II INTERNATIONAL CONFERENCE
ON

MODERN PROBLEMS IN PHYSICS
OF SURFACES AND NANOSTRUCTURES
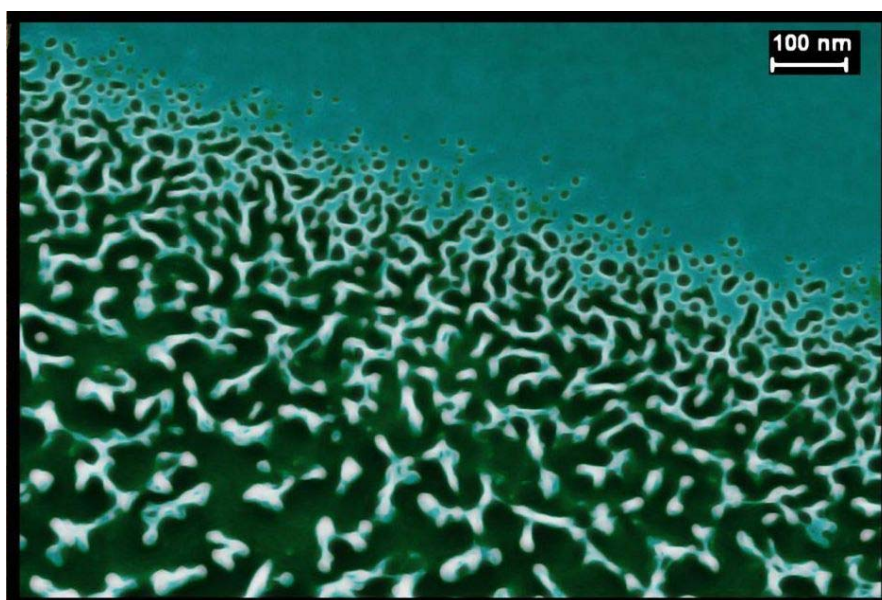
BOOK OF ABSTRACTS

YAROSLAVL, RUSSIA
2012

International Advisory Board:

Alexander Orlikovsky, director of IPT RAS*, Moscow, Russia
Alexander Rusakov, rector of the Yaroslavl Demidov State University, Yaroslavl, Russia
Vladimir Lukichev, deputy director of IPT RAS*, Moscow, Russia
Tapio Ala-Nissial, Aalto University, Helsinki, Finland
See-Chen Ying, Brown University, Providence, USA
Talat Rahman, University of Central Florida, Orlando, USA
Enzo Granato, Institute of Space Research, San Jose dos Campos, Brasil
Oleg Trushin, YB IPT RAS**, Yaroslavl, Russia
Ildar Amirov, deputy head of YB IPT RAS**, Yaroslavl, Russia
Alexander Scundin, IPCE RAS, Moscow, Russia

The Local Organizing Committee:

Alexander Rudy (head of orginizing committee), head of YB PTI RAS , Yaroslavl, Russia
Arkady Berdnikov , YB IPT RAS**, Yaroslavl, Russia
Oleg Trushin (dep. head of organizing committee), YB IPT RAS**, Yaroslavl, Russia
Valery Rudakov, YB IPT RAS**, Yaroslavl, Russia
Ildar Amirov, deputy head of YB IPT RAS**, Yaroslavl, Russia
Vladimir Bachurin, Yaroslavl Demidov State University, Yaroslvl, Russia
Irina Kuznetsova, Yaroslavl Demidov State University, Yaroslavl, Russia

* - Institute of Physics and Technology, Russian Academy of Sciences

** - Yaroslavl Branch of the Institute of Physics and Technology, Russian Academy of Sciences

Cover: Scanning Electron Microscope image of Gd-Co thin film surface.

CONTENTS

Session 1. <u>Physics and Technology of Nanostructures</u>

Session 2. <u>Physics of thin film growth</u>

Session 3. <u>Modeling of Surface Phenomena</u>

Session 4. <u>Spintronics and Magnetic Nanostructures</u>

Session 5. Electronic transport in nanostructures

Session 6. Perspective devices of micro and nanoelectronics

Session 7. Self-organization on the surface

Session 8. Nanocomposites and porous media

Session 9. Properties of micro and nanostructures

Session 10. Ion to surface interactions

Poster Session I

Poster Session II

I1-1: Epitaxial graphene on Ir(111) – a playground for the fabrication of graphene hybrid materials

T. Michely

II. Physikalisches Institut, Universität zu Köln, Germany, michely@ph2.uni-koeln.de

Carefully optimizing the growth of graphene on Ir(111) by scanning tunneling microscopy and low energy electron microscopy yields a virtually defect free epitaxial monolayer of macroscopic extension.

With the help of the aforementioned microscopies, ab initio calculations, resolved photo emission, X-ray standing waves, high resolution X-ray core level spectroscopy and electron diffraction we develop a consistent picture of the electronic and geometric structure of graphene on Ir(111) and its bonding to the substrate.

Graphene on Ir(111) can be used as a laboratory to construct new types of graphene based compound materials. Specifically, patterned adsorption of atoms and molecules takes place resulting in cluster superlattices with exciting magnetic and catalytic properties. Intercalation underneath the graphene allows one to manipulate the properties of graphene itself, e.g. its ability to adsorb atoms and molecules as well as its magnetism.
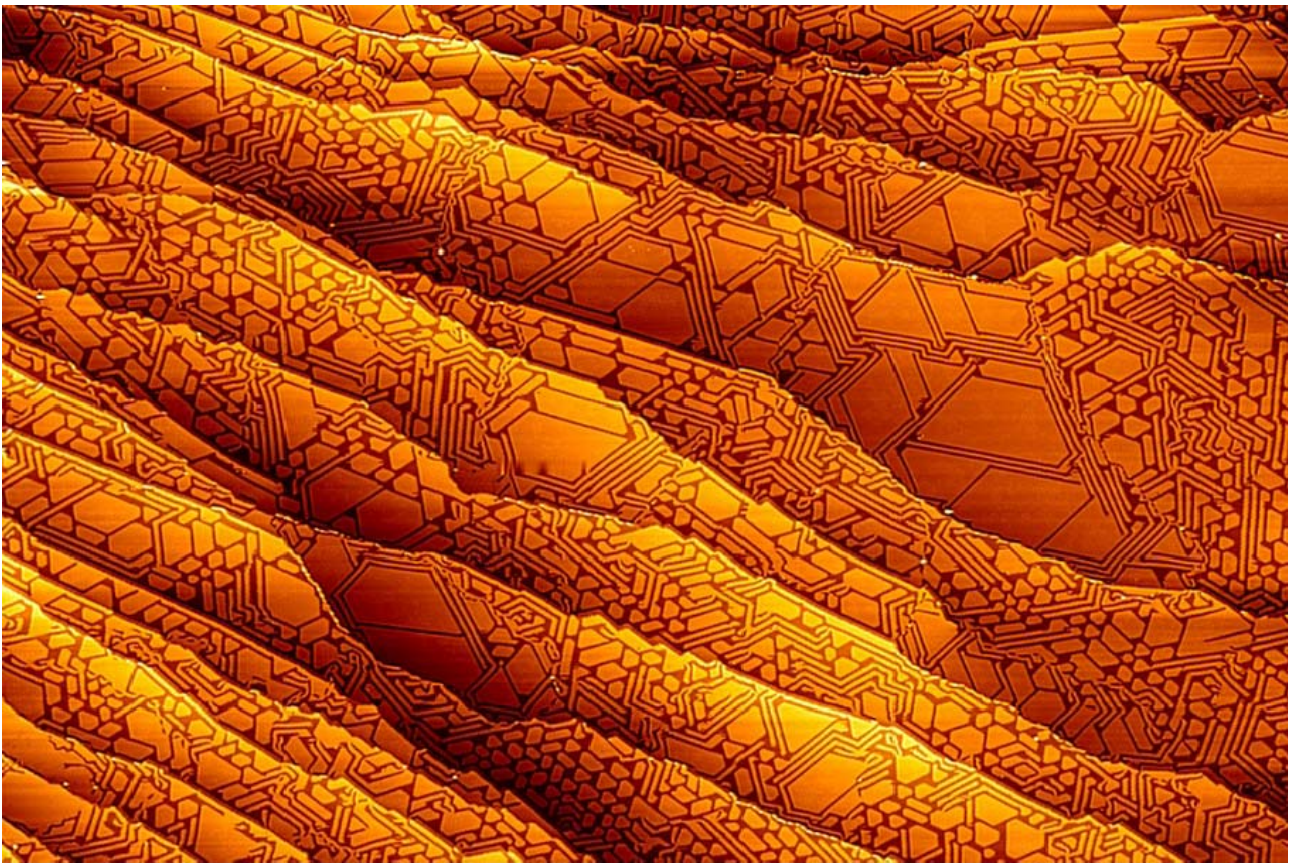
Figure 1: Scanning tunneling microscopy topograph taken at 300 K after intercalation of Eu at 720 K underneath a full graphene layer on Ir(111). The pattern of intercalation Eu islands and stripes results from the interplay of chemically inhomogeneous binding of graphene to the substrate and graphene strain relaxation. Image width is 600 nm.

I1-2: Diffusion and growth of para-sexiphenyl molecular films

Gregor Hlawacek[1,4], Fawad S. Khokhar[1], Paul Frank[2], Peter Puschnig[3], Raoul van Gastel[1], Claudia Ambrosch-Draxl[3], Adolf Winkler[2], Harold J. W. Zandvliet[1], Christian Teichert[4], Bene Poelsema[1]

1. Physics of Interfaces and Nanomaterials, MESA+ Research Institute, University of Twente, PO Box 217, 7500AE Enschede, The Netherlands
2. Institute of Solid State Physics, Graz University of Technology, Petersgasse 16, 8010 Graz, Austria
3. Chair of Atomistic Modelling and Design of Materials, University of Leoben, Franz Josef Strasse 18, 8700 Leoben, Austria
4. Institute of Physics, Montanuniversitaet Leoben, Franz Josef Strasse 18, 8700 Leoben, Austria

Although organic electronics with devices like organic thin film transistors (OTFT), organic light emitting diodes (OLED) and various types of sensors have entered the consumer market, there is still a severe lack of understanding of the basic growth mechanisms. However, the full understanding of growth mechanisms and molecular processes is a prerequisite to utilize the full potential of this materials class. In particular devices based on small molecules are not able to show their full potential. The limitations arise at least partially from rough film morphology, misaligned grains and a high number of grain boundaries.

In an effort to gain insight into some of the fundamental diffusion processes during thin film growth of small conjugated molecules, para-sexiphenyl (6P) was grown under various conditions. A combination of state of the art characterization techniques – including atomic-force microscopy (AFM), low energy electron microscopy (LEEM), and spot profile analysis micro low energy electron diffraction (SPA-µLEED) – allows observing local as well as ensemble behavior ex-situ and in-situ in real time. I will discuss the different growth modes in this model system and describe ways to extract fundamental diffusion parameters.

The growth of small organic molecules often results in the formation of growth mounds [1] or one dimensional needles [2]. It is important to realize that different applications require different molecular orientations. Using a brief ion bombardment of mica we could change the molecular orientation from flat lying to upright standing. While on crystalline mica needles of flat lying molecules are formed [2], deposition of 6P on the anisotropic surface results in growth mounds formed by upright standing molecules. Figure 1a is an AFM image of such a growth mound. The step height (see Figure 1b) between the individual terraces corresponds to the length of the 6P molecule. The shape of the mound is controlled by the height of diffusion barriers – in particular the Ehrlich Schwoebel barrier. We measured the height of this step edge barrier to be 0.67 eV. Molecular dynamics simulations helped to understand the precise diffusion mechanism of such a molecule over the step edge (see Figure 1c,d). We could show that the barrier height depends on the bending angle of the molecular backbone during the step crossing. Consequently we observe smaller barriers for the initial layers, where the molecules have a different tilt angle.
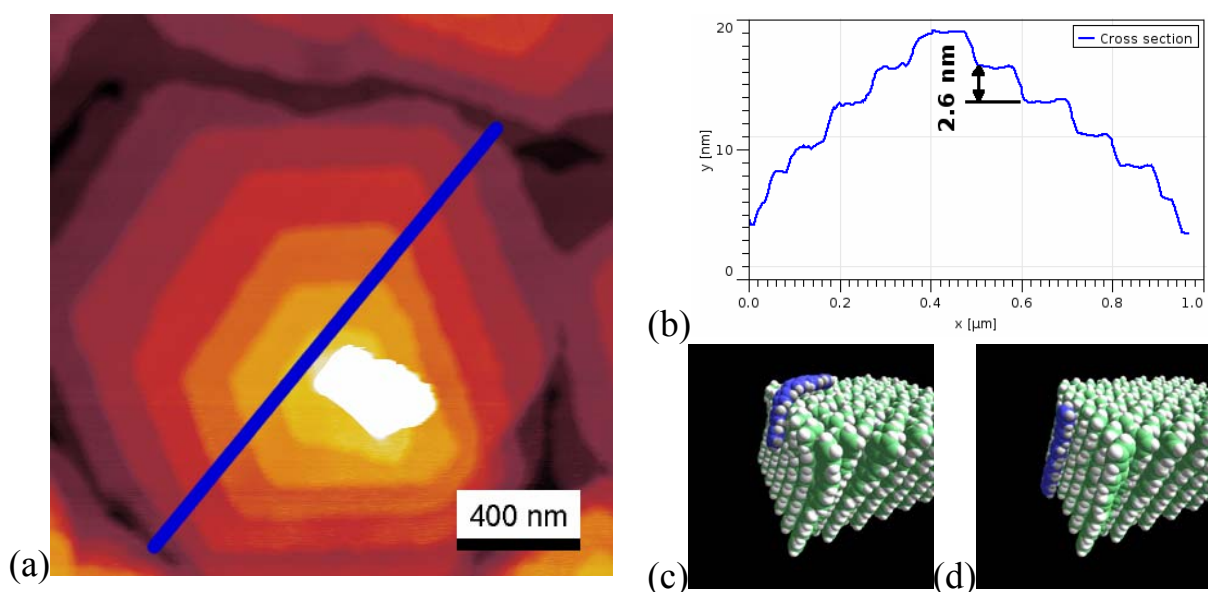
Figure 1: (a) A six sided growth mound with a height corresponding to several layers of upright standing 6P. (b) Corresponding cross section marked in (a). (c,d) Snapshots of the 6P molecules diffusing over a step edge.

For the growth of high-efficiency OLEDs, metal supported graphene has been used as the substrate. Graphene is a flexible, transparent and highly conductive electrode material allowing for the fabrication of bendable all organic devices. Using low temperature (240 K) growth we monitored layer-by-layer growth of small conjugated molecules in-situ and in real time using LEEM (see Figure 2). With the help of SPA-
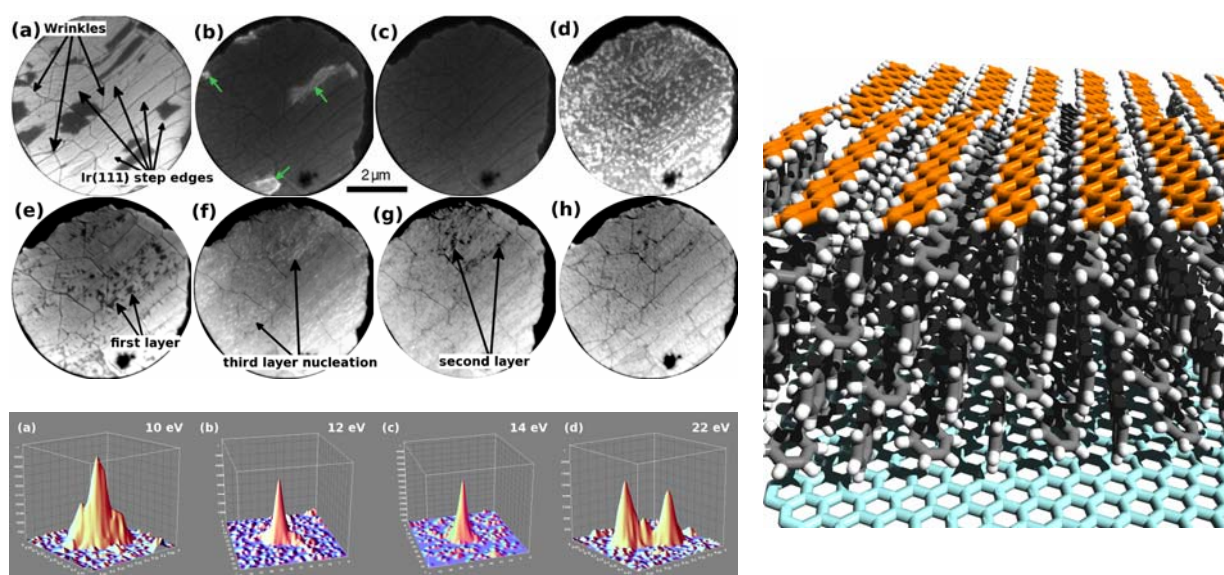
Figure 2 Layer-by-Layer growth. Top left: Sequence of LEEM images taken during the growth of the first 3 monolayers. The initial islands (a) form a closed film with an initial structure (b) that transforms into a bulk like structure (b,c). This sequence repeats for each additional layer (d-h). Bottom left: Spot profiles obtained from O(01) spot at different energies. These LEED results were obtained form a thick film. Right: Proposed structure of the final film. Light blue: graphene; Gray: Layer-by-Layer grown bulk of 6P; Orange: growing ad-layer exclusively built from flat lying face-on molecules.

μLEED we revealed a two step film formation process. Each layer first grows in a low density structure. This structure is formed exclusively from face-on flat lying molecules. With ongoing deposition this layers transforms into a bulk like structure with alternating edge-on/face-on molecules. The layer-by-layer growth proceeds by repeating this sequence (see Figure 2).[3]

The first initial islands show a remarkable mobility which is related to their metastable structure. The observed diffusion of islands which are built from several thousand molecules can be explained with the strain interplay between the Ir crystal, graphene flakes, and 6P islands. This island mobility stops once the film obtains a bulk like structure [4].

A detailed investigation of this system at different growth temperatures reveals a transition to Stranski-Krastanov growth at moderate temperatures (320 K). However, at high temperatures (405 K) no structures are formed on graphene due to the increased mobility of 6P [5].

1. Hlawacek, G. *et al.*, Characterization of Step-Edge Barriers in Organic Thin-Film Growth. *Science* **321**, 108-111 (2008).

2. Teichert, C. *et al.*, Spontaneous rearrangement of para-sexiphenyl crystallites into nano-fibers. *Appl. Phys. A* **82**, 665-669 (2006).

3. Hlawacek, G., Khokhar, F. S., van Gastel, R., Poelsema, B. & Teichert, C., Smooth growth of organic semiconductor films on graphene for high-efficiency electronics. *Nano Lett.* **11**, 333-337 (2011).

4. Hlawacek, G., Khokar, F. S., van Gastel, R., Teichert, C. & Poelsema, B., Diffusion and submonolayer growth of para-sexiphenyl on Ir(111) and Ir(111)-supported graphene. *IBM J. Res. & Dev.* **55** (4), 15 (2011).

5. Khokhar, F. S. *et al.*, The influence of substrate temperature on growth of para-sexiphenyl thin films on Ir. *Surf. Sci.* **606**, 475-480 (2012).

I1-3: Novel low-dimensional phases of carbon and inorganic materials: insights from DFT simulations and TEM experiments

Arkady V. Krasheninnikov,[1,2] Hannu-Pekka Komsa,[1] Natalia Berseneva,[2] Simon Kurasch,[3] Jani Kotakoski,[1,4] Ossi Lehtinen,[1] Torbjörn Björkman,[2] Ute Kaiser,[3] Jannik Meyer,[4] Risto M. Nieminen[2]

1. Department of Physics, University of Helsinki, P.O. Box 43, 00014 Helsinki, Finland, E-mail: akrashen@acclab.helsinki.fi, 2. Department of Applied Physics, Aalto University, P.O. Box 1100, 00076 Aalto, Finland, 3. Central Facility for Electron Microscopy, Group of Electron Microscopy of Materials Science, Ulm University, 89081 Ulm, Germany, 4. Department of Physics, University of Vienna, Boltzmanngasse 5, 1090 Wien, Austria

Unique electronic and mechanical properties of low-dimensional carbon and inorganic materials gave rise to extensive research in this area aimed at finding new low-dimensional phases of these materials and further tailoring of their characteristics. In particular, recent experiments on electron and ion bombardment of 2D materials demonstrate that irradiation can have beneficial effects on such targets and that electron or ion beams can serve as tools to change the morphology and tailor mechanical, electronic and even magnetic properties of low-dimensional materials.

In the first part of the presentation, I will briefly touch upon some of the low-dimensional materials which were recently discovered, such as graphene ribbons inside carbon nanotubes [1] and two-dimensional (2D) silica structures [2] observed on graphene layers. In particular, I will show that the proper account for van der Waals interactions is required to adequately described the properties of these materials.

In the second part of this presentation, our latest theoretical results on the response of graphene [3-5], h-BN [6] and several dichalcogenides (MoS_2, $MoSe_2$, WS_2, etc) [7] to irradiation will be presented, combined with the experimental data obtained in collaboration with several groups. The electronic structure of graphene sheets with defects will be discussed, and possible avenues for tailoring the electronic structure of graphene by irradiation-induced defects [8] and impurities will be introduced. We will also discuss how electron irradiation and electron beam-assisted deposition can be used for engineering hybrid BN-C nanosystems by substituting B and N atoms with C atoms. Finally, we present the results of firs-principles calculations [6] for displacement thresholds in various dichalcogenides. We will further touch upon the most frequent defect structures which appear in these materials under electron irradiation and compare the calculated defect configurations to those found in the transmission electron microscopy experiments. Similar to h-BN, we explore how electron-beam-assisted deposition can be used to change the atomic structure of dichalcogenides and tailor their electronic properties through doping

1. A.V. Talyzin, I.V. Anoshkin, A. V. Krasheninnikov, R.M. Nieminen, A.G. Nasibulin, H.Jiang, and E.I. Kauppinen "Synthesis of Graphene Nanoribbons Encapsulated in Single-Walled Carbon Nanotubes" Nano Letters 11, p. 4352, 2011.
2. P. Y. Huang, S. Kurasch, A. Srivastava, V. Skakalova, J. Kotakoski, A. V. Krasheninnikov, , R. Hovden, Q. Mao, J. C. Meyer, J. H. Smet, D.A. Muller, and U. Kaiser, "Direct Imaging of a Two-Dimensional Silica Glass on Graphene", Nano Letters 12, p. 1081, 2012.
3. J.C. Meyer, F. Eder, S. Kurasch, V. Skakalova, J. Kotakoski, H.J. Park, S. Roth, A. Chuvilin, S. Eyhusen, G. Benner, A. V. Krasheninnikov, and U. Kaiser "An accurate measurement of electron beam induced displacement cross sections for single-layer graphene", Phys. Rev. Lett. in press, 2012.
4. J. Kotakoski, D. Santos-Cottin, and A. V. Krasheninnikov, "Stability of graphene edges under electron beam: equilibrium energetics vs. dynamic effects", ACS Nano 6, p. 671, 2012.
5. J. Kotakoski, A. V. Krasheninnikov, U. Kaiser, and J.C. Meyer "From point defects in graphene to two-dimensional amorphous carbon", Phys. Rev. Lett. 106, p. 105505, 2011.
6. N. Berseneva, A. V. Krasheninnikov, and R.M. Nieminen "Mechanisms of post-synthesis doping of boron-nitride nanostructures with carbon from first-principles simulations" Phys. Rev. Lett. 107, p. 035501, 2011.
7. H.-P. Komsa, J. Kotakoski, S. Kurasch, O. Lehtinen, U. Kaier, and A. V. Krasheninnikov, submitted.
8. F. Banhart, J. Kotakoski and A. V. Krasheninnikov, "Structural defects in graphene", ACS Nano 5, p. 26, 2011.

I1-4: Plasmons enhance near-field radiative heat transfer for graphene-covered dielectrics

V. B. Svetovoy[1] , P. J. van Zwol[2] , J. Chevrier[2]

MESA+ Institute for Nanotechnology, University of Twente, PO 217, 7500 AE Enschede, The Netherlands,
V.Svetovoy@utwente.nl. 2. Institut Néel, CNRS and Université Joseph Fourier Grenoble, Boîte Postale 166, FR-38042
Grenoble Cedex 9, France

Radiative heat transfer (RHT) in vacuum at small distances between bodies is much increased in the near-field regime as compared to that given by the black body law [1]. It happens due to interaction of evanescent waves at distances small in comparison with the thermal wavelength $\lambda_T = \hbar c / T$ (here $k_B = 1$). Particularly strong enhancement occurs when bodies can support surface modes such as plasmon-polaritons and phonon-polaritons [2]. This effect can be used to improve performance of near-field photovoltaic devices [3], in nanofabrication [4], and in near-field imaging systems [5].

Graphene attracted recently enormous attention as a two dimensional carbon material with unusual electronic properties [6]. It is considered as a promising material for the development of high-performance electronic devices. Plasmons in graphene show favorable behavior for applications such as large confinement, long propagating distances, and high tunability via electrostatic gating [7]. The plasmon frequencies lie in the terahertz region that is interesting for radiative heat transfer, but the topic was not explored yet. Plasmons were shown to change significantly the thermal Casimir force for graphene-covered materials [8].

We show theoretically that plasmon excitations in graphene have striking effect on the near-field RHT between bodies if at least one of them is covered with graphene. The effect is related to the fact that graphene is essentially nonlocal material and its plasmon frequency changes with the wavenumber. Moreover, it varies significantly with the doping level. Possibility to tune the plasmon frequency is a convenient tool to control the heat transfer between bodies. Enhance of the heat transfer is demonstrated experimentally by measuring the heat transfer coefficient (HTC) between a glass ball and SiC substrate covered with graphene.

To evaluate the HTC ($W/m^2 K$) between two bodies 1 and 2 one has to know the reflection coefficients r_1 and r_2 for each body as functions of the frequency ω and the wave vector q. There coefficients can be expressed via the dielectric functions of the substrates $\varepsilon_{1,2}(\omega)$ and the dielectric function of the graphene layer $\varepsilon(q,\omega)$. The latter can be evaluated in the random phase approximation as it was done in a number of papers [6]. Space dispersion (dependence on q) is an important property of graphene. If the separation d between two parallel plates is small in comparison with the thermal wavelength, $d \ll \lambda_T$, only evanescent waves will contribute to the heat transfer. Moreover, the contribution of graphene can be calculated in the non-retarded approximation taking into account only transverse magnetic polarization [8]. Retardation effect and transverse electric polarization both are suppressed at least by the factor $v_F/c \approx 300$, where $v_F \approx 10^6 \, m^2/s$ is the Fermi velocity in graphene. For example, if optically inactive substrate (can be described frequency independent dielectric constant) is covered with a layer of graphene, the reflection coefficient of such a body will be $r(q,\omega) = 1 - (1 - r_0)/\varepsilon(q,\omega)$, where r_0 is the reflection coefficient of the substrate.

The reflection coefficient has a pole when $\varepsilon(q,\omega) = 0$. This pole corresponds to plasmon excitation in graphene. The frequency of this plasmons is given by the equation $\hbar \omega_p \approx \left(2\alpha_g G(\varepsilon_F) \hbar v_F q T \right)^{1/2}$, where α_g is the coupling constant in graphene and $G(\varepsilon_F)$ is a function of the Fermi level in graphene ($\varepsilon_F = E_F/T$) [8]. For the best heat transfer, the resonances in the opposing bodies have to match each other [2]. When one body is covered with graphene, one can always find a value of the wavenumber q for which the plasmon resonance matches the resonance in the opposing body. This simple principle gives qualitative explanations for rich physics that can be realized between bodies covered with graphene.

Figure 1 illustrates the situation for the heat transfer between a dielectric covered with graphene (body 1) and a dielectric (body 2) that has a plasmon-polariton resonance at the frequency ω_r. In dependence of the value of q ($x = 2qd$) one can always find a plasmon, which frequency matches ω_r as shown in Fig. 1a. Integration over q gives the spectral density of the HTC that is concentrated around ω_r (see Fig. 1b). Graphene contribution to the HTC scaled as $\Delta h = (100 nm/d)^2 \Delta R$ is shown as a function of distance (Fig. 1c) and as

a function of the Fermi level (Fig. 1d). The maximal heat transfer is realized between two identical dielectrics covered with graphene and it can be as large as $\Delta h = 3000 \, W/m^2 K$ at $d = 50 \, nm$ and $T = 300 \, °K$ to be compared with that between black bodies $h_{bb} = 6 \, W/m^2 K$. This value is larger than that between the best known materials. The effect is especially pronounced at lower temperatures. Significant dependence of the HTC on the Fermi level allows deep modulation of the heat flux at very high frequencies up to 100 GHz.
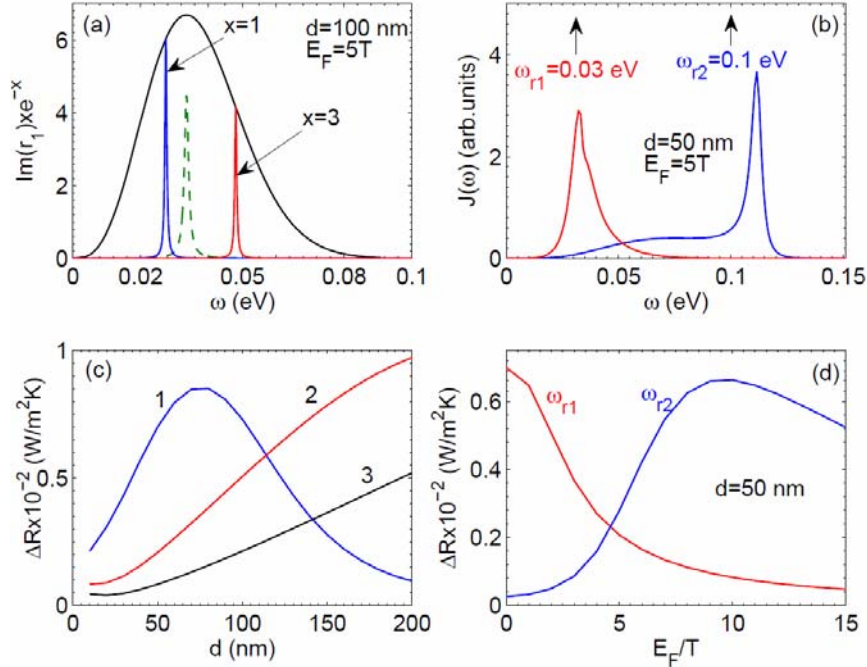
Figure 3 Inactive dielectric covered with graphene (body 1) against a dielectric without graphene described by the Lorentz model (body 2). (a) Resonances in the reflection coefficients. The dashed line (green) shows the fixed resonance in $Im \, r_1$. Plasmon resonances in the body 1 are shown for $x = 1$ and $x = 3$ together with the enveloping line (black). (b) Spectral density for two values of the Lorentz resonance. (c) ΔR as a function of distance. Curves 1, 2, 3 correspond to $e_F = 0, 5, 10$, respectively. (d) ΔR as a function of the Fermi level.

1. D. Polder and M. van Hove, "Theory of Radiative Heat Transfer between Closely Spaced Bodies", Phys. Rev. B 4, pp.3303-3314 (1971)
2. K. Joulain, J.-P. Mulet, F. Marquier, R. Carminati, and J.-J. Greffet, "Surface electromagnetic waves thermally excited: Radiative heat transfer, coherence properties and Casimir forces revisited in the near field", Surf. Sci. Rep. 57, pp.59-112 (2005).
3. M. Laroche, R. Carminati, and J.-J. Greffet, "Near-field thermophotovoltaic energy conversion", J. Appl. Phys. 100, 063704 (2006).
4. Z. W. Liu, Q. H. Wei, and X. Zhang, „Surface Plasmon Interference Nanolithography", Nano Lett. 5, 957 (2005).
5. Y. De Wilde, F. Formanek, R. Carminati, B. Gralak, P.-A. Lemoine, K. Joulain, J.-P. Mulet, Y. Chen, and J.-J. Greffet, "Thermal radiation scanning tunnelling microscopy", Nature 444, 740 (2006).
6. A. H. Castro Neto, F. Guinea, N. M. R. Peres, K. S. Novoselov, and A. K. Geim, "The electronic properties of graphene", Rev. Mod. Phys. 81, pp.109-162 (2009).
7. M. Jablan, H. Buljan, and M. Soljaĉić, "Plasmonics in graphene at infrared frequencies", Phys. Rev. B 80, 245435 (2009).
8. V.B. Svetovoy, Z. Moktadir, M. C. Elwenspoek, and H. Mizuta, "Tailoring the thermal Casimir force with graphene", EPL 96, 14006 (2011).

I1-5: Defects and electronic structure of CIS thin films: revision

L.E. Oikkonen[1], M.G. Ganchenkova[1,2], A.P. Seitsonen[3], and R.M. Nieminen[1]

1. Aalto University, Espoo, Finland, Laura.Oikkonen@aalto.fi. 2. National Research Nuclear University, Moscow, Russia, g_maria@mail.ru. 3. University of Zurich, Zurich, Switzerland

Understanding and controlling the electronic properties of the solar cell absorber material $CuInSe2$ (CIS) is an important step when pursuing higher conversion efficiencies. A ternary material where a variety of intrinsic defects and their complexes can contribute to the electronic structure poses a definite challenge for characterization. In practice, it has not been possible to correlate observed defect energy levels with specific defect structures by experimental techniques [1,2]. Consequently, defect identification in this material remains at a speculative stage.

In lack of direct evidence, the experimental development of CIS solar cells has relied on 'trial and error', and conclusions have been drawn from indirect observations which completely depend on interpretation. In this situation, theoretical first-principles calculations have been served as a helpful tool for interpreting experimental results for the past 15-20 years. The calculations have been used to study defect formation energies in order to reveal energetically most favorable defects, and to obtain defect ionization levels that could be compared with experimental ones. Early theoretical studies [3–7] have highlighted the role of several Cu-related defects: V_{Cu}, In_{Cu} as well as some of their complexes have been suggested to have particularly low formation energies among the considered defects and are predicted to exist in CIS samples in substantial quantities. The ionization levels induced by these defects have been computed and related to experiment, interpreting V_{Cu} as a p-type acceptor, and bringing forth new candidates for donor-type defects, notably, In_{Cu} [5]. However, it should be noted that not all possible point defects have been systematically studied; even the most thorough and cited report published on the topic [3] ignored Se-related.

All along, theoretical calculations have pointed the direction where experimentalists should look, but the basis of these early calculations is not solid based on what we know today and should be brought under critical evaluation. At the time when the studies were conducted, until very recent years, the state-of-the-art defect calculations were performed with density-functional theory (DFT) and the (semi)local-density approximation. The local-density approximation (LDA) inherently underestimates semiconductor band gaps, and in the case of materials with strongly localized Cu-d orbitals such as CIS, it can even lead to a vanishing band gap. Uncertainties related to defect level positions due to the band gap underestimation were often tried to remove by applying a posteriori corrections that could, for instance, stretch out the gap up to its experimental value. Their reliability has been questioned since they have not shown consistent improvement over plain LDA results [8]. This is one of the reasons why the speculative assignments of defects to experimentally observed defect levels should be treated with great caution. Indeed, the agreement between theory and experiment for this material has not been satisfactory, and the calculations have been criticized for not reproducing experimental results [2].

Only recently new methods overcoming the band gap problem have emerged for wider use. The local-density exchange-correlation functional can now be replaced by a hybrid functional, where a portion of exact exchange has been incorporated, there by describing localized orbitals more correctly than LDA [9]. Hybrid functionals have been shown to open up the band gap for CIS [10–12, 13], thus giving hope of shedding light on the defect structure of CIS.

In this paper, we present a fresh look at defects in CIS by employing the range-separated hybrid functional (HSE06) [14]. Our results differ from the generally held view of CIS defect physics. We demonstrate, in particular, the importance of Se-related defects in CIS, which have been often overlooked compared to Cu-related defects. We show that Se-related and not Cu-related defects can be responsible for defect levels within the band gap. Se-related defects therefore play a decisive role when controlling the electronic properties of CIS. We believe that these new findings will be useful when interpreting experimental observations.

1. S. Siebentritt, M. Igalson, C. Persson, and S. Lany, 'The electronic structure of chalcopyrites—bands, point defects and grain boundaries', Prog. Photovolt.: Res. Appl., 18, pp.390-410, 2010.
2. W.N. Shafarman and S. Siebentritt and L. Stolt, *Cu(InGa)Se2 Solar Cells*, in Handbook of Photovoltaic Science and Engineering, John Wiley & Sons, 2011.

3. S. B. Zhang, S.-H. Wei, A. Zunger, and H. Katayama-Yoshida, 'Defect physics of the $CuInSe_2$ chalcopyrite semiconductor', Phys. Rev. B, 57, pp.9642-9656, 1998.

4. S. Lany and A. Zunger, 'Anion vacancies as a source of persistent photoconductivity in II-VI and chalcopyrite semiconductors', Phys. Rev. B, 72, p.035215, 2005.

5. C. Persson, Y. J. Zhao, S. Lany, and A. Zunger, 'n-type doping of $CuInSe_2$ and $CuGaSe_2$', Phys.Rev. B, 72, p.035211, 2005.

6. S. Lany and A. Zunger, 'Light- and bias-induced metastabilities in $Cu(In,Ga)Se_2$ based solar cells caused by the (V_{Se}-V_{Cu}) vacancy complex', J. Appl. Phys., 100, p.113725, 2006.

7. S. Lany and A. Zunger, 'Intrinsic *DX* Centers in Ternary Chalcopyrite Semiconductors', Phys. Rev. Lett., 100, p.016401, 2008.

8. P. De´ak, A. Gali, B. Aradi, and T. Frauenheim, 'Accurate gap levels and their role in the reliability of other calculated defect properties', Phys. Status Solidi B, 248, pp.790-798, 2011.

9. T. M. Henderson, J. Paier, and G. E. Scuseria, 'Accurate treatment of solids with the HSE screened hybrid', Phys. Status Solidi B, 248, pp.767-774, 2011.

10. J. Vidal, S. Botti, P. Olsson, J.-F. Guillemoles, and L. Reining, 'Strong Interplay between Structure and Electronic Properties in $CuIn(S,Se)_2$: A First-Principles Study', Phys. Rev. Lett., 104, p.056401, 2010.

11. J. Pohl and K. Albe, 'Thermodynamics and kinetics of the copper vacancy in $CuInSe_2$, $CuGaSe_2$, $CuInS_2$, and $CuGaS_2$ from screened-exchange hybrid density functional theory', J. Appl. Phys., 108, p.023509, 2010. Errata: J. Appl. Phys., 110, 2011.

12. H. Xiao, J. Tahir-Kheli, and W. Goddard, 'Accurate Band Gaps for Semiconductors from Density Functional Theory', J. Phys. Chem. Lett. 2, pp.212-217, 2011.

13. L. E. Oikkonen, M. G. Ganchenkova, A. P. Seitsonen, and R. M. Nieminen, 'Vacancies in $CuInSe_2$: new insights from hybrid-functional calculations*', J. Phys.: Condens. Matter 23, pp.422202-422206, 2011.*

14. J. Heyd, G. Scuseria, and M. Ernzerhof, 'Hybrid functionals based on a screened Coulomb potential', J. Chem. Phys., 118, pp.8207-8215, 2003.

I1-6: Next Generation Lithography – mythes and reality

S. I. Zaitsev

IMT RAS, Chernogolovka, Russia, e-mail: zaitsev@iptm.ru

The empirical regularity first formulated by Moore, by the efforts seem primarily of Intel, has been elevated to the rank of a "law." Physical limit of the current optical lithography using 193nm light source is a quarter wavelength. This limitation can be bypassed by exposure in the immersion fluid. Double patterning is planned to use for further progress. However, during more than ten past years an active search for technologies that could replace the modern photolithography has been performing. The technology has a special name «next generation lithography» (NGL).

It is believed that the most mature pretendent is technology of extreme ultraviolet lithography (EUVL). However, along with it other approaches are seriously considering and developing. This report examines these, so called. alternative technologies. The technologies are based on the use of electron beams, and also they are called as technologies of direct drawing or technology maskless lithography. Now there are quite a few projects:

- Multi- beam lithography Mapper, the company Mapper
- reflectance electron lithography, REBL, the company KLA-Tencor
- a multi-beam projection lithography, PML2, IMS Nanofabrication Company
- MultiShaped Beam, the company VISTEC
- Multi Column E-beam, the company ADVANTEST
- the system of projection cells, CellProjection System
- complementary electron lithography, Complimentary EBL, Japan
- autoemission electron lithography, SelfEmission Litho, company CRESTEC

Extremely tough competition claims arising from the modern photolithography are imposed on all the next-generation technologies. Such is, for example, the requirement for performance of 100 wafers per hour at a cost of 30-50 million dollars per setup.
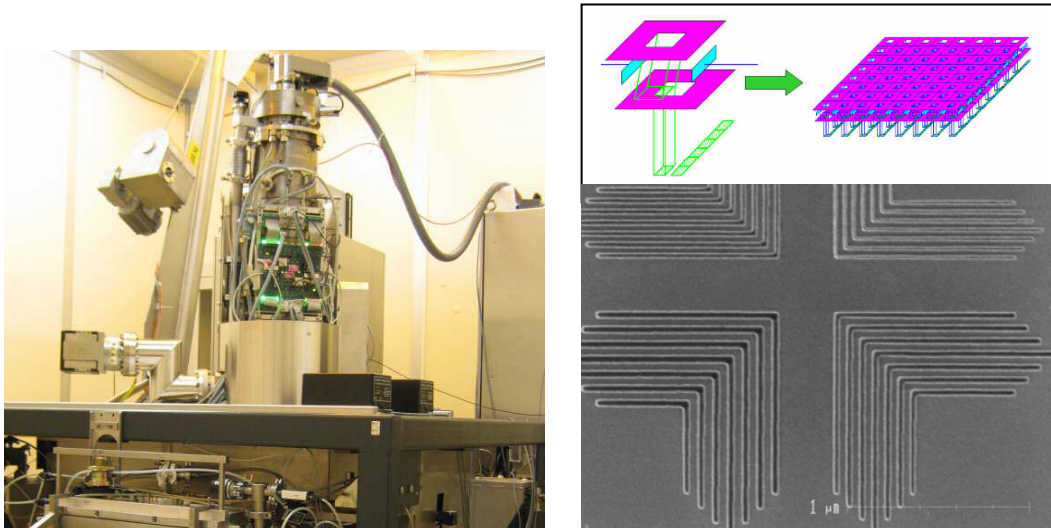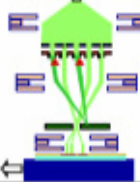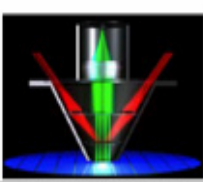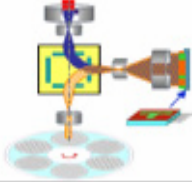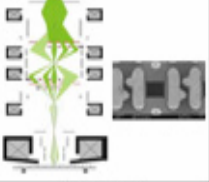
Fig.1 Pilot setup implementing the MultiShaped Beam technology, the company VISTEC; top right - schematic illustration of the differences in VariableShaped Beam and MultiShaped Beam, right-bottom, the limiting resolution reached to date.

The report briefly describes the technologies, analyzes the claimed potentials. In general, all the technologies demonstrate high resolution, or clearly demonstrate the possibility of achieving. However, the main difficulty of the direct drawing technologies is the need to satisfy two mutually exclusive requirements - high-resolution at high throuput. Performance can be improved by increasing the current, but it inevitably

increases the diameter of the beam and decreases the resolution. Therefore, all the technology of direct drawing consider creating a multi-cathode (columns) systems to overcome these difficulties. And even when considering a multi-cathode system requirements for current and stability of a single electron source are extremely high.

	IMS Nanofabrication	MAPPER Lithography	KLA-Tencor	Vistec Electron Beam	ASET/ADVANTEST
Name	eMET / PML2	MAPPER	REBL	MSB	MCC
Spec.					
	Massive parallel			Multi VSB	Multi column
	50kV	5kV	50kV	50kV	50kV
	Point beam/Gray scale			VSB / CP	VSB / CP
	~ 20M beams (256k beams for mask writing: eMET)	13k beams	Reflective (REBL) >1M pixels	64 shaped beams for mask writing	16 columns
α	2500 beams	110 beams	-	16 beams	4 columns
TPT	5wph [≤16nm hp] (50wph by clustering 10 tools)	10wph [≤22nm hp] (100wph by clustering 10 tools)	40wph (Via), 2wph (Metal) [45nm node]	~4wph [≤22nm node] (1024 beams)	~5wph [≤45nm hp] (16 columns)
Verify	2012 (eMET)	2011	2013	2012	---
Project/ Support	EU FP7 MAGIC project		DARPA / KLA-Tencor	TBD	ASET Mask D2I

Fig.2 Summary table of the declared project phases of next generation lithography.

Selection criteria for the next-generation technologies are derived from the competitive requirements, form which one should come to pessimistic conclusion that in spite of the promises and plans (collected in a fresh table Fig. 4), hardly any one of the announced projects will reach potential to replace the current lithography in 2015. The most promising, if not the only project is the project MAPPER, which the report describes in great detail.

I1-7: Quantum Mechanical nanoscale magic:the growth of single 7-layer height Pb islands

M. C. Tringides

Department of Physics Iowa State University
Ames Laboratory –USDOE

The discovery of ways to control the dimensions of nanostructures is essential for Nanotechnology. Experiments over the past 8 years have shown a novel low temperature pathway to grow metallic islands of a single height on Si surfaces. This is an intriguing and unexpected growth mode. Mass transport of heavy atoms like Pb is controlled by the discrete levels of the confined electrons in the islands according to textbook particle-in-a-box model of Quantum Mechanics. This is labeled Quantum Size Effects (QSE)[1]). The selected height is determined by how well the confined electron wavefunction fits the island height .
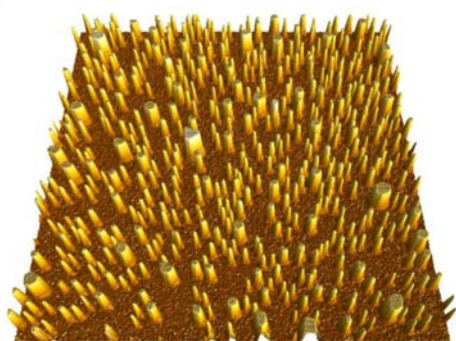
Fig.1 Uniform 7-layer growth of Pb islands on Si(111)-7x7 1.6ML T=200K 1x1μm^2

As in any physical phenomenon this only answers the energetic reason for the "magic" nanoislands to form, but there is still the issue of kinetics, i.e. how the metal atoms move so efficiently to build these islands. The phenomenon requires extraordinary degree of self organization, since a million perfect 7-layer islands with on average ~10^5 Pb atoms each, are built within 1-2 minutes from random deposition at low temperatures ~180K.

Recent experiments have identified a collective super-diffusive mass transport mechanism that carries material very efficiently at low temperatures. This motion has been directly seen with Scanning Tunneling Microscopy and Low Energy Electron Microscopy in real time. The dense wetting layer between the islands moves collectively like a "liquid" transferring atoms to the stable islands at rate much higher than normal diffusion. In normal diffusion transport is stochastic, with the

Fig.2 LEEM diffusion experiments showing an unusual fast diffusion of Pb. The wetting layer moves unperturbed and with constant speed similar to "liquid-like" diffusion as seen in the 5 frames to the right (top 186K and bottom 300K). The plots to the left show unperturbed profiles at different times.

displacement x~ $\sqrt{t}$, while in Pb/Si(111) the motion is ballistic x~t. The theoretical explanation of this unusual behavior is still unclear.

These experiments point to the existence of very novel mass transport at low temperatures, which is coupled to the confined electrons, and is the reason for the very efficient island height selection.

1. M. C. Tringides, M. Jalochowski and E. Bauer Phys. Today 60, No. 4, 50 (2007).
2. K. L. Man, M. C. Tringides, M. M. T. Loy, and M. S. Altman PRL 101, 226102 (2008)
3. M.C. Tringides, M. Hupalo K.L. Man, M.M.T. Loy, M.S. Altman Nanophenomena at Surfaces: Fundamentals of Exotic Condensed Matter Properties Springer ed. M.Michailov (2010)

I1-8: Advances in the Self Learning Kinetic Monte Carlo Method and their application to cluster diffusion and morphological evolution on metal surfaces*

Talat S. Rahman

Department of Physics, University of Central Florida, Orlando, Florida 32816, USA, (email: Talat.Rahman@ucf.edu)

Together with accurate techniques for calculations of diffusion parameters, the kinetic Monte Carlo (KMC) method is an important tool for simulation of temporal and spatial evolution of surface phenomena such as epitaxial growth, adatom-island diffusion, coarsening, and morphological transformations. To enhance its predictive capacity, we had introduced a self-learning KMC method (SLKMC) [1], in which the standard technique is combined with automatic generation of a table of microscopic events, facilitated by a 2D pattern recognition scheme. Each time the system encounters a new configuration, the algorithm initiates a procedure for saddle point search. Nontrivial paths are thus selected and the fully characterized transition path is permanently recorded in a database for future usage. Once the data base of all possible single and multiple atom processes is built, the system evolves automatically and efficiently by picking diffusion processes of its choice. The initial method was limited to adatom occupancy of only the fcc sites. We have now introduced a new 2D pattern recognition scheme which fully accounts for the both the fcc and the hcp sites, together with the top sites, as represented by the substrate atoms in the top layer. This SLKMC-II [2] is thus more versatile and has uncovered several new processes by which adatom islands diffuse on fcc(111) surfaces. For further flexibility in simulating surface morphological evolution and heteroepitaxial growth, we have also proposed a 3D pattern-recognition scheme that is suitable for off-lattice occupancy and for simulating three dimensional structural evolution [3]. This later method is simple and flexible enough that it can be applied to all types of surfaces. In this scheme, to uniquely identify the local environment and associated processes involving three-dimensional (3D) motion of an atom or atoms, space around a central atom is divided into 3D rectangular boxes. The dimensions and the number of 3D boxes are determined by the accuracy with which a process needs to be identified and a process is described as the central atom moving to a neighboring vacant box accompanied by the motion of any other atom or atoms in its surrounding boxes.

I will present application of SLKMC-II to the diffusion and coalescence of 2-dimensional Ag, Cu, and Ni adatom clusters on the (111) surface of these three metals. Of interest are multiple atom processes revealed in the simulation whose presence may have been ignored otherwise. For adatom clusters varying in size from 2 to 100, I will discuss the dependence of the diffusion coefficient, effective energy barriers, and dominant mechanism (periphery atom or concerted-cluster motion), on cluster size. I will highlight the role played by specific diffusion processes and show that a crossover from collective island motion to periphery diffusion takes place at critical sizes which are specific to the metallic system in question. I will also discuss the case of heteroepitaxial growth. Also, for the case of early stages of sub-monolayer island coarsening, I will point to the kinetic stabilization of certain island sizes resulting from specifics of adatom detachment /attachment processes [4]. Furthermore, results of application of the off lattice pattern recognition scheme to examine the decay of 3D Cu islands on Cu(100) will be presented. Results will be compared with those from experiments, where available, and with those from KMC simulations based on a fixed catalog of diffusion processes.

1. O. Trushin, A. Karim, A. Kara , and T. S. Rahman, Phys. Rev. B **72,** 115401 (2005); A. Karim, A. et al., Phys. Rev. B **73**, 165411 (2006).
2. S. I. Shah, G. Nandipati, A. Kara, and T. S. Rahman, submitted to J. Phys. Condens. Matt.
3. G. Nandipati, A. Kara, S. I. Shah, T. S. Rahman, J. Comp. Phys. 231, 3548 (2012).
4. G. Nandipati, A. Kara, S. I. Shah, T. S. Rahman, J. Phys. Condens. Matt.(Fast Track) 23, 262001 (2011).

O1-1: Influence of doping on the properties of Ge-Sb-Te thin films for phase – change memory devices

A. Sherchenkov[1], S. Kozyukhin[2], A. Babich[1], P. Lazarenko[1]

1. National Research University "MIET", 124498, Moscow, Russia, aa_sherchenkov@rambler.ru. 2. Kurnakov Institute of General and Inorganic Chemistry, Moscow, Russia sergkoz@igic.ras.ru

During the last years thin films of chalcogenide semiconductors of Ge-Sb-Te (GST) system were intensively studied due to their possible application in phase change memory (PCM) devices. The work of such devices is based on rapid reversible phase transformations between amorphous and crystalline states, which take place in nanovolume of material under low-energy external influences. These phase transformations are accompanied by the abrupt changes in optical and electrical properties. The work of two types of memories is based on such abrupt changes of the materials - optical and electrical PCM.

At present the most widely investigated and used PCM materials have compositions along the GeTe-Sb_2Te_3 pseudobinary line due to the rapid crystallization. Three intermetallic compounds exist on this pseudobinary line: $Ge_2Sb_2Te_5$, $GeSb_2Te_4$ and $GeSb_4Te_7$ (so named GST materials). The most interesting of them is $Ge_2Sb_2Te_5$, which exhibits appreciable stability at room temperature, high crystallization rate and good reversibility between amorphous and crystalline phases.

Nowadays phase change optical recording discs with different formats [CD-RW, DVD-RW, DVDRAM, and Blu-ray] have obvious commercial success. In addition, phase change electrical memory devices [phase-change random access memory (PRAM)] are considered as most promising candidates for the next generation of memories due to non-volatility, low power consumption, fast operation speed, high endurance, extended scalability, low manufacturing cost.

However, despite of successful commercial application of chalcogenide alloys large investigation work must be carried out to clarify phase transition mechanism, which determines phase transition temperature, rate and thermal cycling life.

The doping can be used for controlling the changes in thermal, electrical, optical properties, and increasing stability of thin films of semiconductors, and so modifying and improving main PCM parameters. However, most chalcogenide glasses are insensitive to the doping due to high density of intrinsic defects pinning the Fermi level near the center of the band gap. In this case, controlling the electrical and optical properties of the PCM materials is a complex problem. Therefore, it is necessary to find alloying elements which have a positive influence on the properties of amorphous and crystalline phases.

In this connection, the general aim of this study is to investigate the influence of In, Ti, Sn, and Bi doping on the thermal, electrophysical characteristics, and cyclability of $Ge_2Sb_2Te_5$ thin films. The choice of the dopants is explained by their isomorphism with the main components. In addition it was assumed that the isovalent elements with covalent atomic radius close to that of the elements in GST will give the least strain in the matrix structure of the material.

The initially doped $Ge_2Sb_2Te_5$ alloys with different amounts of In, Ti, Sn, and Bi (0, 0.5, 1 and 3 wt.%) were synthesized in evacuated sealed quartz ampoules at 850°C for 10 h. The amorphous thin films were deposited by the thermal evaporation of synthesized materials in vacuum.

The composition of thin films was studied by the Rutherford backscattering (RBS) spectroscopy of deuterons with energies E_d = 0.4 and 1 MeV at 135^0 scattering angle, by SEM JSM-6460LV(*JEOL*) with energy dispersive x-ray analyzer Inka-Sight (*Oxford*), X-ray fluorescence analysis (XRF), and Auger spectroscopy. Rigaku D/MAX 2500 with Cu $K\alpha$, λ=0.15418 nm was used for X-ray diffraction (XRD), and determination of phase compositions of the films.

The morphology of thin films was studied by AFM (NT-MDT SolverPro) and SEM (Carl-Zeiss NVision 40). Planar structures containing Al electrodes with fixed inter electrode distances (1, 5, 10 μm), and deposited upon them doped GST thin film were fabricated on oxidized c-Si substrates for investigation of temperature dependences of resistivity of thin films.

Differential scanning calorimetry (Shimadzu DSC-50) was used to study the thermal properties of the materials. Thin films were scraped off from the c-Si substrates with sapphire spatula. Portions of thin films powder were pressed and sealed in aluminum pans. Heating rate was 10 °C/min, maximum heating temperature was 630 °C, and high-purity nitrogen was used to provide an inert atmosphere.

The problem of determination of film content is connected with the overlap of the peaks for Sb and Te.

However, compositions of the films were estimated, and our results show that dopants are successfully incorporated into the deposited layers.

According to DSC measurements synthesized alloys had only one endopeak due to the melting of samples. A number of heat effects were revealed for the as-deposited films. Two first exopeaks in the ranges 140-190°C and 200-230°C were attributed to the transitions from amorphous to metastable *fcc* structure, and from *fcc* to the stable *hcp* phase, respectively. In general, addition of In, Ti, Sn, and Bi to $Ge_2Sb_2Te_5$ leads to the decrease of the amorphous to metastable *fcc* structure transition temperature, which decreases with the increase of dopant content. However, for high concentration of In, Ti, and Bi (3 wt.%) this transition temperature begin to increase.

In addition, endothermic peak in the temperature range 390-415°C was observed for $Ge_2Sb_2Te_5$ composition. With the following measurements the value of endopeak sharply increased. After the repeated DSC measurements endopeak in this temperature range appeared also for all doped materials and increased with the number of DSC measurements. However, kinetics of the endopeak is lower than that of the undoped $Ge_2Sb_2Te_5$.

The temperatures of this endothermic peaks are quite close for all investigated materials, which indicates on the similar nature of the processes leading to the appearance of these heat effects. The nature of this endopeaks is connected with the phase separation due to the diffusion of the mobile Te atoms to the grains boundaries, and melting of Ge-Te eutectic phase, which is supported by the XRD measurements. In this case, doping can block diffusion of the mobile Te atoms to the grain boundaries preventing phase separation, and increasing stability of the material.

According to the resistivity measurements amorphous to metastable *fcc* structure transition is accompanied by drastic decrease of resistivity. The low content of the dopants (up to 1 wt.%) leads to the increase of the resistivity of amorphous thi films, and the value of drop between the resistivities of amorphous and crystalline states, which is important for the reliable work of PCM cell. In addition, low content of the dopants except for Sn leads to the decrease of the phase transition temperature. Low content of Sn increased transformation temperature. Both of these effects can be attributed to the modification of bond energies and local atomic order. On the contrary, high content of dopants (3 wt.%) except for Sn increased transition temperature, while for Sn lowered it. This deviation for high content of dopants can be associated with phase separation, which is supported by DSC measurements.

Exponential temperature dependences of resistivity were established for all investigated thin films in the range from room temperature to the temperature of amorphous to crystalline state transition. This is typical for the amorphous GST, and is associated with the jumping mechanism of carrier transport. Meanwhile, the activation energy of the amorphous phase conductivity slightly increases, which can be attributed both to the lowering of the band gap width, and the shift of the Fermi level due to the increase of the valence band tail density of states.

According to SEM the drastic changes in the structure and morphology occurred in undoped samples above the transformation temperature from amorphous to crystalline state, which was accompanied by the unpredictable changes in resistivity. This is connected with the change of the film value with the phase transformation (about 8%), and can be slightly softened by the doping.

Thus, doping of $Ge_2Sb_2Te_5$ with In, Ti, Sn, and Bi impurities can significantly change thermal characteristics, phase transition temperature, electrophysical characteristics, and sufficiently improve stability of the material during thermal cycling. This is key issues for the fabrication of PCM cells with optimized parameters and increased reliability. However, the content of the dopant must be carefully determined.

O1-2: Metal nanolayer formation on crystal faces with unlike electric charge

V. Haiduchok, R. Krukovsky

Institute of materials, SCR "Carat" Lviv, Ukraine, E-mail addres: haiduchok@carat.lviv.ua

Thin metal film deposition on the surface of lithium niobate $LiNbO_3$ using vacuum deposition methods is one of the technological links in the process of manufacturing devices for acoustoelectronics, optoelectronics and acoustooptics, where the mentioned monocrystal is used as an active element [1]. That is the reason why investigating the structure and growth of these materials is of significant practical interest. Apart from lithium niobate crystals being ferroelectrics, they are also characterized by pyroelectric and piezoelectric properties [2]. Heating and/or deformation of monocrystal blocks of lithium niobate leads to accumulation of unlike electric charges on their faces, which are perpendicular to the crystallographic axis Z. During the process of metal deposition on the crystal using vacuum deposition methods, the crystal is preheated for enhancing adhesion to its surface. Due to this, the $LiNbO_3$ crystal faces, perpendicular to polarization vector, will have unlike electric charge. It should be expected that the processes of metal atom deposition and thin-film coating formation will pass differently depending on the charge sign of crystal surface, where deposition occurs.

The electric field induced effects on the metal film growth processes were described in the work [3]. The effects of the substrate treatment with electron beams during a film deposition process were investigated in [4,5]. It was determined that in case of electron bombardment of the wafer, an increase in nuclei concentration is observed, film growth uniformity is increased and its structure is improved.

However, the results stated in these works cannot be fully implemented to the case, when metal films are deposited on electrically charged surfaces of ferroelectric crystal, i.e. lithium niobate, as the surfaces under deposition may have both positive and negative charges.

Thus, the aim of this work was to investigate the metal layer surfaces deposited on lithium niobate block faces with unlike electric charge for determination of the optimal modes for vacuum deposition of high-quality metal coatings.

Metal film deposition on $LiNbO_3$ crystal surfaces, perpendicular to the crystallographic axis Z, was conducted using thermal and magnetron deposition methods with the help of a combined facility manufactured by TORR International (USA). Crystallographic orientation, lapping and polishing of the faces were conducted and the polarity was determined before deposition.

The morphology of the films deposited on lithium niobate faces of different polarity were investigated using Neophot 21 Optical Microscope, as well as Akashi DS 130C Scanning Electron Microscope and SOLVER P47-PRO Scanning Probe Microscope.

The start of the process of film growth on the crystal surface is predetermined by the energy barrier of nuclei creation, i.e. the necessity of forming a critical nucleus with high positive free energy ensuring its further growth and finally a solid coating creation. Electric charge presence on the substrate surface leads to the change in nucleus formation energy.

In the process of chrome evaporation there are some positive ions Cr^+, as well as its compounds CrO^+, CrN^+ present in the condensed vapour [6,7]. On reaching the negatively charged $LiNbO_3$ crystal surface positive ions tightly hold on its surface, and become nuclei formation centers. As a result, homogeneous metal films without visible bumps are formed on a negatively charged $LiNbO_3$ surface already at a thickness of ~ 2 nm .

On the lithium niobate crystal faces with a positive charge, chrome film had a bumped structure at 2 nm thickness This is, probably, connected with repulsion of positively charged ions of chrome and its compounds with relatively low kinetic energy from lithium niobate surface, and as a result with nuclei formation barrier increase.

Compared to thermal method, the concentration of positive ions in the pairs significantly increases at magnetron sputtering due to the peculiarity of a method, providing for chrome target bombardment, which is under the effect of electric and magnetic fields, with argon ions Ar^+. Using this deposition method it was possible to obtain the homogeneity of chrome films deposited on both negatively and positively charged faces of $LiNbO_3$ crystal even at a layer thickness of 2 nm .This may be connected with significantly higher velocity of the sputtered matter particles, compared to thermal sputtering. The increase in sputtered particle kinetic energy leads to the decrease in the value of nuclei formation barrier.

It was also found out that a tendency to bump structure formation increases at film deposition velocity decrease.

As a result of the conducted work, optimal conditions for chrome and copper film deposition on lithium niobate crystal faces with unlike polarity were determined. The received results may also be used for ohm contact deposition on certain semiconductor compounds A_3B_5.

1. Chopra K. L. Growth of thin metal films under applied electric field// *Appl. Phys. Letters.* − 1965.− N 7.− p. 140.

2. Lewis, B . & Campbell, D. S. Nucleation and initial-growth behavior of thin-film deposits *Vacuum Sci.Technol.*−1967− N4.− p.209–218.

3. Stirland D.J. Electron-bombardment-included changes in the growth and epitaxy of evaporated gold films// *Appl. Phys. Lett.*−1966−N8. p.326.

4. Gladkih N.T., Hotkevych V.I. Dispersed metal films. // K. Phys. Inst. 1972.

5. Pines B.Ya. Metal physics outlines. // Kharkiv, Kharkiv State Univ., 1961, 371 p.

6. Palatnik L.S., Obolyaninova O.A., Naboka M.N., Gladkih N.T., *AS USSR Letters, Metals,* #6 − 1972, p. 171- 176

7. Palatnik L.S., Obolyaninova O.A., Naboka M.N., Gladkih N.T., Hotkevych V.I. // *Crystallography,* vol.17, 1972. – p. 1222-1229

8. M. S. H. Zhao, D. A. Bonnell, and J. M. Vohs, *J. Vac. Sci. Technol.* 27, 1337 (2009).

O1-3: Deposition of HfO$_2$ gate dielectric in ALD processes and its properties

A. Miakonkikh, A. Rogozhin, K. Rudenko, and A. Orlikovsky

Institute of Physics and Technology, Russian Academy of Sciences, Moscow, Russia, miakonkikh@ftian.ru

In this paper the results of atomic layer deposition (ALD) of high-k dielectric (HfO$_2$) are presented. Subsequent ellipsometry measurements showed thickness uniformity of 1.5% over 100 mm wafer, and good wafer-to-wafer reproducibility. Optical constants of oxide were also measured and were shown to be in excellent agreement with reference values.

Decrease of the gate dielectric electrical thickness providing physical thickness which is enough for suppressing tunneling current lead to implementation of high-k metal oxides as the gate dielectric, for example HfO$_2$[1]. Homogeneity and electrical properties of these thin HfO$_2$ layers are of great importance for transistors qualities. Perspective FinFET transistors wll definitely need gate dielectric deposition technology with high degree of conformity. ALD allows to produce ultrathin films with atomic level control of film thickness, excellent conformal coverage.

The oxide layer was formed by ALD FlexAl system (Oxford Instruments) system. Woolam Co. M-2000x ellipsometer, and Keithley 4200 SCS were used for measurements and analysis.

The films were deposited in plasma assisted ALD process with TEMAH (Hf(N(C$_2$H$_5$)(CH$_3$))$_4$) as metal precursor and O$_2$ as non-metal plasma precursor. This process is truly self limited and hence process dependence on external parameters (stage temperature, duration of the process, pressure) is flat in wide interval. That provides "process window", in which stable and reproducible film properties can be achieved.

Ellipsometry of 47 nm thick hafnium oxide shows n=2.27 @ λ=280 nm and n=2.05 @ λ=500 nm which is in perfect agreement with the results of previous studies [2].

CV and IV characteristics of formed gate structures were measured. They are presented on fig. 1. Obtained capacitance values correspond to dielectric constant 25.2. Leakage current values obtained at gate voltage of 1V do not exceed 0.16A/cm^2.

Optical and electrical properties of non stoichiometric hafnium oxides produced with the process parameters outside of the "process window" were also studied.
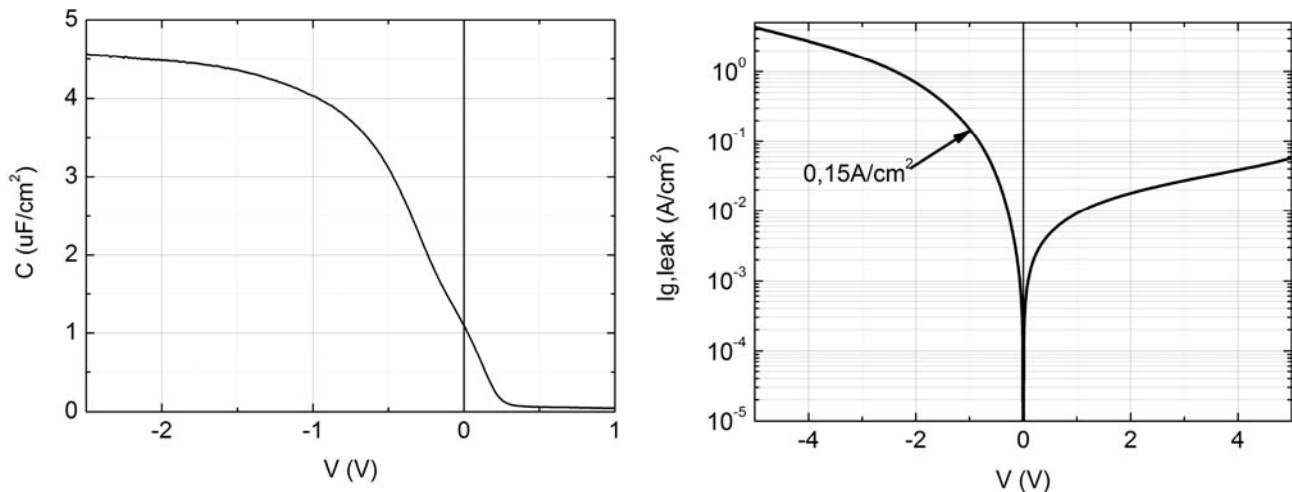
Fig. 1. CV and IV characteristics of formed gate structures.

1. J.H. Choi, Y. Mao, J.P. Chang, "Development of hafnium based high-k materials. A review", Materials Science and Engineering, **R 72**, 97–136, 2011
2. R. Rammula, J. Aarik, H. Mandar, P. Ritslaid, V. Sammelselg, "Atomic layer deposition of HfO2: Effect of structure development on growth rate, morphology and optical properties of thin films", Appl. Surf. Sci., **257**, 1043–1052, 2010

I2-1: Electrostatic interactions in nanoscale systems

Sahin Buyukdagli

Department of Applied Physics and COMP center of Excellence, Aalto University School of Science, P.O. Box 11000, FI-00076 Aalto, Espoo, Finland.

Electrostatic interactions are omnipresent in various nanoscale systems. These interactions regulate several biological phenomena, such as the stability of membrane assemblies and the ionic selectivity of biological nanopores. Electrostatic forces are also at the origin of important industrial applications, to name but a few, paint and ink making, water purification in artificial nanofiltration technology, and the conception of new generation energy storage devices. For several decades, these forces have been mainly modeled within mean-field level electrostatic formulations that neglect important ionic correlation and ion specific effects. The talk will focus on improving the current formulation of electrostatics by including these effects for a better understanding of the biological and industrial systems.

The first part of the talk will be devoted to a discussion of the electrostatic forces in these systems and their modeling within the classical formulation of electrostatics. Then, I will show the importance of correlation effects considered in extended theories on the ionic selectivity of artificial membrane nanopores used in water purification and desalination technology [1]. Namely, I will discuss the role played by the surface polarization (or image charge) effect and the surface charge in the ionic exclusion mechanism. It will be shown that in cylindrical ion channels, the same correlation effects lead to a new type of discontinuous phase transition from a good to a poor ionic conductor state [2,3]. The electrostatic mechanism behind this phase transition provides a natural and universal explanation for ionic current oscillations observed in biological and artificial membrane nanopores [4,5]. I will also explain the inclusion of finite ion-size into the current formulation of electrostatics, and the resulting excluded volume effects on the stability of macromolecules in water solvent [6,7].

The second part of the talk will focus on carbon based supercapacitors, which are efficient energy storage devices where electrostatic interactions bring the most important contribution to the structure of the double layer in the neighborhood of the electrode surface. The current state of the art in the theoretical modeling of these devices is based on the mean-field level Gouy-Chapman model that overestimate the experimental differential capacitance data by one order of magnitude. Indeed, this mean-field formulation neglects surface polarization effects and the electrostatic nature of solvent molecules. I will present a recent non-mean-field dipolar Poisson-Boltzmann formalism that overcomes these limitations and exhibits a good agreement with experimental capacitance data of carbon based materials, thus correcting the previous mean-field Gouy-Chapman theory by one order of magnitude [8]. I will conclude by presenting a brief summary of open questions in the field of charged heterogeneous fluids.

1. S. Buyukdagli, M. Manghi, and J. Palmeri, Phys. Rev. E 81, 041601 (2010).
2. S. Buyukdagli, M. Manghi, and J. Palmeri, Phys. Rev. Lett. 105, 158103 (2010).
3. S. Buyukdagli, M. Manghi, and J. Palmeri, J. Chem. Phys. 134 074706 (2011).
4. A.A. Lev et al., Proc. R. Soc. Lond. B 252, 187 (1993).
5. C.A. Pasternak et al., Colloids Surf. A 77, 119 (1993).
6. S. Buyukdagli, C.V. Achim and T. Ala-Nissila, J. Stat. Mech. P05033 (2011).
7. S. Buyukdagli, and T. Ala-Nissila, J. Chem. Phys. 136, 074901 (2012).
8. S. Buyukdagli, and T. Ala-Nissila, "*Dipolar depletion effect on the differential capacitance of carbon based materials*", arXiv:1203.2285v1

I2-2: Unifying model of driven polymer translocation

T. Ala-Nissila

Department of Applied Physics and COMP Center of Excellence, Aalto University School of Science, P.O. Box 11000, FI-00076 Aalto, Espoo, Finland and Department of Physics, Box 1843, Brown University, Providence, Rhode, Island, USA

Driven translocation of biopoymer chains through nanopores has been suggested as a fast and inexpensive way to sequence DNA molecules. To explain the dynamics of this process, we present a Brownian dynamics model, in which non-equilibrium memory effects arising from tension propagation (TP) along the cis side subchain are incorporated as a time-dependent friction. To solve the effective friction, we develop a finite chain length TP formalism, based on the idea suggested by Sakaue [Sakaue, PRE 76, 021803 (2007)]. We validate the model by numerical comparisons with high-accuracy molecular dynamics simulations, showing excellent agreement in a wide range of parameters. Our results show that the dynamics of driven translocation is dominated by the non-equilibrium TP along the cis side subchain. Furthermore, by solving the model for chain lengths up to 1010 monomers, we show that the chain lengths probed by experiments and simulations are typically orders of magnitude below the asymptotic scaling limit. This explains both the considerable scatter in the observed scaling of translocation time w.r.t. chain length, and some of the shortcomings of other present theories. Our study shows that for a quantitative theory of polymer translocation, explicit consideration of finite chain length effects is required.

I2-3: Self-organization of nanostructures in ultra-thin films

K. R. Elder[1], G. Rossi[2], P. Kanerva[2], F. Sanches[1], S-C Ying[3], E. Granato[3,4], C. Achim[2] and T. Ala-Nissila[2,3].

1. Department of Physics, Oakland University, Rochester MI, USA, elder@oakland.edu. 2. Aalto University School of Science, Espoo, Finland. 3. Brown University, Providence RI, USA. 4. Laboratorio Associado de Sensores e Materiais, Sao Jose dos Campos SP, Brazil.

Thin heteroepitaxial overlayers have been proposed as templates to generate stable, self-organized nanostructures at large length scales, with a variety of important technological applications. However, modeling strain-driven self-organization is a formidable challenge due to different length scales involved. In this talk a method for predicting the patterning of ultra thin films on micron length scales with atomic resolution will be presented. The model is used to make quantitative predictions for the type of superstructures (stripes, honeycomb, triangular) and length scale of pattern formation of two metal/metal systems, Cu on Ru(0001) and Cu on Pd(111). The findings are in excellent agreement with existing experiments and call for future experimental investigations of such systems.

O2-1: Detailed structure and transformations of grain boundaries in graphene

Ossi Lehtinen[1], Simon Kurasch[2], Jani Kotakoski[1,3], Viera Skákalová[4], Jurgen Smet[4], Carl E. Krill III[5], Arkady V. Krasheninnikov[1,6], and Ute Kaiser[2]

1.Department of Physics, University of Helsinki, P.O. Box 43, 00014 Helsinki, Finland 2.Central Facility for Electron Microscopy, Group of Electron Microscopy of Materials Science, Ulm University, 89081 Ulm, Germany 3.Department of Physics, University of Vienna, Boltzmanngasse 5, 1090 Wien, Austria 4.Max Planck Institute for Solid State Research, Heisenbergstr. 1, 70569 Stuttgart, Germany 5.Institute of Micro and Nanomaterials, Ulm University, Albert-Einstein-Allee 47, 89081 Ulm, Germany 6.Department of Applied Physics, Aalto University, P.O. Box 1100, 00076 Aalto, Finland

Graphene has been attracting ever increasing scientific attention due to its unique electrical and mechanical properties. The chemical vapor deposition technique can be nowadays used to grow large crystalline domains in the millimetre-range [1,2]. However, grain boundaries are present also in such samples and, more importantly, graphene samples with much smaller crystallite sizes can be grown. Further on, grain boundaries strongly affect the properties of polycrystalline materials in general and those of graphene spesifically.

Several works have been dedicated to the structure of graphene grain boundaries, but the detailed structure of grain boundaries observed in, e.g., high-resolution transmission electron microscope (HRTEM) experiments [3] often differs significantly from theoretical predictions [4].

In this work the gap between the experimental and theoretical observations is bridged by means of multiscale atomistic simulations and HRTEM experiments. A theoretical model is presented, which reproduces charasteristic features observed in real grain boundaries and predicts low energy transformation routes connecting different low-energy boundary configurations.

1. L. Gao, et al., *Repeated growth and bubbling transfer of graphene with millimetre-size single-crystal grains using platinum*, Nat. Commun. 3 (2012) 699

2. X. Li, et al., *Large-Area Graphene Single Crystals Grown by Low-Pressure Chemical Vapor Deposition of Methane on Copper*, J. Am. Chem. Soc. 133 (2011) 2816

3. P. Y. Huang, et al., *Grains and grain boundaries in single-layer graphene atomic patchwork quilts*, Nature 469 (2011) 389-392

4. O. V. Yazyev and S. G. Louie, *Topological defects in graphene: Dislocations and grain boundaries*, Phys. Rev. B. 81 (2010) 195420

O2-2: Controlling of the size and density of three-dimensional islands self-assembled in kinetic Monte Carlo simulations

F. F. Leal[1] , S. C. Ferreira[2] , S. O. Ferreira[2]

1. Instituto de Educação, Ciência e tecnologia Fluminense, Itaperuna, Rio de Janeiro, Brazil, ffleal.iff@gmail.com
2. Universidade Federal de Viçosa, Viçosa, Minas Gerais, Brazil.

The epitaxial growth of three-dimensional (3D) islands is of both scientific interest and technological importance. These structures grown of both elemental and compound semiconductor thin films have shown great use as quantum dots (QD). The usefulness of and other applications depends on how well their size distributions can be understood and controlled. However, to obtain a high density of QD with regular sizes is a challenge for industry. Fortunately, for some systems, these nanostructures can be obtained spontaneously by an epitaxial growth system by controlling of some parameters. There is a considerable number of systems but the majority of ones follow the Stranski-Krastanow (SK) growth mode characterized by the transition from the two-dimensional to three-dimensional growth regime. Commonly, in SK mode, the density of islands on substrate decreases whereas the size increases as the growth temperature.

In recent experiments, Ferreira et. al. showed that the growth of CdTe on Si(111) substrates by hot wall epitaxy (HWE) follows the Volmer-Weber (VW) growth mode, with nucleation of self-organized CdTe 3D islands on the Si substrate for less than 1 monolayer of evaporated material [1]. In contrast, in this system the density of islands increases whereas the size decreases as the growth temperature.

Computational solid-on-solid models are useful tools for the understanding of the film growth dynamics. Therefore, we are proposing a thermally activated model for the growth of the CdTe/Si system, in which a two-dimensional triangular lattice with periodic boundary conditions represents the Si substrate. The one dimension version of the model was recently studied [2,3]. Deposition and diffusion processes are included in the model. In addition, Ehrlich-Schoebel (ES) barriers were included in the present work. While deposition occurs at constant rates, Arrhenius-like law rule diffusion. An important ingredient of the model is the difference between energies for diffusion of CdTe particles on Si and CdTe on previously deposited CdTe, but the main ingredient is an ES barrier heuristically dependent on growth temperature. For such procedure are considered both bond and activation energies, also ES barrier. The model was studied through kinetic Monte Carlo simulations in which, the system size, the growth time and growth temperature are the parameters of the simulation. Size distributions and density (number of dots/area) of the CdTe islands were used to characterize the self-assembled structures and to compare the simulation results with the experimental finds. Distributions for size of the QD were obtained in agreement qualitative with experimental observations. This model is able to reproduce as the SK typical results as that VW presented [1]. Indeed, the two-dimensional version of model has a better quantitative agreement with experiments if compared with the one-dimensional case. Recently, this model (with some variations) has been able to study mounding instability [4,5].

1. S. O. Ferreira et.al., "Characterization of CdTe quantum dots grown on Si(111) by hot wall epitaxy.", J. Appl. Phys., 93, pp.1195-1198, 2003
2. S. C. Ferreira and S. O. Ferreira, "A one-dimensional model for the growth of CdTe quantum dots on Si substrates.", Phys. Lett. A, 352, pp.216-221, 2006
3. S. O. Ferreira and S. C. Ferreira, "Volmer-Weber growth of CdTe on silicon: a one-dimension Monte Carlo model.", Braz. J. Phys., 36, pp.294-297, 2006
4. F. F. Leal, S. C. Ferreira, S. O. Ferreira, "Modelling of epitaxial film growth with an Ehrlich Schwoebel barrier dependent on the step height.", J. Phys.: Condens. Matter, 23, pp. 292201, 2011.
5. F. F. Leal, T. J. Oliveira, S. C. Ferreira, "Kinetic modelling of epitaxial film growth with up- and downward step barriers.", J. Stat. Mech., v. 2011, p. P09018, 2011.

O2-3: Modeling the evolution of the surface profile of materials at low-energy ion sputtering

A.S.Shumilov, I.I.Amirov

Yaroslavl branch of the Institute за Physics and Technology of Russian Academy of Science, Yaroslavl, Russia.
ashumilov@inbox.ru

Modeling of the surface profile for the low-energy ion sputtering of materials for which there is a formation of nano-and microstructures, or vice versa, smoothing irregularities, it is necessary to understand the surface processes which responsible for changes in its morphology. The developed method of dynamic Monte Carlo method [1-3] allows us to explore the atomic scale mechanisms of nucleation of nanostructures, the evolution of the surface profile of materials by ion sputtering. However, in the framework of this method is impossible to simulate the processes of formation of high aspect ratio nanostructures when become important the redeposition of sputtered atoms. The aim of this work was to develop a method of two-dimensional simulation of the surface profile of materials at low-energy ion sputtering processes, taking into account redeposition.

The developed method is based on the cellular method of representation of the surface profile and the Monte Carlo method to simulate the ion transport to the surface. Method uses special algorithms to calculate the surface normal for accurate determination of the ion's strike angle and the emission angle of sputtered atoms. Based on the specified functions of sputtering probability of atoms from the ion's energy and incidence angle, the atomic balance in the cells is calculated. Sputtered atoms of material are redeposited on the surface with a given sticking probability.

In this work we simulated the sputtering of wave-like and triangular -like profile nanostructures on silicon surface by low energy argon ions (E_i <200 eV). The sputtering rate depends of the ion's energy and the type of ion's incident angle-dependent sputtering probability function (Fig. 1a, b). It is shown that under typical conditions for ion-plasma sputtering, surface irregularities are smoothed.
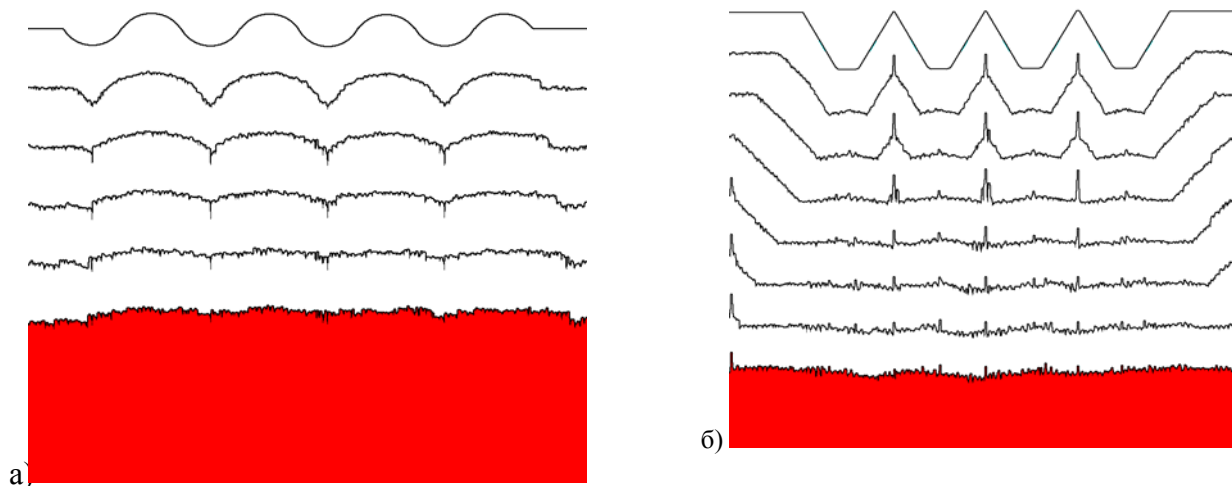
Fig. 1. Simulation of a sputtering a) - wave-like surface of Si and b) - the triangular –like profile of Si nanostructures with period of 100 nm with different ion's incident angle-dependent sputtering probability functions.

1. W.L. Chana_ and E. Chason, Making waves: Kinetic processes controlling surface evolution during low energy ion sputtering, J. Appl. Phys., 101, pp.121301, 2007
2. Y. Ishii, W.L. Chan, E. Chason. Kinetic Monte Carlo simulation of ripple formation by sputtering: Effects of multiple defects and Ehrlich–Schwoebel barriers, Nuclear Instruments Methods in Phys. Res., B 272, pp.188–192, 2012
3. M. S. Bharathi, H. Ramanarayan, and Y. W. Zhang. Pattern formation and nonlinear evolution in alloy surfaces by ion-beam sputtering, Appl. Phys. Lett. 99, p.083103 2011

I2-4: Electric-field control of magnetic domain wall motion and local magnetization reversal in multiferroic heterostructures

Sebastiaan van Dijken

NanoSpin, Department of Applied Physics, Aalto University School of Science, P.O. Box 15100, FI-00076 Aalto, Finland E-mail: sebastiaan.van.dijken@aalto.fi

Spintronic devices currently rely on magnetic switching or controlled motion of domain walls by an external magnetic field or spin-polarized current. Achieving the same degree of magnetic controllability using an electric field has potential advantages including enhanced functionality and low power consumption. Here, an approach to electrically control local magnetic properties, including the writing and erasure of regular ferromagnetic domain patterns and the motion of magnetic domain walls, will be discussed. The method is based on recurrent strain transfer from ferroelastic 90º stripe domains in ferroelectric $BaTiO_3$ substrates to continuous magnetostrictive CoFe films with negligible magnetocrystalline anisotropy. The dominance of magnetoelastic anisotropy in these multiferroic heterostructures causes full imprinting of the ferroelectric domain pattern into the ferromagnetic counterpart and strong pinning of magnetic domain walls onto narrow ferroelastic boundaries in the as-deposited state [1,2]. Optical polarization microscopy of both the ferroelectric and ferromagnetic domain structures reveals that domain correlations and strong inter-ferroic domain wall pinning are maintained in an applied electric field [3]. This leads to unprecedented electric-field control over the formation of ferromagnetic domains and lateral motion of magnetic domain walls, an accomplishment that opens the way to electric-field driven spintronics.

The sequence of images in Fig. 1 illustrates the writing of ferromagnetic stripe patterns during the application of an out-of-plane bias voltage across the $BaTiO_3$ substrate. We note that no magnetic field is applied during these room temperature measurements. The micromagnetic response to the applied electric field is induced by a gradual increase of ferroelectric domains with out-of-plane polarization at the expense of in-plane domains, i.e. by lateral ferroelectric domain wall motion. As a result, the strain states in the overlaying CoFe film change locally and this results in the writing (or erasure) of growth induced ferromagnetic domains via inverse magnetostriction. The electric-field controlled magnetic writing process is reversible.

Another intriguing observation is electric-field control of magnetic domain wall motion. Two different types of magnetic domain walls form in our samples as shown in Fig. 2(a). The walls labeled by (1) and (2) are strongly pinned at locations where the local magnetoelastic anisotropy abruptly changes in strength or rotates by 90º. Strong pinning of magnetic domain walls onto 90º ferroelastic domain boundaries is also confirmed by micromagnetic simulations (Fig. 2(b)). From these simulations, the spin rotation within the domain wall and the pinning energy are extracted. As illustrated in Fig. 2(c) and 2(d), the pinning energy profile provides an ever increasing barrier for lateral wall displacement which cannot be overcome by thermal activation. Pinning of magnetic domain walls onto ferroelastic boundaries is therefore robust and the strong link between both ferroic domain walls is only broken if one of the walls is destroyed by ferromagnetic or ferroelectric saturation. These results thus demonstrate the possibility to accurately control the position of magnetic domain walls by sideways motion of ferroelastic boundaries in an applied electric field.

1. T.H.E. Lahtinen, J.O. Tuomi, and S. van Dijken, Adv. Mater. 23, 3187 (2011)
2. T.H.E. Lahtinen, J.O. Tuomi, and S. van Dijken, IEEE Trans. Magn. 47, 3768 (2011)
3. T.H.E. Lahtinen, K.J.A. Franke, and S. van Dijken, Nature Scientific Reports 2, 258 (2012)
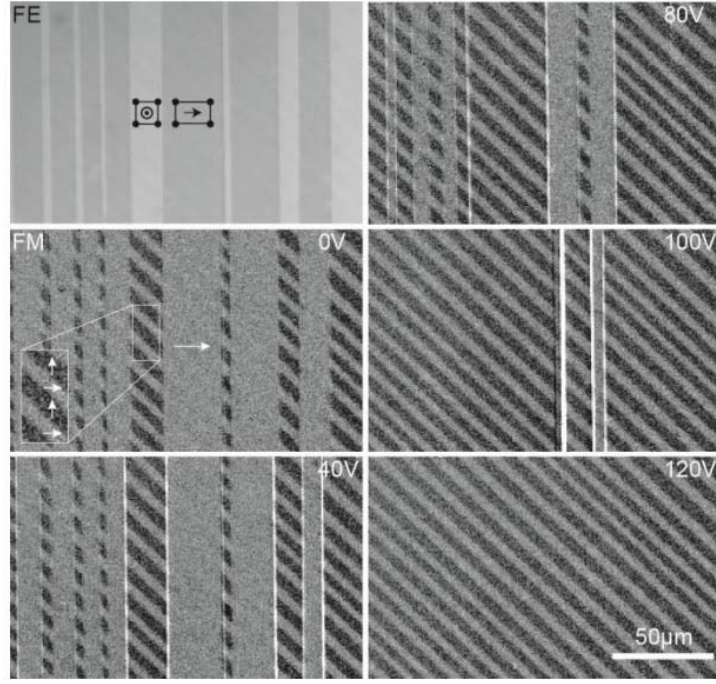
Figure 1: Polarization microscopy images of the ferroelectric (FE) and ferromagnetic (FM) domain structure during the application of an out-of-plane bias voltage across the BaTiO$_3$ substrate. In this experiment, the CoFe film is used as top electrode and conducting silver paint on the back of the substrate is used as bottom electrode. The BaTiO$_3$ substrate is 0.5 mm thick.
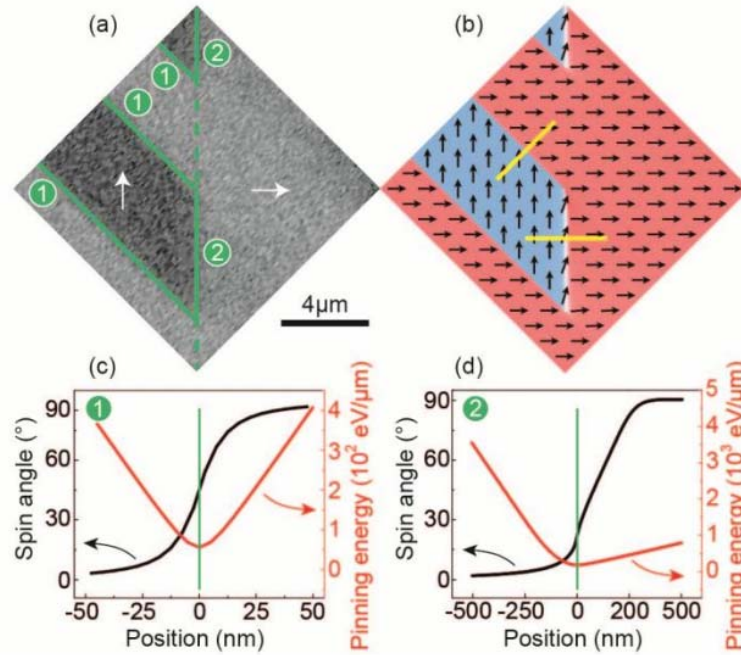
Figure 2: (a) Polarization microscopy image of the ferromagnetic domain structure on top of out-of-plane (left) and in-plane (right) ferroelectric domains. (b) Micromagnetic simulation of the magnetic microstructure. (c) and (d) Spin rotation within the magnetic domain walls and pinning energies indicating strong clamping of magnetic domain walls onto ferroelastic domain boundaries.

O2-4: New magnetic and magnetoelectric phenomena in tetrahedron single molecule magnets

V.V. Kostyuchenko

Institute of Physics and Technology RAS, Yaroslavl Branch, Universitetskaya 21, Yaroslavl, 150007, Russia,
vkqubit@mail.ru

The experimental observations of amazing properties of single molecule magnet Ni_4Mo_{12} have stimulated the appearance of present theoretical work. The core of single molecule magnet Ni_4Mo_{12} contains four ions Ni^{2+} (*S=1*) placed in the vertexes of a tetrahedron. Ligands form isolating shells that encapsulate the magnetic core. Thus the interaction between magnetic ions located in different molecules is small. The spin structure of Ni_4Mo_{12} looks rather simple. But the theoretical interpretation of magnetic properties Ni_4Mo_{12} is not a simple problem. The proper choice of spin Hamiltonian remains unclear despite intense discussions during several years [1-4].

At the present time two models can more or less describe the magnetic properties of Ni_4Mo_{12}. The first one [2] is based on assumption of essential role of non-Heisenberg exchange interactions in spin tetrahedron (biquadratic and three-spin). The second one [4] comprises two assumptions, strong violation of symmetry of exchange interactions, and strong single-ion anisotropy.

The present work is devoted to the theoretical analysis of both these models. The attention is focused on the forecasting power of these spin models. Mechanism responsible for non-Heisenberg exchange interactions is the same as mechanism resulting in interaction of spin chirality with external magnetic field. As an example, additional level splitting in magnetic field can be observed in the case of model [2]. In the case of model [4] quite different phenomena are expected. The violation of symmetry of exchange interactions inevitably leads to nonzero toroidal moment of the ground state. This effect can be observed via set of magnetoelectric phenomena.

Thus the experimental investigation of spin chirality Ni_4Mo_{12} and magnetoelectric phenomena can play a crucial role in defining the character of the magnetic interactions in Ni_4Mo_{12}. It allows us to obtain a decisive support for one of the two spin models, or reject both models.

1. J. Schnack, M. Bruger, M. Luban, P. Kogerler, E. Morosan, R. Fuchs, R. Modler, H. Nojiri, R. C. Rai, J. Cao, J. L. Musfeldt, X. Wei, Phys. Rev. B, "Observation of field-dependent magnetic parameters in the magnetic molecule {Ni4Mo12}", 73, 094401, 2006

2. V.V. Kostyuchenko, "Non-Heisenberg exchange interactions in the molecular magnet Ni4Mo12", Phys. Rev. B, 76, 212404, 2007

3. J. Nehrkorn, M. Hock, M. Bruger, H. Mutka, J. Schnack, O. Waldmann, "Inelastic neutron scattering study and Hubbard model description of the antiferromagnetic tetrahedral molecule Ni4Mo12", Euro. Phys. J. B, 73, pp. 515-526, 2010

4. A. Furrer, K. Kramer, T. Strassle, D. Biner, J. Hauser, H. Gudel, "Magnetic and neutron spectroscopic properties of the tetrameric nickel compound [Mo12O28(м2-OH)9(м3-OH)3{Ni(H2O)3}4]·13H2O", Phys. Rev. B, 81, 214437, 2010

O2-5: Mössbauer study of magnetite nanoparticles surface

M. Shipilin[1], V. Alekseev[1], V. Bachurin[1], I. Zakharova[2], A. Shipilin[3]

1. Yaroslavl State University named after P.G. Demidov, Yaroslavl, Russia, E-mail: ship.yar@gmail.com;
2. Yaroslavl State Technical University, Yaroslavl, Russia;
3. Moscow State University named after M.V. Lomonosov, Moscow, Russia, E-mail: amship@mail.ru.

The study of highly dispersed iron-containing materials including nanomagnetic Fe_3O_4 (magnetite) has reached the new level nowadays. The distinguishing feature of nanoparticles is the considerable volume of their surface area comparable with the whole volume of the particle. In case of magnetic sample, magnetic properties of nanoparticle's surface can greatly differ from the bulk properties. Mössbauer spectroscopy allows to get the local information about the state of ions and hence about the magnetic properties and structure of nanoparticle as a whole and its surface area as a great part.

Magnetite has the spinel crystal structure with two nonequivalent crystalline positions tetrahedral A-places and octahedral B-places occupied by divalent and trivalent iron ions. In case of massive sample with particles size ~ 1 mkm Mössbauer spectrum has the standard appearance and includes two sextets corresponding to two different magnetic states of iron ions: divalent and trivalent iron ions in B-places where the Verwey transition takes place above 118K and trivalent iron ions in A-places [1]. The values of effective magnetic field H_n on ^{57}Fe nuclei for these ions are ≈ 459 kOe and ≈ 489 kOe respectively.

a) $d_p = 45$ nm
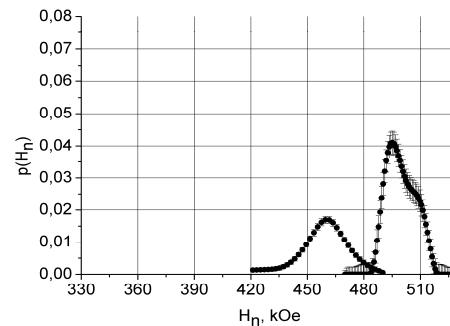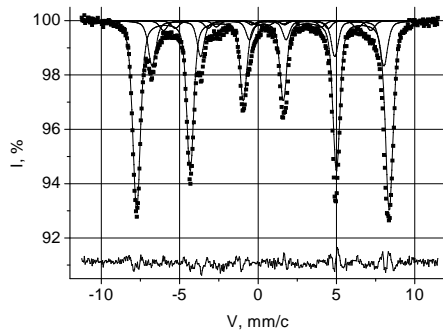
b) $d_p = 24$ nm
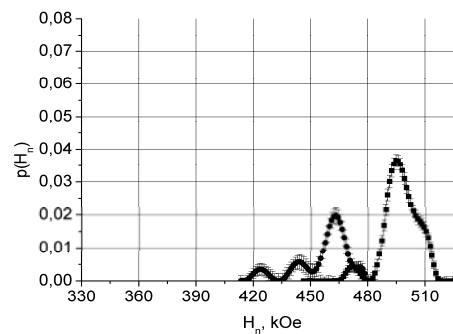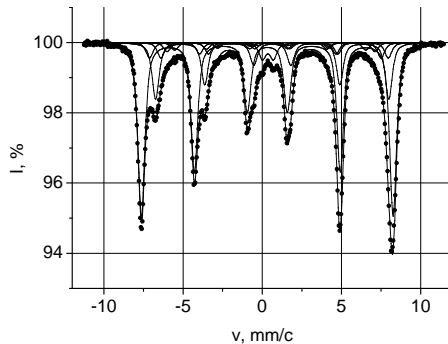
c) $d_p = 7.5$ nm
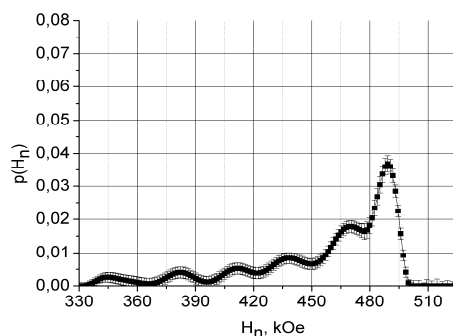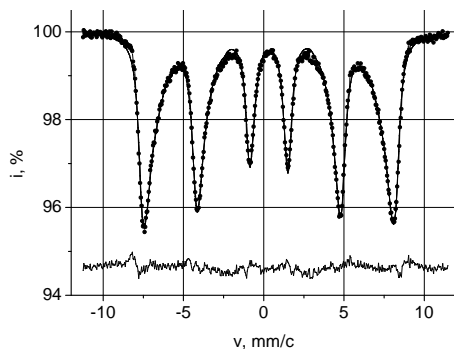
Fig. 1. Mössbauer spectra of magnetite samples with different particle size d_p (left column) and corresponding distribution functions of effective magnetic fields on ^{57}Fe nuclei (right column)

For 45 nm magnetite particles the distribution function of effective magnetic fields H_n on ^{57}Fe nuclei (*fig.1.a right*) obtained on the base of Mössbauer data (*fig.1.a left*) by means of MS Tools Software package [2] represents three maxima that is most probably due to termination of Verwey transition. Reference data [3] exhibits that characteristic temperature of Verwey transition (118K for massive particles of magnetite) increases with the decrease of particles size and reaches the value of room temperature for 20 nm particles. In our experiment this phenomenon is observed for particles with size less than 45 nm. Besides it with the decrease of particles size down to 24 nm and then to 7.5 nm the additional maxima of distribution function (*fig.1.b,c.right*) in lower magnetic fields diapason appear.

The comparison of characteristic values of Mössbauer spectra exhibits the following. For the spectra of studied nanoparticles systems there are contributions to the effective magnetic fields H_n that are almost equal to the same values for massive samples. These contributions apparently correspond to the iron ions in the internal area of nanoparticles that are in the same state as in the bulk material. Besides it there are contributions with lower values of effective magnetic fields. Increasing of intensities of corresponding Mössbauer lines with the decrease of particles size and the fact that corresponding values of δ and ε are higher than the same values for the bulk material allow to link these contributions with the surface layer of nanoparticles with iron ions that are deprived of exchange bonds. In simple terms this surface layer can be divided into two parts: surface cations (1) deprived of half of magnetoactive neighbouring ions and the next layer of cations (2) that are in the state different of internal area. The increase of corresponding values of δ and ε is in agreement with modern conception of considerable distortion of crystal structure of nanoparticles surface layer.

The mentioned decrease of H_n conforms by order of magnitude with the values obtained by method of molecular orbitals for ideal crystal lattice of ferrit-spinel: the absence or substitution of magnetic cation in A-place with nonmagnetic leads to the decrease of effective magnetic field on ^{57}Fe nucleus in B-place on ~ 12 kOe. Similar estimation for A-place – ~ 8 kOe.

1. I.P. Suzdalev, *Dynamic Effects in Gamma-Resonance Spectroscopy*. Atomizdat, Moscow, 1979.
2. V.I. Nikolaev, V.S. Rusakov, Mössbauer studies of ferrites. Moscow State University publishing, Moscow, 1985.
3. I.P. Suzdalev, V.N. Buravcev, U.V. Maksimov, A.N. Nikolaev, "Electric and magnetic first order phase transitions in nanostructures", Russian nanotechnologies, Vol. 6, Is. 1-2, pp. 105-108., 2011.

O2-6: Fabrication of InGaAs/GaAs light-emitting diodes with GaMnSb and GaMnAs ferromagnetic injector layer

M.V. Dorokhin, Yu.A. Danilov, A.V. Kudrin, E.I. Malysheva, M.M. Prokof'eva, B.N. Zvonkov

Physico-Technical Research Institute of Nizhny Novgorod State University, Nizhny Novgorod, Russia,

E-mail: dorokhin@nifti.unn.ru

The fabrication of light-emitting diodes (LEDs) that include the option for spin injection and circularly polarized light emission is a subject of strong interest [1-3]. The basic elements of such LEDs are a ferromagnetic layer that provides injection of spin-polarized carriers into a semiconductor and an active region where spin polarized carriers recombine with the emission of circularly polarized light. For last 10 years great success has been made in fabrication of such LEDs with the variety of ferromagnetic injectors and active regions [2,3]. Despite this only few types of injectors [1] fit the conditions set for an efficient device: room temperature ferromagnetism, high spin injection efficiency. For that reason much effort is being made to the appropriate selection and insertion of a ferromagnetic (FM) injector layer. The set of the prospective materials is $(A^3,Mn)B^5$ diluted magnetic semiconductors which are compatible with GaAs based LEDs and which have proven to provide efficient spin injection [1-3]. In the present paper we have investigated light-emitting diodes based on InGaAs/GaAs quantum well (QW) heterostructures with ferromagnetic GaMnSb or GaMnAs injection layer. Our early studies have proven that both are the prospective ferromagnetic materials with Curie temperature above 300 K for GaMnSb and about 40 K for GaMnAs. The main advantage of GaMnAs is a better ferromagnetic layer/GaAs interface quality [2].

Investigated samples were fabricated by means of two-stage epitaxial growth technique. At the first stage a 0.5 μm buffer GaAs:Si ($n \sim 10^{17}$ cm^{-3}) layer, In$_x$Ga$_{1-x}$As (width $d_{QW} = 10$ nm, In content $x \approx 0.16$) quantum well (QW) and 30 nm undoped GaAs spacer layer were grown subsequently on n-GaAs (100) substrates at 600°C by means of metal-organic chemical vapor deposition. At the next stage ferromagnetic GaMnSb (GaMnAs) layer was grown by sputtering of Mn and GaSb (GaAs) targets with pulse Nd:YAG laser. Finally 6 nm undoped GaSb (GaAs) layer was grown on sample surface to prevent oxidation of a ferromagnetic semiconductor. Growth temperature was lowered to 400°C, it allowed to decrease Mn diffusion into GaAs. The Mn content was established by the ratio between sputtering time of Mn and GaSb (GaAs) (Q_{Mn}). Two types of samples was studied in the present work: 1) sample#1: GaMnSb layer with the thickness of 10 nm and 2) GaMnAs layer with the same thickness.

To investigate magnetic properties of GaMnSb films anomalous Hall effect measurements were carried out. In this case Van Der Paw type ohmic contacts were made on the samples surface. The current between contacts flows only in GaMnSb(As) and is affected only by its properties provided there is no alloying of ohmic contacts into GaAs. Light-emitting diode fabrication started from the thermal vacuum deposition of Au contact on samples surface. Back ohmic contact was fabricated by means of sparkling of Sn foil. Finally photolitography and etching was applied to form 500 μm mesa structures. The properties of fabricated diodes were tested via measurements of forward bias electroluminescence (EL) in 10-120 K temperature range. The magnetic field $B = 0 - 0.4$ T was applied normal to the QW plane. The degree of circular polarization (CP) of the EL was evaluated with the equation: $P_C = (I^+ - I^-)/(I^+ + I^-)$, where $I^+()$ are the intensities of the left (right)-hand polarized QW emission spectrum.

Experimental results. The electric measurements taken at 10 K revealed that both GaMnSb and GaMnAs films are p-type conductivity, which is because Mn acts as an acceptor in A3B5. Sample#1 demonstrates nonlinear dependence $R_H(B)$ with hysteresis loop. Such behavior is the evidence of FM properties of GaMnSb, it reflects the magnetic field dependence of GaMnSb film magnetization. In the sample#2 the anomalous Hall effect could not be measured because of the large magnetoresistance between Van Der Paw contacts. However the negative magnetoresistance may as well be the evidence of ferromagnetic properties of the GaMnAs layer. Ferromagnetic properties vanish at about 300 K for the sample#1 and 40 K for the sample#2, evidencing that the Curie temperature of fabricated GaMnSb layer is much higher than that of GaMnAs. That is not typical for GaMnSb layer fabricated by the molecular beam epitaxy technique [4].

The forward bias electroluminescence spectra of the samples (not shown) contain the peak at 1.378 eV corresponding to radiative transitions in the QW with above-mentioned parameters. The EL intensity of sample#2 is about 100 times higher than that of sample#1 that is probably due to better interface quality of GaMnAs/GaAs in comparison with GaMnSb/GaAs. In the magnetic field the EL of sample#1 becomes

circularly polarized (fig.1b), i.e. the intensity of left circular polarized component becomes higher than right circular polarized one. The degree of polarization is much higher than that of reference samples containing no FM layers. The circular polarization degree dependence in the magnetic field can be approximated by a linear function. The effect is observed up to 90 K. The circular polarization of the EL is the evidence of an injection of spin polarized holes from the ferromagnetic GaMnSb layer into the semiconductor.
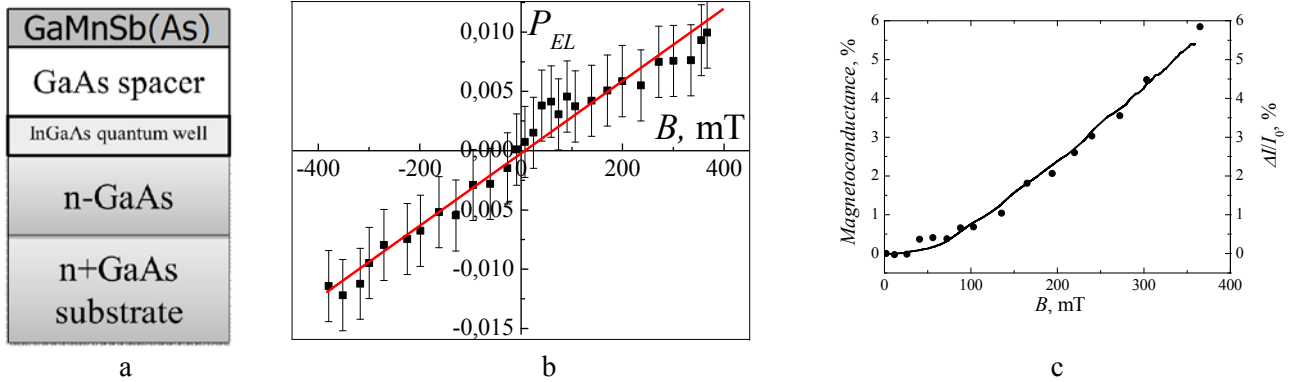
Fig.1. a. The schematics of the diodes; b. Dependence of circular polarization degree on the magnetic field for sample #1; c. Dependence of magnetoconductance (curve) and relative change of the EL intensity (dots) on the magnetic field. Measurement temperature = 10 K.

In our measurements the magnetic field is applied perpendicular to the easy magnetization axis of a GaMnSb, thus the saturation of magnetization occurs at rather high field of about 2 T [5]. In the investigated range of fields (0 – 0.4 T) one would expect nearly linear dependence of $P_c(B)$. In other words the picture observed at fig.1a is in a good agreement with the results obtained for similar samples [5].

The application the magnetic field in the same geometry to the sample#2 leads to a increase of the diodes series conductance by about 5 %. The dependence of magnetoconductance on the magnetic field is shown at fig.1c (curve). This effect takes place because the carriers transport through a GaMnAs layer is affected by spin-dependent scattering. The scattering decreases with the increase of a magnetic field aligning magnetization on GaMnAs. In the voltage source mode the decrease of the diode resistance leads to the increase of a diode current in the magnetic field which in turn leads to the increase of the EL intensity (fig.1c dots). As can be seen in the magnetic field of 0.4 T the EL intensity increases by 5 %. The magnetic field dependence of EL intensity is in qualitative agreement with the magnetic field dependence of magnetoconductance. The effect is observed up to the temperature of 40 K which is the Curie temperature for (Ga,Mn)As. The reference non-magnetic sample revealed neither conductance dependence on B nor EL increase effect.

Thus we have investigated the light-emitting diodes based on InGaAs/GaAs heterostructures with GaMnSb/GaAs or GaMnAs/GaAs ferromagnetic contact. It has been demonstrated that GaMnSb/GaAs diode reveals circularly polarized EL which is due to the spin injection of holes from GaMnSb into the QW. The GaMnAs/GaAs diode revealed the effect of magnetic field controlled EL intensity. Although the operating temperature is higher for the sample#1, GaMnAs sample reveals higher EL intensity and bigger value of magnetic field controlled effect.

1. M Holub, P Bhattacharya, "Spin-polarized light-emitting diodes and lasers" J. Phys. D: Appl. Phys. **40**, p.R179-R203, 2007.
2. Y. Ohno, D.K. Young, B. Beschoten, "Electrical spin injection in a ferromagnetic semiconductor heterostructure" et.al., Nature, **402**, pp.790-792, 1999.
3. R.P. Borges, C.L. Dennis, J.F. Gregg, et. al., "Comparative study of spin injection into metals and semiconductors" J. Phys. D:Appl. Phys., **35**, pp.186-191, 2002.
4. M. Ramsteiner, H. Y. Hao, A. Kawaharazuka, et. al. "Electrical spin injection from ferromagnetic MnAs metal layers into GaAs", Phys. Rev. B, **66**, p.081304(R), 2002.
5. Y. Nishitani, M.Endo, F.Matsukura , H.Ohno "Magnetic anisotropy in a ferromagnetic (Ga,Mn)Sb thin film", Physica E, **42**, pp.2681–2684, 2010.

O2-7: The conductivity of DNA molecules

T.I. Sharipov, F.F. Nafikov, R.Z. Bakhtizin

Bashkir State University, Ufa, Russia, sha-t@yandex.ru

Last years interest to processes of charge transport in DNA molecules has considerably increased. That is connected with the prospects of their use in nanoelectronic devices. The attempts to measure electric resistance of DNA resulted in contradictory conclusions: the molecule can show properties of a dielectric [1], a semiconductor [2], a metal [3] and even a superconductor [4]. The reasons of such ambiguity of results is complexity of the DNA molecule structure, and also uncertainty in treatment of experimental results.

There are two most often used methods for conductivity research of the DNA molecule. In the first case the isolated DNA molecule is placed between two electric contacts. The distance between electrodes should be small (about 1-10 nm), but sufficient enough to interfere with tunneling of charges. Such experiment is rather hard to carry out and particularly difficult to control.

The second approach to measurement of conductivity of individual molecules is based on the use of a scanning tunneling microscope (STM) [5]. The very first experiments with the use of STM have shown that it is the most suitable tool for researches of both single DNA molecules and molecules in monolayer films. However, running of qualitative and unambiguous experiments on measurement of charge transport through a single molecule by means of STM is extremely difficult, and interpretation of the received results appears even more difficult.

After a series of STM images receiving and identification of the DNA molecules on these images, the current-voltage curves of the DNA molecules have been measured (Fig. 1).
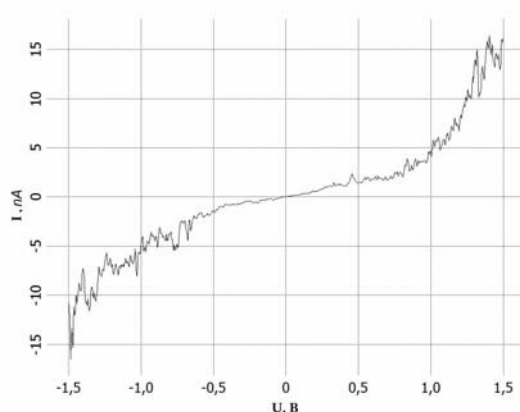
Fig. 1. Current-voltage curve of the DNA molecules.

The current-voltage curve has shown a symmetric appearance concerning zero values. The kind of curve is nonlinear. On sites of the current-voltage curve with the pronounced manifestation of nonlinearity, the growth of a tunnel current dispersion of fluctuations has been observed.

1. Brauns E B, Madaras M L, Coleman R S, Murphy C J, and Berg M A, J. Am. Chem. Soc., 121, p.11644, 1999;
2. Porath D, Bezryadin A, Vries S De and Dekker C, Nature London, 403 p.635, 2000;
3. H.W. Fink and C. Schonenberger, Nature, 398, p.407, 1999;
4. Kasumov A Y, Kociak M, Gueron S, Reulet B, Volkov V T, Klinov D V, and Bouchiat H, Science, 291 p.280, 2001;
5. H. Cohen, C. Nogues, R. Naaman, D. Porath, Direct measurement of electrical transport through single DNA molecules of complex sequence, PNAS, v. 102, № 33, pp. 11589-11593, 2005.

O2-8: Electron transport in relaxed high doping transistor Si/Si$_{1-x-y}$Ge$_x$C$_y$ heterostructures

M.L. Orlov[1], V.N. Neverov[2] , N.L.Ivina[3], Yu.A.Nozdrin[1], A.A.Melnikova[4], L.K.Orlov[1]

1.Institute for Physics of Microstructures, Russian Academy of Sciences, N.Novgorod,   orlov@ipm.sci-nnov.ru
2.Institute of Metal Physics of the Ural Branch of the Russian Academy of Sciences, Ekaterinburg,
3.Nizhny Novgorod Management Institute,   4. Nizhny Novgorod State Alexeev University, Russia,

Increasing the doping level of Si/Si$_{1-x}$Ge$_x$ transistor heterocompositions often leads to the exhibition of specific features in the behavior of their transport characteristics associated with both the fundamental properties of two-dimensional electron subsystem [1], and with quite a noticeable influence of the free carriers charge to the form of the quantum well potential and barrier layers adjacent to it. This fact was the main motivating factor for discussion in the present work of the dependencies observed in the magnetotransport experiments using partially relaxed Si$_{1-x}$Ge$_x$/Si/Si$_{1-x}$Ge$_x$ transistor heterostructures. Samples of the two-dimensional silicon transport channel thickness of about 10 nm [2] were characterized by the value of the surface electron density which is higher than n$_{cr}$ = 10^{12} cm^{-2}. The typical form observed in the samples the magnetic-field dependence in high magnetic fields up to 10T at liquid helium temperature is shown in Figure 1. In these structures with a high doping level of the formation of a narrow potential barrier in the vicinity of one of the heterojunction enhances the probability of the interlayer charge transport, which in some cases, a noticeable effect on the transport characteristics of the system [3]. We can assume that observed in our experiments, the scatter of points on the measured dependences of magnetotransport is also associated with the specifics of the potential distribution in the layers of the investigated heterostructures, deter an effective transfer of electrons between the parallel transport channels of the system.
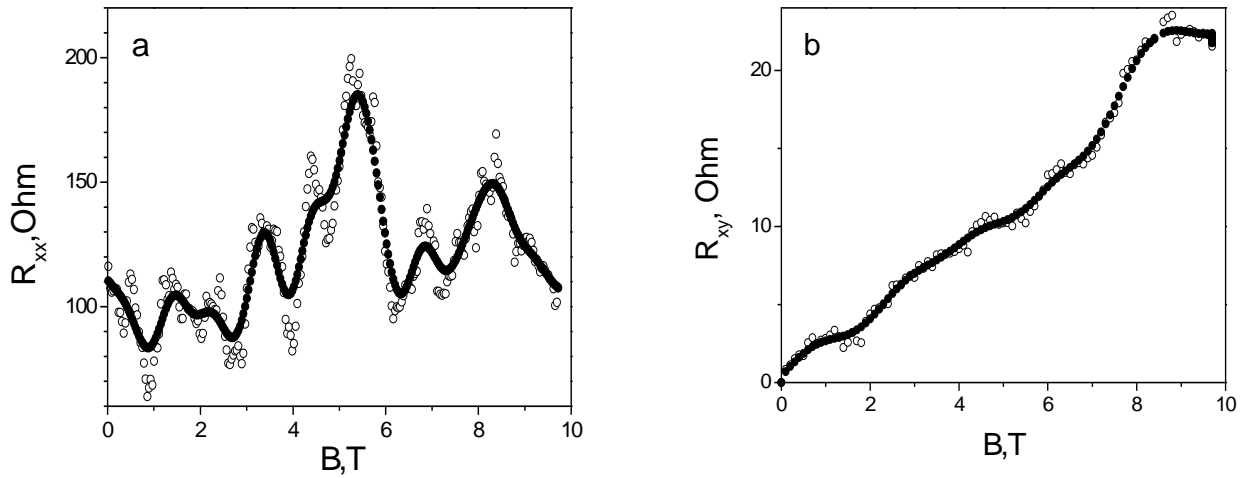
Fig. 1. Magnetoresistance (a) and Hall (b) characteristics of the structure 414 in a magnetic field. Open symbols - experimental data, averaged over 10 neighboring points. The lines in the figures obtained by smoothing the averaged data using the FFT (10) procedure

To better understand the observed patterns of our samples with the different character of the elastic strain in the layers and different doping detailed calculation of the potential and the distribution of electrons in layers of the structure have been carried out in the frame of the quasihydrodynamical approximation. Relaxation and not relaxation Si/SiGeC/Si and SiGe/Si/SiGe heterocompositions have been considered in comparison. Potential distribution and equilibrium and nonequilibrium concentration have been determined by the way of a differential equation solution. System of differential equations includes the equation of Poisson and the continuity equation for the charges and currents. Calculation has been conducted by a method of finite differences under Gumbold scheme. Boundary conditions have been carried out taking into account inexact parameters of system near to heterobordary. The numerical analysis was carried out for various types of heterocompositions. The form potential, field structure and a distribution of a charge carriers have been

analyzed for each layer of system. Character of accumulating of a nonequilibrium charge in narrow heterobase of the diode (in a transport channel) is necessary for practical phototransistor application.

An assessment of the potential barrier formed in the vicinity of the heterojunction, and the characteristics of the silicon layer formed in the quantum well. The characteristic form of these dependences for a sample of 414 is shown in Figure 2. Evaluation of the barrier width W_b in its half-height ($h_b/2$=73meV) relative to the bottom of the conduction band in the upper doped SiGe layer gives the value of W_b = 2 nm. The calculation shows a strong dependence of the characteristics of the building, which is formed in the vicinity of a silicon transport channel on a number of initial parameters of the system. The narrowness of the barrier layer is formed and the presence of embedded in the potential well of the electric field, providing a deviation of its shape from the rectangular form and propellant levels of size quantization of the hole, it can provide a variation of the measured transport properties of samples obtained even in relatively the same technological conditions. Transitions of charge carriers from the 2D into 3D state, due to interlayer tunneling transition of an electron, it is possible to explain the instability, manifested in the measurements in strong fields.
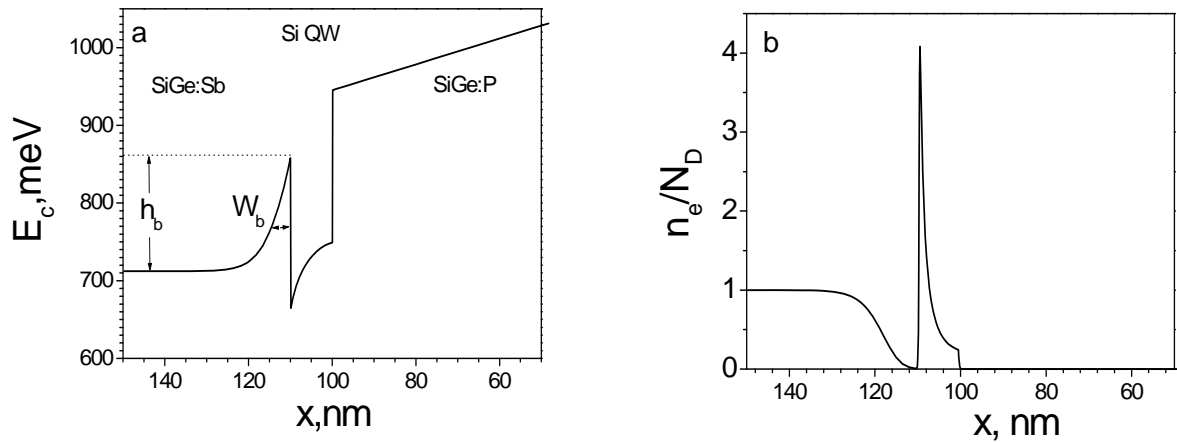
Fig. 2. The form of the potential of the quantum well for electrons in Si layer and the adjacent barrier layers (a), as well as the characteristic distribution of the layers of the structure of the electron density n_e (b), referred to the donor concentration $N_D = 2*10^{18}$ cm^{-3} in the barrier layer, for the sample [2] with the maximum elastic layer of strained Si (d_{Si}=10 nm) and the parameters of the structure of E_g (Si) = 0.93 eV, E_g (Si$_{0.75}$Ge$_{0.25}$) = 1.07 eV, ΔE_v = 0.056 eV [4].

Si/SiGe/Si diode compositions with elastically stressed SiGe heterobase are optimum for accumulating of holes in SiGe transport channel. Effective accumulating of no equilibrium electrons in a structure occurs in the Si/SiGeC/Si compositions with Si$_{1-y}$C$_y$ or Si$_{1-x-y}$Ge$_x$C$_y$ base layer. Accumulating of a no equilibrium charge is probably in relaxed SiGe/Si/SiGe diode heterocompositions also with not deformed Si layer. In SiGe/Si/SiGe heterocompositions, holes are accumulated near the boundary of the lower solid solution layer. Accumulating of nonequilibrium electrons and holes in base of the diode structure is probably only for Si/SiGeC/Si system.

1. E. B. Olshanetsky, V. Renard, Z. D. Kvon, J. C. Portal, N. J. Woods, J. Zhang, and J. J. Harris, "Conductivity of a two-dimensional electron gas in a Si/SiGe heterostructure near the metal-insulator transition: Role of the short- and long-range scattering potential", Phys. Rev. B. 68, pp.085304, 2003.
2. L.K. Orlov, Z.J. Horvath, M.L. Orlov, A.T. Lonchakov, N.L. Ivina, L. Dobos, "Anomalous Electrical Properties of Si/Si$_{1-x}$Ge$_x$ Heterostructures with an Electron Transport Channel in Si Layers", Phys. Solid State, 50, p.330-340, 2008.
3. M.L. Orlov, L.K. Orlov, "Mechanisms of negative resistivity and generation of terahertz radiation in a short-channel InGaAs/InAlAs transistor " Semiconductors, 43, p.652-661, 2009.
4. M.M. Rieger, P. Vogl, "Electronic-band parameters in strained Si$_{1-x}$Ge$_x$ alloys on Si$_{1-y}$Ge$_y$ substrates." Phys. Rev. B. 48, p.14276-14287, 1993.

O2-9: Antihysteresis in voltage-capacitance characteristic of MIS with multilayer insulator

A.A.Popov, A.V.Perminov, A.A.Mironenko, A.E.Berdnikov, V.D.Chernomordick, V.N.Gusev

Yaroslavl Branch of the Institute of Physics and Technology, Institution of Russian Academy of Sciences; 150007 Universitetskaya 21, Yaroslavl, Russia, e-mail imiraslab4@yandex.ru

We investigate metal-insulator-semiconductor (MIS) structures with thin multilayer insulator. Crystalline silicon wafers with boron or phosphorus doping were used. Three layers insulator, deposited on semiconductor, have structure silicon oxide – silicon nitride – silicon oxide (ONO). Five layers insulator have ONONO structures. Thickness of the top layer of silicon oxide is 40-60 nanometers, thicknesses of the other layers are 3-8 nanometers. Metal electrodes were formed from aluminum.. Back side of silicon wafers also were covered by aluminum, which have ohmic contact to semiconductor.

Insulator layers were formed by low frequency (55 kHz) plasma enhanced chemical vapor deposition (LF PECVD). Temperature of depositions was 380 C. For nitride deposition gas mixture of SiH_4 and NH_3 were used, and for oxide deposition gas mixture of SiH_4 and NO were used. Character features of materials formed by LF PECVD include nonstoichiometric composition, incorporated in film silicon nanoclusters, amorphous structure.

Voltage-capacitance characteristic were investigated by analog setup and by digital device from "Keithley". C-V plot have hysteresis-like shape. Word "hysteresis" means delay, which usually observed in the case of hysteresis plot. Contra verse in our case we can view lead in function changing. Because it, we can named same type of plot as antihysteresis. Typical C-V plot presented in figure 1.

Antihysteresis showed as in 5 layers structures, so in 3 layers structures. But in the case of 5 layers structures antihysteresis loop is greater. Antihysteresisis observed in two or three regions of plot, but only one of they is significant. Antihisteresis in voltage-capacitance characteristic can be explained by tunneling of charge carrier through oxide layer to nitride layer and accumulating there.
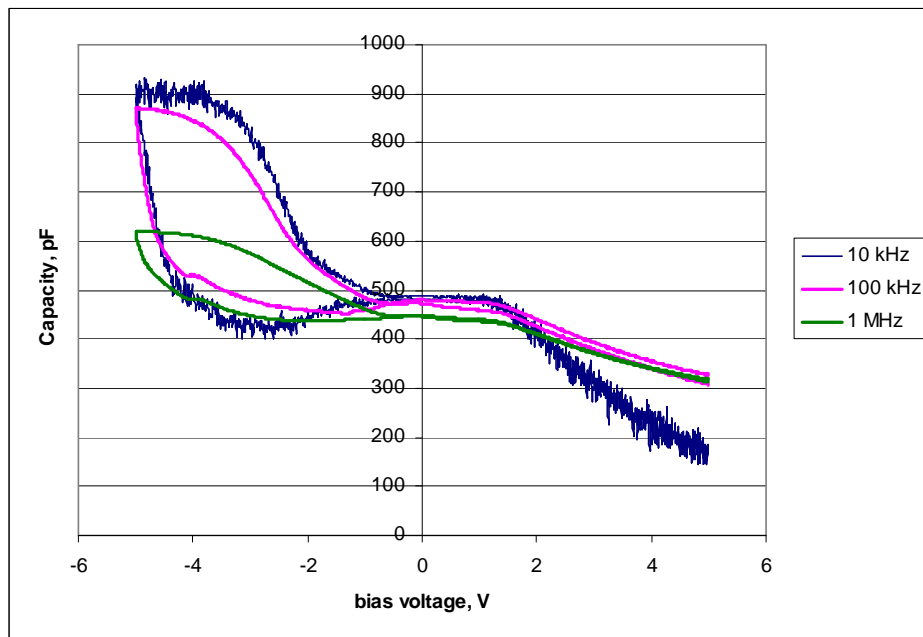
Fig.1. Typical C-V plots for MIS structure with 5 layers ONONO structure of insulator for 3 test frequency.

O2-10: Tunneling and current instability in two-miniband superlattices with unsymmetrical unit cell

J.Yu. Romanova, M.L. Orlov, Yu.A. Romanov

Institute for Physics of Microstructures, Russian Academy of Sciences, Nizhny Novgorod, Russia, orlovm@ipmras.ru

Earlier we have analytically shown [1] that the superlattices (SL) with a compound unit cell and non-harmonic dispersion law are the most promising objects for the creation of sources of terahertz radiation on the Bloch oscillations. However, even in the absence of scattering by optical phonons in the SL with parabolic dispersion law it is possible to separate the areas of low- and high-frequency instabilities. Such dispersion law can be formed, for example, in the lower miniband of the system containing several closely spaced minibands (ε_g <0.02 eV), that takes place in the SL with a compound unit cell. In this paper we study the probability of interminiband tunneling, current flow peculiarities in semiconductor SL with non-harmonic dispersion law of electrons.
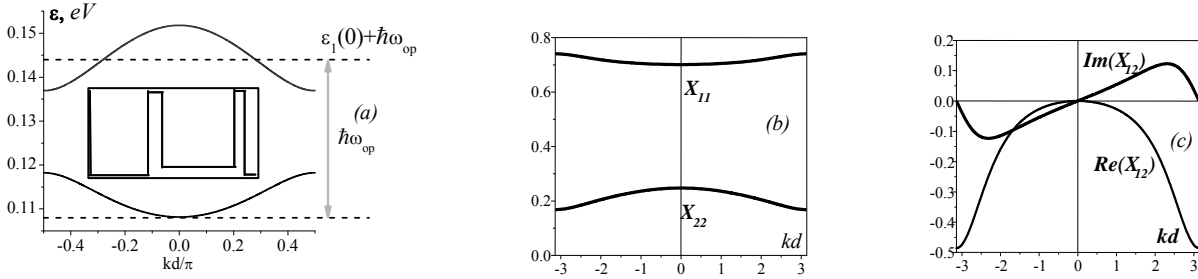
Fig.1. Energy diagram (a), diagonal (b) and nondiagonal (c) coordinate matrix elements ($X_{nv}d$). Potential profile for SL is on the inset to (a).
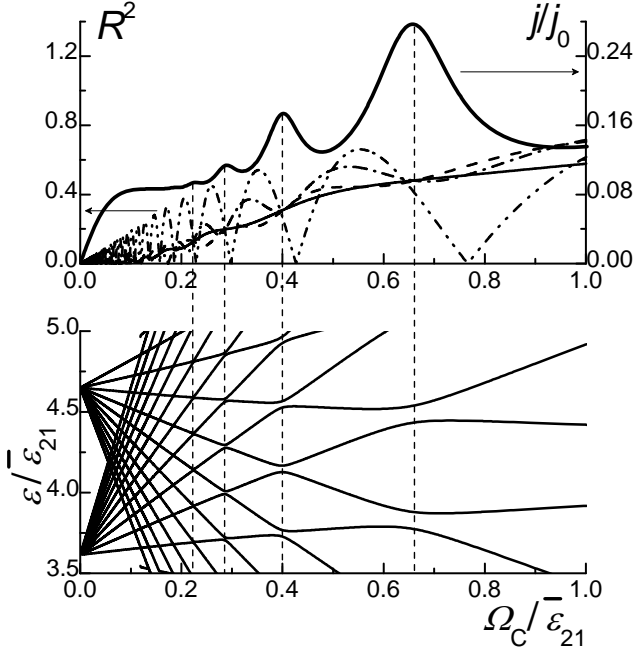
Fig. 2. (a) The probability of the electron tunneling in second miniband as a function of field for different k_0. $k_0d=0$ – solid line, $-\pi/2$ – dash, $-2/3 \pi$ – dash-dot, $-\pi$ – dash-dot-dot; bold line represent VAC; (b) two-miniband WSL.

The results are illustrated by the example of SL with narrow allowed minibands ($\Delta_{1,2}$): GaAs(45Å) - AlAs(11Å) – $Al_{0.05}Ga_{0.95}As$(51Å)-AlAs(9Å). Electron tunnel along whole Brillouin miniband with small probability in this SL. The interaction between the minibands is taken into account using the coordinate operator $r = i\delta_{mn} \partial/\partial k + x$ with the components

$$x_{mn}(k) = i2\pi/d \int_0^d u_{mk}^*(x)(\partial u_{nk}(x)/\partial k)dx, \qquad \text{where}$$

$u_{mk}(x)$- is the Bloch function amplitude periodic in the coordinate space, d – SL period, k - quasi-wave vector (Fig. 1). Optical phonon emission is accompanied by tunneling into the lower miniband ($\Delta_{1,2}<\hbar\omega_{op}$).

Using the model developed in [2] we studied the dependencies of probability of the interminiband tunneling (R^2) and the Wannier-Stark ladders (WSL) position from the static electric field magnitude (E), and $R^2(k)$ (fig.2,3). Far from WSL anticrossing in the spectrum of the electron dominates the Bloch frequency $\Omega=eEd/\hbar$ (fig.3a), in anticrossings SL behaves like a two-level system (fig.3b) making the integer number of transitions between the minibands for the reciprocal SL period $K=2\pi/d$ (so $R^2(k_0,k_0+K)$

for the period is close to 0). In strong fields ($\hbar\Omega/\overline{\varepsilon_{21}} > 1$, where $\overline{\varepsilon_{21}}$ is the distance between the centers of minibands) the electron is greatly localized and therefore makes interminiband transitions within a single

unit cell (fig.3c). At the same time the interminiband tunneling probability $R^2(k_0, k_0 + K, E)$ become monotonic function from field.

Volt-ampere characteristics (VAC) were calculated using the density matrix in τ - approximation [3] and taking into account the emission of optical phonons. The characteristic time is τ_{op}. τ is the velocity relaxation time.

It is shown, that:

1. The dependence of the tunneling probability for a single period of reciprocal SL from the static field is oscillatory. R^2 is independent of the initial value of the quasi-wave vector k_0 in the fields corresponding to the WSL anticrossing (dashed). Its values aren't maximum, and in weak fields, even zero (fig.2).

2. VAC is a set of maxima and minima of the current, more pronounced for the SL with narrow allowed minibands (fig.3a). The first current peak at $E \sim \hbar/ed\tau$ is associated with intraminiband processes of scattering and the Bragg reflections. It can decrease significantly by interminiband transitions and even disappear. That complicates the determination of the characteristic time τ using the position of the first peak of the experimental VAC for the SL with narrow forbidden minibands. The following maximums of current are determined by interminiband scattering and correspond to the WSL anticrossing (opposite to the tunneling probability). Formation of maxima of the current in these fields is due to the fact that (1) collisions disturb high frequency electron oscillations periodicity, but interminiband tunneling probability stays high, (2) the motion of electrons is not limited to one period of the reciprocal SL.

Fig. 3. Time evolution and spectra of the probability of electron being in the second miniband as it moves from the initial state $k_0 d$ =0 in the first miniband for $\widetilde{E}$ =: a – 0.1, b – 0.2865 (anticrossing), c – 1.41.

3. One can see in fig.4a,b the calculated VAC in one-(curve 2) and two-miniband (curves 1,3,4) approximations and various probability of optical phonon emitting. Taking the second miniband into account increases current and shifts the region of static NDC to higher fields. Strong scattering by optical phonons prevents the reflection of electrons from the minibands boundaries, and current reaches saturation.

High-frequency conductivity calculated without consideration of the optical phonons (fig.4b). Areas of low-frequency instability alternate with areas of high frequency. Conductivity sign change occurs near $\omega/\overline{\varepsilon_{21}} = n/2$, where n is integer.
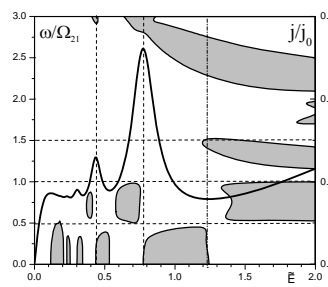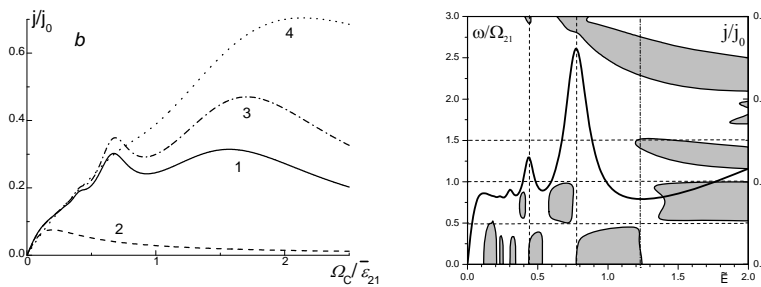
Fig. 4. a – VAC: (1,3,4) – two-miniband approximation, (2) – one-miniband approximation; (1,2) – nonmetering scattering on optical phonons; (3) – $\tau_{op}/\tau = 1$; (4) – $\tau_{op}/\tau = 0.1$; b – dynamic instability areas ($\sigma_\omega < 1$) CP D nonmetering scattering on optical phonons, and VAC for comparison.

1. Romanov Yu.A., Romanova J.Yu., "On a superlattice bloch oscillator" Physics of the Solid State 46, pp.164-169, 2004; IJN 3, 177-185, 2004.

2. J.Yu. Romanova et.al., "Zener tunneling in semiconductor superlattices" J. Phys.: Cond. Mat., 23, pp.305801-1-17, 2011.

3. L.K. Orlov, Yu.A. Romanov. "Nonlinear resonant peculiarities of electrical properties of superlattices provided strong intersubband tunneling of electrons" Sov.Phys.Semicond, **19**, pp.1157-1161, 1985; "Features of electromagnetic signals amplification in quantum superlattices with high inter-subband tunneling current", Izv. VUZ. Radiofizika (in Russian), **32**, pp.282-288, 1989.

I2-5: Gas Sensors Based on MEMS Platforms

<u>A.A.Vasiliev</u>[1], A.S.Lipilin[2], A.M.Mozalev[3], A.S.Lagutin[1], A.V.Pisliakov[1], N.P.Zaretskiy[1], N.N.Samotaev[1], A.V.Sokolov[1]

[1]*Institute of Applied Chemical Physics, NRC "Kurchatov Institute", Moscow, Russia,* <u>A-A-Vasiliev@yandex.ru</u>
[2]*Institute of Electrophysics of Ural Branch of RAS, Ekaterinburg, Russia*[3] *Belarus State University of Radioelectronics and Informatics, Minsk, Belarus*

Summary
We present a novel approach to the fabrication of MEMS devices, which can be used for sensors (gas, pressure, temperature, etc.) operating in harsh environment in wireless and autonomous information systems. MEMS platforms based on ZrO_2/Y_2O_3 (YSZ) and alumina membranes are applied in these devices. The methods of fabrication of these MEMS are considered. It is shown that the application of such membranes permits a decrease in MEMS power consumption at 450^0C down to ~75 mW at continuous heating and down to ~ 2 mW at pulse heating of gas sensor.

Motivation and results
One of important requirements to the sensors based on semiconductor, thermocatalytic, and electrochemical gas detection principles, which are applied in autonomous and wireless systems, is the minimization of their power consumption. Recently, the most prospective is the application of microelectromechanical (MEMS) structures as a basis for such sensors. In these structures, a dramatic decrease in power consumption is reached due to very strong decrease in heat dissipation of hot sensing element heated up to $300 – 600^0C$, which is located not on a massive substrate, but on thin dielectric membrane. Traditional MEMS structures fabricated with silicon technology can not be used in harsh environmental conditions because of hydrolysis of Si_3N_4 at high temperature, poor adhesion of Pt to SiO_2 or Si_3N_4, and difference in properties of the materials used for such MEMS devices.

A possible solution of these problems is the application of ceramic MEMS (Fig. 1). The membrane of this MEMS can be made by spark electrolyte oxidation of aluminum [1]. A disadvantage of this membrane is high porosity of Al_2O_3 preventing wire bonding of Pt elements of the MEMS platform. The application of anodic oxidation of aluminum gives high quality membranes (Fig. 2) with thickness of $10 – 20$ µ, which can be fixed on ceramic alumina substrate with laser drilled holes (Fig. 3). Membrane (Fig. 2, 3) was annealed before gluing to the substrate at 1150^0C, therefore whole MEMS device can operate at temperature up to 1000^0C at high humidity and aggressive atmosphere. Relatively high heat conductivity of alumina membrane fabricated by anodic oxidation of aluminum (25 W/m·K) leads to relatively high power consumption of MEMS device operating at high temperature typical of semiconductor and thermocatalytic gas sensors.

This problem can be solved by the application of ceramic materials with lower heat conductivity. The most suitable material for such application is yttria stabilized zirconia, a material with lowest heat conductivity coefficient among all ceramics (2.5 W/m·K). The film of this material is produced by slip casting with consequent annealing under mechanical load. Ceramic slip consists of small particles with size of about 20 nm, therefore satisfactory quality of the film sintering was obtained at relatively low temperature of about 1150^0C and sintering time of 12 hours. Resulting membrane has thickness of about 10 µ, photo of the membrane with dimension of 48 x 60 mm (this is the size of YSZ substrate with laser drilled holes used for membrane gluing) is presented in Fig. 4, and SEM image of the cleaving of the membrane is given in Fig. 5.

Thermal characteristic of the Pt heater formed by magnetron sputtering through shadow mask (heater size is 200 x 400 µ) is presented in Fig. 6. Low heat conductivity of the material of the membrane enables the fabrication of methane gas sensors (sensing layer is Pd doped tin dioxide) with power consumption of about 70 mW at continuous heating and less than 2 mW at pulsing heating of the sensor.

It is planned to apply these devices for the prevention of hard accidents in nuclear power reactors for the measurement of H_2, humidity, and O_2 concentrations under high temperature/humidity conditions.

1. A.A.Vasiliev, R.G.Pavelko, S.Yu.Gogish-Klushin, et al. Sensors and Actuators B, 132 (2008) 216–223.
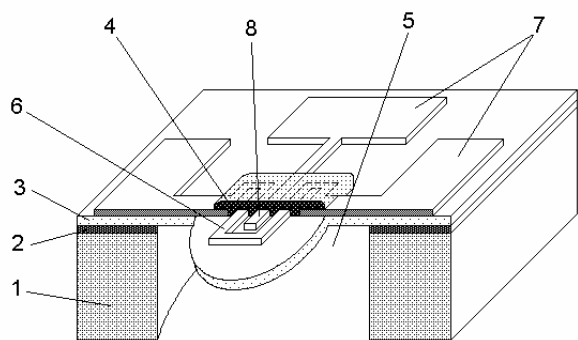
Fig. 1: The structure of the ceramic MEMS gas sensor. 1 – ceramic substrate; 2 – glue layer; 3 – thin ceramic membrane; 4 – sensing layer; 5 – laser drilled hole in ceramic substrate; 6 – platinum heater of the gas sensor; 7 – contact pads to the heater and sensing layer; 8 – measuring electrode for the measurement of the resistance of semiconductor sensing layer [1].
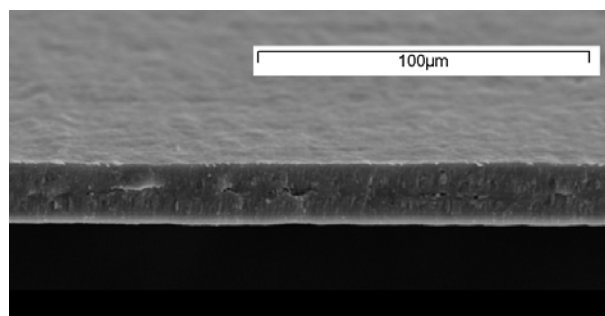
Fig. 2: Cross-section of the 20-micron membrane fabricated by anodic oxidation of aluminum foil. The photo was made after annealing of the membrane at 11500C.
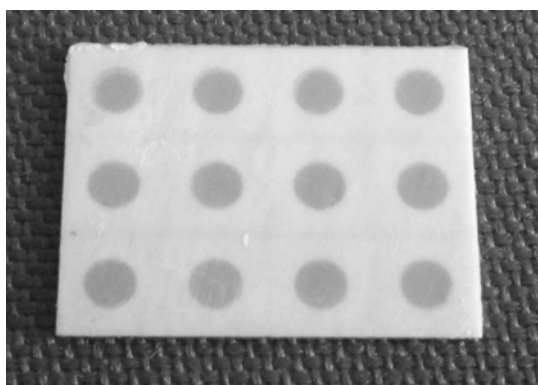
Fig. 3: Top side view of alumina substrate with anodic membrane glued with glass. The size of each individual chip is 6 x 6 mm, hole diameter is of 3 mm. The thickness of the membrane is of 10 microns.
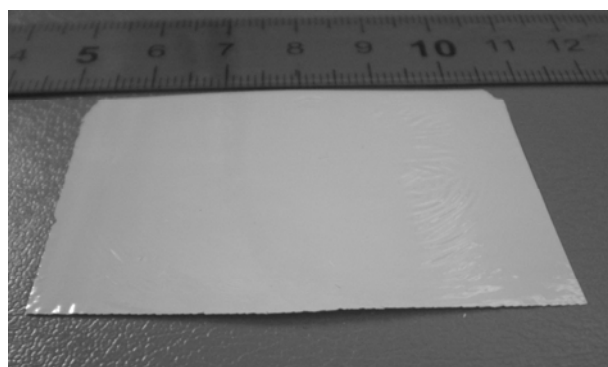
Fig. 4: Ceramic film made of yttria stabilized zirconia. Size of the membrane is 48 x 60 mm, thickness 10 microns. Annealing temperature is 11500C.
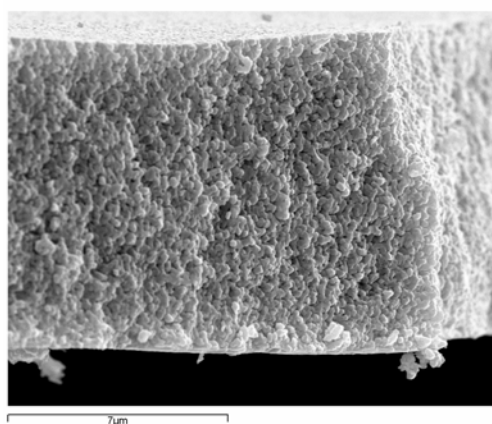
Fig. 5: SEM photo of the cross section (cleaving) of the ceramic membrane made of yttria stabilized zirconia.
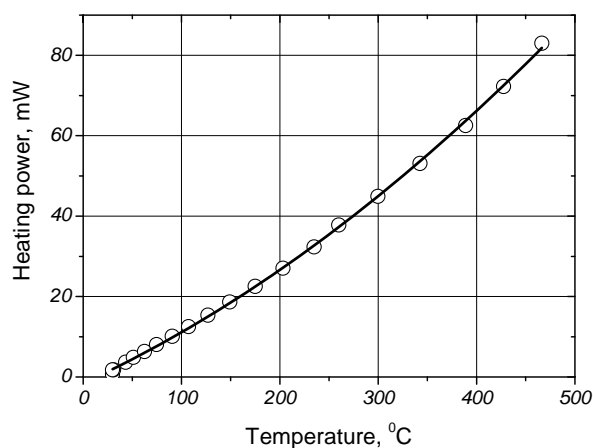
Fig. 6. Heating power of the heater on 20 micron YSZ membrane presented in Fig. 1 (heater size 400 x 200 microns) as a function of its temperature.

O2-11: Principal Physical and Technological Problems and Technical Solutions for Creating a New Generation of High-Temperature Microelectromechanical SOIMT Strain Sensors

L.Sokolov[1], N.Parfenov[2], S. Igochin[3]

1. Filial, MAI, "Strela" Zhukovsky, Moscov Region, Str.Zhukovsky. 8, Russia, E-mail:sokol@niiao.com. 2. Moscov, MAI, Volokolamskoe higway,4, Russia, E-mail: sedennik@mail.ru. 3. Moscov, OOO "Interlab" Tikvin lane,11, p. 2, Russia, E-mail: igochin@interlab.ru.

Under severe operational conditions for electronic systems of aerospace equipment there is an acute problem of creating high-temperature, high-reliability and also competitive sensors of mechanical quantities [1].

This problem can be resolved on the basis of innovative microelectronics and micromechanics technologies, which allow integral strain sensors without isolation p-n-junctions to be produced in batches [2].

The analysis results of physical and technological problems, as well as some basic technical solutions are given for manufacturing an experimental batch of strain sensor modules and integral MEMS-SOI membrane-type pressure sensors with a monolithic tensoframe (SOIMT) based on a "monosilicon-glass-monosilicon" heterostructure by group method.

VEECO, TM-3000, as well as Quanta 200 3D FEI electronic scanning microscopes, that include an EDAX detector for the X-ray microanalysis, are used to analyze the physical and technological problems of precision microprofiling of a 3D micromechanical structure for a MEMS-SOIMT sensors, which are caused by the contact photolithography process on a relief surface, and the problem of jointing a MEMS-SOIMT sensor chip, which contains glass nanocluster fragments on its contact surface, with a Pyrex glass support element, in the electrostatic field.

1. Sokolov L.V., Zhukov A.A., Kapustian A.V., Physical and Technological Problems of Producing New Generation High-Precision Semiconductor Pressure Sensors with Digitized Output for Information Measuring, Control and Diagnostics Systems // Proceedings of All-Russian Scientific&Technical Conference "Actual Problems of Space Rocket Instrument Engineering and Information Technologies", Moscow, 28-30 April, 2008, Fizmatlit, 2009, pp. 364-367.

2. Leonid V. Sokolov. Conceptual Basis for Creating New-Generation High-Stable High-Temperature Microelectromechanical Sensors Based on a Silicon-On-Isolator Heterostructure with a Monolithic Integral Tensoframe for Intelligent Transducers // Proceedings of ISMTII-2009, Volume 3, 9th International Symposium on Measurement Technology and Intelligent Instruments. St.-Petersburg, 29 June – 2 July 2009, pp. 248-251.

O2-12: Application of Amplitude Response of Scanning Differential Heterodyne Microscope for Characterization of Triangular and Trapezoidal Plasmon Waveguides

I. M. Akhmedzhanov, D. V. Baranov, E. M. Zolotov

A. M. Prokhorov General Physics Institute, Russian Academy of Sciences, Vavilov str.38, Moscow 119991, E-mail: eldar@kapella.gpi.ru

Surface plasmon-polariton (SPP) components as expected will be widely used in future nanofotonic devices. First of all, perspectives for the application of the SPP components are based on the possibility of their confinement in substantially smaller space volumes as compared with usual surface optical waves. The main reason for such possibility follows from the fact that the wavelength of SPP, which propagates along the metal-dielectric boundary, is smaller then the wavelength of the optical wave with the same frequency, therefore the diffraction effect is less significant for such type of waves. The main problem in practical SPP applications is a contradiction between a localization of surface wave field and propagation losses. Tight SPP localization leads to high propagation losses and reduction of propagation losses leads to poorer localization. To overcome this problem several types of SPP waveguiding structures were proposed and investigated by various research groups [1]. It was shown that for the near infrared and visible spectral region $0.5 \div 1$ μm V-groove waveguides is most promising taking into account the trade-off between a localization and a propagation length. For these waveguides the typical depth is about 1 μm and base ~0.5 μm. Distortions of V-groove profile influence on the properties of the guided SPP modes. Thus the task of a characterization of the V-groove waveguide with the accuracy better then 100 nm becomes important. The scanning differential heterodyne microscope (SDHM) seems to be an appropriate tool for this purpose due to its non-destructive optical design. In our previous works [2,3] we have used SDHM in conjunction with RCWA theory [4] for the solution of the direct characterization problem. There was enough to process only one component of the complex SDHM response, namely phase one. Here we consider the inverse problem and both components of the complex response should be analysed to overcome the ambiguity of the solution.
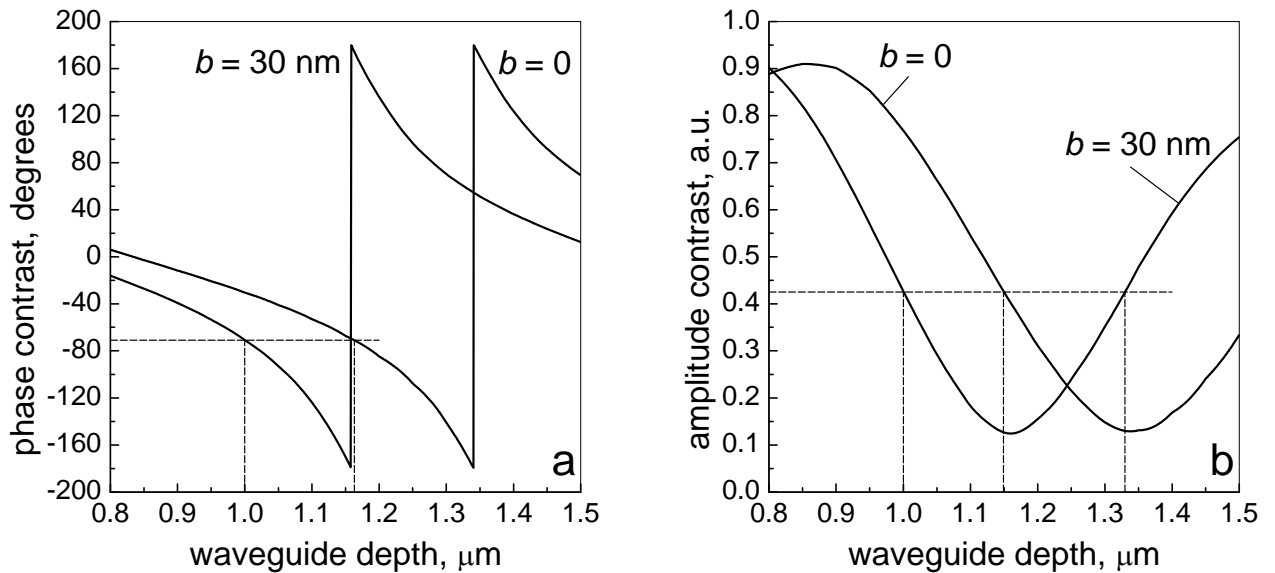
Fig. 1. Phase (a) and amplitude (b) contrast of a SDHM response vs CPP waveguide depth for two bottom base values of waveguide profile.

Possible approach to the solution of inverse problem we shall consider for following special case. Let us suppose that two SPP waveguides on gold–air interface is given. One of the waveguides has triangular profile with the upper base $w = 0.5$ μm and bottom base $b = 0$ and another has trapezoidal profile with upper base 0.5 μm and bottom base 30 nm. The depth values d of both waveguides is in the interval $0.8 \div 1.5$ μm. One should determine the actual parameters of the waveguide if complex SDHM response is characterized

by phase contrast $\Phi = -70°$ and amplitude contrast $A = 0.425$ on TE polarization. With other words, it should be determined profile of the SPP waveguide by using SDHM response and some a priori information about expected profile parameters. As it could be seen in Fig.1a, two possible sets of parameters correspond to the phase response $\Phi = -70°$ in considered depth region: (b=30nm, d=1.0μm) and (b=0nm, d=1.16μm). The ambiguity of the phase response is obvious. Similarly we obtain other sets from the amplitude response (see Fig.1b): (b=30nm, d=1.0μm); (b=30nm, d=1.33μm); (b=0nm, d=1.15μm). Only one pair (b=30nm, d=1.0μm) belongs to both sets, and this pair is the solution of the formulated problem. It can be shown that for another value of the complex SDHM response the procedure will be the same. It is important to note that in proposed approach only one (TE) polarization for the probing SDHM optical beam is sufficient. Thus we have shown that using both amplitude and phase response of SDHM on TE polarization state allows to determine two parameters of trapezoidal SPP waveguide with a priori information.

1. D. K. Gramotnev, and S. I. Bozhevolnyi, "Plasmonics beyond the diffraction limit", Nature photonics., **4**, pp.83-91, 2010.
2. I. M. Akhmedzhanov, D. V. Baranov, and E. M. Zolotov, "Influence of V-shaped groove profile distortion on the response of a heterodyne microscope", *22nd Congress of the International Commission for Optics: Light for the Development of the World*, ed. Ramón Rodríguez-Vera, Rufino Díaz-Uribe, Proc. SPIE, **8011**, pp.80118G-1–80118G-7, 2011.
3. I. M. Akhmedzhanov, D. V. Baranov, and E. M. Zolotov, "Implementation of the coupled-wave method for V-shaped groove characterization with a scanning differential heterodyne microscope", *J. of Phys.: Conference Series*, **274**, 012005, 2011.
4. M. G. Moharam, D. A. Pommet, and E. B. Grann, "Stable implementation of the rigorous coupled-wave analysis for surface-relief gratings: enhanced transmittance matrix approach," JOSA A, **12**, pp.1077–1086, 1995.

O2-13: KELVIN PROBE method in scanning probe microscopy

[1]Salimov R. R., [2]Zhunusbekov A.M., [2]Kainarbai A. Zh., [2]Karipbaeyv Zh.T.
1.Bashkir State university, Ufa, Russia, 2. L.N.Gumilyov Eurasian National University, Astana, Kazakhstan,
sunaman@mail.ru

Scanning probe microscopy (SPM) is one of the most powerful modern methods of investigation of the morphology [1-3] and the local properties of the solid surface with a high space resolution. The scanning probe microscope can measure the physical properties of surfaces such as surface conductivity, the distribution of static charges, magnetic fields and elastic modulus, properties of lubricating films, etc. Modern applications of SPM are very diverse [4].

Kelvin probe method is a electric force microscopy in SPM, also known as surface potential microscopy. It allows to research of the distribution of surface potential of the sample. The Kelvin Probe is a non-contact, non-destructive measurement device used to investigate properties of materials. It is based on a vibrating capacitor and measures the work function difference or, for non-metals, the surface potential, between a conducting specimen and a vibrating tip. The work function is an extremely sensitive indicator of surface condition and is affected by adsorbed or evaporated layers, surface reconstruction, surface charging, oxide layer imperfections, surface and bulk contamination, etc.

The aim of this work was to study, mastering and application of the method Kelvin probe in scanning probe microscopy. Samples, the most satisfying that aim, were selected as objects of research. Surface potential distributions of the samples should be contrast for clarity of the results. As known, compounds with a different electron works function have also the different surface potentials.

Therefore, the following samples were prepared:
• Si (111) single crystal substrate, Au thin film is partially deposited to the crystal surface;
• Si (111) single crystal substrate, Ti thin film is partially deposited to the crystal surface.

Logical choice of the two research objects lies in the fact that the work function of titanium is less than the work function of silicon, and conversely, the work function of gold more than the work function of silicon. Qualitative demonstration of these differences is the expected result of the research.

Investigations of electrical properties of the samples surface were carried out on scanning probe microscope NTEGRA-PRIMA.

For contrast substance a lot of scratches have been done on the first sample surface with using paper. The maximum depth of the scratches reached the substrate surface. Then from this set one scratch has been selected as most suitable for research. The relief of the surface which obtained by semi-contact AFM, is shown in Figure 1. Then distribution of surface potential in this sector of the sample was measured. The results are shown in Figure 2.
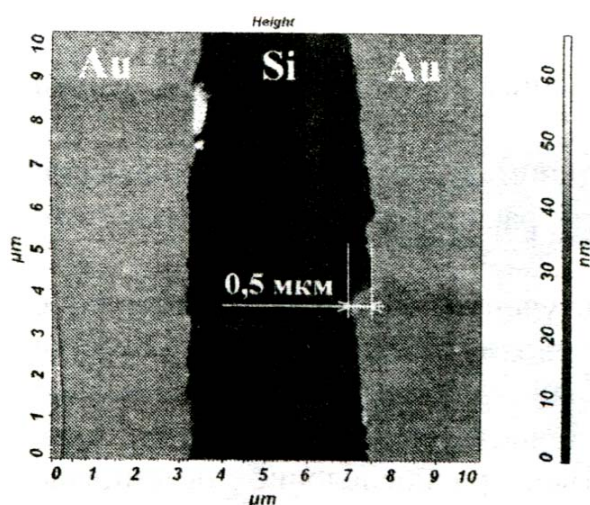
Fig. 1. The relief of the surface which obtained by semi-contact AFM
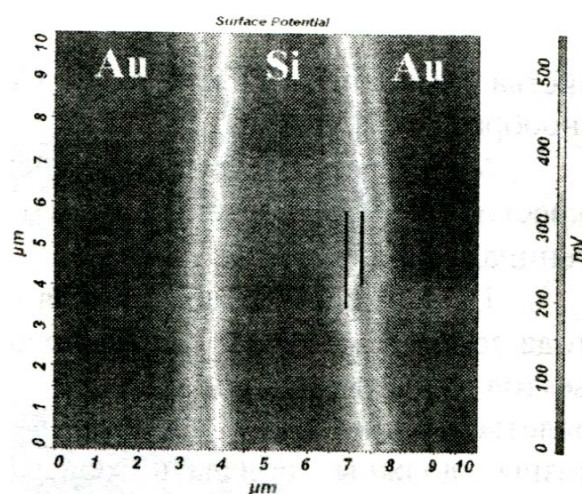
Fig. 2. Surface potential in this sector of the sample
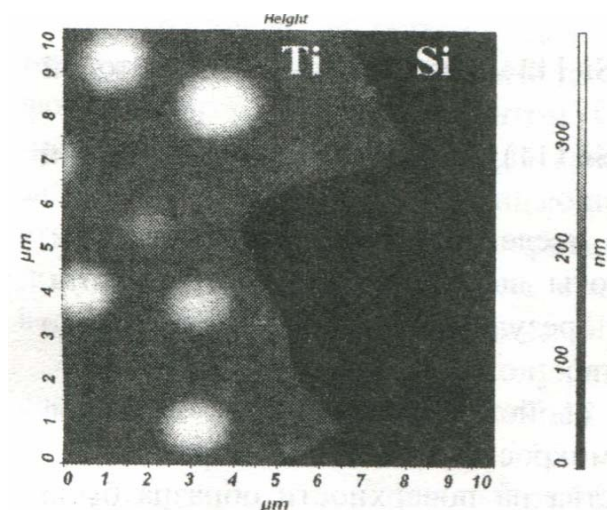
Fig. 3. Image of scratches edge which obtained by semi-contact AFM
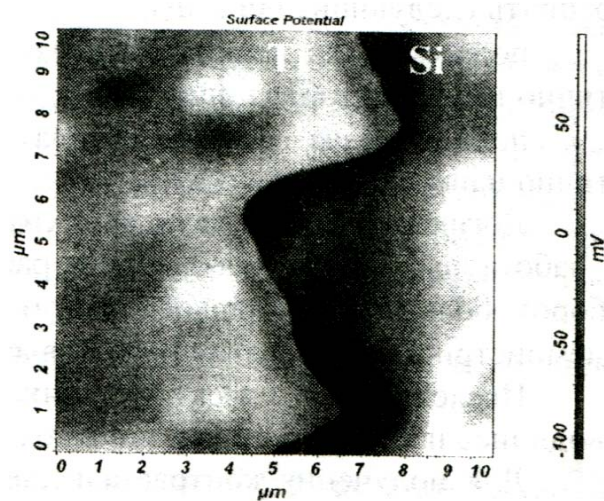
Fig. 4. Surface potential scratches edge in this sector of the sample

Similarly, as in the case of gold, for the contrast substance on the second substrate the scratch was made by sharp end of tweezers. Image of scratches edge which obtained by semi-contact AFM is shown in Figure 3. The results coincide with theoretical data. Resolution of the method is less than 500 nm. Thus, contrast of the electron work function is measured at the nanometer level.

1. G.Binnig, C.F.Quate, Ch.Gerber—*Atomic force microscope.* // Phys. Rev. Lett., v. 56, № 9, p. 930 - 933 (1986).
2. V.S.Edelman.-   // Pribory i technika experimenta, № 1, p. 24 - 42 (1991).
3. D.Sarid - "*Exploring scanning probe microscopy with "Mathematica"*", John Wiley & Sons. Inc., New York, 1997, 262 p.
4. Internet web site "NT-MDT": http://www.ntmdt.ru/.

I3-1: Evolution of Non-Equilibrium Profile in Compressive Strained Adlayer

E. Granato, S. C. Ying

1. Laboratório Associado de Sensores e Materiais, Instituto Nacional de Pesquisas Espaciais, Saõ José´ dos Campos, SP 12227-010, Brazil
2. Department of Physics, Brown University, Providence, RI 02912, USA

The system of an adsorbate layer with a lattice mismatch to the underlying substrate has been extensively studied both from the experimental and theoretical side. In the monolayer regime, it provides a realization of many two dimensional phases and has also been used as a simple model for studying sliding friction phenomena on surfaces]. In particular, the rich phenomena of commensurate to incommensurate phase transition depends on the competition between the adsorption energy and the strain energy from the lattice mismatch. Recently, Tringides and co-workers have done an extensive study of the Pb/ Si(111) system and found the ''Devil's Stair Case'' within a narrow range of coverage as predicted by the theory. They have further found that the adsorbate layer exhibited anomalous mass transport through the time evolution of step profile created by desorbing the adatoms in a small region[1]. This anomalous transport is characterized by a sharp non-diffusive profile at all times as well as a critical coverage below which the rate of the profile evolution slows down exponentially with decreasing coverage. Up to now, there is still no detailed understanding of the microscopic origin of this anomalous mass transport. In this talk, we present a study of a generic two-dimensional adsorbate system with a well understood transition from a commensurate c(2x2) phase to an incommensurate phase.[2] A non-equilibrium profile is created in the adsorbate layer and the time evolution of the profile is then studied numerically via molecular dynamics simulation. In particular, we focus on the rate of profile evolution as a function of the lattice mismatch, the coverage, and the strength of the substrate potential. We find that the results are qualitatively similar to those observed for the Pb/Si(111) system. The main results can be understood via microscopic mechanisms that are generic to an adsorbate layer under a compressive strain near a commensurate–incommensurate transition. In particular, the time evolution of the non-equilibrium profile is governed by the rate of domain wall creation at the boundary and its subsequent diffusion into the interior of the adsorbate layer. The profile remains sharp during its evolution because it is continuously being driven by the unbalanced compressive stress at the boundary. When the stress at the boundary is increased via increasing the coverage beyond the ideal commensurate coverage, the interior of the adsorbate layer has intrinsic defects or domain walls to accommodate the extra adatoms. Depending on the substrate potential and the coverage, these defects can be either pinned or depinned. The transition between these two phases correspond to the ''Aubry transition''well studied in the literature .When the domain walls are ''pinned'', the propagation of the boundary generated domain wall into the interior will be blocked by the pinned domain walls and the time evolution of the nonequilibrium

profile will also stop. The anomalous fast transport can only be achieved when the system is in the unpinned side of the incommensurate phase. The transition to this side of the ''Aubry phase'' leads to a critical coverage for the rapid time evolution of the non-equilibrium profile as observed in the experiments. Although this study is for a specific model system with a relatively simple commensurate– incommensurate phase transition, the generic features of the profile evolution is applicable to a wide class of adsorbate layer under compressive strain. The mechanism of anomalous mass transport via activation and propagation of boundary domain walls should play an important role in tribological systems.

1. Man, K.L., Tringides, M.C., Loy, M.M.T., Altman, M.S.:"Anomalous mass transport in the Pb wetting layer on the Si(111) surface" Phys. Rev. Lett. 101, 226102 (2008)
2. Granato Enzo, Ying,S-C: " Evolution of Non-Equilibrium Profile in Adsorbate Layer Under Compressive Strain" Tribology Letter, in press.

O3-1: Forming of self-organizing nanostructures at laser heating

A.A. Antipov, S.V. Kutrovskaya, A.O. Kucherik A.V. Osipov

Department of Physics and Applied Mathematics, Stoletov's Vladimir State University, Gorky st. 87, Vladimir, 600000 Russia, E-mail: kucherik@vlsu.ru

Opportunity of nanostructure formation is one of most actively developing directions of laser physics. Advance of the given direction is connected by dependence of properties formed nanostructures from parameters of laser radiation (length of a wave, duration of a pulse, form of a beam). The modern laser systems allow to control of the laser radiation parameters and to generate nanostructures with the set properties.

In the given work the objects of research are the various samples (carbon materials, metals, semiconductors). In the carried out experiments the dependences of morphological properties of generated nanostructures from condition of experiments are found out. It is shown, that mechanisms of their formation have the different character. The investigation has been carried out at action to target by radiation of the continuous, nanosecond and femtosecond pulse lasers in various environments: atmospheric air, vacuum, liquids.

Properties of the samples after laser action were investigated by raster electronic (REM), atomic force (AFM) microscopes and Raman spectroscopy (RS).
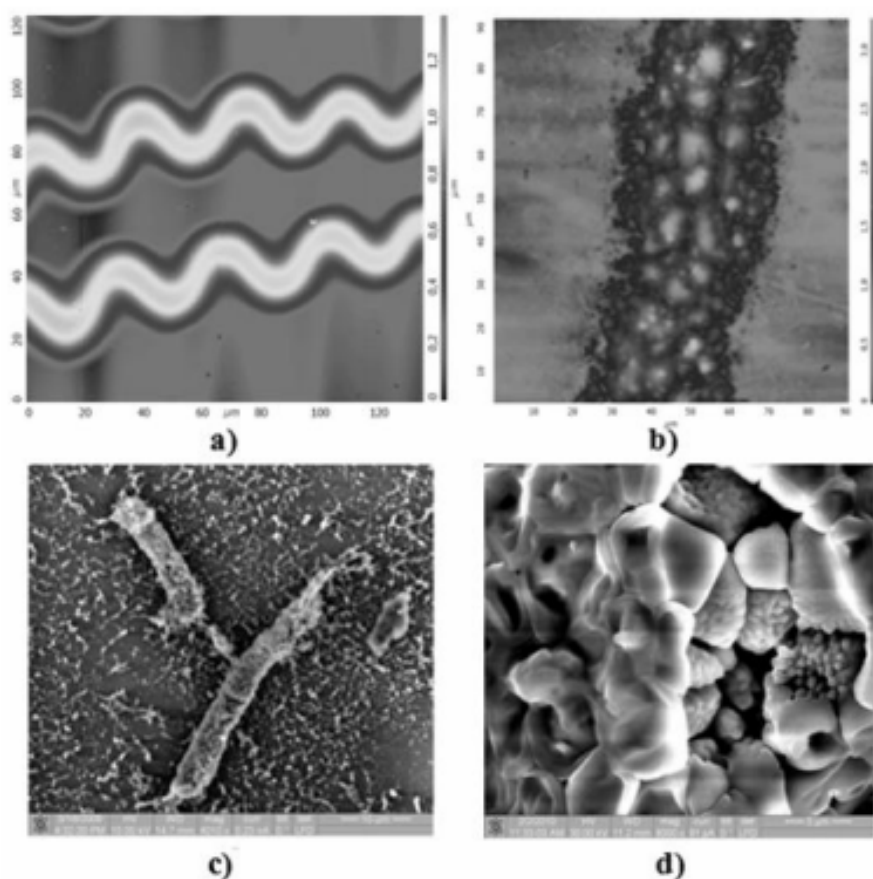
Fig. 1 Examples of organized nanostructures: a) AFM-image of self-organized surface of carbon deposition; b) AFM-image of nanostructure array deposited from colloidal solution; c) REM-image of self-organized titan oxide deposition; d) REM-image of metal-carbon crystalline-like structures;

O3-2: Self-organization in adlayers on metallic nanosystems

N..Socolova, A.Tsivadze

Frumkin Institute of Physical Chemistry and Electrochemistry, Russian Academy of Sciencies, Leninskii pr,31,
Moscow,119991, Russia, E-mail; socolova@phyche.ac.ru

The study of nanostructures formation is one of the basic trends in modern fundamental and applied science. The data concerning peculiarities and physical-chemical properties of nanosystems are necessary for a more detailed understanding of the process of metallic surface formation in particular adsorbents and catalysts.

In this work we discuss the results of the research of state and changes in the surfaces of nanometallic systems in the cours of self-organization in adlayers including mutual transformations in metal-gas systems and enrichment of bimetallic surface and its reasons.

The metals of VIII and 1 b groups of periodical table are used The determination of a particle size has been performed by means of x-ray scattering (T.Purjaeva and A.Shirjaev).The information concerning of the surface sites has been obtained by studying the chemisorption of the test-molecule (CO) using IR spectroscopy. The approach was suggested by authors of the paper.

It is known that superficial layer of reacting atoms and molecules is an open non-ideal system in which a phenomen of spatio-temporal self-organization may take place. On monocrystal metallic systems the surface layer may change its geometrical structures either spontaneously or under the effects of adsorbed atoms and molecules. The their data about nanometallic systems are practically absent. The existence in this systems of a great number sites in which atoms differ in their structural (neighborhood) and electronic properties (unsaturated coordination) leads to self-organization.

The changes in the state of adlayers depending on the duration of the contact with the gas ,on the pressure and the effect of thermal desorption are discussed in detail. To study the changes depending on the time of the contact with gas we recorded the spectra of adsorbed CO molecules both immediately upon the gas inlet at certain pressure and after the exposition to gas atmosphere for 72 hours.

To distinguish new species a spectrum of freshly prepared specimen was subtracted from the spectrum recorded upon the 72 hours exposure. Depending on the duration of the contact the superficial distribution of active sites change in different ways ; in one case (Rh-Ir) the amount of defect forming dicarbonyl species increases in the other case (Rh-Gd) multicenter species become prevailing.

The changes in the composition and structure of surface take place under effect of thermal desorption. Desorption at high temperature is accompainied by complex processes. Their mechanism has been studied insufficiently because in is difficult to observed the processes on originalle heterogeneously surface. In order to clarify whether the changes in the composition and structure of the surface induced by chemisorption by reversible the gas was again let on the specimen after the adsorption – desorption cycle. It is shown that at high temperatures not only MCO complexes are broken but also the surface is reorganized so that the structures involving several metals atoms appear:

$$MCO \rightarrow M_n CO$$
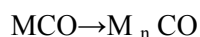
We also found that the surface formation depends on the way of gas supply .When the gas concentration increases gradually from very low values ,then even upon thermal desorption the surface structure is completely restored. We suppose that at the successive adsorption starting from low coverage ,the adsorption complexes are stabilized due to the electron density redistribution between the metal atoms which are directly involved in the interaction with CO molecules and the neighboring atoms. When large amount of gas is rapidly supplied, such stabilization has no time to take place, and gas molecules are more mobile, which result in their migration over surface and the accompanying change in the original structure.

O3-3: Research of gas-sensitive cobalt-containing polyacrylonitrile films using the theory of self-organization

S. Konovalenko[1] , T. Semenistaya[2]

1. Taganrog Pedagogical Institute named after A.P. Chekhov, Taganrog, Russia, E-mail svetlana_s12@mail.ru
2. Taganrog Institute of Technology – Southern Federal University, Taganrog, Russia, E-mail semenistaya@yandex.ru

Nanosized materials with fractal structure and unique properties due to their structural, topological and morphological features, allow realizing the latest technological and engineering developments in the field of creation of gas sensors. Semiconductor gas sensors based on metal-organic polymer composites attracted considerable attention owing to their exclusively high sensitivity to the composition of the gas phase of the atmosphere at low working temperatures.

Films of polyacrylonitrile (PAN) doped with cobalt, have good gas-sensitivity (S) to Cl_2 at room working temperature $(17 \div 22\,°C)$. The technological parameters of the formation of the polymer and the mass content of cobalt in the organic component of the film influence the gas sensitive properties of this material. PAN is an organic polymer, whose linear form is an insulator, after heat treatment gains semi-conductor nature of conductivity thanks to structural transformation of the polymer chain [1]. As a result of self-organization in the system there are new collective properties, which initially did not have. These properties are shown in the form of correlations, creating and supporting reproduced relationship between remote parts of system [2]. Thus, PAN is capable of detecting gaseous impurities by change electrophysical characteristics and morphological features of formed layer of its film. Mathematical methods were used to research the relationship of the surface morphology of the material with the characteristics of gas-sensitive films of PAN: basic analysis method of nonlinear self-organizing systems – F. Takens embedding method, the theory of information, which leads to non-linear representations of the relationships between different parts of the system [3].

The films of PAN/Co (cobalt content by weight: 0.25 wt.%, 0.5 wt.%, 0.75 wt.%, 1 wt.%) were formed of film-forming solutions on a dielectric substrate by the method of incoherent IR-radiation. IR-annealing carried out in IR-chamber in two stages at a low vacuum (80 mTorr). Intensity of radiation at the first stage corresponded to $250\,°C$ and $300\,°C$, and the intensity of radiation at the second stage – $300 \div 500\,°C$. Time of exposure of infrared radiation were different $(5 \div 20\ minutes)$ at each temperature.

Resistance of the films was measured by teraommetre E6-13A to study the gas-sensitive properties of a material of the received films. Sensitivity of the films was evaluated using factor of a gas-sensitivity S, which is calculated as:

$$S = R_o - R_g / R_o, \text{ when } R_o > R_g, \tag{1}$$

where R_o – value of resistance of a film on air, R_g – value of resistance of a film in the atmosphere of detected gas.

Parameters of non-linear dynamics and value of factor of a gas-sensitivity to Cl_2 (69 ppm, 22 ºC) of Co - containing PAN films are calculated (tab. 1).

The values of fractal dimension D_f equal to the self-affine surface of PAN films which are from 2.41 to 2.50 have been calculated. Interpretation of fractional dimension is that the studied surface of Co-containing PAN films are close to two-dimensional one $(D_f = 2)$, but also have some properties of three-dimensionality.

Considering parameters of nonlinear dynamics it is possible to draw a conclusion on existence or absence of self-assembled structures in studied nanocomposite materials PAN / Co: a surface of a film sample with the optimum content of cobalt (0.25 wt.%) is formed by two and three levels of similar structures. These samples also have the highest factors of a gas-sensitivity to the detected gas.

For studied samples Lyapunov's first spatial indicators λ_r which appeared positive have been calculated. This fact may mean that substance distribution in space for studied films differs from the equilibrium.

Researches of samples showed that the maximum and minimum values of average mutual information AMI (I) have a rather large scatter of values. It is observed the increase in values of factor of increase of the area K and factor of a gas-sensitivity S with increase temperature of the second stage of the IR-annealing at one concentration of dopant. The above-listed factors are reduced with increasing of cobalt concentration in the received films. Relatively high AMI values are observed in the samples with small surface roughness (peak-to-peak height ~ 30 nm) and quiet good sensitivity (about $S = 0,61 \div 0,88$). The maximum AMI value corresponds to the maximum of gas sensitivity. High AMI values indicate the presence of long-range

correlations in the system; the order can be considered as a result of self-organization [4]. It was found that a greater AMI value corresponds to a more ordered structure of the material and to the highest value of factor of gas sensitivity.

Table 1
Nonlinear dynamic parameters and gas sensitivity value of Co - containing PAN films

№	ω (Co), wt.%	$T_1, {}^0C$- t_1, min.	$T_2, {}^0C$- t_2, min.	S (Cl$_2$)	D	D_f	K	λ_r	I
*1**	0	250-5	450-10	0,83	0,344	2,44	1,15	0,0679	0,4668
2	0	250-5	500-2	0,68	1,535	2,41	1,136	0,0277	0,2112
3	0,25	250-5	450-10	0,44	3,718	2,44	1,1330	0,0304	0,1456
4	0,25	250-5	500-2	0,81	1,345 1,137 0,983	2,44	1,1540	0,0423	0,4649
5	0,25	250-5	450-10	0,44	1,433	2,44	1,1334	0,0385	0,2927
6	0,25	250-5	500-2	0,87	1,935 3,894	2,44	1,1487	0,0534	0,6613
7	0,5	250-5	450-10	0,74	1,929	2,48	1,143	0,0303	0,25041
8	0,5	250-5	500-2	0,66	1,228	2,42	1,1217	0,0298	0,2882
9	0,75	250-5	450-10	0,25	1,294	2,47	1,1389	0,0373	0,2794
10	0,75	250-5	500-2	0,14	1,417	2,45	1,1605	0,0721	0,6070
11	0,75	250-5	350-10	0,66	2,760	2,49	1,1739	0,0558	0,6044
12	0,75	250-5	450-5	0,30	1,101	2,44	1,1256	0,0300	0,2545
13	0,75	250-5	500-2	0,23	0,536	2,47	1,1309	0,0610	0,4191
14	1	250-5	450-10	0,09	1,032	2,49	1,1703	0,0309	0,1826
15	1	250-5	500-2	0,13	1,402	2,46	1,1270	0,0371	0,2419

* pre-drying samples (in an oven T = 160 ° C, t = 30 min.)

Nanocomposite materials, whose self-organizing processes are most apparently expressed, show the highest gas-sensitive properties. Processes of self-organizing confirm presence of structures of several correlation dimensions and high AMI values. The parameters of self-organization are dopant concentration and the technological parameters of forming PAN/Co material. Studying of influence of technological parameters on properties of materials will allow to operate process of growth of disordered materials effectively, and also to program the synthesis of materials for micro-and nano-electronics with new unique properties.

1. A.N. Korolev, T.V. Semenistaya, I.S. Al-Hadrami, T.P. Loginova, M.Bruns "Nanocomposite copper-containing polyacrylonitrile films: composition, structure, surface morphology", Advanced Materials, 5, pp. 52 – 56, 2010
2. N.V. Bodyagin, S.P. Vikhrov "Patterns of evolution of technology materials", ISSN 1995-4565. Supplement to the journal "Bulletin RSREU", 4, p.25, 2009
3. N.A. Makeyev, P. Lu, V.A. Iwaniec, T.V. Semenistaya, N.K. Plugotarenko, A.N. Korolev "Prediction of response on nitrogen dioxide of gas-sensitive material based on polyacrylonitrile using methods of the theory of self-organization", Proceedings of the SFU. Engineering, 117, №4, pp. 149 – 156, 2011
4. M. Yablokov, S.A. Zavialov, E.S. Obolonkova "Self-organization of nanoparticles in the formation of palladium metal-polymer coatings", Journal of Physical Chemistry, 73, №2, pp. 219 – 223, 1999

O3-4: Formation of ordered structure of porous silicon in outside the electrodes discharge plasma

M. Novozhenin, V. Kolpakov, V. Podlipnov

Samara State Aerospace University (national research university) Podlipnovvv@ya.ru

In papers [1, 2] great perspectives of off-electrod plasma highvoltage discharge gas in the technology of optical micro-relief are shows, because it is free from such drawback as the effect of load, the need to control a large number of technological parameters of traditional methods of plasma generation. Besides this kind of plasma is widely used in soldering technology semiconductor components, surface cleaning materials, increasing the adhesion of thin films. In this work, preliminary study of the formation of ordered porous structures in silicon using off-electrod plasma is carried out, since the structures of porous silicon have a number of unique properties that make it a promising material for optics and nanophotonics, electronics, as micro-and nanosensors for rapid analysis of the content various chemicals and gases [3].

For research, we used specially prepared samples of monocrystalline silicon, whose surface is oriented along the crystallographic plane (100). On the wafer surface a binary photoresist mask is formed by photolithography with a period of lines 3.5 microns and a height of 700 nm (Fig. 1, a). Parameters control of the resistive mask and the structures obtained after plasma treatment was performed with a scanning electron microscope (SEM) Carl Zeiss Supra 25. After the etching process in off-electrod plasma was micro-relief obtained, which is a triangular projection with height of 250 nm. Etching was performed in the mode of voltage U = 2kV, current I = 150 mA, the working gas pressure in the chamber was maintained at 0,2-0,25 mbar (20-25 Pa). The control parameters of obtained microrelief was conducted using a scanning probe microscope NANOINK, the profile view is shown in Fig. 1 b.
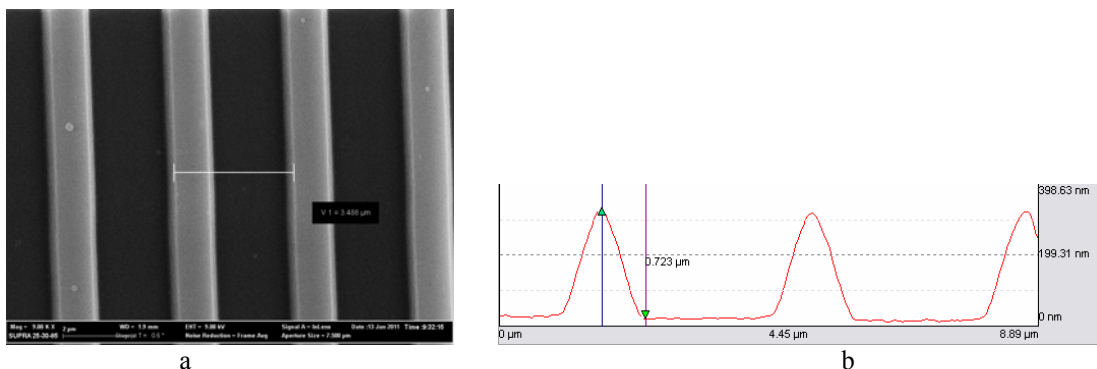
Figure 1. Images of the silicon surface: a - silicon with photoresist mask on the surface;
b - after etching in the off-electrode plasma.

Then the obtained samples were additionally treated in off-electrode plasma for 5 min time in the mode: voltage U = 1,8 kV, current I = 20mA in the medium of working gas mixture CF_4 with O_2. In the course of processing of the microrelief mesopores in silicon were obtained, forming a line with width of 80-nm, 200 nm depth (Fig. 2).

The main mechanism for the formation of these pores is formation of Si^{2+} ions by the electron and the ion stimulating in the strong heterogeneity of the electric field at protrusions of the microrelief. Further formed ions are able to participate in the disproportionation reaction with the formation of secondary silicon, usually amorphous, and Si^{4+} ions forming volatile compounds SiF_4 later in the presence of etching radicals of working gas, these assumptions are also consistent with works [2, 3].

Thus, using the technology of photolithography and etching in off-electrode plasma ordered structures were obtained, which represent the line of porous silicon, without the use of electrolytes and chemical solutions, allowing this technology to be compatible with plasma technology, technology, microelectronics and MEMS technology. The possibility of production of ordered structures of porous silicon is shown, a configuration which can be formed, creating of microelectronics and nanoengineering masking layers of required form by the standard methods.
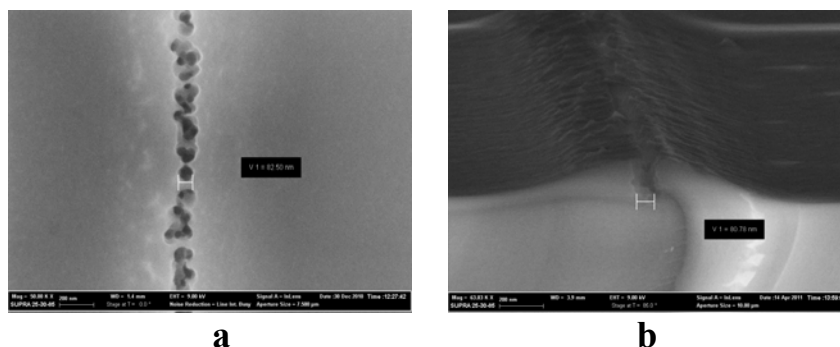
Figure 2. Images of the structures of porous silicon on the SEM: a - 10000 times increase; b - 50000 times increase; c - image cleaved sample.

1. Kazan, N.L., Kolpakov, A.I., Kolpakov, V.A. "Investigation of the features of the anisotropic etching of silicon dioxide in a gas discharge plasma high-voltage type" Microelectronic.– V. 33. No. 3 – P. 218-233. – 2004. – [in Russian].
2. Kazansky, N.L., Kolpakov, V.A. *Formation of an optical micro-relief in off-elektrod plasma high-voltage gas discharge. Monograph* M.: Radio and Communications, 2009. – 220 p. – [in Russian].
3. Goryachev, D.N., Belaykov, L.V., Sreseli, O.M. "On the formation mechanism of porous silicon" Physics and Technology of Semiconductor, V.34, No. 9, P. 1130-1134, 2000 – [in Russian].

O3-5: Formation of fractal porous clusters in silicon

N. A. Arzhanova, A. V. Mozhaev, A. V. Prokaznikov

Yaroslavl Branch of Physical – Technological Institute, Russian Academy of Sciences, Yaroslavl, Russia,
E-mail addres: prokaznikov@mail.ru

In the present time permanent increasing of interest is observed in creation and usage of novel class of materials that are called metamaterials. In these materials a significant role plays theirs artificially created structure rather than chemical composition. The basis of such materials is the substances with modified morphology. The base of such a modification can be anodization processes that result in porous space formation which can be fractal one [1, 2].

In the present work on the base of analysis of experimental and theoretical results [1] it was demonstrated that besides of different regimes of pores formation a special regime takes place which is determined by holes delivery to the place where electrochemical reactions occur in *n*-type silicon under illumination by an external source of light [3]. The basis of this approach is an equation which is obtained by application of underlying equation of continuity neglecting recombination processes:

$$\frac{\partial p}{\partial t} = D_p \frac{\partial^2 p}{\partial x^2} - \mu_p E \frac{\partial p}{\partial x}, \tag{1}$$

where p is holes concentration, D_p is diffusion coefficient of holes, μ_p is a mobility of holes, $E = E^{ext} + E^{clust}$ is a strength of electrical field in cluster which consists of two parts E^{ext} being external field applied and E^{clust} being a field of a cluster. Equation (1) is scaling invariant with respect to the following transformations of spatial and temporal variables: $x' = \lambda^{1/2}x$, $t' = \lambda t$ without an electric field, where λ is dimensionless numerical coefficient. In order to do the solutions of equation (1) being automodelling by applying an electric field one should put some requirements on electric charge transformation. It should transform in accordance with following: $q' = \lambda^{1/2}q$ what results in scaling invariance of electric potential as well as Coulomb forces. The second term in (1) in the case of $q/r = inv$ transforms analogously to the first terms in right and left sides of (1). In this case charge density transforms as $\rho = q/V$, V is a volume where charge is distributed, i.e. it transforms as reciprocal area ($[\rho] = [\lambda]^{1/2}[\lambda]^{-3/2} = [\lambda]^{-1}$). A value that behaves itself such a way is a Gauss curvature K, which is equal to the product of two main curvatures in a given point $K = k_1 \cdot k_2$, so that $[k] = [1/r]$, where r is a curvature radius.
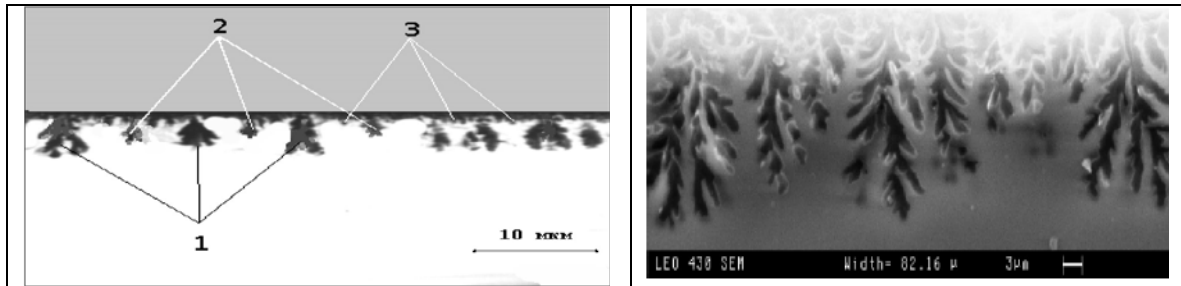
Fig. 1. Photos of cross sections of fractal structures of porous clusters in silicon [4]. Numbers (left) corresponds to self-similar structures of three different scales.

By porous space formation a border between silicon and electrolyte looks like a surface which is vastly bent. It is an equipotential surface in the case of conducting electrolyte (see Fig.1). A charge density such a surface is proportional to the curvature in a given point. Conditions mentioned above are necessary for formation of self-similar fractal porous clusters (see Fig.1).

Motion of particles (holes) in superposition of constant and random fields is governed by external field. The motion was simulated on the base of equations:

$$\frac{d\vec{r}}{dt} = \vec{U}(\vec{r}, t), \quad \vec{r}(t_0) = \vec{r}_0, \tag{2}$$

where $\vec{U}(\vec{r}, t) = \vec{u}_f(\vec{r}, t) + \vec{u}_t(\vec{r}, t)$, $\vec{u}_f(\vec{r}, t)$ is determined component of fields of velocities and $\vec{u}_t(\vec{r}, t)$ is a

random component of fields of velocities, moreover

$$c\vec{u}_f = -\frac{1}{2}c\frac{\partial\phi}{\partial\vec{r}}, \quad \rho\vec{u}_t = -D\frac{\partial\rho}{\partial\vec{r}}, \tag{3}$$

where $\rho \equiv \rho(t,\vec{r})$ is distribution function for charge carriers, D is diffusion coefficient, γ is coefficient which describes a medium resistance, ϕ is a potential of electric field and is obtained from Poison's equation: $\Delta\phi = -4\pi\rho$, $\vec{u}_f = \mu_p\vec{E}$, μ_p is holes mobility, $\vec{E}$ is a strength of an external field. Using continuity conditions in the case of thermolization of holes distribution one obtains an equation which is analogous to Fokker-Plank one:

$$\frac{\partial\rho}{\partial t} = D\frac{\partial^2\rho}{\partial\vec{r}^2} + \frac{1}{\gamma}\frac{\partial\phi}{\partial\vec{r}}\frac{\partial\rho}{\partial\vec{r}}, \tag{4}$$

that is entirely equivalent to (1). New position of particle is determined by equation $\vec{r}(t+\Delta t) = \vec{r}(t) + (\vec{u}_f + \vec{u}_t)\Delta t$, that is a solution of equation (2). Such a procedure with corresponding border conditions was carried out for *2D* and *3D* cases. Silicon crystal has a crystal structure of a diamond type so that a space was divided by cubic cells with corresponding orientations. The motion of holes was described in isotropic approximation of spherical zones with a centre in Γ- point according to electronic structure of silicon. The results of computer calculations in *2D* case are presented on Fig. 2, where the dimensions of fractal clusters are presented.
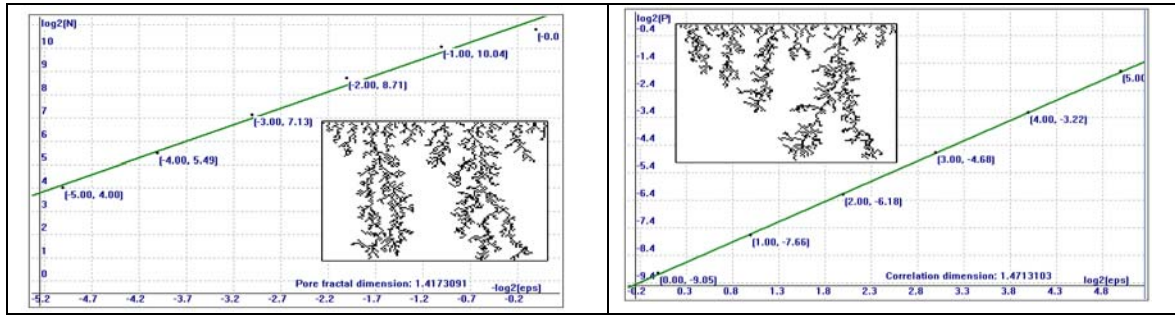
Fig. 2. The results of calculation of fractal D_f = 1.417 (left) and correlation dimensionalities D_{cor} = 1.471 (right) and corresponding fractal structures (inserts).

Thus, by a good enough conductivity of an electrolyte a surface of division with silicon is an equipotential surface. A charge on a surface is distributed proportional to a curvature of this surface. Pores formation processes are determined by participation of holes in corresponding electrochemical reactions and therefore by theirs delivery to the surface of division what is typical for *n*-type silicon [3]. In the case when a contribution of an external electric field does not exceed a contribution from electric field of clusters a fractal structure is formed. Confirmations of this fact are experiments on computer simulations as well as numerous experimental data.

1. E.Yu. Buchin, A.B. Churilov, A.V. Prokaznikov, "Different morphology aspects in n-type porous silicon", Applied Surface Science, **102**, pp.431 – 435, 1996.
2. T. Nichiporuk, V. Lysenko, D. Barbier, "Fractal nature of silicon nanocrystallites", Phys. Rev. B, **71**, 115402, 2005.
3. A.V. Prokaznikov, E.Yu. Buchin, "Controllable formation of porous structures on *n*-type silicon", Phys. Low-Dim. Struct., **5/6**, pp. 47 – 52, 1997.
4. E.Yu. Buchin, A.V. Prokaznikov, "Synchronization effects of microscopic regions during silicon anodization in HF solutions", Phys. Low-Dimen. Structures, **7/8**, pp. 69 – 76, 2003.

O3-6: Variation of the pore morphology for the porous lead selenide layers on silicon substrates

S.P. Zimin[1] , E.S. Gorlachev[1,2] , V.V. Naumov[2] , F.O. Skok[1]

1. Microelectronics Department, Yaroslavl State University, Yaroslavl, Russia, E-mail: zimin@uniyar.ac.ru.
2. Yaroslavl Branch of The Institute of Physics and Technology of Russian Academy of Sciences,Yaroslavl, Russia

One of the most prospective fields of modern day nanotechnology is the fabrication of porous nanostructured materials that can be applied for a wide range of practical applications due to their unique properties, such as the possibility to store nanoinclusions in the pore volume, quantum size effects due to the small dimensions of the interpore material, and many others. While porous silicon is the first and the most-studied porous material, an important growing trend in this field is the reserarch of new compound materials in porous form. Thus, the fabrication of porous IV-VI materials, and in particular lead chalcogenides (PbTe, PbSe, PbS), which are fundamental for the optoelectronics and thermoelectrics, presents an extremely important and prospective scientific and technological challenge. Recently, we were first to demonstrate the pore formation in lead chalcogenide layers and study their properties [1-3]. In this report we will discuss the varied morphological and structural parameters of porous PbSe layers obtained under different conditions.

The experiment was based on a technological approach that allows us to prepare porous lead chalcogenide layers on sillicon wafer substrates with an anodic electrochemical etching treatment using a vertical type electrochemical cell. For the discussed study, the fist batch of the initial epitaxial PbSe films with 3-5.2 μm thickness on $CaF_2/Si(111)$ substrates were anodized using a KOH based electrolyte [2], that was first introduced for PbTe polishing by M. Norr [4]. Scanning electron microscopy (SEM) studies were performed on Supra-40 (Zeiss), chemical energy-dispersive spectroscopy (EDS) microanalysis was carried out simultaneously with SEM using INCA-Energy (Oxford Instruments). As a result, depending on the initial film surface relief and with a variation of etching parameters, porous PbSe layers with island-like morphology and hierarchical mesoporous films (Fig. 1a) were obtained using Norr's electrolyte, as discussed thoroughly in [2].
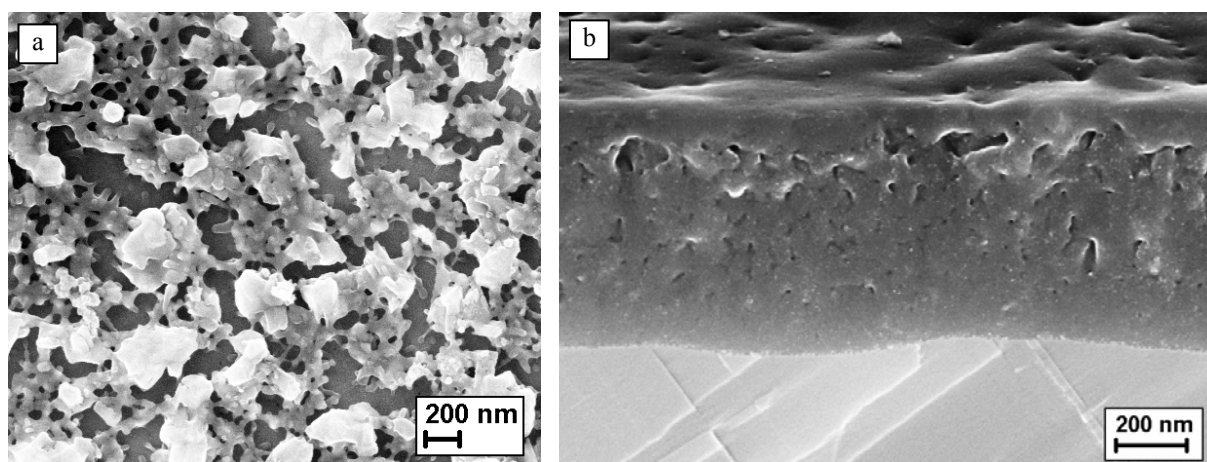
Fig. 1. Scanning electron microscopy images for the porous PbSe layers obtained using potassium hydroxide (a, surface, normal view) and nitric acid and glacial acetic acid (b, cross-section, 70° tilted view) based electrolytes

It became obvious, that the main problem for the results discussed above was the undesirably high etch rate of PbSe that did not allow the formation of a developed thick porous layer. Thus, it was necessary to find a new electrolyte with low-speed electropolishing. We have proposed to use a solution of 10 ml HNO_3, 10 ml glacial (undiluted) acetic acid CH_3COOH, 40 ml glycerol (first used by E.H. Tompkins and G.L. Johnson [4] for the electropolishing of lead selenide at high current densities), for which, by analogy with porous silicon, we reduced the current density (1 mA/cm^2) and processing temperature (20°C). Here, nitric acid is the etching agent and acetic acid is the wetting agent that slows down the material removal. SEM showed that the anodic treatment resulted in the formation of a well-defined porous layer with 750 nm thickness (Fig. 1b), while the thickness of the underlaying unmodified PbSe (3% Sn) film indicated that ~750 nm thick layer

was etched away. The average size of the mesopores was 22 nm with their density on the surface of $\sim 10^{10}$ cm^{-2}. X-ray investigations did not show a formation of any new compounds additionally to the PbSe cubic structure. EDS analysis, however, showed that the stoichiometry of PbSe for the porous layer was strongly modified. The EDS chemical mapping of the elements lead and selenium (which is given in full detail in [5]) showed a high chemical heterogeneity between the porous layer and the underlaying unmodified layer. For the initial film the atomic ratio between Pb and Se atoms on the surface was 0.96, and for the porous layer it became 0.07. We assume that during anodic etching the positive lead ions dissolve into the electrolyte, while the negative selenium ions redeposit on the pore walls. As a result, the matrix remains a monocrystalline PbSe. This conclusion is supported by the SEM images in back-scattered electrons (Fig. 2), which exposed the fact that many of the pores on the surface are obviously closed due to the active redeposition of the products of the electrochemical reactions. More specifically, it showed a darker areas around the pores, which became more profound with the increase of the electron energy, meaning that the yield of the back-scattered electrons for these areas decreases. The reason for that is the increase in the proportion of inelastic collisions of electrons with the sample surface. This is possible if the atoms are not rigidly fixed, i.e. have the ability to move under electron impact. Hence, the electrons will pass such a large amount of energy to atoms, while they themselves will lose it and won't be detected as back-scattered. Therefore, this process indicates the "soft", amorphous regions. We can conclude that for the areas around the pores during anodoc etching the Pb leaves to the electrolyte solution and the amorphous friable Se layer remains.
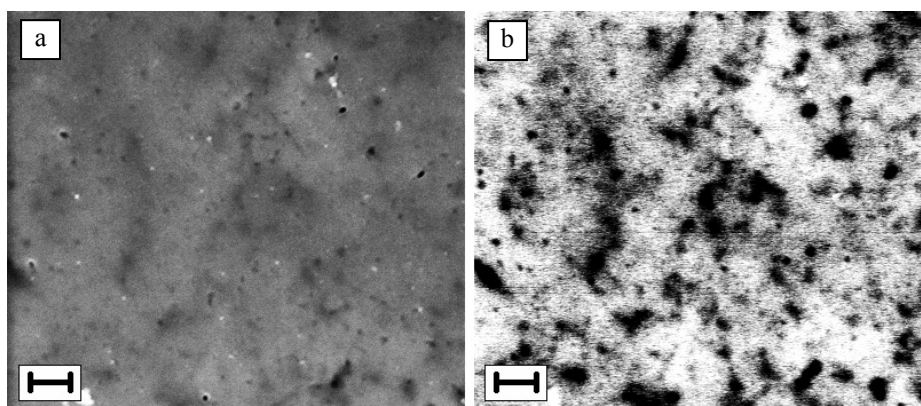
Fig. 2. Scanning electron microscopy image of the surface of the mesoporous PbSe layer (a) and the image in back-scattered electrons with 10 kV bias (b) for the same area. Scale mark is 200 nm

1. S.P. Zimin, E.A. Bogoyavlenskaya, E.Yu. Buchin, A.P. Petrakov, H. Zogg and D. Zimin, "Formation of porous nanostructured lead telluride films by an anodic electrochemical etching method", Semicond. Sci. Technol., 24, pp. 105008-1-6, 2009

2. S.P. Zimin, V.M. Vasin, E.S. Gorlachev, E.Yu. Buchin and V.V. Naumov, "Investigations of PbSe layers after anodic electrochemical etching by scanning electron microscopy", Phys. Stat. Sol. (c), 8, pp. 1918-1922, 2011

3. S.P. Zimin, E.S. Gorlachev, V.V. Naumov, E.Yu. Buchin and H. Zogg H., "Fabrication of porous nanostructured lead chalcogenide semiconductors for modern thermoelectric and optoelectronic applications", J. Phys.: Conf. Ser., 291, pp. 012023-1-6, 2011

4. M.K. Norr. *Polishes and etches for tin telluride, lead sulfide, lead selenide, and lead telluride*. Naval Ordnance Laboratory Report NOLTR 63-156, 1963

5. S.P. Zimin, E.S. Gorlachev, V.V. Naumov and F.O. Skok, "Investigations of the pore formation in the lead selenide films using glacial acetic acid based electrolyte", Materials of the 8th Intern. Conf. "Porous Semiconductors – Science and Technology", Spain, pp. 340-341, 2012

O3-7: Calcium hydroxyapatite (HAp) and methylcellulose (MCel) interaction by their coprecipitation from aqueous solutions in the course of HAp/MCel nanosized biocomposites synthesis

N. Zakharov, M. Sentsov, T. Zakharova

Kurnakov Institute of General and Inorganic Chemistry of the Russian Academy of Science, Moscow, Russian Federation, zakharov@igic.ras.ru

Structure of calcium hydroxyapatite $Ca_{10}(PO_4)_6(OH)_2$ (HAp) is similar to that of the human bones inorganic component, thus HAp is used in medicine as bone implant material. However, in spite of its biocompatibility, osteoconductivity and osteoinductivity, pure HAp cannot be used under high loading conditions due to its high fragility and insufficient mechanical strength. In some cases the problem of obtaining materials with satisfactory mechanical properties can be solved by development of composite materials (CM) based on calcium phosphates (CPH) and different polymers, which could function under high stress conditions. In the meantime, the improvement of the HAp based biomaterials' mechanical characteristics is still the problem of high interest.

Since natural bone tissue is a composite material based on nanosized rod-like HAp and collagen fibres there were different attempts to reinforce HAp with various fibrous polymers such as chitosan, collagen, polylactic acid etc. In this area great attention is payed to biopolymers due to their biocompatibility. Methylcellulose ($[C_6H_7O_2(OH)_{3-x}(OCH_3)_x]_n$ MCel) is an ether of cellulose –one of the most common biopolymers in nature. In the current work nanosized HAp and HAp/MCel composite materials were synthesized and analysed.

HAp was synthesized by coprecipitation from water solution in the system $Ca(OH)_2$–H_3PO_4–H_2O at 37°C (ratio Ca/P = 1,67). Composite materials were obtained from a similar system (with addition of biopolymer) under similar conditions. Composition and structure of the composites and HAp crystallographic characteristics and sizes of HAp nanoparticles were determined by XRD analysis, FTIR spectroscopy, scanning and transmission electron microscopy and electron diffraction method.
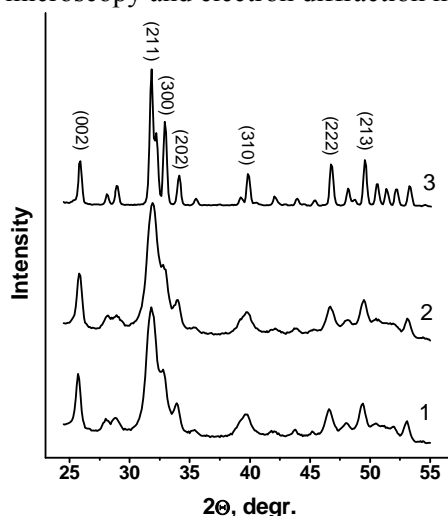
Figure 1. XRD patterns of HAp (1), HAp/MCel composite material (2) and calcined HAp (3)

Figure 1 shows XRD patterns of HAp, HAp/MCel composite material and calcined HAp. According to the XRD data HAp nanoparticles with sizes about 40 nm lengthwise and 20 nm across were obtained. All the peaks on XRD patterns of HAp and HAp/MCel samples are similar to those of the reference HAp. That means that MCel macromolecules do not alter the HAp structure.

FTIR spectra (diffuse reflection) of HAp and HAp/MCel composites (Fig. 2) show that products based on stoichiometric HAp were synthesized. Specific reflection bands relative to HAp were observed for all the samples obtained. For both the pure HAp and composite materials with the biopolymer FTIR spectra show OH group bands (3570 cm^{-1}) as well as valent (1090, 1034, 962 cm^{-1}) and bending (605, 565, 472 cm^{-1}) PO_4 group bands. The bands at 1489, 1420 и 875 cm^{-1} could be

associated with CO$_3$ groups which replace OH and PO$_4$ groups of HAp during its synthesis.
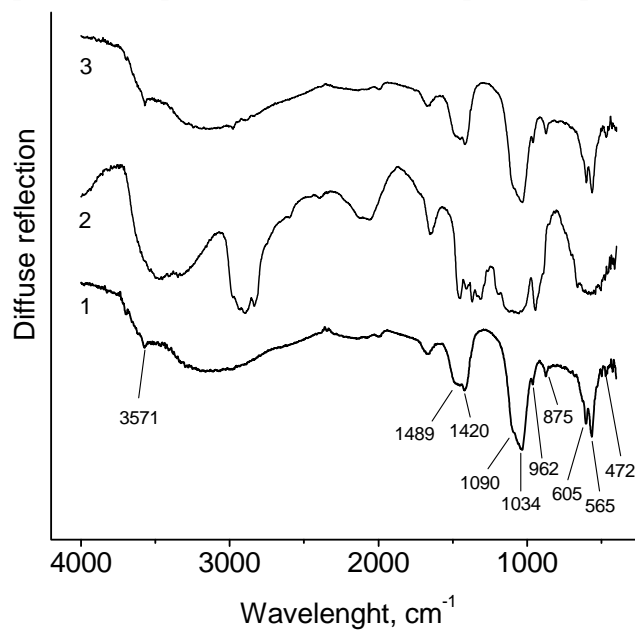
Figure 2. FTIR spectra of HAp (1), HAp/MCel composite material (3) and MCel (2)

O3-8: New Generation of Lithium-ion Batteries: Role of Nanostructured Materials

T. Kulova, A. Skundin

Frumkin Institute of Physical Chemistry and Electrochemistry, Russian Academy of Sciences, Moscow, Russia,
e-mail: askundin@mail.ru

Chemical power sources and their place in human activities. Modern rechargeable batteries. The brief history of lithium-ion batteries. Basic concepts of lithium-ion batteries. Power and maintenance characteristics of lithium-ion batteries. Ragone plots. Lithium-ion batteries as a foundation of modern portable electronic devices. Chemistry of today's batteries. Advantages and disadvantages of the batteries-of-today

Goals and ways of progress: enhancement of energy density, increase in rate capability, cost reduction, safety increase, scaling up.

Advanced electrochemical systems for lithium-ion batteries. Review of electrode materials. Negative electrode: alternatives to carbon. Positive electrode: alternatives to lithiated oxides of cobalt and manganese.

Silicon as the best choice for negative electrodes. The main problem in silicon electrodes functioning: giant expansion at lithium insertion. Thin amorphous films and nanomaterials. Nanocomposites "silicon/carbon". Technological aspects of silicon electrodes manufacturing. Different techniques for thin films application (physical vapor deposition, chemical vapor deposition, rf magnetron sputtering, pulsed laser deposition, electron beam evaporation, others) and for nanocomposites manufacture (pyrolysis or chemical/thermal vapor deposition, ball milling or mechanically milling, combination of pyrolysis/CVD/TVD and mechanical milling, chemical reaction of gels, others). The performances of thin-film and composite electrodes. Cycle-life and degradation mechanisms.

Advanced positive electrodes. The nearest challenge: lithium iron phosphate. Charge-discharge behavior. The main problem: very low conductivity. Nanomaterials with nanocoating. Partial doping of iron phosphate.

Cardinal solution: vanadium oxides instead of iron phosphate. Crystal instability at deep discharges. Nanomaterials based on vanadium pentoxide − xerogels, nanotubes, whiskers, composites.

O3-9: Structure, composition distribution and properties of the (Ga,Mn)Sb/GaAs and MnSb/GaAs heterosystems

Yu.A. Danilov[1], M.V. Dorokhin[1], A.V. Kudrin[1], O.V. Vikhrova[1], B.N. Zvonkov[1], A.I. Bobrov[2], V.S. Dunaev[2], E.D. Pavlova[2], E.A. Pitirimova[2], S.M. Plankina[2], R.R. Yakubov[2], M.N. Drozdov[3], Yu.N. Drozdov[3], A.I. Suchkov[4]

1. Physico-Technical Research Institute of University of Nizhni Novgorod, Nizhni Novgorod, Russia. E-mail addres: danilov@nifti.unn.ru. 2. Physics Department of University of Nizhni Novgorod, Nizhni Novgorod, Russia. 3. Institute for Physics of Microstructures, Russian Academy of Sciences, Nizhni Novgorod, Russia. 4. Institute of High-Purity Substances, Russian Academy of Sciences, Nizhni Novgorod, Russia.

The GaSb semiconductor, which forms the basis of infra-red optoelectronic devices [1], is in particular of great interest for spintronic applications. However, ferromagnetic semiconductors of (III,Mn)Sb type and methods for their fabrication are poorly understood. In context of spintronic applications also attractive are the binary compounds MnB^V, which have high Curie temperature (in particular, T_C = 587 K for MnSb).

In this work, the properties of the (Ga,Mn)Sb semiconductor and MnSb magnetic half-metal compound layers grown by laser deposition were investigated. Process was performed at depressed pressure ($\approx$ 50 torr) in a hydrogen flow. *i*-GaAs wafers with (001) orientation were used as substrates. The (Ga,Mn)Sb layers were deposited by alternate sputtering of Mn and undoped GaSb targets by Nd:YAG laser pulses (λ = 1.06 μm). The substrate temperature was T_g = 300 and 400°C. The quantity of introduced manganese controlled by targets sputtering time ratio and characterized by a parameter $Y_{Mn} = t_{Mn}/(t_{Mn}+t_{GaSb})$, where t_{Mn} and t_{GaSb} are a time of Mn and semiconductor targets sputtering, respectively. The layers were about 100 nm thick. The Y_{Mn} parameter was varied in range of 0 – 0.5. The layers of MnSb were grown also on *i*-GaAs substrates by the method of alternating laser ablation of solid Mn and Sb targets. The parameter $Y_{Mn} = t_{Mn}/(t_{Mn}+t_{Sb})$ was varied in range 0.33 – 0.83. The MnSb layers were grown at T_g =300°C.

We used a lot of techniques for study of properties of the (Ga,Mn)Sb/GaAs and MnSb/GaAs heterostructures. In the X-ray diffraction curves corresponding to $\Theta/2\Theta$ scanning (Fig.1), there are peaks related to the (002) reflections from the GaAs substrate ($\approx$ 31.6°) and GaSb layer ($\approx$ 29.2°). The system of these two peaks changes negligibly with increasing Mn concentration (curves 2 and 3 in Fig. 1), though a slight shift of the peak from GaMnSb toward higher angles is observed, which corresponds to a decrease in the lattice parameter of a layer. This correlates with the data reported in [2]. The X-ray diffraction data also showed that GaMnSb layers grow epitaxially at both 400 and 300°C.

The SIMS analysis of the elemental concentration profiles across the (Ga,Mn)Sb layers revealed considerable arsenic diffusion from the substrate to the layer at nonzero Mn concentrations and Mn diffusion into the substrate during the growth process. It leads the formation of a thin epitaxial $Ga_{1-x}Mn_xSb_{1-y}As_y$ layer near the nominal (Ga,Mn)As/GaAs interface. The last-named feature was confirmed by cross-section TEM investigations for the (Ga,Mn)Sb/GaAs heterostructure. Besides the thin transition layer we observed the formation of GaMn inclusions in slightly Mn doped GaSb matrix.

In the Raman scattering spectra for a GaSb layer without doping with Mn (T_g = 400°C), there is a predominant peak at 235.9 cm^{-1} that corresponds to the longitudinal optical (LO) phonon (curve 1 in Fig. 2). Doping with manganese leads to a monotonic decrease in the intensity of the LO peak and an increase in the intensity of the TO peak (curves 2–4 in Fig. 2), which is qualitatively consistent with the enhancement of disordering, according to the XRD data.

The electrical properties of the (Ga,Mn)Sb layers were investigated in the temperature range T = 10– 300 K. An undoped GaSb layer (Y_{Mn} = 0) exhibited hole conductivity (the acceptor behavior is typical of native point defects in GaSb) with concentration and mobility of $1.6 \cdot 10^{17}$ cm^{-3} and 220 cm^2/(V s), respectively. All the (Ga,Mn)Sb layers also exhibited hole conductivity over the entire temperature range. As Y_{Mn} increased, the carrier concentration grew as a consequence of the acceptor character of the Mn impurity. For layers grown at T_g = 400°C, the rise of Y_{Mn} from 0.06 to 0.5 leads to an increase in hole concentration from $1.5 \cdot 10^{19}$ to $2.9 \cdot 10^{20}$ cm^{-3}. Studies of the Hall effect show that the dependence of Hall resistance R_H on magnetic field H upon the doping of layers with Mn atoms is nonlinear. At a sufficiently high Mn content ($Y_{Mn} \geq 0.33$), the $R_H(H)$ dependence contains a hysteresis loop with saturation in a magnetic field over 2000 Oe. For (Ga,Mn)Sb layers grown at T_g = 400°C, a hysteresis loop is observed in the $R_H(H)$ dependence up to room temperature. A feature of the anomalous Hall effect in the (Ga,Mn)Sb layers is that the sign of the term

corresponding to the anomalous Hall effect in the $R_H(H)$ dependence can either coincide with the sign of the term corresponding to the normal Hall effect or be opposite to it, depending on the (Ga,Mn)Sb growth parameters (Fig.3). In addition, the sign of the term responsible for the anomalous Hall effect can change with temperature.
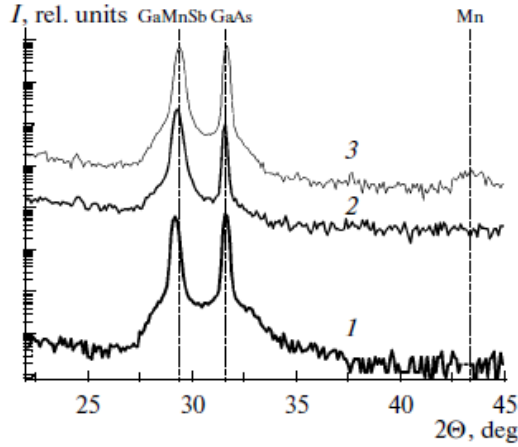
Fig.1. X-ray diffraction spectra ((002) reflection) for (1) the GaSb/GaAs structure and (2) (Ga,Mn)Sb/GaAs structures with $Y_{Mn} = 0.2$ and (3) 0.33.
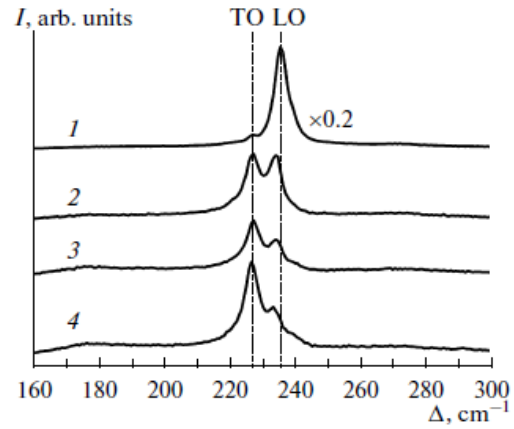
Fig.2. Raman scattering spectra of (1) GaSb and (Ga,Mn)Sb layers with Mn contents (2) $Y_{Mn} = 0.2$, (3) 0.33, and (4) 0.5, grown at $T_g = 400°C$.

Cross-section TEM analysis of MnSb/GaAs heterosystem revealed that the MnSb layers are not uniform in thickness, contain numerous grains (in sizes up to ~ 50 nm), incorporating the atoms of Mn, Sb, Ga, and As in variable compositions. The investigations of Hall effect revealed that MnSb layers are ferromagnetic in temperature range from 10 K to at least 300 K. The magnetic field dependence of Hall resistance at all temperatures had clear ferromagnetic hysteresis shape. In Fig.4 the $R_H(H)$ dependence is shown for MnSb layer with two value of Y_{Mn} (dependences were obtained at 300 K). It is clear that the sign of anomalous Hall effect depends on Mn content in the layers.
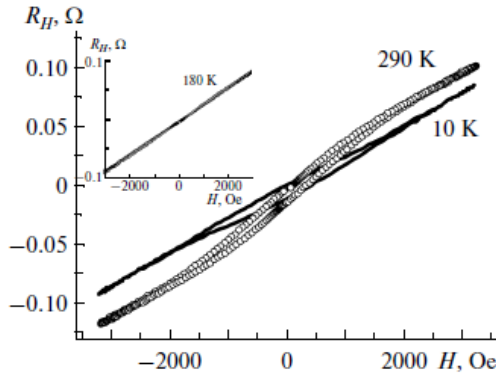
Fig.3. Magnetic field dependences of the Hall resistance at 10 and 290 K for (Ga,Mn)Sb layer with $Y_{Mn} = 0.5$. The insert shows the $R_H(H)$ dependence at 180 K.
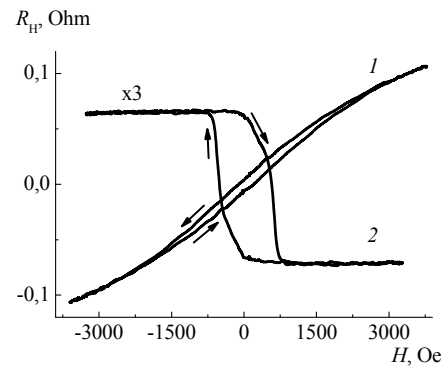
Fig.4. Magnetic field dependences of R_H at 300 K for (1) MnSb/GaAs structure with $Y_{Mn} = 0.5$, $T_g = 200°C$ and (2) MnSb/GaAs structure with $Y_{Mn} = 0.83$, $T_g = 200°C$.

In summary, we can assert that the (Ga,Mn)Sb grown by laser deposition are crystal, but not single-phase, ferromagnetic semiconductor that can be used as a spin injector in spintronic devices. The MnSb layers are also ferromagnetic; the conditions of their formation should be optimized.

1. P.S. Dutta, H.L. Bhat, V. Kumar, "The physics and technology of gallium antimonide: An emerging optoelectronic material", J. Appl. Phys., **81**, pp.5821-5870, 1997
2. K. Ganesan, H.L. Bhat, "Magnetic and magnetotransport properties of diluted magnetic semiconductor (Ga,Mn)Sb crystals", J. Supercond. Novel Magn., **21**, pp.391-397, 2008

O3-10: Structure and properties of ZnSSe nanostructures embedded into nanoporous Al$_2$O$_3$ films

R. Valeev[1,2], A. Beltukov[1,2], V.Mukhgalin[1], E. Romanov[2], A. Eliseev[3]

1.Physical-Technical Institute of Ural Branch of Russian Academy of Sciences, Izhevsk, Russia, fti@fti.udm.ru
2.Udmurtia State University, Izhevsk, Russia, ftt@uni.udm.ru 3.Material Sciences Faculty of Lomonosov's Moscow State University, Moscow, Russia

Semiconductor nanostructures in dielectric matrixes are of current interest due to absorption and luminescent properties improved in comparison to thin films of materials [1, 2]. In nanocrystals, the surface-to-volume ratio is considerably large, therefore there is a high contribution of surface in the luminescence properties. The unsaturated bonds on the surface create band-gap states that can easily capture the excited electrons and holes and relax the energy in non-radiative ways [3]. In addition, matrix isolation allows to protect nanostructures from external influences.

ZnSSe films are interesting because by choosing the composition of the ternary compound there is a possibility of controlled changing of band gap value, which led to the development of band gap engineering. Early was shown that the value of E_g in ZnSSe can be described by the formula [4]:

$$E_g = 2.77 + 0.21x + 0.6x^2 \qquad (1)$$

were x is the concentration of sulfur in the compound.

The work is focused on development of formation of ordered ZnSSe nanostructures in nanoporous alumina oxide films used as the dielectric matrix. The proposed method is based on thermal deposition of material into the nanopores of highly-ordered anodic alumina films. Obtained ZnSSe/AAO composites were study by SEM, XRD, XPS, UV-VIS, luminescent and Raman spectroscopy methods in comparison with ZnSSe thin films. SEM studies shown that the semiconductor crystallized in cubic structure and fill AAO nanoporous. Chemical composition was controlled by XPS method. The samples exhibit luminescence in a visible region depending on chemical composition of ZnSSe.

1. S. Vijayalakshmi, H. Grebe, Z. Iqbal and C.W. White, "Artificial dielectrics: Nonlinear properties of Si nanoclusters formed by ion implantation in SiO$_2$ glassy matrix", J. Appl. Phys., **84**, p.6502, 1998

2. P. Persans, T. Hayes and L. Lurio, "Size-dependent composition of semiconductor nanoparticles in glass", J. Non Cryst. Solids, **349**, pp.315-318, 2004

3. N. Taghavinia and T. Yao, "ZnS nanocrystals embedded in SiO$_2$ matrix", Physica E, **21**, pp.96-102, 2004

4. A. Ben Fredj, M. Debbichi and M. Said, "Influence of the composition fluctuation and the disorder on the bowing band gap in semiconductor materials", Microelectronics Journal, **38**, pp.860-870, 2007

O3-11: Nano-porous silicon produced by helium plasma immersion ion implantation as a material for photovoltaic applications

A. Rogozhin and A. Miakonkikh and K. Rudenko

Institute of Physics and Technology, Russian Academy of Sciences, Moscow, Russia, rogozhin@ftian.ru

As known high dose He-implantation can dramatically affect Si properties. Basically it changes crystalline structure of silicon producing layers of amorphous, nanoporous, disordered and defected silicon. Among others the optical properties of the semiconductor can be considerably changed. Because of direct band structure of nano-porous Si and its higher band gap energy (~1.8eV) [1] amorphized Si:He (a-Si:He) could be more attractive for optical applications like photo detectors and solar cells.

Plasma immersion ion implantation (PIII) has a number of advantages compared with beam-line implantation. It allows to achieve doses up to 10^{17}cm^{-2} in time of several seconds, has scalability up to 500 mm and produce implantation of high conformity which is important for structures with complicated surface design. The structures a-Si:He/c-Si had electroluminescence spectrum within the wavelength range 400-800 nm [2], which covers about 80% of energy of solar radiation spectrum. This raises interest to investigation of a-Si:He/Si structures solar cell application.

In this study a structure made by PIII of He$^+$ into boron-doped p-type Si(100) with resistivity of 12 Ohm·cm is presented. Formation process consisted of cleaning wafers, implantation, thermal annealing, and deposition of back contact and transparent top contact.

The layer of native SiO$_2$ was removed by HF:H$_2$O (6:50) preliminary rinsing for 5 min. He+ energy in implantation process varied from 1 to 5 keV. It produced Si amorphization for depth of about 100-200 nm. Implanted ion doses was in the range $5 \cdot 10^{16}$-$2 \cdot 10^{17}$cm^{-2}, which forms layer of nano-porous silicon. Thickness of modified layer was calculated in a free software TRIM and measured by spectral ellipsometry. After annealing at 600ºC for 60 min the semi-transparent gold layer (~200Å) for photo-current collection was deposited. Top Ni electrode was formed by magnetron sputtering through mask with subsequent annealing. Area of transparent section of the devices was equal to 0.5cm^2.

Electrical characteristics of these devices was measured and analyzed. Dark current-voltage and capacitance-voltage characteristics were measured. As it was estimated from the assumed energy band structures the devices shows diode-type characteristics with relatively high reverse current (~100 uA/cm^2 at −10 Volts). Light characteristics were obtained under radiation of the 20W-halogen lamp at constant energy flux, showing photovoltaic effect. The ways for optimization of photovoltaic parameters has been targeted.

1. F.P. Romstad, E. Veje, "Experimental determination of the electrical band-gap energy of porous silicon and the band offsets at the porous silicon/crystalline silicon heterojunction", Phys. Rev. B, **V. 55**, pp. 5220-5225, 1997.

2. P. R. Desautels, M. P. Bradley, J. T. Steenkamp, and J. Mantyka, "Electroluminescence in plasma ion implanted silicon," Phys. Status Solidi (a), **V. 206**, pp. 985-988, 2009.

O3-12: Study on water adsorption on oxygen passivated silicon nanoparticles

R. Fedyuk

Far Eastern Federal University, Vladivostok, Russia, roman44@yandex.ru

Synthesis and characterization of silicon (Si) nanoparticles (NPs) is triggered by the observation of strong emission in the visible region from porous silicon. Variety of methods has been adopted to prepare Si NPs. These include electrochemical etching, ion implantation, laser ablation and gas phase decomposition of silane. Solution chemistry routes have been attractive due to the control on both, the size and surface chemistry. It has been well demonstrated that the emission wavelength from these NPs can be controlled by the size of NPs since the quantum confinement plays an important role in the electron energy state distribution of these NPs. Si NPs are recognized as potential candidates for light emitting devices and photo pump tunable lasers. Although, initial focus was on hydrogen terminated Si NPs, later it was shifted on various terminations to further functionalize the surfaces. This was needed since the envisaged application required the NPs to be selective in the surface reactivity. Thus, proper choice of capping agent can make Si NPs biocompatible, stable against photobleaching and can have high photoluminescence quantum efficiency. Thus these can be used as to monitor living cells *in-vivo* by tracking the luminescence from the NPs bioconjugate to target species. Also porous Si NPs can carry a drug payload and the intrinsic near-infrared photoluminescence property enables monitoring of both accumulation and degradation *in-vivo*. The feasibility of oral delivery of Si-based NPs by means of *in-vitro* cellular responses and interactions, as well as in *in-vivo* biodistribution, stability, and safety is also proved recently. These NPs are strong candidates for replacing fluorescent dyes in biological assays. Such applications require tailored functionalization of NPs surface. Further, its reaction with water molecules is of importance in biofluid environments. It is known that water can be adsorbed on SiO, and SiO_2 surfaces in various forms. This involves formation of various silanol groups leading to different forms of adsorption. Hence, the oxidation at the surface of Si NPs is an important means for studying interaction of such surfaces with water. The NPs with oxidized surfaces are likely to provide better stability.

In single electron transistors (SET), the device consists of such NPs which are surrounded by oxide. Also the surface passivated NPs, when subjected to the atmosphere, can lead to partial oxidation. Thus, effect of oxygen and corresponding limitations need to be understood for Si NPs. Effect of oxidation of Si crystallites of size less than 2 nm in porous silicon has been shown that they reveal a red shift on oxidation. This was explained on the basis of defect states being introduced by Si=O configurations at the surface. In another study, Si NPs were coated with siloxanes, involving Si–O–Si surface bonding, terminated into alkenes.23 In all these cases, the interaction with water has not been mentioned or is of no significance.

In the present work we have prepared oxygen passivated siloxane like bonded Si NPs. These NPs of size less than 2 nm show strong absorption around 265 and 1400 nm. Photoluminescence is observed at 325 nm. Clearly the optical behavior of oxidized particles in porous silicon of the same size is different than the NPs obtained in our case. Further, these tend to form larger clusters capable of holding water molecules.

This affects the optical behavior. We have characterized these particles with X-ray diffraction (XRD), transmission electron microscopy (TEM), environmental scanning electron microscopy (ESEM), scanning tunneling microscopy (STM), atomic force microscopy (AFM), and Fourier transform infrared spectroscopy (FTIR). The water adsorption is studied using temperature dependent FTIR and STM measurements as described below.

Si NPs passivated with oxygen (O) were synthesized by adapting the method suggested by Tilley et al. In Ref. [1] the purpose was to obtain 1-heptene capping on Si. The preparation route is slightly modified to obtain oxygen capping. This method is based on inverse micelle (water-in-oil) formation. Toluene is used as a solvent and tetraoctylammonium bromide (TOAB) is dispersed in it forming micelle cores. The cores are hydrophilic. Anhydrous ionic salt $SiCl_4$ is injected in the micelle solution which dissolves in hydrophilic cores. The Si NPs are nucleated in the cores and grow. Size is limited by the micelle core diameter. The Si is however in the oxidation state Si(IV). Anhydrous lithium aluminium hydride ($LiAlH_4$ is used to reduce this oxidation state to Si(0). In this process, the Si NPs are formed with some H on the surface. If this solution is exposed to air without reduction then SiO_2 is formed. Hence step of controlled reduction is important. We have observed that by varying the ratio of $SiCl_4:LiAlH_4$ it is possible to cap Si NPs with oxygen. In Ref. [1],

the molecular ratio is 1:1. By decreasing the amount of $LiAlH_4$ and exposing the solution to air, oxygen capping is obtained. We have used 2:1 ratio for most of the Si NPs reported here. Thus we obtain oxygen capped Si NPs. The Si NPs were isolated from the reaction solution by centrifugation and dried in vacuum. The measurements were carried out by dispersing Si NPs in methanol in the presence of relative humidity between 40 to 50%.

Phase as well as average size of NPs was determined by using X-ray diffraction (XRD). XRD measurements were performed on Bruker D8 advance powder X-ray diffractometer, with an incident radiation of Cu K_α ($\lambda=1,5402\ \mathring{A}$). Transmission electron microscopic (TEM) measurements were carried out using a Philips CM200 microscope operating at 200 kV. These Si NPs were deposited on the carbon coated copper grid for the TEM image and electron diffraction pattern. Environmental scanning electron microscopy (E-SEM) measurements were carried out using FEI Quanta operating at 30 kV and with 850 Pa pressure, along with energy dispersive X-ray analysis.

Optical absorption spectra were measured on JASCO V-670 spectrophotometer. For photoluminescence (PL) studies, Perkin Elmer LS55 spectrophotometer was used.

In-situ IR spectra of the samples (15 mm x 10 mm x 0,4 mm thick) were recorded in transmission mode at temperatures from 25 to 105 ^{o}C, using a JASCO 610 FTIR spectrophotometer equipped with a DTGS detector. An indigenously developed stainless steel cell fitted with water cooled CaF_2 windows and with a provision of heating of the sample under vacuum or in a gas flow was employed for this purpose. Normally 300 scans were collected for each spectrum at a resolution of 4 cm^{-1}.

This shows that the particle size distribution is homogeneous. Electron diffraction pattern of these NPs reveals the diffraction rings corresponding to (1 1 1), (2 1 1), and (2 2 0) lattice planes of cubic diamond structure of Si (JCPDS # 27-1402). The Si bond length calculated from electron diffraction measurements is 2,33±0,01 Å which is short compared to the bulk value. The comparison between O passivated Si NPs and bulk values indicate that the NPs are in compressed state. Hence the diffraction pattern confirms presence of core Si clusters. Thus, we have obtained Si clusters with fourfold co-ordination core. The FTIR spectrum is presented in Figure 3. Si–O–Si asymmetric stretching mode is located at 1097 cm^{-1}. It also exhibits contribution in the range of 3200 to 3500 cm^{-1} which is due to OH related vibrational frequencies. Existence of OH at 3400 cm^{-1} indicates presence of water in the sample at room temperature (RT) [3].

In the present case, Si NPs along with some encapsulating molecules are enveloped with O. X-ray photoelectron spectroscopy (XPS) was employed to determine stoichiometry of Si and O in NPs (not shown here). In order to calculate the amount of O present over the surface of Si NPs, the ratio of intensity of Si $2p$ in SiO_2 to Si is determined. The ratio is calculated using the method given by Yang et al.[5] Oxygen content is around 40% of the total mass in Si NPs. Thus, the large fractions of particles are covered with O. Above results indicate that fourfold Si cores are covered with mainy oxygen and to some extent with OH and methyl groups.

In conclusion, Si NPs capped with oxygen are formed using chemical route method show water adsorption. These NPs show strong absorption at 265 nm along with one at longer wavelength of 1400 nm and an emission at 320 nm. When coated on Si surface a temperature dependent surface opacity is observed within a range of 30 to 100 ^{o}C. This is due to the water adsorption of Si NPs which tends to form agglomerates and appears as nanopores. The agglomerates are of 200 nm while the NPs are of 1,0 ± 0,3 nm in diameter. The optical inspection and STM measurements show reversible adsorption–desorption of water with temperature [4].

1.R. D. Tilley, J. H. Warner, K. Yamamoto, I. Matsui, and H. Fujimori*, Chem. Commun. 1833 (2005), DOI:10.1039/B416069J.*
2. J. P. Wilcoxon, G. A. Samara, and P. N. Provencio, *Phys. Rev.B60, 2704 (1999).*
3. B. D. Cullity, *Elements of X-ray Diffraction, Addison-Wesley (1978).*
4. M. Arold, F. Piuzzi, C. Jager, and F. Huisken*, Chem. Phys. Lett. 484, 100 (2010).*
5. D. Q. Yang, J. N. Gillet, M. Meunier, and E. Sacher*, J. Appl. Phys.97, 024303 (2005).*

O3-13: Mechanism of microtribometric interaction of semiconductor wafers in assessment of surface cleanliness

V. Kolpakov[1,2], N. Ivliev[1,2], D. Novomeiskiy[2]

1. Image Processing Systems Institute of the RAS, Samara, Russia. 2. Samara State Aerospace University (national research university), Samara, Russia, e-mail: ivlievn@gmail.com

One of the set of technology processes to improve the quality of the microrelief diffractive optical elements (DOEs) manufactured by vacuum-plasma methods and techniques of lithography, is a control of the concentration of organic contaminants on the surface of materials [1].

In this paper a method for rapid assessment of surface cleanliness on the basis of tribometric interaction of substrates is proposed. The method provides the possibility of determining the coefficient of sliding friction to estimate the concentration of surface contamination in the range of $10^{-7} - 10^{-10}$ g/cm^2, which corresponds to the technologically clean surfaces used in the manufacture of optical microrelief.

Substrate surface which is necessary to measure the degree of contamination, is placed at an angle to the horizon (α), and a substrate-probe at an angle to studied substrate (β), thereby forming the driving force and a point contact with certain characteristics.

Disadvantage of rapid monitoring, as described in [1], is the lack of physical and mathematical model of quantifying determination the concentration of the adsorbate.

In this work an analytic dependence coefficient of friction on the number of adsorbed atoms due to the presence of dangling bonds on the surface of the substrate is defined. If there are two acceptor surface electronic states (SES) in a single point of contact semiconductor, the formation of stable chemical bonds will be possible. [2]. From the standpoint of the theory of first-order reaction the rate of formation of chemical bonds, depending on the number of atoms that interact, is [3]:

$$\frac{dN_b}{dt} = fN_aW , \qquad (1)$$

where f – oscillation frequency of atoms; N_a – number of interacting atoms, W – probability of chemical bonds formation.

Based on the theory of adhesive friction [4] and (1), the coefficient of friction is determined from the relation:

$$\mu = \frac{(N_s - N_{ad})WE_b}{Nd} , \qquad (2)$$

where E_b – adhesion energy; d – length of the elementary slip; N – ground reaction force; N_s – common number of surface atoms; N_{ad} – number of adsorbed atoms.

Thus, the experimental determination of coefficient of sliding friction at elementary movement acts allows to determine accordingly to number of bonds the number of atoms neutralizing the active centers of SESs and preventing the formation of covalent bonds between the matrix surface atoms.

1. N.L. Kazanskiy, S.V. Karpeev, V.A. Kolpakov, S.V. Krichevsky, N.A. Ivliev, "Interaction of dielectric substrates in the course of tribometric assessment of the surface cleanliness", Optical Memory and Neural Networks. V.17, 1, pp.37-42, 2008.
2. N.S. Maslova, V.I. Panov, "Scanning tunneling microscopy of atomic structure, electronic properties and surface chemical reactions", UFN. V.157, 1, pp.185-195, 1989.
3. V.A. Kolpakov, "The mechanism of adhesion in metal-insulator structures after the bombing of a stream of charged particles", Physics and chemistry of materials processing. 5, pp. 13–19, 2006.
4. G.V. Dedkov, "Adhesion mechanism of friction in nanotribocontacts" Technical Physics Letters. V.24, 19, 44-50, 1998.

O3-14: Particle trapping in various materials under low energy plasma irradiation.

A. Ayrapetov, L. Begrambekov, A. Gordeev, A. Grunin, A. Yevsin, V. Ermakov, A. Mischenko, Ya. Sadovskiy, A.Kuzmin, A. Kapleuski, P. Shigin.

National Research Nuclear University MEPhI, Moscow, Russia, lexxair@plasma.mephil.ru

The paper discusses conditions and mechanisms of trapping and retention of low energy hydrogen particles in solids that would not be able to penetrate into the bulk only due to their kinetic energy. Retention of gases was measured using thermodesorption spectrometry.

This phenomenon was proposed to be named "potential" trapping (trapping by means of "potential" mechanism), and, accordingly, trapping due to kinetic energy of bombarding particles is named "kinetic" trapping (trapping be means of "kinetic" mechanism) [1].

"Potential" mechanism takes place when trapping is supported by potential interaction energy of impinging particles with the surface and is realized when, for example, non-elastic collisions of atoms and ions with the surface occur or non-elastic interaction of sorbed molecules with the surface is stimulated by bombarding ions, atoms or electrons.

This type of trapping was observed on graphite materials [1-2] and metals (stainless steel and zirconium)[3]. In all cases there was a "slightly conductive" layer on the surface of the sample, which was ion modified and eroded layer in case of graphite materials and surface oxide layer in case of stainless steel and zirconium.

Experimentally found potential trapping regularities are:
1. Potential trapping occurs when the surface is irradiated with hydrogen atoms or any components of hydrogen plasma (ions, atoms or electrons).
2. Not only low energy bombarding atoms but also atoms, sorbed on the surface in form of hydrogen-containing molecules (H_2, H_2O) are trapped.
3. "Potential" trapping is observed in a broad irradiation hydrogen ions energy range.
4. In case of low energy ($E_i \leq 200$ eV) hydrogen ions most part of the trapping is due to "potential" trapping.
5. Hydrogen atoms that penetrate the surface by "potential" mechanism could be trapped in already existing traps (structural defects, grain boundaries, dislocation centers, pores etc.) and also in traps that are formed by high energy irradiating particles in the ion stopping range.
6. "Potential" trapping increases with irradiation time. Total trapping was found to be higher when graphite sample was irradiated with the same fluence but lower flux and accordingly increased irradiation time.
7. "Potential" trapping of hydrogen atoms from hydrogen containing molecules on the surface occurs when the surface is irradiated with oxygen or noble gas ions.
8. Oxygen ion irradiation stimulates hydrogen trapping from hydrogen containing molecules sorbed on the surface.

1 A. Airapetov, L. Begrambekov, C. Brosset, J.P. Gunn, C. Grisolia, A. Kuzmin, T. Loarer, M. Lipa, P. Monier-Garbet, P. Shigin, E. Tsitrone, A. Zakharov, Journal of Nuclear Materials, Volumes 390-391, 2009, Pages 589-592

2 A. Airapetov, L. Begrambekov,S. Vergazov, A. Kuzmin, V. Smirnov, P. Shigin, Bulletin of the Russian Academy of Sciences: Physics, 2010, V. 74, № 2, Pages. 227-232.

3 A. Airapetov, L. Begrambekov, S. Brémond, D. Douai, A. Kuzmin, Ya. Sadovsky, P. Shigin, S. Vergasov, Journal of Nuclear Materials, Volume 415, Issue 1, Pages S1042-S1045

O3-15: The investigation of hydrogen sorption-desorption process by carbon material with content of carbon nanotubes

L.Gulidova, A.Lider, A. Zherlicyn, V.Shiyan

Institute of Physics and Technology, Tomsk Polytechnic University, Tomsk, Russia, l_gulidova@sibmail.com

As a result of energy resources depletion and problems of environmental pollution hydrogen has been recognized as an ideal fuel because it has specific properties. As high-performance and ecological energy carrier it has big perspectives for general using in power engineering, particularly as fuel for transports. The using of hydrogen economy is based on three important aspects of using hydrogen as the fuel for our energy needs, namely production, storage and transportation. One of the general problems is lack of effective methods of storage and transportation of hydrogen. At this time no one method of storage meets the demands of storage system [1]. Recently carbon materials, in particular, carbon nanotubes, have been regarded as reservoirs for hydrogen storage. In the recent decade these materials have been very popular and different laboratories have published experimental results of sorption capacity [2, 3, 4]. The studying of all peculiarities of sorption and desorption of hydrogen by carbon nanotubes is important for science.

The superfine carbon material synthesis method was created in Institute of Physics and Technology of Tomsk Polytechnic University [5]. The peculiarity of this method is combination of metal catalysts and influence of microwave field on the catalysts and methane. Scientists used the flow reactor of waveguide type. As catalysts are used metals Ni, Fe, Mo, Ti. The material produced by conversion of natural gas has different modifications of carbon as nanotubes, nanofibres, onion-particles, microcrystals of graphite and amorphous carbon. The content of nanotubes in the final product is not more than 70%. The received material was chemically treated against impurities (other modifications of carbon) and metallic catalysts.

The samples of carbon material were researched with the help of transmission microscope. It allows detecting nanotubes with diameters from 50 to 150 nm (fig.1). Different modifications of carbon in the samples were detected with the help of diffractometer Shimadzu XRD-6000. The sample of carbon material produced by conversion of natural gas consists of 55% MCNTs, 38% ONIONs and amorphous carbon.
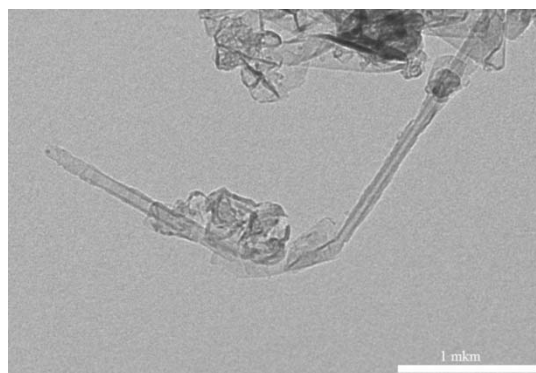
Fig.1 Transmission micrograph of carbon material

The Advanced Materials Corporation's Gas Reaction Controller was used for measuring the sorption of hydrogen by carbon materials. The samples were used in compressed state. The carbon materials were hydrogen saturated with the temperature 243K and 300 K and the pressure of the hydrogen 0-8atm.
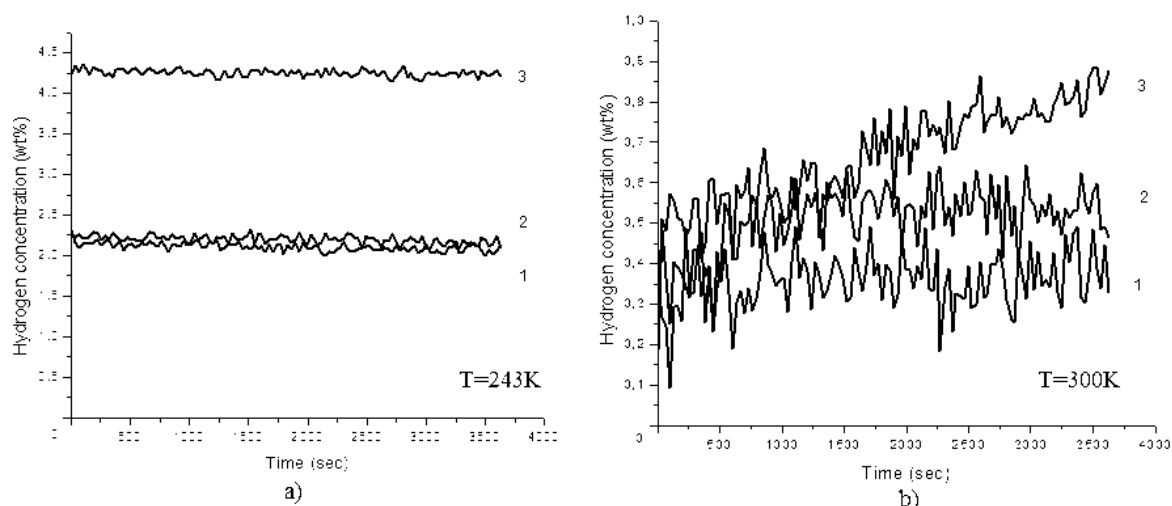
Fig.2. Concentration-time sorption diagram with low (a) and room (b) temperatures
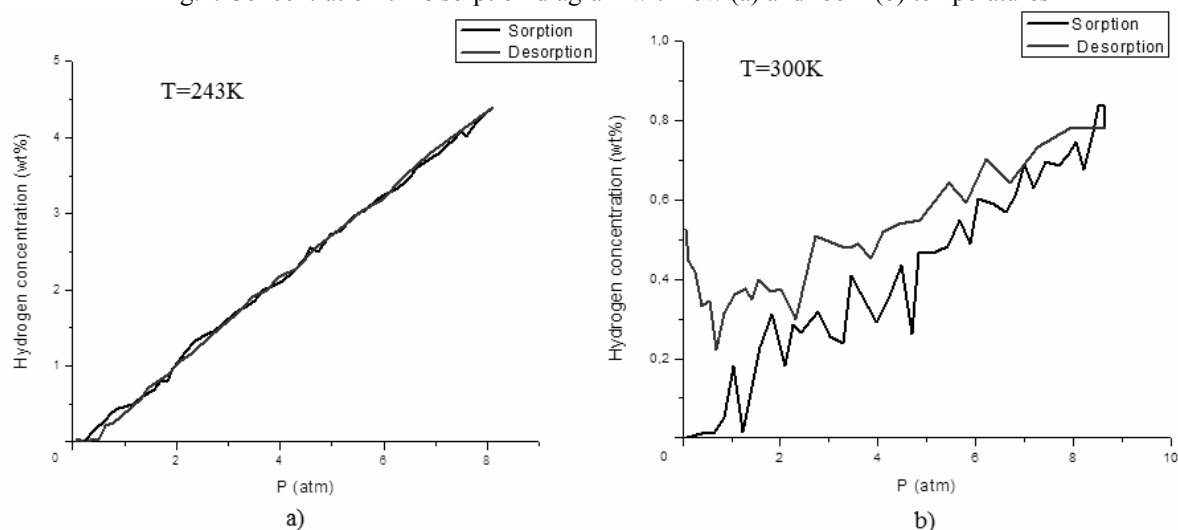
Fig.3. Concentration-pressure sorption diagram with low (a) and room (b) temperatures

Hydrogen concentration grows with cycles of sorption (fig.2). Hydrogen concentration by room temperature is more than five times less than by low temperature (fig.3). The maximum hydrogen sorption capacity of carbon materials is more 4 wt% by high pressure and low temperature. All this results prove high efficiency of using the carbon material, which produced by conversion of natural gas, as a hydrogen sorbent.

1. Елецкий А.В. "Углеродные нанотрубки", Успехи физических наук, 167, 9с., 1997.
2. Yuda Yurum, Alpay Taralp, T. Nejat Veziroglu, "Storage of hydrogen in nanostructured carbon materials", International journal of hydrogen energy, 34, 15 p., 2009.
3. Chang Liu, Hui-Ming Cheng, "Carbon nanotubes for clean energy application", J. Appl. Phys., 38, p.22, 2005.
4. Тарасов Б.П., Гольдшлегер Н.Ф, "Сорбция водорода углеродными наноструктурами", Альтернативная энергетика и экология, 3, с.20-38, 2002.
5. Жерлицын А.Г., Шиян В.П., Медведев Ю.В., Галанов С.И., Сидорова О.И. "Получение углеродного наноматериала и водорода из природного газа под действием СВЧ-излучения", Известия вузов. Физика, 10, с.280-284, 2007.

O3-16: Changes of surface layers composition, surface morphology and mechanical properties of carbon steel due to various parameters of ion irradiation

P.V. Bykov, V.L. Vorob'ev, V.Ya. Bayankin

Physical-Technical Institute of the Ural Branch of the Russian Academy of Sciences, Izhevsk, Russia
E-mail: less@fti.udm.ru

One of the trends in modern mechanical engineering is the surface strengthening of moderately cheep steels and alloys for making parts of machines and mechanisms operating under severe conditions. This provides a saving in costly high doped steels and alloys and makes products cheaper. One of the currently evolving methods is the ion- beam and ion-plasma doping of the surface. By choosing purposefully a doping element and irradiation conditions one can provide a vide range of useful properties of surface layers of materials: rise in limits of strength and leakage, toughness, cracking resistance, resistance to corrosion and wear resistance, etc. [1, 2]. Methods of ion and ion-plasma treatment by high-current beams are widely used and studied [3]. But in a number of cases the use of the intensive ion or ion-plasma treatment causes degradation of properties of the base material because of high temperatures at which this action is realized.

The ion implantation, while increasing the concentration of structural defects of the subsurface layer, promotes the increase of resistance to the movement of dislocations that is one of the mechanisms of an increase of fatigue strength [4]. On the other hand, irradiation of the surface with ions of chemically active elements may give rise to fine-disperse inclusions of new phases which provide higher mechanical properties at the cost of the disperse strengthening of the surface layer [5].

The influence of pulse beaming with Ar and N ions upon the fatigue strength of carbon steel St.3 is studied. Energy of ions is 20 keV, irradiation dose is 10^{18} ion/cm^2, ion current density varies from 10 to 40 mkA/cm^2. Non-monotonous dependency of microhardness and fatigue strength from ion current density and flattening of surface under irradiation is shown.

1. E.V. Legostaeva and Yu.P. Sharkeev, "Lows and mechanisms of wear of ferrite-pearlite steel implanted by molybdenum ions", Trenie Iznos, 23/5, pp.529-536, 2002. (in Russian).
2. N.V. Pleshivtzev and E.A. Krasikov, "Protection of metals, alloys, and steels by ion bombardment (survey)", Metally, №4, pp.98-129, 1995. (in Russian).
3. A.N. Didenko, et al., "Physico-chemical state of surface layers and functional properties of alloy VT18U that has been subjected to the action of a powerful ion beam", Fiz. Khim. Odrab. Mater., №5, pp.14-23, 1991. (in Russian).
4. F.F. Komarov, *The Ion Implantation into Metals*, Metallurgy, Moscow, 1990. (in Russian).
5. T.D. Radzhabov and A.S. Bagdasarjan, "Variation of surface micro-hardness and wear resistance of titanium alloy as a result of ion nitration", Poverkhnost'. Fiz., Khim., Mechanica, №11, pp.104-111, 1986. (in Russian).

O3-17: Nanomaker-the means of electron lithography for ultimate resolution

B. N. Gaifullin[1], I. S. Stepanov[1], S. I. Zaitsev[2], A. A. Svintsov[2]

1. Interface Ltd, Moscow, Russia,
2. IMT RAS, Chernogolovka, Russia, e-mail: zaitsev@iptm.ru

The two key and non-breaking technologies:
-electron-beam lithography (for making masks) and
-optical lithography (for mass, industrial production with the use of the masks) constitute the basis of modern micro-and nano-electronics. However, electron-beam lithography is certainly more important, because it is universal. It is used in mass production, not only for mass making, but also directly in the production of limited-edition products. In addition, advanced research and development are made using only the electron-beam lithography. In this case the electron-beam lithography provides the major means of nanostructuring and due to its versatility is significantly ahead of other well-known lithography, for example, ion-beam lithography or lithography based on scanning probes.

Electron-beam lithography allows structuring with the utmost accuracy of 5-10nm in the squares above 100h100mm2.

The report will focus on describing the achievements of electron-beam lithography of ultimate resolution achieved in IPTM Academy of Sciences. In particular, the hardware-software system NanoMaker (www.nanomaker.com) will be presented. The basic physical and instrumentation limitations such as proximity effect, static and dynamic distortions of electron columns with a focused electron beam leading to a decrease in the accuracy of electron-beam lithography will be discribed. The technical solutions implemented in NanoMaker for compensation and correction of the sources for accuracy and resolution losses in modern electron lithography will be presented. One of the important achievements is the system's ability to provide NanoMaker writing in a large field with a good steaching without the use of expensive laser table. Features of NanoMaker will be compared with similar systems capabilities that are available on the market. Examples of using electron-beam lithography with high resolution will be shown
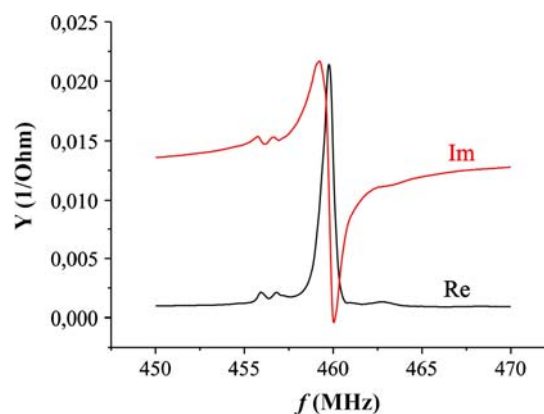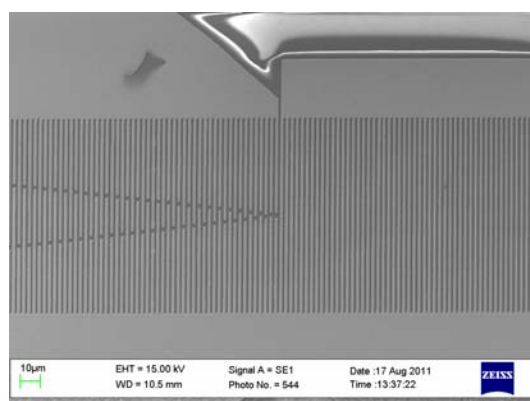
Fig.1 An example of MEMS device to be used as high-temperature wireless temperature sensor in aggressive environments; left the apodized interdigital transducer (IDTs) created by electron lithography, right, a narrow resonance the amplitude - frequency characteristics of apodized SAW resonator shows its high operational properties. From DV Roshchupkin, DV Irzhak, O. Plotitsyna, RR Fahrtdinov, EV Emelin, INVESTIGATION OF STRUCTURAL PERFECTION AND ACOUSTIC PROPERTIES OF PIEZOELECTRIC CRYSTAL CA3TAGA3SI2O14, preprint, 2011.
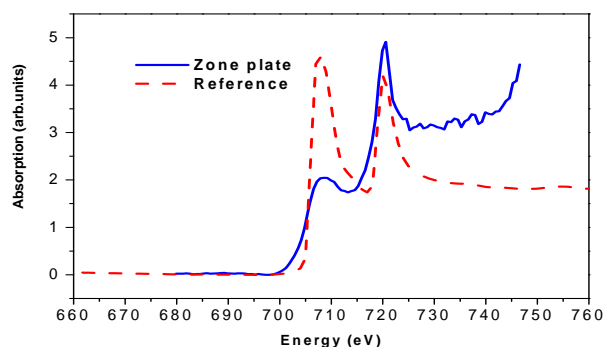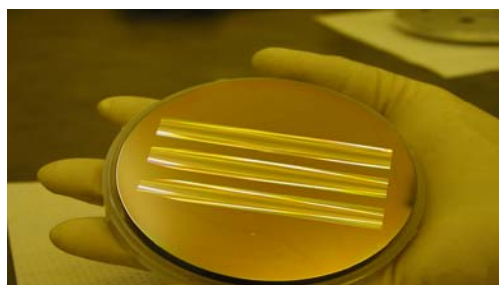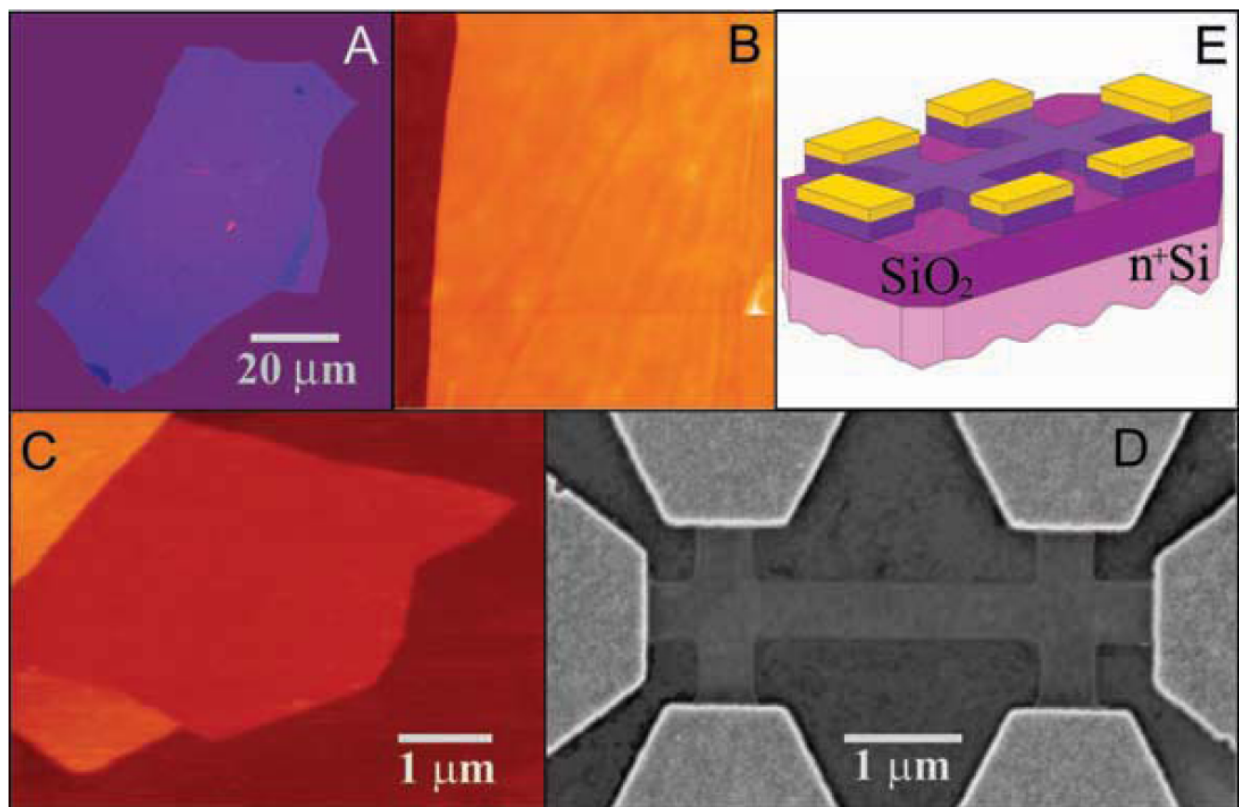
P2-1: Electric current mechanics in reverse-biased p-i-n- structures under strong electrical field

V.S. Kuznetsov, P.A.Kuznetsov

Yaroslavl State University, Yaroslavl, E-mail: vskuzn@uniyar.ac.ru

Investigations of electric current mechanics under strong electrical field are of theoretical and working significance. Although there are a lot of publications on this topic, still we don't have general consensus. In this abstract we investigate generation-recombination influence on electrical current and generation of spatio-temporal structures.

Assume there is an impurity with concentration N in i- region of p-i-n- structures. Impurity fulfills the function of generation and recombination centers. These centers can be in two states: neutral state (concentration N^0) and the one charged negotively (concentration N^-).

Current density vector is a sum of two components: first component is parallel to i-p boundary; second component is perpendicular to this boundary (OZ direction). In OZ direction we will neglect diffusion current, because of the i- region's thinness and because voltage value is close to breakdown voltage: $j_{nz} = ev_n n$ and $j_{pz} = ev_p p$, e- absolute elementary electron charge value, v_n and v_p – electron and hole saturation velocity. Current density components parallel to the boundary have both field and diffusion parts and usually are:

$$j_{n\square} = e\mu_n(n\vec{E}_\square + \frac{kT}{e}\nabla_\square n), j_{p\square} = e\mu_p(p\vec{E}_\square + \frac{kT}{e}\nabla_\square p).$$

Here μ_n and μ_p − electron and hole motilities, $\vec{E}_\square$ − electrical field component, which is parallel to i-p boundary, k – Boltzmann constant, T − temperature.

Continuity equation for n-, p-, N- concentrations:

$$\frac{\partial n}{\partial t} - \frac{1}{e}\nabla \cdot \vec{j}_n = \varphi_n,$$

$$\frac{\partial p}{\partial t} + \frac{1}{e}\nabla \cdot \vec{j}_p = \varphi_n - \varphi_-,$$

$$\frac{\partial N^-}{\partial t} = \varphi_-.$$

(1)

φ_n and φ_- − generation-recombination rates:

$$\phi_n = \gamma - \alpha np + \gamma_{1n}vn + \gamma_{1p}vn + \left[s_2 N_c N^- - s_1 n\left(N - N^-\right)\right];$$

$$\phi_- = \left[s_4 N_v\left(N - N^-\right) - s_3 pN^-\right] + \left[s_1 n\left(N - N^-\right) - s_2 N_c N^-\right],$$

where N_c and N_v - effective density of states in conduction and valence bands, respectively, γ, α - band-to band generation and recombination coefficients. s_1, s_2 are conduction band impurity center emissions and capture coefficients. s_3, s_4 are valence band impurity center emissions and capture coefficients, and $N^0 = N - N^-$.

The solution of the differential equation system (1) was found in [1] for a stationary state. Dimensionless coordinates were introduced (marked with $'$) with x which is a new dimensionless variable which characterizes an electronic component of the current, i.e. $j'_{nz} = (0,5 - x)(j'_{nz} + j'_{pz})$. In these designations:

$$x(z') = x_1 \frac{x(0)Ch(kz') - x_1 Sh(kz')}{x_1 Ch(kz') - x(0)Sh(kz')}$$

(2)

where $k = x_1 j_z' \dfrac{2 + j_z' + N'}{2 + j_z'}$ and $x_1^2 = \dfrac{\left(j_z' + 2\right)\left(j_z'^2 + \left(N' - 4\gamma_1'\right)j_z' - 4\gamma_0' - 2N'\right)}{4 j_z'^2 \left(2 + j_z' + N'\right)}$, $j_z' = j_{nz}' + j_{pz}'$. $x(0)$

substitution at the first boundary $z' = 0$ and $x(-w)$ at the other one $z' = -w$ in (2) will make an equation for current-voltage characteristics. The Fig. 1 shows different dependence j_z' from E_z (V/cm) for
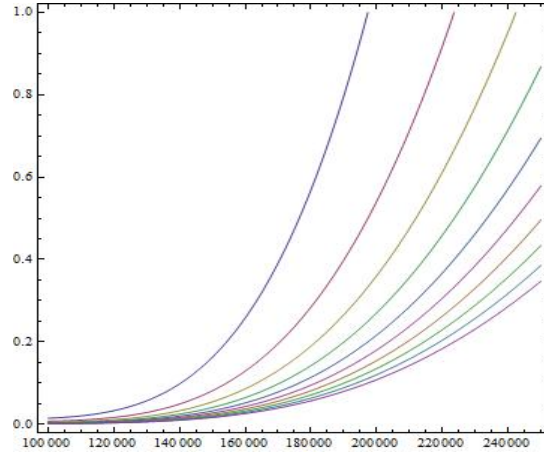
Fig.1. Current-voltage characteristic j_z' from E_z V/cm

$x(0) = 0,1$ and $x(-w) = 0,1$; $0,09$; $0,08$; $0,07$; $0,06$; $0,05$; $0,04$; $0,03$; $0,02$; $0,01$; 0. The upper curve describes $x(-w) = 0,1$ and the lower one $x(-w) = 0$. Crystal inhomogeneity leads to huge numbers of regions with different $x(0)$ and $x(-w)$ values, therefore multiple current-voltage characteristics can be obtained for simple structures. Under weak field conditions these characteristics do not differ much but in strong electrical fields slight changes in the current can lead to great voltage jumps. This accounts for microplasma phenomena observed in experiments. Current inhomogeneity leads to the generation of spatio-temporal structures and hysteresis.

1. В.С. Кузнецов, П.А. Кузнецов, "Пространственная самоорганизация свободных носителей тока в электрических полях", Вестник ЯрГУ. Серия Естественные и технические науки. № 1. pp. 29–34, 2011
2. Ю.А. Астров, "Токовые структуры в Si(Zn)", ФТП, том 27, № 11/12, pp. 1971-1989, 1993; Ю.А. Астров, С.А. Хореев, "Исследование структуры токовых нитей в Si(Zn)", ФТП, том 27, № 11/12, с. 1024-2029, 1993

P2-2: Geometric constraints of orbital entanglement production in normal conductors

S. Rodríguez-Pérez and M. Novaes

Departamento de Física, Universidade Federal de São Carlos, São Carlos, SP, 13565-905, Brazil, E-mail: sigmund_r_p@yahoo.com

Quantum entanglement has been one of the most intriguing phenomenon predicted by quantum mechanics. Because of its essential role in new emergent technologies like quantum computation and quantum cryptography [1], as well as its own fundamental nature, physicists from many areas have concentrated their efforts trying to understand how entanglement can be produced, manipulated, and detected in real physical systems. With this aim in mind, many solid-state devices were studied in the last decade, in the context of quantum transport phenomena. In particular, it was realized that carriers can be entangled after scattering processes, even without a direct interaction between them [2].

In principle, any normal conductor may orbitally entangle the scattered state of two incident carriers, if a left-right bipartition is established. Based on this idea, a chaotic quantum dot built from a two-dimensional electron gas in a semiconductor heterojunction was proposed as quantum entangler [3]. In this system, the outgoing state of two scattered electrons can be expressed as the superposition of three components,

$$\left|\Psi_{\text{scat}}\right\rangle = \left|\Psi_{\text{LL}}\right\rangle + \left|\Psi_{\text{RR}}\right\rangle + \left|\Psi_{\text{LR}}\right\rangle \qquad (1)$$

Two of them are separable, corresponding to both electrons being scattered to the left or to the right. The other component, $\left|\Psi_{\text{LR}}\right\rangle$, may be no separable and represents the state of one electron being scattered to the left and the other one to the right. Its degree of entanglement can be measured by the concurrence C. The average value and variance of C were considered first, and later its probability distribution was found [3, 4, 5].

In this work [6], we investigate the entanglement production in a generic normal conductor, connected to two single-channel left leads and two single-channel right leads. We consider the joint statistics of the number of entangled pairs produced during a given time and the amount of entanglement carried by them. We find a constraint which implies that more entangled states are less likely to be detected. Namely, if N is the norm of $\left|\Psi_{\text{LR}}\right\rangle$, then production occurs only if

$$N(1+C) < 1. \qquad (2)$$

For the particular case of a chaotic quantum dot working as quantum entangler, we obtain explicit expressions for the joint distribution of C and N, both for systems with and without time-reversal symmetry.

1. M. A. Nielsen and I. L. Chuang. *Quantum Computation and Quantum Information.* Cambridge University Press, Cambridge, 2000

2. C. W. J. Beenakker, C. Emary, M. Kindermann, and J. L. van Velsen, "Proposal for Production and Detection of Entangled Electron-Hole Pairs in a Degenerate Electron Gas", Phys. Rev. Lett., 91, pp.147901, 2003

3. C. W. J. Beenakker, M. Kindermann, C. M. Marcus, and A. Yacoby, *Fundamental Problems of Mesoscopic Physics,* edited by I. V. Lerner, B. L. Altshuler, and Y. Gefen, NATO Science Series II Vol. 154, Kluwer, Dordrecht, 2004

4. V. A. Gopar and D. Frustaglia, "Statistics of orbital entanglement production in quantum-chaotic dots", Phys. Rev. B, 77, pp.153403, 2008

5. F. A. G. Almeida and A. M. C. Souza, "Statistics of orbital entanglement production in a chaotic quantum dot with nonideal contacts", Phys. Rev. B, 82, pp.115422, 2010

6. The results presented in this work were submitted to Physical Review B

P2-3: Molecular dynamics simulations of energy and impact angle of incidence of ions on the ion-plasma sputtering of copper

A.N. Kupriyanov, O.C.Trushin, I.I. Amirov

Yaroslavl branch of the Institute за Physics and Technology of Russian Academy of Science, Yaroslavl, Russia. ildamirov@yandex.ru

The possibility of ordered nanostructures on the surface of materials in the processes of ion and ion-plasma sputtering causes of great interest to them [1]. Such structures are usually formed at certain angles of incidence of ions. Modelling of these processes is an integral part of the research aimed to development of the technology of surface nanostructuring. In contrast to traditional monoenergetic ion sputtering an ion-plasma sputtering is characterized by wide distribution of energies of the incident ions. In addition, the ion flow is characterized by a certain angular distribution.

In this paper molecular dynamics (MD) simulation was used to study the sputtering of copper by low energy argon ions (E_i <200 eV). MD simulation was done using home made computer code (IMPACT) with numerical algorithm Leap-frog [2] with a time step of 10^{-15} s. The substrate is modeled by a single crystal of copper with orientation of surface FCC (100) consisting of 6000 atoms. Interatomic forces were modeled by generalized form of the Lennard-Jones potentials [2].
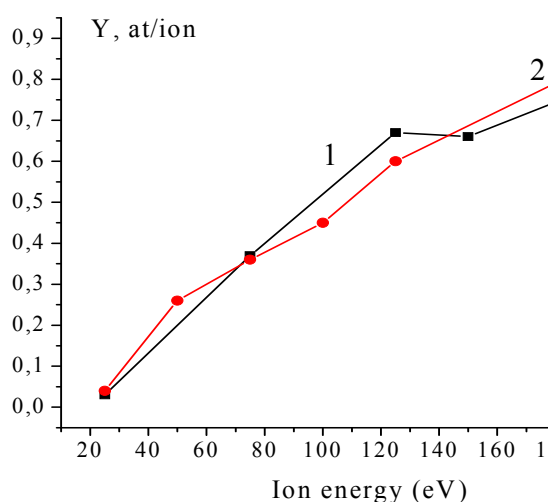
Figure 1. The dependence of the yield of the Cu atoms per ion on impact energy of the incident ions at σ; 1 – 0; 2 - 2 degrees.
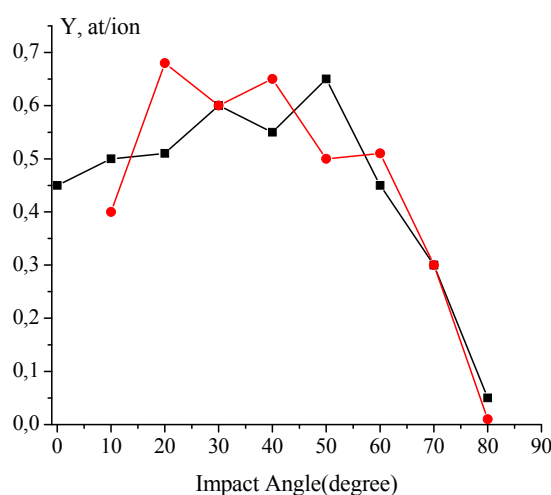
Figure 2. The dependence of the yield of the Cu atoms per ion on the angle of incidence ions with equal σ, 1 – 0; 2 - 2 degrees.

The simulation showed that the dependences of the yield of Cu atoms sputtering per ion (Fig. 1) on impact energy and the angle of incidence of the ions (Fig. 2) are in satisfactory agreement with experimental data [3,4]. A small angular deviation of the ion flux is not affected by this dependence.

1. Y.-M. Chang, S.R. Jian, J.-Y. Juang. Nanogrids and Beehive-Like Nanostructures Formed by Plasma Etching the Self-Organized SiGe Islands, Nanoscale Res. Lett. 5, pp.1456–1463, 2010
2. В.Экштайн. Компьютерное моделирование взаимодействия частиц с поверхностью твердого тела. М.: Мир, 1995
3. http://www.npl.co.uk/nanosciencesurface-nanoanalysis/ products-and-services/sputter-yield-values
4. D. Kress, D. E. Hanson, A. F. Voter, C. L. Liu, X.-Y. Liu, and D. G. Coronell, Molecular dynamics simulation of Cu and Ar ion sputtering of Cu (111) surfaces, J. Vac. Sci. Technol. A 17, pp. 2819-2827, 1999

P2-4: Surface alloying during Pd/Cu(100) deposition

O.S. Trushin[1], T. Ala-Nissila[2], S.C. Ying[3], and E.Granato[4]

[1] *Institute of Physics and Technology of Russian Academy of Sciences, Yaroslavl Branch, Yaroslavl, Russia,*
otrushin@gmail.com
[2]*Department of Applied Physics and COMP CoE, Aalto University School of Science, Espoo, Finland*
[3]*Department of Physics, Brown University, Providence, USA*
[4]*Laboratrorio Associado de Sensores e Materiais, Instituto National de Pesquisas Espaciais, Sao Jose dos Campos,*
SP, Brazil

Alloy formation during thin film growth is of interest for fundamental science and technological applications. In some cases surface alloying is an undesireable phenomenon when a sharp interface between layers is needed. However, it can be important mechanism for obtaining surfaces with unique properties, such as for creating catalytic systems.

Thin film growth in many cases is a nonequilibrium process. The growing structure is the result of competition between thermodynamic and kinetic factors, in particular in the case of energetic deposition, where adatoms land on the surface with a considerable amount of kinetic energy (typically in the range 1-100 eV). Such energies promote exchange processes on the surface, where an adatom exchanges position with a substrate atom. This phenomenon makes it possible to create surface alloys in systems immiscible in the bulk [1].

In this work we study this phenomenon on the Pd/Cu(100) system using Molecular Dynamics and Molecular Static simulations. Our model comprises an atomic slab with fcc(100) geometry. There are ten atomic layers of the substrate with 400 atoms in each layer. Periodic boundary conditions are applied in the plane parallel to the surface. Two bottom layers of the substrate are fixed to simulate a semi-infinite substrate and to prevent the system from moving as a whole. Interatomic forces are modeled by Embedded Atom Method potentials [2].

First we performed numerical estimates of the energy barrier corresponding to exchange diffusion process using the Nudged Elastic Band method [3]. In Fig. 1 we show atomic configurations for the initial and final states of the exchange process, and the corresponding energy profile along the minimal energy path.

| A | B | C |
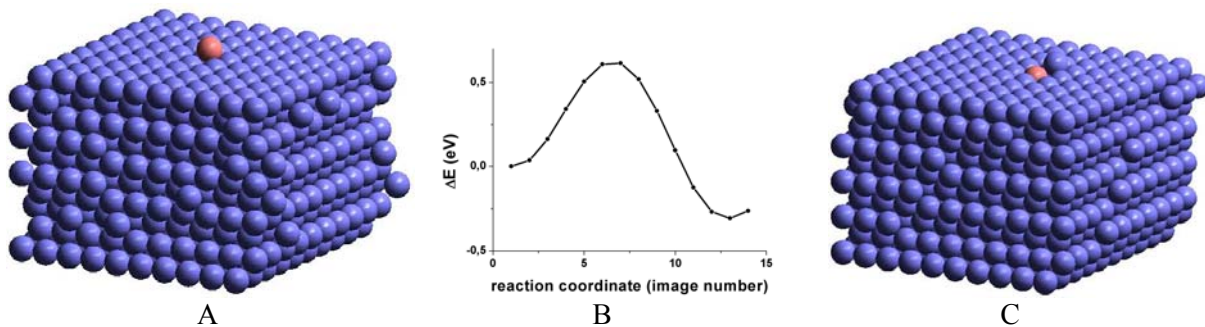
Fig. 1 Exchange process on the surface: A,C: Initial and final states; B: Energy profile along the minimal energy path for the exchange process.

The results show that the energy barrier for a single atom exchange process is equal to 0.62 eV, and the final state (where the Pd atom is buried inside the Cu substrate) is lower in energy than the initial state. This means that alloying is energetically favorable for this system. However, the high energy barrier for this process creates a strict kinetic limitation for alloy formation. Taking into account this consideration we performed the second set of simulations. We used standard MD simulations with the NVT ensemble to estimate the probability of a Pd adatom landing on the Cu(100) surface with different kinetic energies to exchange positions with substrate atoms (impact activated exchange). In Fig. 2 we show a map of exchange events on the fcc(100) surface (A), and dependence of the probability to exchange on the kinetic energy of the atom deposited.
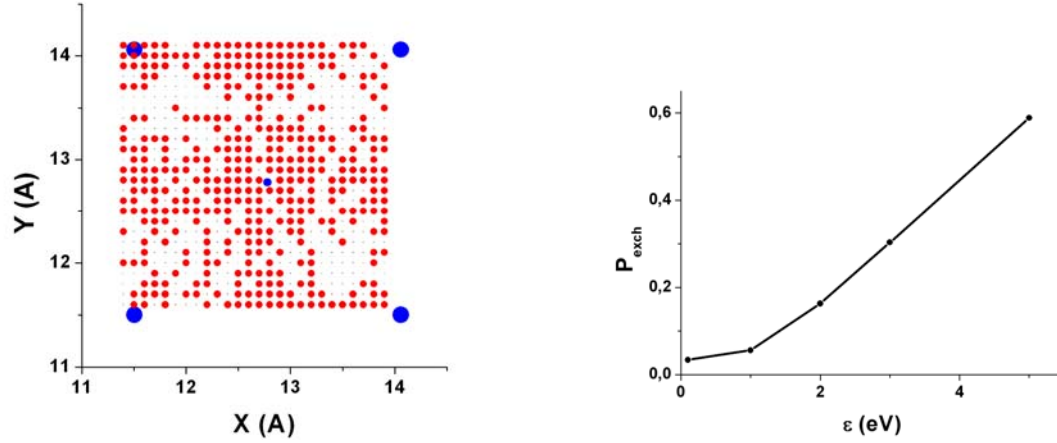
Fig. 2 Statistics of exchange processes in Pd/Cu(100) energetic deposition. A: Distribution map of exchange events on the substrate surface at 5 eV (blue color balls represent substrate atoms); B: Probability of exchange as function of impact energy.

From the results we find that the probability of exchange increases with the impact energy. Thus, as expected energetic deposition promotes alloy formation in the film.

We also performed MD simulations of a Pd film growth using the NVT ensemble. In Fig. 3 we show a side view of the MD cell after 10^6 time steps (1 ns in real time) (A) and the corresponding time evolution of the level of coverage (Ni/No) in the layers showing strong intermixing near the film-substrate interface.
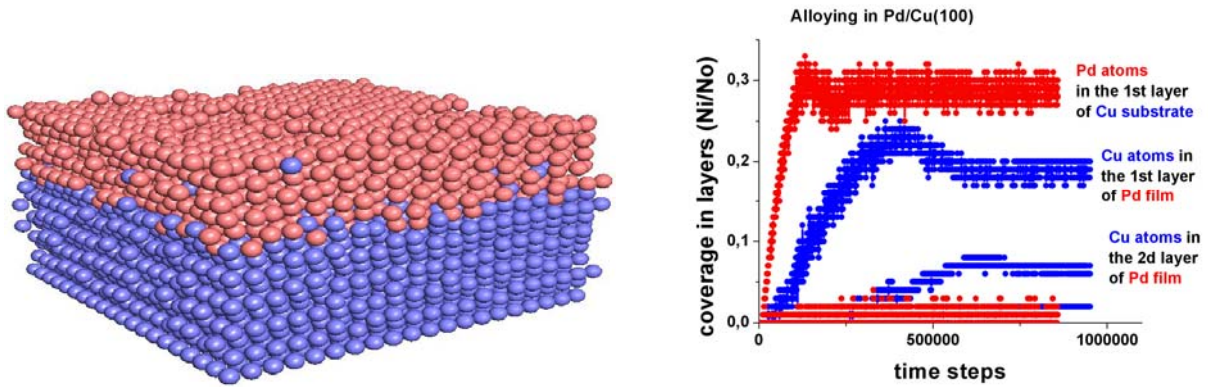
Fig. 3 Pd/Cu(100) structure grown by energetic deposition with energy equal to 10 eV. A: Side view on the MD cell; B: Level of coverage in layers as a function of time.

In summary, we can conclude that the conditions of Pd film growth can strongly influence surface alloying. It is possible to hamper alloying by reducing the kinetic energy of the deposited atoms and simultaneously increasing the deposition flux.

1. O. Trushin, K. Kokko, P. Salo, *Film-substrate interface mixing in the energetic deposition of Ag on Cu(001)*, Surf. Sci. **442**, 420 (1999).
2. S.M. Foiles, M.I. Baskes, and M.S. Daw, *Embedded atom method functions for fcc metals Cu, Ag, Au, Ni, Pd, Pt and their alloys*, Phys. Rev. B **33**, 7983 (1986).
3. H. Jónsson, G. Mills, and K.W. Jacobsen, in *Classical and Quantum Dynamics in Condensed Phase Simulations*, ed. by B. J. Berne *et al.* (World Scientific, Singapore, 1998).

P2-5: Modeling LINEAR defects in graphene and NANOGRAPHENE

V. Stelmakh[1] , I. Yadgarov[1], A. Dzhurakhalov[1,2]

1.Arifov Institute of Electronics, Akademgorodok, 33, Do'rmon yo'li Street, Tashkent, Uzbekistan, iyadgarov@mail.ru
2 Dept. of Mathematics and Computer Sciences, University of Antwerp, Antwerp, Belgium, dzhurakhalov@mail.ru

The ideal structure of graphene is a two-dimensional hexagonal lattice. The presence of defects in graphene leads to a disruption of this structure and to changes in physical and chemical properties of graphene.

Using Metropolis Monte Carlo method, the formation of linear defects and stable configurations of graphene and nanographene (which has a small finite size with free boundary atoms) have been studied. The interatomic interactions have been described by the Brenner's reactive empirical bond order potential which was parametrized specifically for carbon and hydrocarbon systems [1].

Nanographene has been modeled by 112 carbon atoms arranged in a flat plane and in the appropriate configuration for graphene with a lattice constant of 2.46 Å. To simulate a graphene the periodic conditions were superimposed on the boundary atoms of nanographene along its plane. The presence of linear defects has been modeled as point vacancies, which is located along the same line in the lattice. We studied their effects on changes in the lattice structure and binding (cohesive) energy of atoms. In particular, it was found that linear defects results in decreasing the cohesive energy of studied systems. Figure 1 shows how the energy of cohesive varies on the number of point vacancies in a linear defect for graphene and nanographene.
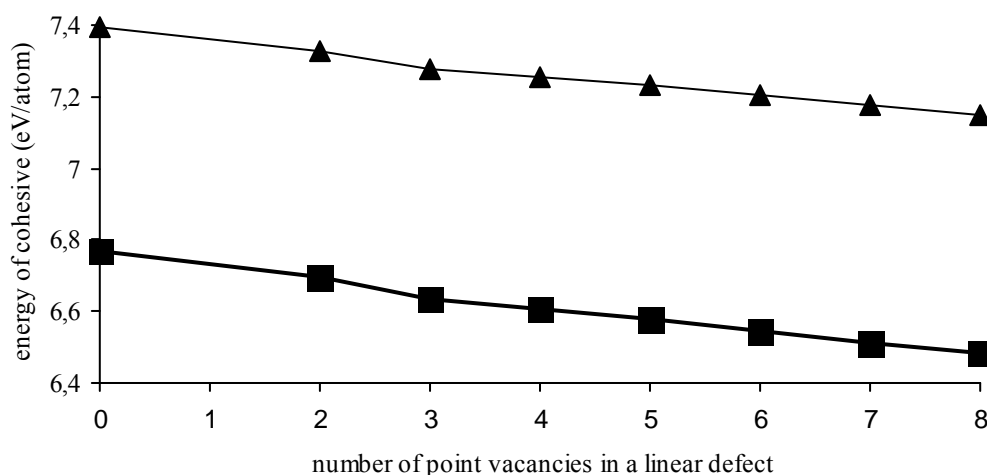
Fig.1. The dependence of the cohesive energy of the number of point vacancies in a linear defect for graphene (marked by triangles) and for nanographene (marked by squares)

1 D.W. Brenner, O.A. Shenderova, J.A. Harrison, S.J. Stuart, B. Ni, S.B. Sinnot. "A second-generation reactive empirical bond order (REBO) potential energy expression for hydrocarbons", J.Phys: Condens. Matter, **14**, pp.783-802, 2002

P2-6: Micromagnetic modeling of spin-valve structure with technological imperfections

O.S. Trushin[1], N. Barabanova[2], V.P. Alexeev[2]

[1]*Yaroslavl Branch of the Institute of Physics and Technology of RAS, Yaroslavl, Russia,*
[2]*Department of Physics, Yaroslavl State University, Yaroslavl, Russia*

Magnetic field sensors based on Giant Magnetic Resistivity(GMR) effect find wide range of applications in modern technology[1]. High sensitivity at low fields and low cost make these sensors very competitive at a market. The most popular design of these sensors based on spin-valve structures[2]. Typical such structure consists of several metallic layers such as FREE magnetic layer ($Ni_{80}Fe_{20}$ - permalloy), nonmagnetic spacer (Cu) and PINNED magnetic layer ($Fe_{80}Ni_{20}/Fe_{50}Mn_{50}$). Combining ferromagnetic FeNi and antiferromagnetic FeMn layers provides strong pinning of permalloy layer due to exchange bias effect. Modern studies of these structures are aimed on further improvements of its functional characteristics.

It is well known that quality of spin valve multialyer structure determines its functional characteristics. In particular, presence of pinholes in spacer layer may create ferromagnetic connections between layers and lead to worsening functional characteristics. Another important factor is substrate roughness. Waving interface lead to additional magnetic interactions between ferromagnetic layers (Neel effect). Thus magnetic reversal of spin-valve may contain signature of imperfections in multilayer structure. It might be used for express diagnostics of spin-valve structures for technology optimization. In this work we present the results of micromagnetic modeling of the effect of technological imperfections on magnetic reversal of spin-valve structure. Our own, home made micromagnetic package MICROMAG4 was used for this study. Minimization of total energy of the system is performed through numerical solution of LLG equation. Rectangular shape mesh is used for numerical scheme.

To study the effect of spacer layer imperfections we used the model which consists of two ferromagnetic layers of rectangular shape with variable size ferromagnetic bridge between them. The bridge simulates ferromagnetic connection through pinhole in spacer layer. One of those magnetic layers is exchange biased.

A   B
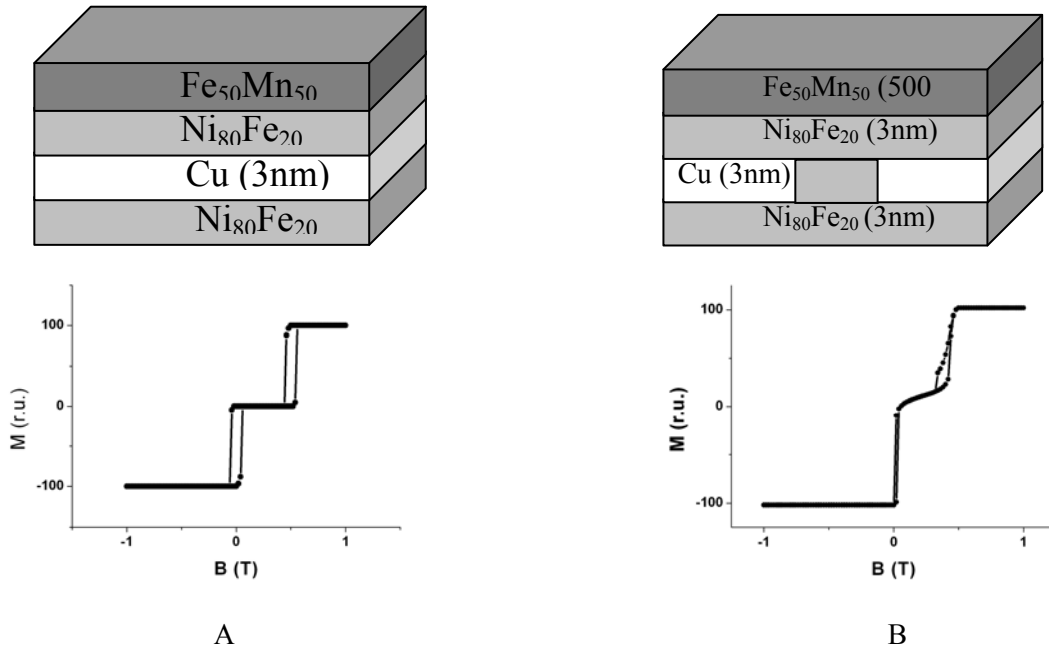
Fig.1 Schematic presentations of spin-valve structures and its magnetic reversal loops obtained by micromagnetic simulation: A) ideal spin valve with no pinholes in nonmagnetic spacer, B) spin valve structure with ferromagnetic connetcion through pinhole in the center.

The results obtained for this model show trend in changing shape of magnetic reversal loop of spin-valve with increasing ferromagnetic connection through pinholes.

We have also studied the effect of substrate roughness on the magnetic characteristics of spin valves. In that

case we used the model which consists of two ferromagnetic layers of rectangular shape with different interface roughness. We compared magnetic reversal loops obtained for ideal flat interface and for waving shape interface (rough substrate) (shown in Fig.2).

A   B
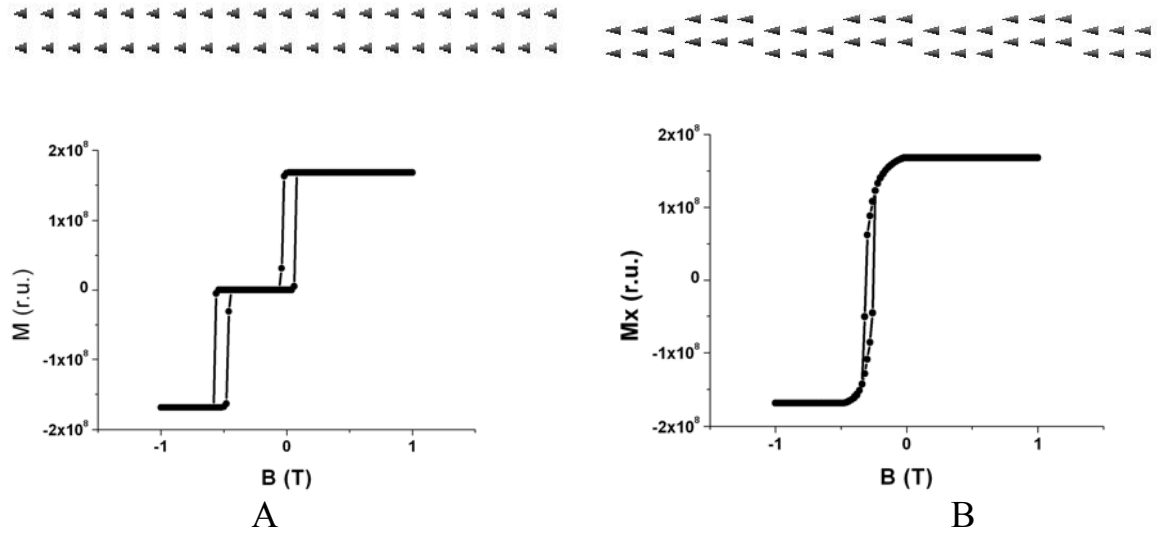
Fig.2 Schematic presentations of spin-valve structures (upper panel) and its magnetic reversal loops obtained by micromagnetic simulation (bottom panel): A) ideal spin valve with flat interface, B) spin valve structure with pronounced interface waving (rough substrate).

The results show strong distortion of hysteresys loop with increasing amplitude of interface waving. Substrate roughness may lead to degeneracy of spin-valve characteristics and reducing GMR effect.
Thus analysis of magnetic reversal loops of spin-valve structures may be used for diagnostics of different imperfections in structure and help in optimization of the technology.

1. S. Tumanski *Thin magnetoresistive sensor*s, IOP publishing Ltd., Bristol, 2001.
2. R. Coehorn "Giant magnetoresistance and magnetic interactions in exchange-biased spin-valves", in *Handbook of magnetic materials*, volume **15**, Elsevier Science, Amsterdam, 2003.

P2-7: Variational calculation of the image potential near a surface, taking into account the three-dimensional distribution of screening charge

S.E. Efimovsky

Northern State Medical University, Russia, Arkhangelsk, seefim@rambler.ru

There has recently renewed interest in studying the interaction of a point charge with a metallic surface. The precise form of this interaction is of importance for a number of phenomena, such as field evaporation and desorption, field emission, low-energy-electron diffraction, electron tunneling, etc. From classical electrostatics, one knows that the interaction energy E of point charge of strength q with ideal conductor is just

$$E=-q^2/4d, \tag{1}$$

where d is distance of the charge from metal surface. Since this expression is singular as one approaches the metal surface it is very important to know in what way the energy saturates for a real metal surface as d→0.

In [1, 2, 3] problem of the interaction of charge with metal surface has been solved numerically using various modifications of density functional theory. However these calculations do not allow their use in analytical applications.,it appears that the singularity of the interaction with d = 0 can be eliminated by replacing the classical electron two-dimensional density

$$n(\rho,z) = \frac{qd}{2\pi(\rho^2 + d^2)^{3/2}} \delta(z)$$

in the three-dimensional:

$$n(\rho,z) = \frac{qR}{2\pi(\rho^2 + R^2)^{3/2}} st(z)$$

where δ(z) – Dirac δ – function, z, ρ – the cylindrical coordinates, st (z) = γ_0 / 2 if | z | <1/γ_0 and zero outside this interval. 1/γ_0 is «thickness" of the screening charge and can be evaluated from the quantum-mechanical calculations [3]. The interaction energy was calculated as the sum of the Coulomb interaction energy of a point charge with the screening charge plus the Coulomb energy of the "response", that is interaction energy of the screening charge with itself. The value of R is a variational parameter and is chosen by minimizing the energy E.

The calculation results show that the dependence found at all distances d is below the classical curve (1) and terminates with the value of E = -0,845 q^2 γ_0 for d = 1 / γ_0, thereby eliminating the previously mentioned singularity. It should be noted that the theorem-Irwin Shaw does not allow to classically perform calculations for d <1/γ_0. We have tried to analyze influence of calculated value of energy on the reduction of the potential barrier for desorption of ions in strong electric fields (the effect of Schottky).

The author would like to thank Dr. L. Ushakova for helpful discussions.

1. J.R. Smith, S.C.Ying, W. Kohn «Charge densities and binding energies in hydrogen chemisorption », Phys.Rev.Lett., Vol. 30, N 13, 1973, p 610-613.
2. J.A. Appelbaum, D.R. Hamann «Variational calculations of image potential near a metal surface», Phys. Rev. B, Vol. 6 ,N 4, 1972, p 1122-1130
3. С.Е.Ефимовский, Г.Г.Владимиров, «Взаимодействие заряда с поверхностью металла в статистическом методе функционала плотности». Препринт 1103, Физико-технический институт им. А.Ф.Иоффе АН СССР, Ленинград, 1987.

P2-8: Application of ion implantation for making MIS nanotransistors with local area of the buried insulator

S.A. Krivelevich , D.D. Korshunova , N.P. Pron

Yaroslavl Branch of the Institute of Physics and Technology , Russian Academy of Sciences, Russia, E-mail addres: s.krivelevich@mail.ru

The main elements of modern microprocessor-based devices and integrated circuits are silicon memory MOS - transistors. Currently, the world began the process of transition to planar transistors with lateral dimensions less than 100 nm. The greatest successes in this direction, apparently, achieved using the so-called " strained silicon technology" [1], which allows creating transistors with effective channel length of ~ 45 nm. The main problem that arises at the creation of such transistors is suppression of short channel effects, which lead primarily to an increase in subthreshold current and a decrease in the mobility of charge carriers in the channel. Therefore, the possibility of further reducing the lateral dimensions of the planar transistor is no very obvious.

It has been shown [2] that the sequential implantation in silicon of oxygen and glass-forming elements such as boron and phosphorus, at the stage of post implantation heat treatment, the formation of hidden layers of silicate glasses is possible. The layers are formed at relatively low temperatures (in 1000 -1050° C) and have a high resistivity (about 10^{14} Ohms cm).
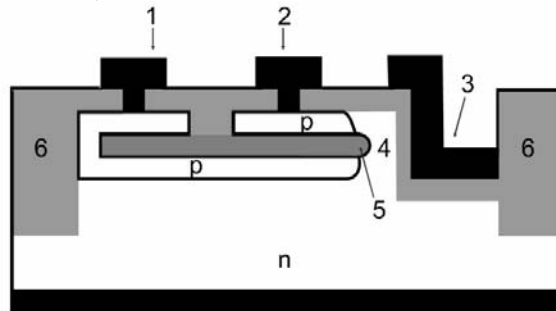
Fig. 1. Nanotranzistor with a buried layer of silica glass.
1-sorse, 2-drain, 3-gate-, 4- channel area, 5- buried layer of silica glass, 6 – isolation area

Theoretical modeling and experimental study of the distributions of the components in the emerging structures have shown that under certain conditions the technology buried layers of silicate glasses provides the formation of three-layer sandwich containing two layers of highly doped silicon and a layer of silicate glass between them. This allows to creating of nanotransistors with vertical structure. That is shown schematically in Figure 1.
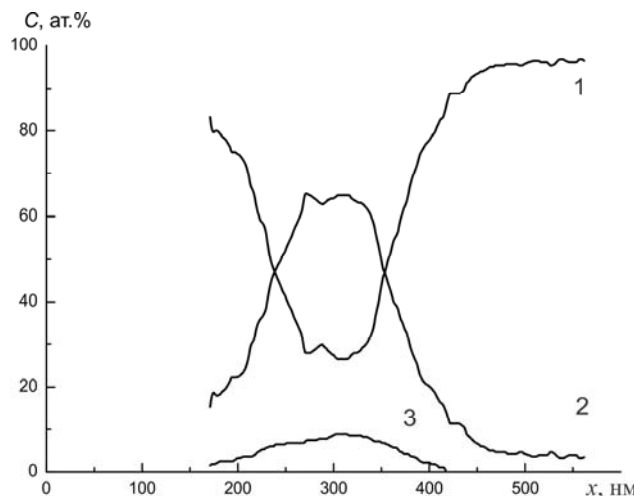
Fig. 2 Distributions of the relative concentrations of oxygen, boron and silicon, obtained after heat treatment at 1000 ° C for 5 minutes. 1 - distribution of silicon atoms, 2 - distribution of oxygen atoms, 3 - distribution of boron atoms. The dose of molecular oxygen $4 \cdot 10^{17}$ cm^{-2}

Where, after the formation on the surface of the silicon substrate the insulating layer around the active regions of the transistor is created. At the boundary layer is created a trench, subsequently filled by a dielectric. Implantation of ions, mainly oxygen is carried out through a mask so as to ensure the closing of drain and source regions. Their isolation is performed by means of the separation grooves. The surface is covered with dielectric. Then we create a contact area and thus form the structure of the transistor with a vertical channel. The effective length of channel is determined by the thickness of a thin buried dielectric layer. The method of forming of transistor with vertical channel allows to avoid short channel effects and to minimize the length of the channel and the parasitic capacitances of the p-n junctions.

The properties of the synthesized layers were studied by IR spectroscopy, Auger - spectroscopy and SIMS. It is shown that the hidden layer of silicate glass is formed in the system, if the dose of molecular oxygen is equal to $4 \cdot 10^{17}$ cm^{-2}. The results of this study confirm the possibility of formation of nano transistor with buried layer of a silicate glass (Fig. 2, 3).
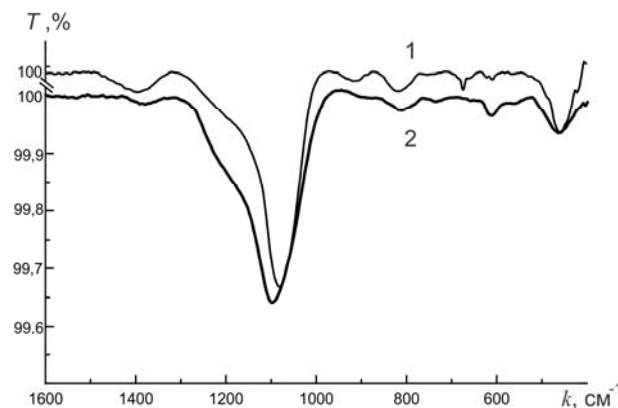
Fig.3. Transmission spectra of samples containing the buried layers of borosilicate glass.
1 - obtained by the sol-gel technology. Temperature heat treatment in 1000 °C, 2 - ion obtained by synthesis. The dose of O -4×10^{17} cm-2

1, A.L. Aseev, "Nanomaterials and nanotechnology for modern semiconductor electronics", Russian nanotechnology, N1, pp.97-100, 2006
2. S.A. Krivelevich, V.I. Bachurin, Yu.I. Denisenko, R.V. Selyukov, "Ion synthesis of buried insulating silica layers", Bulletin of RAS. Physics, **70**, pp.787-789

P2-9: Conductance quantization of nanojunctions dynamically formed between two rough molybdenum surfaces observed in air at room temperature

L. Fedichkin[1,2,3], M. Chernyshev[2], A. Borisov[2], A. Konin[2], R. Petrukhnenko[2], V. Rubaev[2]

1. Institute of Physics and Technology, Russian Academy of Sciences, Moscow, Russia, leonidf@gmail.com . 2. NIX Co., Moscow, Russia, leonid@nix.ru . 3. Moscow Institute of Physics and Technology, Dolgoprudny, Moscow region, Russia, leonid@phystech.edu .

The measurement of dynamics of electrical conductance between metallic contacts being mechanically gradually displaced from each other provides sensitive tool to metal surface characterization [1]. At certain conditions it enables also the fundamental study of quantum behavior of electron transport [2] revealing itself in particular in conductance quantization of nanojunction [3,4].

This report presents recent experiments [5] with mechanically controlled molybdenum contacts. Our goal is to study the transition from the condition of a good electric contact up to the breakage of the connection. We demonstrate that electron transport through molybdenum nanojunction manifests the features of ballistic and quantum motion even in air atmosphere under normal pressure and room temperature. By reiterating the contacts displacement with the use of piezoelements millions and millions times, we obtain a conduction histogram, shown below in Fig. 1, with the pronounced peak corresponding to one conduction quantum and the minimum corresponding to one and a half conduction quantums, in agreement with theory.
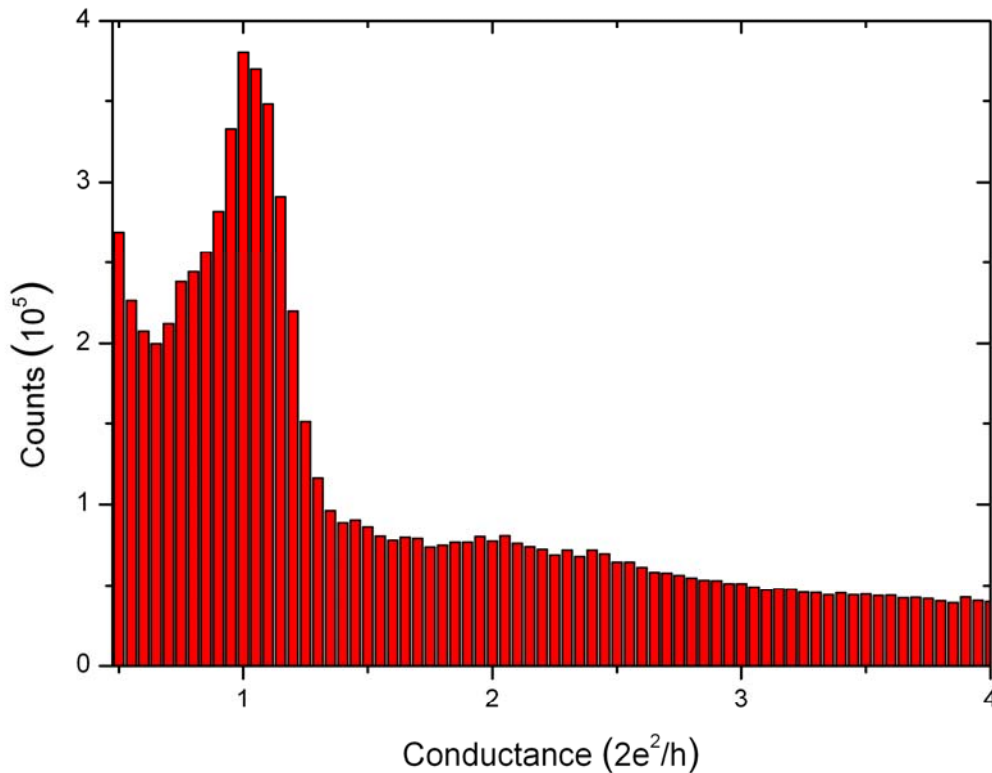
Figure 1. Conduction histogram. Number of events of nanojunction conductance value within +/- 0.025 conduction quantum from the central value of conductance versus conductance.

Although the experiment is carried out in air atmosphere under normal conditions, we do not notice any signs of degradation of the measurement results during tens of minutes. The transition processes in the studied range of conduction data with a duration of 200 μs are excluded from the total data array since the

analog-digital converter response time does not allow us to grasp properly faster conduction dynamics and the fast breaking curves are blurred. Delaying and uncompleted breaking processes with a duration of more than 6 ms are also excluded from the analysis. The unavoidable systematic deviations (less than +/-3%) related to the discreteness of the analog-digital converter output data, were taken into account and excluded from the plot.

The ability to observe quantization peak proves persuasively the validity ballistic and quantum description of electron evolution at least at scales corresponding to nanojunction sizes.

1. Yu.V. Sharvin, Zh. Eksp. Teor. Fiz., 21, p. 655, 1965
2. F. Manders, A.K. Geim, and J.C. Maan, Physica B: Condensed Matter, 294–295, p. 332, 2001
3. D.A. Wharam, T.J. Thornton, R. Newbury, M. Pepper, H. Ahmed, J.E.F. Frost, D.G. Hasko, D.C. Peacock, D.A. Ritchie, and G.A.C. Jones, J. Phys. C, 21, p. 209, 1988
4. B.J. van Wees, H. van Houten, C.W.J. Beenakker, J.G. Williamson, D. van der Marel, and C.T. Foxon, Phys. Rev. Lett., 60, p. 848, 1988
5. L. Fedichkin, A. Borisov, A. Konin, R. Petrukhnenko, M. Chernyshev, and V. Rubaev, Russian Microelectronics, 41, No. 1, pp. 1–4, 2012

P2-10: The effect of surface properties on electric absorption of fine metallic particles

I.A.Kuznetsova, M.E.Lebedev

Demidov Yaroslavl State University, Yaroslavl, Russia, kuz@uniyar.ac.ru

The electric absorption of fine cylindrical particle under effect of plane electromagnetic wave is considered. The particle is reputed to be small if its size is much smaller than the wavelength of electromagnetic radiation. When the frequency is much lower than the plasma resonance frequency and the electric field is directed axially, the contribution of the dipole electric polarization currents dominates over the contribution of eddy currents, so the effect of the magnetic field can be neglected. The radius of the cylindrical particle R is less than the skin depth, therefore the skin effect is not taken in account. The ratio of the mean free path of the main charge carriers λ to the cylindrical particle radius R is not limited. The cylinder radius R is comparable or less than the mean free path of electrons λ, it causes non-local effects due to the interactions between charge carriers and the surface of the sample. These effects have a significant impact on the optical properties of the particle. The consequence is a non-trivial dependence of the optical characteristics (for example, the absorption cross section) on the ratio R/λ.

In such cases, the macroscopic electrodynamics is not applicable, so the kinetic approach only provides correct description of the electromagnetic field energy dissipation in the particle. In metals the conduction electrons are treated as a Fermi gas, which is described by the Fermi-Dirac distribution function in equilibrium state. An oscillating uniform external electric field affects the conduction electrons and causes a deviation of the distribution function from equilibrium. The Boltzmann equation in the time relaxation approximation and in the linear field approximation is solved in order to find the equilibrium distribution function.

Taking into account [1, 2] the contribution of surface scattering in such problems is based on the sequential formulation of the boundary condition due to the Boltzmann equation, which relates the distribution function of the incident electrons on the particle surface and reflected from it. In fact, this boundary condition for the distribution function was formulated by introducing the reflectivity coefficient q, which is equal to the relative number of electrons regularly reflected at the surface, or q is the probability of mirror reflection of electrons $(0 < q < 1)$, and $(1 - q)$ is probability of diffuse reflection, respectively [3]. Electric absorption of small particles in the case of cylindrical diffusion-specular Fuchs boundary conditions is considered in [2].

In this paper Soffer model [4] is used as kinetic boundary conditions for the non-equilibrium electron distribution function, taking into account the dependence of q on the surface defects and on the angle of incidence θ between the electron velocity vector and the normal to the metal surface. At the angles θ close to $\pi/2$, i.e., for electrons that have almost slid to the surface, the difference of the reflectivity coefficient from unity is $(q - 1) \sim cos^2\theta$ [4].

The current density and the absorption cross section are calculated as functions of the external field dimensionless frequency, the dimensionless reciprocal mean free path R/λ, and the parameter of surface irregularity. The limiting cases were considered and the results are compared with theoretical calculations performed for the model the Fuchs boundary conditions.

1. P.M. Tomchuk, B.M. Tomchuk, "Shape and size effects on the energy absorption by small metallic particles",, Phys. Rev. B, **vol. 73**, 155423, 2006
2. E.V. Zavitaev and A.A. Yushkanov, "Influence of the behavior of electrons reflection from the surface on electric properties of a cylindrical particle", Low Temp. Phys., **vol. 31**, no. 12, p. 1048, 2005.
3. K. Fuchs, "The Conductivity of Thin Metallic Films According To the Electron Theory of Metals", Proc Cambridge Phil. Soc., **vol. 34**, no. 1, pp. 100–108, 1938.
4. Soffer, S.B., "Statistical Model for the Size Effect in Electrical Conduction", J. Appl. Phys., **vol. 38**, no. 4, pp. 1710–1715, 1967.

P2-11: Dynamic effects of mossbauer spectroscopy for iron compounds in natural nanostructures.

A. A. Zalutskii[1], P.A. Ivanov[1], R. N. Kuzmin[2], M.V. Lokhanin[3]

1. Yaroslavl State Technical University, Yaroslavl, Russia, zalutskii@mail.ru. 2. Physics Department, Lomonosov State University, Moscow, Russia. 3. Yaroslavl Demidov State University, Yaroslavl, Russia, lokhaninmv@mail.ru

There are presented dynamic and orientation effects that appear at different forms of adsorbed iron in clay minerals. There were used typical represents of natural alum silicates-clay minerals montmorillonite and caolinite (Fig. 1. a) as a carrier. The Mossbauer spectroscopy (MS) in transmission geometry was choused as a basic method, the typical experimental spectra for investigated systems is presented on Fig. 1.b.
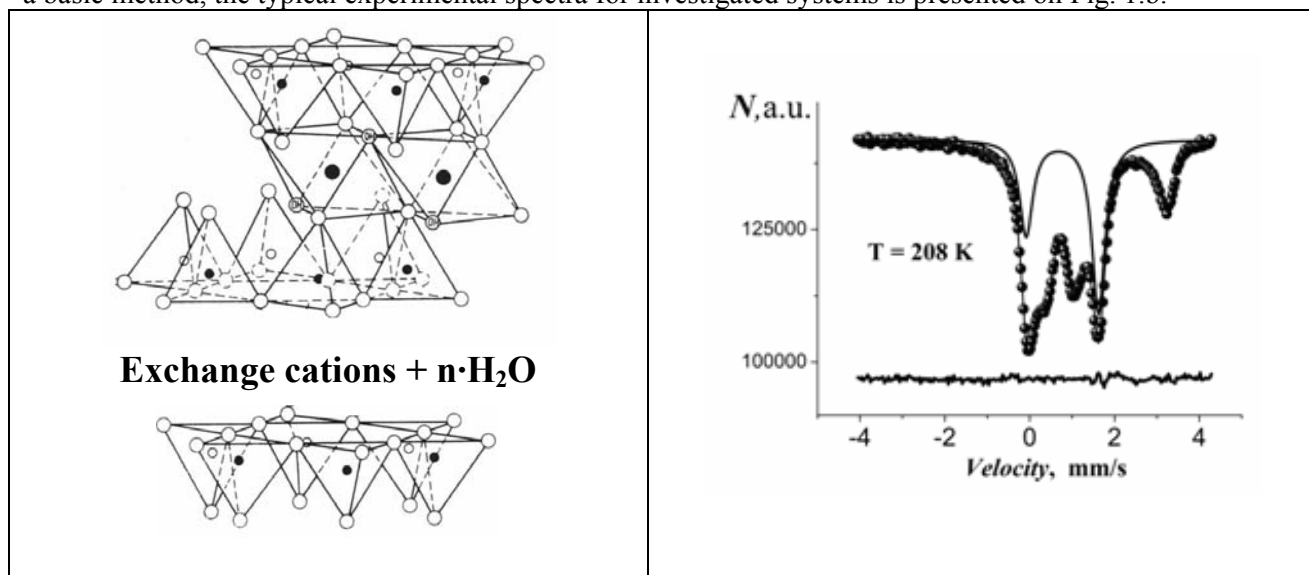
Fig. 1. a). The structure of montmorillonite triplex laminations (*a*): 1 - oxygen (O^{2-}); 2 - hydroxyl (OH^-); 3 – aluminium (Al^{3+}) or iron (Fe^{3+}, Fe^{2+}); 4 – silicium (Si^{4+}) and aluminium (Al^{3+}) or iron (Fe^{3+}, Fe^{2+}) **b)**. Mossbauer spectrums of ^{57}Fe-nuclei in ion exchange products of montmorillonite (clusters (A) and dimers (B))

The behavior of temperature course of mossbauer parameters ($S(T)$, $\delta(T)$, $\varepsilon(T)$, $\Gamma(T)$) for iron compounds in montmorillonite is described by two models of unlimited and limited diffusion movement.

The character of widening of mossbauer line for $Fe^{2+}(H_2O)_6$ ions at temperature change (in presence of "connected" water film in mineral) can be interpreted by two mechanisms: by diffusion at the cost of "jumping" mechanism at low temperature, by "continuous" diffusion at high temperature. The dependence $\ln \Delta\Gamma_D / \Gamma_0$ in function $1/T$ (Fig. 2,a) had a typical inflection at T ≈ 230 K. It is possible to calculate the activation energy of movement: ε_a = 0,24 эB, D_0 = 2,9·10⁻⁶ sm²/s from widening of line upper inflection point in case of submission of diffusion coefficient of exponential dependence from return temperature ($D = D_0 \exp(-\varepsilon_a / kT)$).

In case of absence in mineral of film of "connected" water there is no inflection point in behavior of dependence of $\ln \Delta\Gamma_D / \Gamma_0$ at function $1/T$ (Fig. 2, a), and observed linear dependence can be interpreted by diffusion mechanism at the cost of jumps. In suggestion that jumps are described by markov's process, the quantitative estimation of diffusion coefficient that is received from widening of mossbauer line is as $D = (l^2/12\hbar)\Delta\Gamma$, here l is a distance between neighbor places of localization Fe^{2+} ion.

Complexes of compounds of trivalent iron can be diagnosed in mossbauer spectra by two phases (A and B) (Fig. 1, b) [1]: doublet A is caused by finely divided aggregates of iron concentrated phase (clusters) with structure that is same with roentgen amorphous hydroxide, and doublet B is related to iron dimers

$$\left[Fe_2^{3+}(OH)_2^- \right]^{4+}$$

The theory of limited diffusion movement makes it possible to explain why there is no widening of mossbauer line for iron dimers in presence of diffusion. The enough wide range of mossbauer window

velocities ($\upsilon = \pm 150$ mm/s) is necessary for receiving of quantitative data from experimental line and it is a separate technical problem. Because of that there was specially received the expression for resonance component's square with taking into account of nonzero level of substrate that is registered as a background in usual spectra.
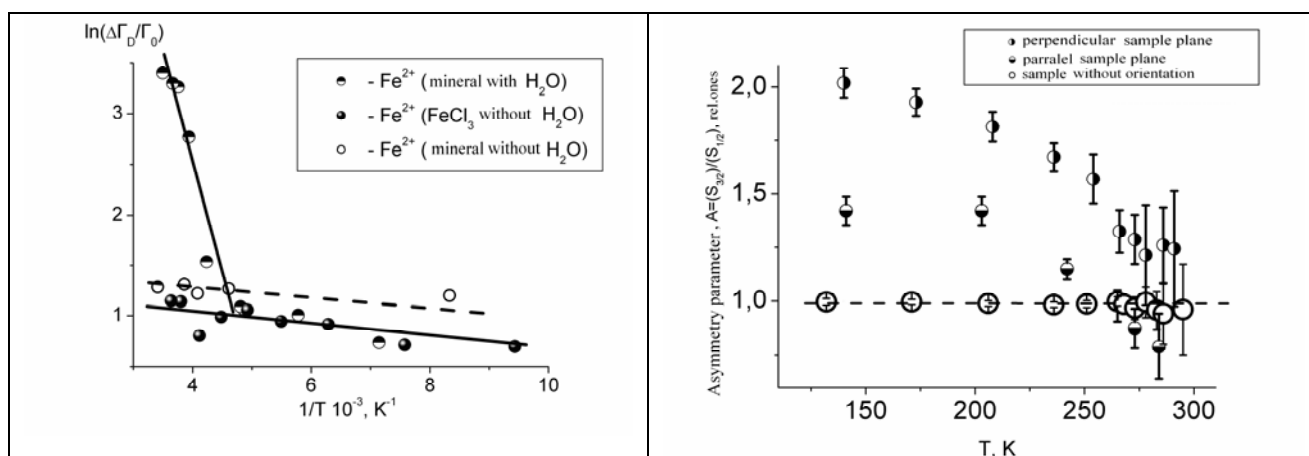
Fig.2. a) Dependence $\ln \Delta \Gamma_D / \Gamma_0$ in functionи $1/T$ for different systems; b) Result of "artificial" texturing for "dimers-montmorillonite" system (temperature dependence of asymmetry parameter)

The numerical calculation for received expressions for line width and resonance part's square give a possibility to determine the change range of area of movement limits L and diffusion coefficient D in that the registered spectra is presented by single component without widening ($L^2/12\lambdabar^2 \langle 0{,}75 + 2D/\lambdabar^2\Gamma$). The

expression for probability of effect in this area is $f' = 1 - a^2 \exp(-a^2) \int\limits_0^1 y^{n(T)} \exp(a^2 y) dy$ that is in good

agreement with experimental results and that bring us to parameters values (D, ε_a) that are in correspondence with parameters that are typical for unlimited diffusion by order of value.

Temperature behavior of asymmetry parameter $A(T)$ in system "iron dimers-mineral" at artificially textured samples can be explained in borders of model of limited diffusion movement that partly breaks orientation of dimers one related to the other. During that the angle between quantization axe and direction of γ-quant is ceased to be fixed and procedure of averaging at ensemble of all particles together with decreasing of lines asymmetry (Fig. 2, b) give a possibility to receive quantitative estimation of an energy of communication of iron dimers with surface of clay mineral. Additionally, there were received expressions for dependence of parameter $A = S_{3/2}/S_{1/2}$ from disorientation range and there were constructed appropriate curves by numerical calculations.

The reason of experimentally detected asymmetry of doublet line for system "iron hydroxide-caolinite" can be explained by diffusion mechanism. The analysis of temperature dependencies of mossbauer parameters showed that anisotropy of diffusion is shown by different widening of components of quadruple spectra super thin structure like anisotropy of Debay-Waller factor brings to the asymmetry in intensities of that components. For value of diffusion coefficient receiving there were used two factors of anisotropy for intensity (A) and half width (B) of mossbauer doublet. The expression for A is equivalent to usual formula for Goldansky-Koryagin effect in polycrystals ($A = S_{3/2}/S_{1/2}$) [2] with the only difference that it was took into account the value of angle between axe that is perpendicular to caolinite plane and direction of electrical field gradient. The second factor is determined by formula as $B = \chi \cdot (\ln A)'_\varepsilon$, where parameter χ gives a possibility to find diffusion coefficient ($\chi = 3\hbar k^2 D$), and parameter of differentiation is determined by formula $\varepsilon = (\langle z \rangle^2 - \langle x \rangle^2)/\lambdabar^2$.

1. Zalutskii A.A., Stepanov E.G. Physical research methods firm phase of reagents and catalysts. (2005) Yaroslavl. 312

2. Goldanskii V.I. and Herber R.H. Chemical Applications of Mossbaur Spectroscopy. Academic Press New York and London (1968)

P2-12: Dependence of magnetic parameters on a thickness and formation conditions of permalloy films

A.V.Morozov[1], V.P.Alekseev[1], V.A.Paporkov[1], V.A.Naumov[2]

1. Yaroslavl State University, Yaroslavl, Russia, avp@uniyar.ac.ru
2. Yaroslavl branch of the Institute of Physics and Technology of RAS, Yaroslavl, Russia, vvnau@rambler.ru

Permalloy thin films find wide application in microelectronics for making of devices of record and information storage. Permalloy at the certain sizes and orientation of the sample possesses a rectangular hysteresis curve and has high residual magnetization I_R. However stability of record low enough because of small coercive force H_C. Reduction of a thickness of a film is one of the methods to improve stability of magnetic recording. The material coercivity in this case the increases because of amplifying influence of the superficial anisotropy [1].

Physical properties including magnetic properties of a film differ from those in a massive state. In the absence of the induced anisotropy a state at which magnetic moments lie in a film plane is energy more favourable in the lack of applied magnetic field. It leads to that such magnetic material have a plane magnetic anisotropy of the shape. Thus all directions in a surface of films are equivalent. Therefore for film magnetization in its plane it is necessary to put a smaller magnetic field, than for a case when the film is magnetized on a normal line to its surface. Easiest magnetic axis (EMA) appears in a film plane during coating of a magnetic film in an exterior magnetic field. Appearance of EMA is caused by magnetic moments orientation in the film plane preferentially along an exterior magnetic field (easy-axis magnetic anisotropy). The actions spotted physically can lead to formation EMA, guided perpendicularly and film planes.

Formation of various types of anisotropy is influenced by such factors, as: the sizes, crystal structure, impurities, defects, elastic stresses, exterior magnetic fields, etc.

In our research influence of permalloy film the thickness on hysteresis curve parameters was studied. One of problems was the investigation of magnetic transition nature "order-disorder" at reduction of film thickness.

1.5 nm; 3 nm; 4.5 nm and 6 nm films were gained by means of an ion-plasma sprayed coating of the permalloy cathode (19 % *Ni* and 81 % *Fe*) and condensation on a cold glass substrate in argon atmosphere. The thickness of films was controlled accurate to 0,3 nm by time of evaporation according to a well-known procedure [2, 3]. Film evaporation was spent in a stray magnetic field and in a longitudinal magnetic field 120 Oe.

Measurings of an initial susceptibility were spent on the industrial device IMV-5 with the sensitivity

$2 \cdot 10^6$ SGSM units.

Hysteresis loops were explored on a high-sensitivity vibrating-coil magnetometer [4].

On the basis of the experimental data and their analysis we conclude:

1. Calculations proved that the initial magnetic susceptibility is directly proportional to the square of the saturation magnetization, and in accordance with the theory of ferromagnetism does not depend on the thickness of the permalloy film.

2. It was established that with decreasing film thickness residual magnetization and loop squareness decrease and the hysteresis disappears for films with a thickness of ~1.5 nm. This means that film remains ferromagnetic up to ~ 2-3 nm. With further decrease of the thickness magnetic order disappears and film becomes superparamagnetic (not paramagnetic since the Curie temperature for permalloy is ~ 800 K). This allows us to estimate the critical size of superparamagnetism ~ 1.5-2 nm.

3. Dependence of measured coercivity on the film thickness at which shows that permalloy grains remain one-domain for films with thickness up to 10 nm, films with a thickness of 10nm have a maximum coercivity.

4. It is revealed that the studied films possess high dispersion of the anisotropy which is incremented with reduction of a film thickness and dominating contribution in anisotropy belongs to amplitude

dispersion.

5. Reduction of saturation magnetisation occurs mainly due to the increase of the proportion of non-magnetic regions with decreasing thickness of permalloy film. The average size of non-magnetic regions has been calculated on the basis of magnetic measurements and the theory of superparamagnetism. For our films the size of these regions is about 2 nm.

1. Zhigalov V.S. Features of the structure, phase states, and magnetic properties of nanocrystalline composite 3-d metal films obtained by ultrafast condensation / Abstract of a thesis D. Sc. - Krasnoyarsk.: Institute of Physics Siberian Branch of the RAS, 2006, – P. 41

2. Naumov V.V., Paporkov V.A., Lohanin M.V. Equatorial Kerr effect dependence on the angle of incidence for the ultrathin films and multilayers of cobalt Co/Cu/Co // Microelectronics. – 2009, V. 38, №4, 273-279.

3. A. I. Stognij, N. N. Novitskii and O. M. Stukalov A method for monitoring thicknesses of nanodimensional bilayer film structures // Technical Physics Letters. - 2003. Volume 29, Number 2, 147-150.

4. Maksimochkin V.I. Trukhin V.I. Garifullin N.M. / An automated high-sensitivity vibrating magnetometer // Instruments and Experimental Techniques. – 2003, N5, 132-137.

P2-13: Comparative study of ultrathin Co films grown by ion-plasma and magnetron sputtering

O.S. Trushin[1], V.F. Bochkarev[1], V.V. Naumov[1], S.V. Vasiliev[2] and V.A. Paporkov[2]

1Yaroslavl Branch of the Institute of Physics and Technology of RAS, Yaroslavl, Russia

otrushin@gmail.com

2 Department of Physics, Yaroslavl State University, Yaroslavl, Russia

Magnetic multilayer nanostructure is of perspective material for spintronic applications [1,2]. Such nanostructures show giant magnetic resistivity effect[3]. Development of cost effective and reliable technology for magnetic layers of high quality fabrication is of important direction for research. Standard way of magnetic multilayer formation is magnetron sputtering deposition. Yet another alternative method for growing mulilayer films is ion-plasma sputtering. The purpose of this work was to check possibility of using ion-plasma method for fabrication of magneto-resistive structures. The most important ingredients of magneto-resistive structures are ultrathin magnetic layers (Co, Py and others). In this work we performed comparative study of ultrathin Co films grown by ion-plasma and magnetron sputtering.

As an example of magnetron sputtering tool we used standard industrial istallation TETRA SCR-600 (produced by Alcatel) equiped with 4 targets for simultaneous deposition of four different materials in single vacuum cycle. Ion-plasma sputtering was done using home made installation (plasma discharge by triod scheme) having 4 targets. We performed two sets of experiments systematically comparing thin Co films produced by those two methods.

In the first set of experiments we were growing Co films on NaCl layer. By dissolving NaCl layer it was possible to separate Co thin film and place it onto Cu gratings for subsequent Transmission Electron Microscopy study of its crystal structure. In Fig.1 we present TEM images and corresponding electron diffraction patters for Co films deposited by two alternative methods.
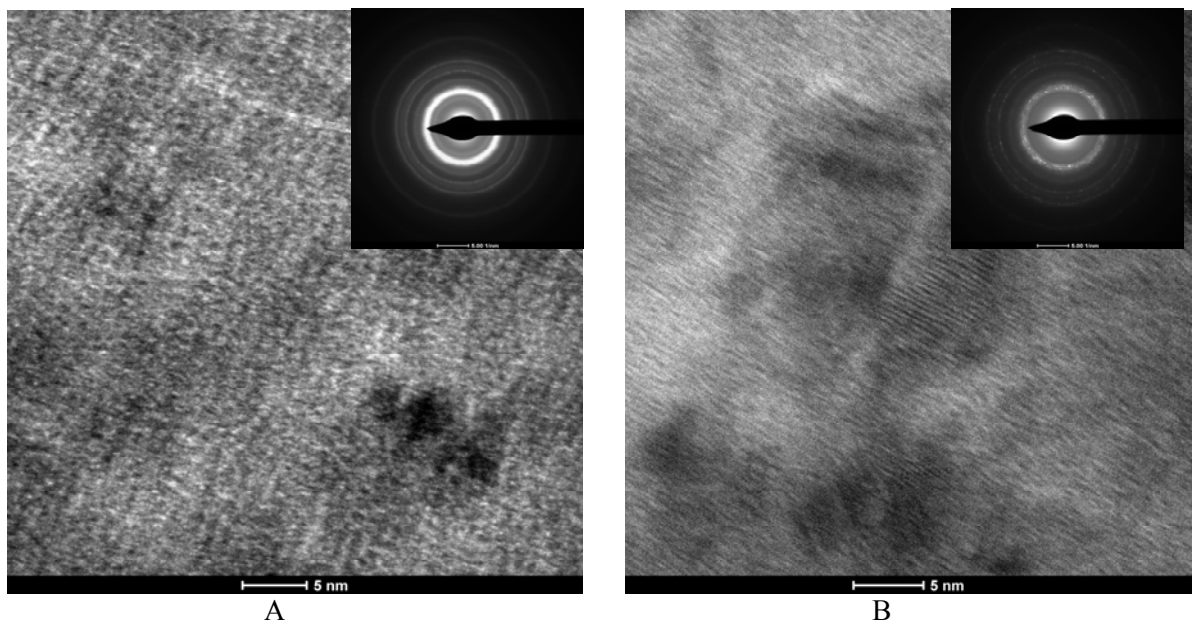
Fig.1 Transmission electron microscopy images (electron diffraction patterns on the insets) taken for two different Co films: A) ion-plasma sputtering, B) magnetron sputtering

From analysis of TEM data we conclude that ion-plasma film has less developed crystal structure (considerable fraction of amorphous phase) in comparison to magnetron film. Electron diffraction patters show presence of Co oxides fraction in the ion-plasma film.

In the second set of experiments we studied physical properties of thin Co films grown on Si(100) substrate with Ta buffer layer. We measured sheet resistivity, AMR effect and magnetic reversal loop for Co films deposited by two alternative methods.
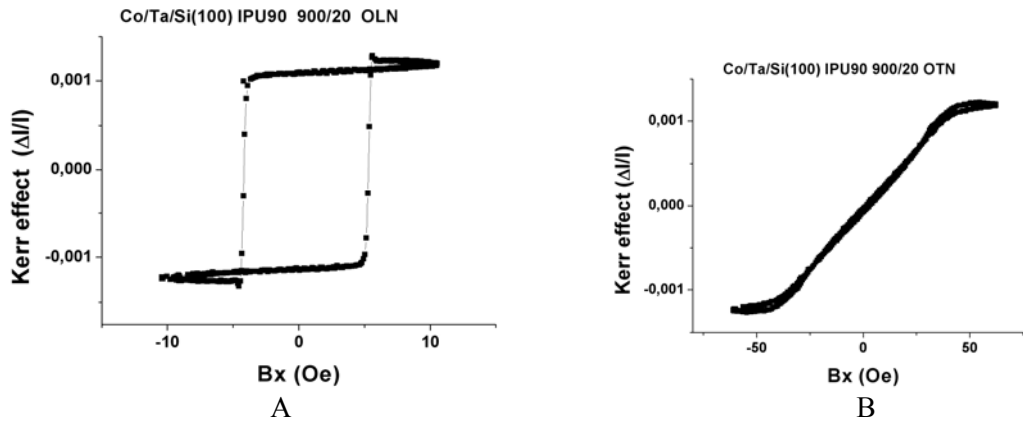
Fig.2 Transverse Kerr effect measurements for Co/Ta/Si(100) grown by ion-plasma sputtering: A) External magnetic filed along easy axis; B) along hard axis

In Fig.2 we show the results of Transverse Kerr effect measurements for Co/Ta/Si(100) grown by ion-plasma sputtering. Two pictures corresponds to two possible orientation of external magnetic field (A – along Easy axis, B – along Hard axis). The analysis of those results showed that Co films grown by ion-plasma method are magnetic with low coercetivity and easy axis oriented along direction of plasma discharge.

In summary, we checked possibility to use ion-plasma method for ultrathin Co film deposition for magnetic multilayer fabrication. We perfomed systematic comparison of as grown films with the films grown using standard magnetron sputtering. The results showed on principle the possibility of growing good quality magnetic films by ion-plasma method under condition of further work on improoving technology.

1. S. Tumanski *Thin magnetoresistive sensor*s, IOP publishing Ltd., Bristol, 2001.
2. R. Coehorn "Giant magnetoresistance and magnetic interactions in exchange-biased spin-valves", in *Handbook of magnetic materials*, volume **15**, Elsevier Science, Amsterdam, 2003.

P2-14: Mössbauer study of ZnO implanted with iron ions at high temperature

E.N. Dulov[1], A.I. Gumarov[1], D.M. Khripunov[1], N.G. Ivoilov[1],
V.F. Valeev[2], R.I. Khaibullin[1,2], L.R. Tagirov[1,2]

1. Kazan (Volga Region) Federal University, 420008 Kazan, Russia, fe57@rambler.ru 2. Zavoisky Physical-Technical Institute of RAS, 420029 Kazan, Russia, rik@kfti.knc.ru

Zink oxide implanted with transition metal ions is considered as a new promising material for spintronics revealing diluted magnetic semiconductor properties. At the present time works concerning $Fe^+ \rightarrow ZnO$ [1,2] demonstrate some contradictions, but lead to a conclusion that the formation of diluted and ferromagnetic at room temperature phase is possible. The work presented is devoted to investigation of phase formation in $Fe^+ \rightarrow ZnO$ by means of conversion electron Mössbauer spectroscopy (CEMS).

In this study, the single crystalline (0001)-face oriented plates of ZnO (CrysTec) were implanted with 40 keV and Fe^+ ions to the high fluence of 1.5×10^{17} $ions/cm^2$ at high (900 K) temperatures of substrate. Implanted iron was enriched by resonant isotope ^{57}Fe to ~30 at.%.

CEMS study was carried out on standard Mössbauer spectrometer with gas-flow (He+5%mol.CH_4) proportional detector of conversion electrons. Obtained Mössbauer spectrum is shown on fig.1.
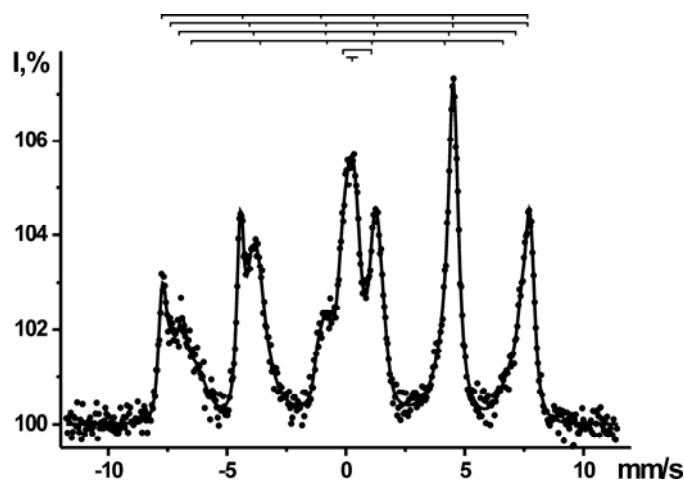
Fig. 1. Mössbauer spectrum of $Fe^+ \rightarrow ZnO$.

Fig.1 shows that most of the implanted ions belongs to ferromagnetic phases (>80%). Sextets may be ascribed to iron oxides diluted by Zn ions, but on the other hand at least some of sextets may be caused by iron substituted ZnO. In any case thin film studied reveals strong ferromagnetism at room temperature.

1. H.P. Gunnlaugsson et al. "Paramagnetism in Mn/Fe implanted ZnO", Appl.Phys.Lett., 97, pp.142501, 2010
2. Krishanlal Bharuth-Ram et al. "A CEMS search for precipitate formation in ^{57}Fe implanted ZnO", Hyp.Int., 207(1-3), pp.49-52

P2-15: The Influence of Superparamagnetism in Magnetic Properties of the Alloy MnAl

V. Boydenko

P.G. Demidov Yaroslavl State University, Yaroslavl, Russia, E-mail exphys@uniyar.ac.ru.

In recent years attracted great interest of researchers spatially modulated structures (SMS), in which the particle size of different phases is of the order of the mean free path of electrons. The materials with SMS include multilayer coatings, heterogeneous alloys, nanocrystalline system.

Among the heterogeneous alloys a wide variety of possibilities of varying the phase composition, the type of magnetic ordering alloys have the system Mn-Al. Non-ferromagnetic elements Mn and Al in the alloys near the equiatomic composition ($51 - 59$ atomic% Mn), in this case 55 at% Mn-Al, form a metastable ferromagnetic τ-highanisotropic phase with a fct lattice, ordered by type CuAu I (L1$_0$). This phase is obtained either by cooling from the region of existence of an antiferromagnetic ε-phase with optimal rate of $6 - 30$ K/s, for example, in this paper from 1100 °C at a rate of 20 K/s, or when annealing in the temperature range $400 - 700$ °C ε-phase, fixed by quenching the alloy in water from 1100 °C.

Equilibrium below 800 °C are non-ferromagnetic η-phase enriched in aluminum (face-centered rhombohedral lattice) and manganese-rich β-phase with a complex cubic lattice.

Measurements of magnetic properties in this paper produced by vibrating sample magnetometer using a nickel standard, which took the form of samples.

The maximum magnetization M_{max}, quenched alloy in the field $H_{max} = 376$ MA/m increases twice when the temperature changes from 300 K to 150 K, which corresponds to the para- or superparamagnetic behavior of the τ-phase nuclei, since the magnetic susceptibility in this case is inversely proportional to the temperature:

$$\chi = \frac{C}{T} \tag{1}$$

After tempering the quenched alloy at 380 °C for 30 minutes ferromagnetic phase was $5 - 10$ % of the samples, and superparamagnetic phase it took $30 - 40$ % of this amount, according to the temperature dependence of $M_{max}(T)$. As the temperature measurement, since the blocking temperature $T_B = 210$ K, there is an increase of the remanent magnetization M_r, which corresponds to the size of the superparamagnetic particles of 18 nm according to the relation:

$$K_A \cdot V = 25 k_B \cdot T_B \tag{2}$$

where $K_A = 108$ Dzh/m^3 – magnetocrystalline anisotropy constant, k_B – Boltzmann constant, V – volume of the particle.

Along with the increase in M_r increases the coercive force. After tempering at 400 °C 50 minutes, change the properties similar to that described above, and the content of superparamagnetic phase, approximately 20 % of the total number of τ-phase component of ~ 40 % by weight of the samples.

For samples with the number of τ-phase, 80 % relative change in properties with temperature is less, because the low-temperature curves $M(T)$ and $K_A(T)$ is almost horizontal.

The course of the magnetization curves of the above powder is not contrary to the assumptions made.

P2-16: Influence of an external magnetic field on the structure of granular Co-Cu films deposited by ion-plasmic method

Ed. Buchin, D. Kokanov, and V. Naumov

Yaroslavl Branch of the Institute of Physics and Technology, Russian Academy of Sciences, Yaroslavl, Russia,
E-mail addres: imi.buchin@rambler.ru

The magnetic granular films equally with other GMR structures are studied actively in respect to magnetic sensors and computer memory. In this case pair Co-Cu was used to obtain granular medium. Experimental films were forming by sputtering deposition on the hot substrate (200°C) from the mosaic target under high vacuum conditions without subsequent annealing. Such one-stage process led to spontaneous phase separation. The structure and magnetic properties of the deposited films greatly depended on the process conditions. For example the films deposited on SiO_2 and c-Si substrates in pari causa considerably differed in surface morphology (Fig.1a, 1d). The film formed on oxidized siliceous substrate was notable for homogeneous wavy surface. The film formed on single-crystal substrate has a lot of the quasi-crystalline inclusions - submicron-size pyramids, which formed mainly on superficial defects. Data of the EDX-spectrometer analysis has shown that these inclusions on the structure differ from the basic material ($Co_{20}Cu_{80}$) of the film [1]. They are phase fluctuations with the low maintenance of cobalt (only 6 % at.).

In this work was investigated influence of an external magnetic field as technological parameter within the limits of one-stage process. Objects of comparison were specified above the films with considerably differing structures. Morphological properties of the samples were studied using high-resolution scanning electron microscopy (Zeiss Supra-40).

During experiments the constant magnet (SmCo) of the cylindrical form has been established from the back party of the sample. If the magnet was placed in parallel to the sample the homogeneous magnetic field by intensity 500 Oe has been registered at its surface. If the magnet was placed perpendicularly to the sample a non-uniform magnetic field has been registered, in the centre of the sample its intensity reached 800 Oe and along edges of the sample only 80 Oe. Deposition of films was made at the same technological parameters at which the samples mentioned above have been received.

In the presence of an external magnetic field films with structure considerably different from the comparative samples were formed. In the case of parallel magnetic field on SiO_2 substrate was formed array of isolated columnar elements with diameter of 30 nm (Fig.1b). On crystal silicon substrates structurally homogeneous films without pyramidal inclusions were formed (Fig.1e). In the case of perpendicular magnetic field on SiO_2 substrate was formed structurally homogeneous film similar to the comparative sample, but with large-scale wavy surface (Fig.1c). On crystal silicon substrates were formed the films having homogeneous structure in the centre of samples and pyramidal inclusions on its edges (Fig.1f).

The general reason of observable structural changes in the investigated granular films, possibly, is diamagnetic nature of copper. During deposition adatoms have superfluous energy and actively move around on a surface of substrate. Their state can be characterised as quasi-liquefaction. Thus diamagnetic atoms of copper are forced out by an external magnetic field in a direction, to perpendicular its field lines. Paramagnetic atoms of cobalt aspire to move in the opposite direction. In a case presented on (Fig 1б), it promotes formation columnar structures. In a case presented on (Fig. 1e), it leads to masking of superficial defects therefore pyramidal inclusions which consist on 94 % of copper are not formed. If the magnet are placed perpendicularly to the sample diamagnetic copper atoms and paramagnetic cobalt atoms move along a surface of the sample. For this reason in a case presented on (Fig.1c), already there are no conditions for columnar structure formation. In a case presented on (Fig.1f), intensity of a magnetic field at edges of the sample is insufficient for masking of superficial defects, therefore pyramidal inclusions here are again formed.

Thus during researches it has been found that the external magnetic field is the technology parameter strongly defining structure and, accordingly, magnetic properties of granulated Co-Cu films.

Films on SiO₂ substrate

Films on c-Si substrate
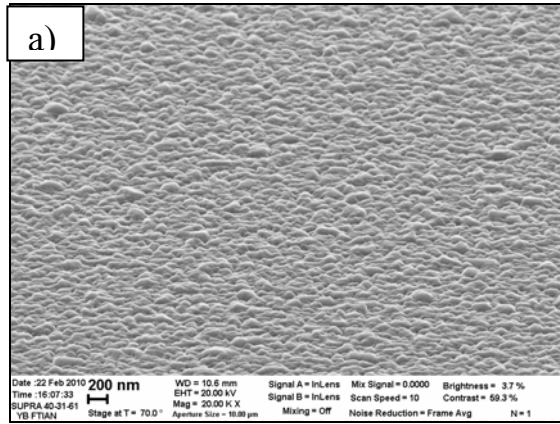
structurally homogeneous film
formed without influence of
an external magnetic field
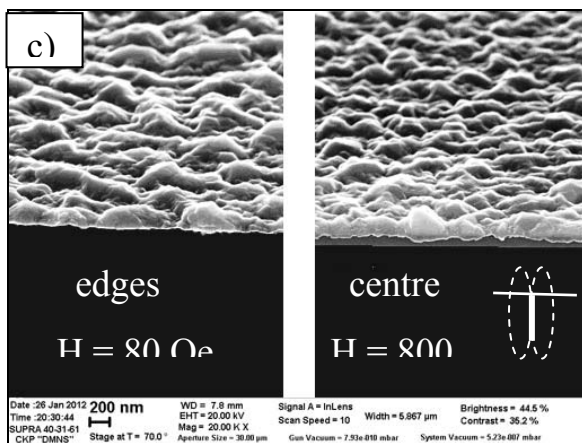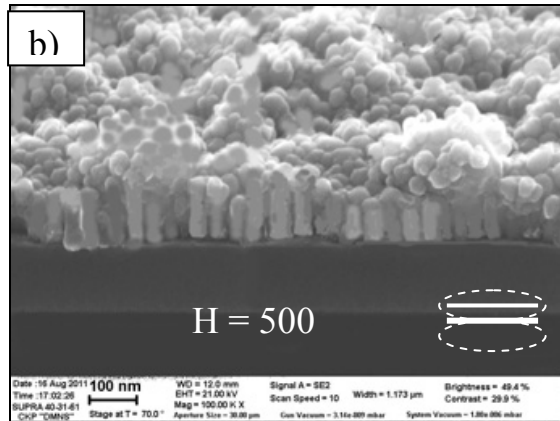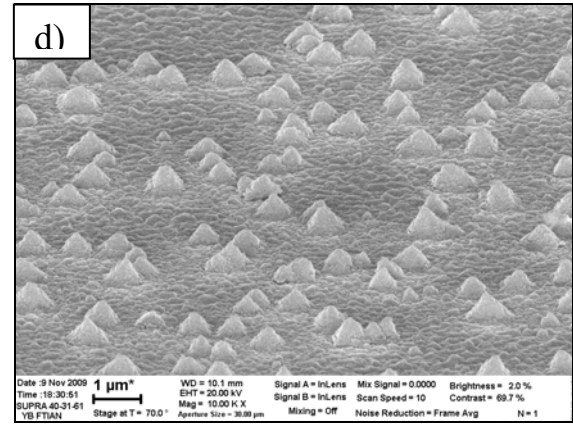
film with the pyramidal inclusions,
formed without influence of
an external magnetic field
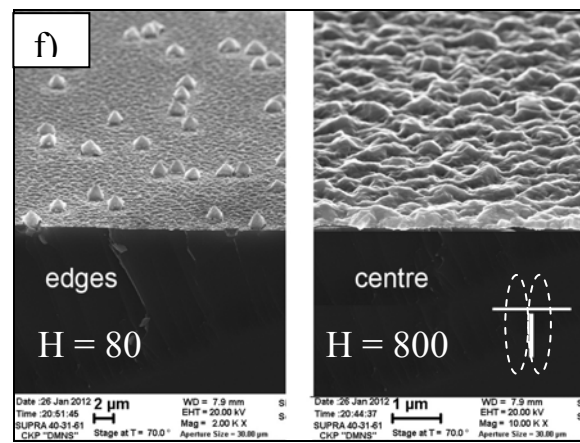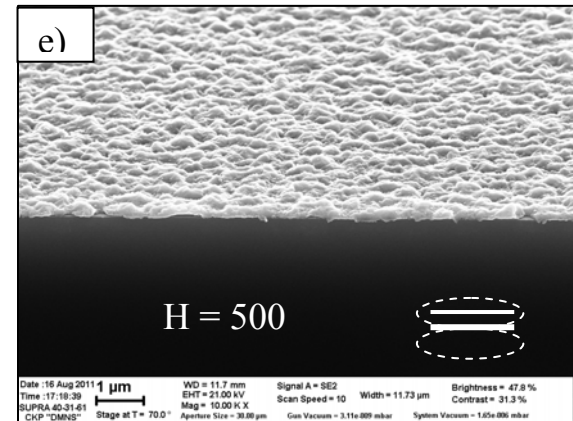
Fig.1. Illustration of influence of an external magnetic field on structure of the formed granular Co-Cu films.

1. E.Yu.Buchin, V.F.Bochkarev, D.A.Kokanov, and V.V.Naumov. *International conference "Modern problems in physics of surfaces and nanotructures",* Yaroslavl, Russia, 2010, Book of abstracts, O2-8.

P2-17: Investigation of thermal characteristics and stability of Ge-Sb-Te-Ti thin films

A. Sherchenkov[1], S. Kozyukhin[2], A. Babich[1]

1. *National Research University of Electronic Technology, Moscow, Russia, aa_sherchenkov@rambler.ru.*
2. *2. Kurnakov Institute of General and Inorganic Chemistry of the Russian Academy of Sciences, Moscow, Russia, sergkoz@igic.ras.ru*

Phase-change memory devices on the basis of $Ge_2Sb_2Te_5$ semiconductor are actively developed now. One of the attractive advantages of phase-change memory in comparison with flash memory is considered cycling endurance (from 10^6 up to 10^{13} cycles against 10^5 for flash memory).

However, it was previously shown [1] that multiple heat treatments of thin films of such material leads to the appearance of the endopeak in the temperature range from 390 to 415°C due to the phase separation. Phase separation is destructive for cycling life, and can initiate reliability issue. It is possible to increase stability by doping the material with different impurities. One of such dopant may by Ti. Therefore, the aim of this work was to investigate thermal characteristics of thin films based on the materials of Ge-Sb-Te-Ti system, and their stability during multiple heat treatments.

The synthesis of materials was carried out in evacuated sealed quartz ampoules at 850°C for 10 h, and $Ge_2Sb_2Te_5$ with different Ti concentration (0, 0.5, 1, 3 wt. %) was obtained. Thin films were deposited by the thermal evaporation of the synthesis materials in vacuum.

The thermal behavior of thin films was investigated with using of differential scanning calorimeter DSC-50 (Shimadzu). Thin films were scraped off from the c-Si wafers and pressed into Al pans. Samples were heated with the rate of 10 K/min in the nitrogen atmosphere. Empty Al pans were used as references.

DSC scans of investigated samples are presented in fig. 1. Exothermic peak corresponding to the transition of amorphous to crystalline state is observed for all investigated compositions in the temperature range from 140 to 180°C. Another exothermic peak due to the transition from cubic to hexagonal state in the temperature range from 200 to 260°C is also seen for all samples. In addition, endothermic peak in the temperature range from 390 to 415°C was found for undoped $Ge_2Sb_2Te_5$. Endothermic peak due to melting of the materials is observed at temperatures above 600°C.
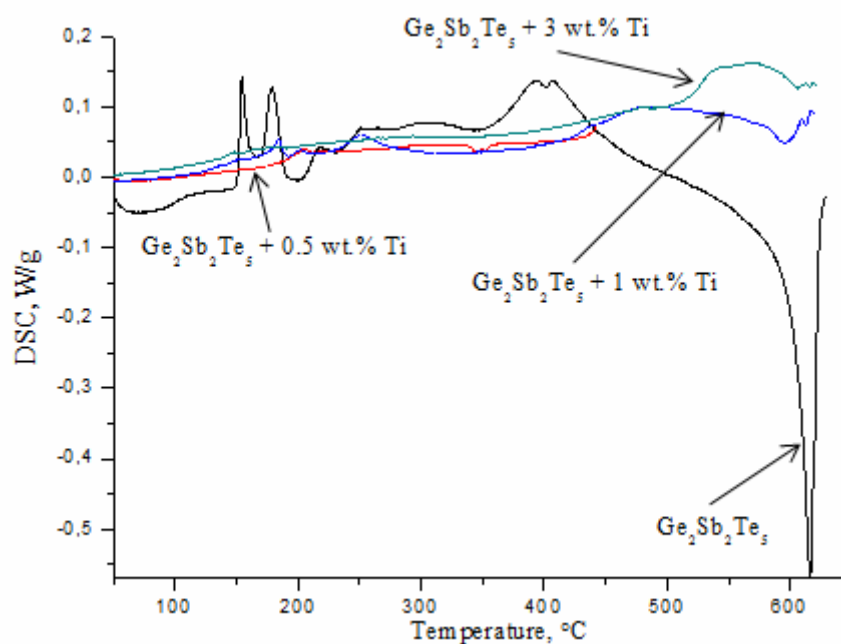
Figure 1 – First DSC measurements for Ti doped $Ge_2Sb_2Te_5$ thin films

In the case of overlapping peaks decomposition with using of Gaussians was carried out. This fitting procedure allowed estimating characteristics of the peaks. Analysis of DSC data showed that introduction of

Ti leads to the modification of crystallization temperature, and decrease of the value of heat effect. The crystallization temperature of $Ge_2Sb_2Te_5$ is 156.2°C. Incorporation of 0.5 wt. % Ti leads to the sharp increase of the crystallization temperature up to 188.1°C. For samples with 1 wt. % and 3 wt. % of introduced Ti crystallization temperature decreases to 137.2 and 140.7C, respectively. The value of the heat effect of crystallization decreases from is 2.95 J/g for $Ge_2Sb_2Te_5$ to 0.452 J/g, 0.683 J/g, and 0.261 J/g for compositions with 0.5 wt. %, 1 wt. %, and 3 wt. % of Ti, respectively. This can be connected with the modification of the chemical bonding by Ti.

To investigate the behavior of materials during repeated heat treatment, multiple DSC measurements were carried out. For undoped $Ge_2Sb_2Te_5$ the peak in temperature range from 390 to 415°C is observed already after the first measurement, and rapidly increased with following DSC measurements. For Ti-doped materials this endopeak also appeared, however not after the first DSC measurement, but later, and its increase with following experiments is slower.

The temperatures of endothermic peaks in the temperature range 390-415°C are quite close for all investigated materials, which indicate on the similar nature of the processes leading to the appearance of these heat effects. The nature of endopeak is connected with the phase separation in the grains during repeated heat treatments due to the diffusion of the mobile Te atoms to the grains boundaries. This results in inhomogeneous composition of the grains, phase separation, and melting of the phases. In this case, Ti doping can block diffusion of the mobile Te atoms to the grains boundaries preventing phase separation, and increasing stability of the material.

Thus, Ti doping of $Ge_2Sb_2Te_5$ can not only changes thermal characteristics, phase transition temperature, but also significantly improve stability of the material during thermal cycling, which is important for fabrication of PCM cells with increasing reliability.

1. A.A.Sherchenkov, S.A. Kozyukhin, E.V. Gorshkova, "Transformations in phase-change memeory material during thermal cycling", Journal of Optoelectronics and Advanced Materials, **11,** pp. 26-33, 2009.

P2-18: Electrical and thermal properties of indium doped $Ge_2Sb_2Te_5$ thin films

P. Lazarenko[1], A. Babich[1], S.Kozyukhin[2], A.Sherchenkov[1], A. Vargunin[2]

1. National Research University of Electronic Technology, Moscow, Russia, aka.jum@gmail.com.
2. Kurnakov Institute of General and Inorganic Chemistry, Moscow, Russia sergkoz@igic.ras.ru

Thin films of chalcogenide semiconductor on the basis of Ge-Sb-Te system (GST) are currently intensively studied due to their possible applications in devices of phase change memory, particularly in nonvolatile memory cells of PCRAM type [1-2]. $Ge_2Sb_2Te_5$ (GST225) is the most promising composition for phase change cells.

Variation and optimization of the properties of materials used in phase-change memory cell are possible by doping and modification of the structural matrix. It was reported that In-doping effectively influences the kinetics of crystallization of $Ge_2Sb_2Te_5$, which provide fast operation speed, and a way to satisfy the compromise between crystallization rate and archival lifetime of the recording materials [3]. However, questions of the influence of In-doping on the properties and stability of $Ge_2Sb_2Te_5$ are not well understood yet.

In this study we investigated the influence of In-doping on the electrical and thermal properties of the $Ge_2Sb_2Te_5$ thin films.

The initially doped $Ge_2Sb_2Te_5$ alloys with different amounts of In (0, 0.5, 1 and 3 wt.%) were prepared using quenching technique. The amorphous thin films were deposited by the thermal evaporation in vacuum. The thicknesses of the films were determined with using of AFM (NT-MDT SolverPro) scans, which were in the range from 50 to 80 nm. The morphology of the thin films was studied by SEM (Carl-Zeiss NVision 40). The chemical and phase compositions of the films were determined by X-ray fluorescence analysis (XRF) and X-ray diffraction (XRD).

The set-up on the basis of KEITHLEY 6486 and a voltage control unit NI6008 was developed and used for investigation of the temperature dependences of resistivity of thin films. Planar structures containing Al electrodes with fixed inter electrode distances (1, 5, 10 μm), and deposited upon them GST thin film were fabricated on oxidized c-Si substrates. In order to reduce flaking of the GST thin film away from the electrode contact boundary due to the phase transformation during the heating [4] silicon dioxide thin film with 0.5 μm thickness was deposited by electron-beam evaporation on the top of GST film. The temperature of the samples during the measurements was varied from room temperature to 350 °C with the heating rate of 1 °C/min.

Differential scanning calorimetry (Shimadzu DSC-50) was used to study the thermal properties of the materials. Thin films were scraped off from the c-Si substrates with sapphire spatula. Portions of thin films powder (2-4 mg) were pressed and sealed in aluminum pans. Heating rate was 10 °C/min, maximum heating temperature was 630 °C, and high-purity nitrogen was used to provide an inert atmosphere.

(a)   (b)
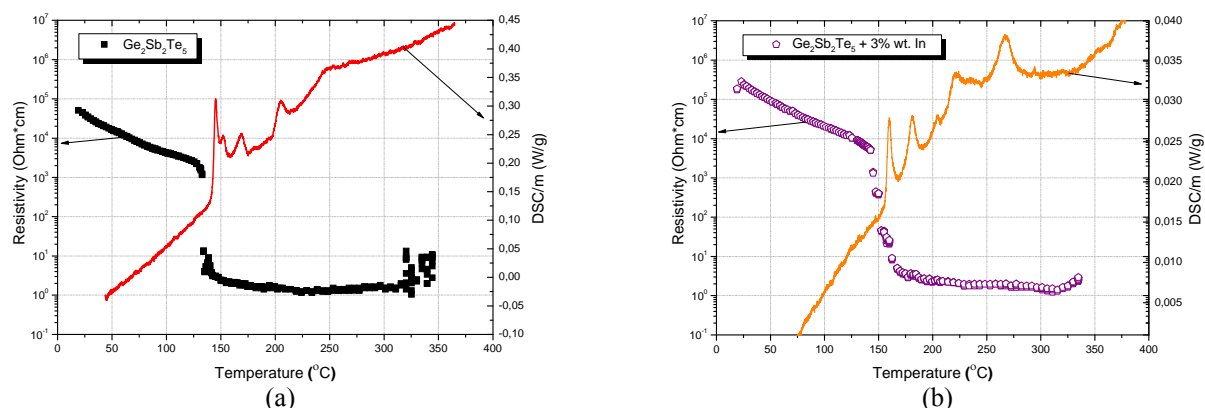
Fig. 1. Temperature dependences of resistivity and DSC-curves: (a) $Ge_2Sb_2Te_5$; (b) $Ge_2Sb_2Te_5$ + 3 % wt. In

Figures 1 (a) and 1 (b) shows the summary graphics of DSC-measurements and temperature dependences of resistivity of the $Ge_2Sb_2Te_5$ and $Ge_2Sb_2Te_5$ + 3 wt. % In thin films, respectively. Table 1 summarizes the results of the measurements of the temperature dependences of resistivity and differential scanning

calorimetry of $Ge_2Sb_2Te_5$ and In-doped $Ge_2Sb_2Te_5$. In the table ρ_{RT} denotes resistivity at the room temperature, while ρ_x and ρ_y - resistivities at the beginning and at the end of the phase transformation, respectively.

Exponential temperature dependences of resistivity were established for the investigated thin films in the range from room temperature to 120 °C, which are typical for the amorphous GST. The activation energy of the amorphous phase's conductivity was determined.

A sharp drop of resistivity and endo DSC-peak were observed in the temperature range from 120 to 170 °C, which are attributed to the transition from amorphous to metastable cubic structure of NaCl-type. The value of resistivity drop increased with the increase of In content.

The results of measurements showed that the incorporation of In in $Ge_2Sb_2Te_5$ shifts the phase transition temperature from amorphous to crystalline state to the higher values, which can be attributed to the change in the local chemical bonding [5]. However, the values of the phase transition temperatures obtained by the resistivity measurements (132 °C for undoped GST225, and 140 °C for GST225 with 3 wt. % In) are lower than that observed by the differential scanning calorimetry (141 °C for undoped GST225, and 154 °C for GST225 with 3 wt. % In), which can be attributed to the different heating rates.

Table 1. Electrical and thermal properties of the In-doped $Ge_2Sb_2Te_5$.

Material	In, wt. %	Temperature range of the phase transition, °C		ρ_{RT}, $\Omega\cdot cm$	ρ_x, $\Omega\cdot cm$	ρ_y, $\Omega\cdot cm$	E_a, эВ
		Resistivity measurements	DSC measurements				
$Ge_2Sb_2Te_5$	-	132-141	141-149	$4.5\cdot10^4$	$1.5\cdot10^3$	3.7	0.28
$Ge_2Sb_2Te_5$	0.5	136-153	147-154	$1.3\cdot10^5$	$4.5\cdot10^3$	3.3	0.29
$Ge_2Sb_2Te_5$	1	139-161	150-159	$7.8\cdot10^5$	$1.2\cdot10^4$	24	0.35
$Ge_2Sb_2Te_5$	3	140-166	154-162	$2.9\cdot10^5$	$6.2\cdot10^3$	3.6	0.31

The obtained data (Table 1) showed that incorporation of a small amount of indium into GST225 material (up to 1 wt. %) led to the increase of the activation energies and resistivities of thin films. At the same time the addition of 3 wt. % In is accompanied by the decrease of the activation energy and resistivity. The deviation from the trends for the dependencies of electrical properties on the dopant concentration with the high dopant content was also observed for the Bi-doped GST225 [4] and was associated with phase separation.

So, incorporated of indium into the GST225 material leads to the modification of thermal and electrical properties, which can be used for the optimization of phase change memory cell technology and increase of the device reliability. However, indium content must be carefully controlled.

1. A.L. Lacaita, "Phase change memories: State-of-the-art, challenges and perspectives", Solid-State Electronics. **50**, 24–31, 2006
2. M. Wuttig, "Towards a universal memory?", Nature Materials. **4**, 265-266, 2005
3. K. Wang, C. Steamer, D. Wamwangi, S. Ziegler, M. Wuttig, "Effect of indium doping on $Ge_2Sb_2Te_5$ thin films for phase-change optical storage", Microsyst Technol, **13**, 203–206, 2007
4. P. Lazarenko, Huy Phuc Nguyen, S. Kozyukhin, A. Sherchenkov, "Influence of Bi doping on electrical and optical properties of phase change material $Ge_2Sb_2Te_5$", Journal of Optoelectronics and Advanced Materials, **13**, 1400 – 1404, 2011
5. H. J. Shin, Youn-Seon Kang, Anass Benayad, Ki-Hong Kim, Y. M. Lee et al.., "Effect of indium on phase-change characteristics and local chemical states of In–Ge–Sb–Te alloys", Appl. Phys. Lett., **93**, 021905, 2008

P2-19: Stress fields within the cantilever console according to raman scattering

A. Kuzmenko[1], D. Timakov[1], P. Abakumov[1], M. Dobromyslov[2]

1. South-West State University, Kursk, Russia, E-mail address: apk3527@mail.ru
2. Pacific National University, Khabarovsk, Russia, E-mail address: mdobr@bk.ru

The change-over to nano-scaled level of measurements prompts qualitative changes in materials science, facilitates the development of notions about the interrelations among composition, structure, and properties of surface layers [1–4]. We report here the investigation results of nano-scaled changes arising from the concentric elastic effects on a microscopic object, the cantilever console. The results have been obtained by the Raman scattering together with atomic-force microscopy (AFM).

Equipment for studying distributions of micro- and nanostresses within the cantilever's console was composed from a Raman spectrometer OmegaScope intergrated with AFM (AIST-NT, Zelenograd-city, Russia). A confocal microscope was used to provide a hgh—accuracy positioning and recording of elastic stresses applied and also the laser radiation at 532 nm with a power of 50 mW. The spatial and spectra resolution was equal to 425 nm and 0.8 cm^{-1}, respectively. As a model sample an elastic cantilever's console with the size of 135x35x2mµ was deformed. The maximum shift of the beam's loose end was 280 µm, which corresponds to the maximum pressure of the order of 4 GPa.

With the use of micro Raman spectroscopy (MRS) data (a total of 900 scan spectra) topological distributions of elastic stresses within a curved cantilever's beam were plotted. Figure 1 shows the characteristic distribution along the beam of Raman shifts and pressures in various points of the cantilever predicted with consideration for the stiffness coefficient. It should be noted the agreed changes in applied pressures and Raman shift variations, substantiating the possible mapping of stress distributions in bends of the beam.
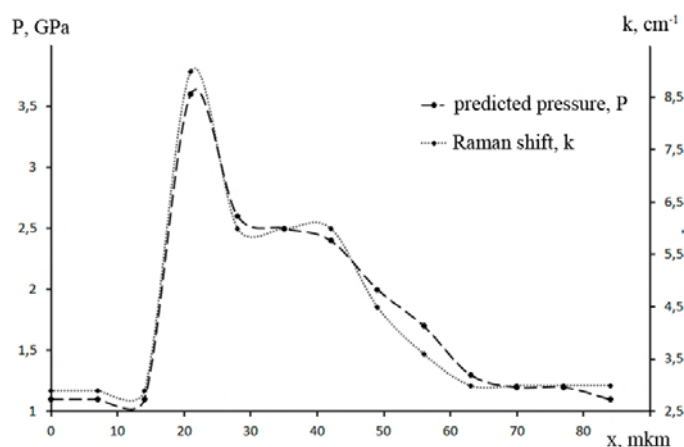
Fig. 1. Raman shift scan and the distribution of predicted pressures along the cantilever beam

With the use of such scanograms the maps of hyperspectral distributions of sresses along the beam have been constructed in two mutually-perpendicular directions, namely, along its plane and perpendicular[4]. The examination of stress distributions in the beam cross section with MRS has shown the change of deformation sign in the beam bend, as seen in Fig.2.
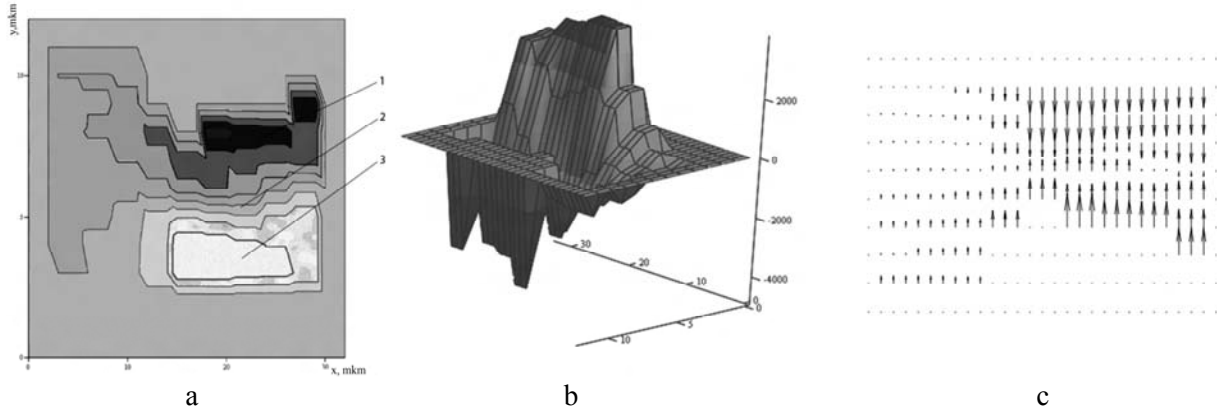
Fig. 2. Volume stress distributions and the change in stress sign in the cross-section of the console: a – compression 1, extension – 2, undeformed region -3; b – volume hyperspectral distribution according to the Raman shift; c – directions of deformation vectors

The dependence of the intensity of the MRS signal on the misrostresses in the cantilever's beam in the general form is dictated by the amplitudes of the incident (E_i) and scattered (E_s) light wave, and also by the Raman tensor (R_j):

$$I = C\Sigma \left| E_i R_j E_s \right|^2, \tag{1}$$

Where C is a dimension factor. For the studied silicon single crystal with a typical for semiconductors orientation (100) the 9- component Raman tensor is considerably simplified taking into consideration the geometry of elastic bend stress. This means that only one main peak (518 cm$^{-1)}$) can appear in the MRS spectrum. In doping of silicon with the hole conductivity formation in addition to this line another two ones appear, namely, 509 and 528 cm^{-1}. We have conducted the investigation with respect to the main peak, making it possible to apply conclusions:

$$\Delta\omega = [pS_{12} + q(S_{11} + S_{12})]\sigma/2\omega_0 \tag{2}$$

Considering the elastic constant values for silicon $S_{11} = 7.68\times10^{-2}$Pa^{-1}, $S_{12} = -2.14\times10^{-12}$Pa^{-1}, $p = 1.43\omega_0^2$ and $q = -1.889\omega_0^2$ for the maximum value of the Raman shift obtained (9 cm^{-1}) one can predict, using (2), the relevant value of the applied bend stress $\sigma = \Delta\omega/2\times10^9$Pa = 4 GPa. So it lead us to conclusion that findings on elastic stresses of the cantilever's console, measured for the first time, to our knowledge, with AFM, quite well agree with theoretical inferences.

Raman spectroscopy opens wide avenues in studying how internal stresses are distributed in materials at external actions in various stages long before the onset of irreversible changes and up to the complete destruction.

1. L. Skatkov, P. Cheremskoy, V. Gomozov , B. Bayrachny , G. Tulskiy and S. Deribo, "The Influence of Space Environment on Substructure of Light-Absorbing Thermoregulating", Coatings, 1, pp. 108-116, 2011
2. C. Himcinschi, M. Reiche, R. Scholz, S.H. Christiansen, and U. Gosele, "Compressive uniaxially trained silicon on insulator by prestrained wafer bonding and layer transfer", Applied Physics Letters, 90, 2007
3. R.S. Dubey, D.K. Gautam Synthesis, "Characterization of Nanocrystalline Porous Silicon Layer for Solar Cells Applications", Journal of Optoelectronic and Biomedical Materials, 1. Num. 1, pp. 8 –14, 2009
4. A.P. Kuzmenko, P.V. Abakumov, M.B. Dobromyslov, "Domain wall structure of weak ferromagnets according to Raman", Journal of Magnetism and Magnetic Materials, 324, pp. 1262–1264, 2012

P2-20: CW laser-induced nanomodification of PbX films

A. Antipov, V. Emel'yanov, A. Kucherik, S. Kutrovskaya

Stoletov's Vladimir State University, Vladimir, Russia, E-mail: 11stella@mail.ru

A nanostructured state of the narrow-gap semiconductors PbSe (band gap Eg=0.29 eV), PbTe (0.32 eV) and PbS (0.41 eV) is of interest for gaining insight into quantum size effects in relatively large systems, tens of nanometres in dimensions [1]. Nanostructures based on PbTe, PbSe, PbS and their solid solutions can be produced by a variety of techniques [1 - 3], including laser and laser-plasma deposition processes, which are of practical importance. Both below-band-gap ($\hbar\omega$ < Eg) and above-band-gap ($\hbar\omega$ > Eg) laser radiation, in different modes (e.g., laser ablation and/or heating), effectively changes the structural and electrical properties of the lead chalcogenides, producing micro- and nanostructures.

Laser exposure of semiconductor and metal surfaces is a promising technique for producing nanoparticle ensembles with tailored geometric characteristics (characteristic size and size distribution of the nanoparticles). To this end, a metallic or semiconductor target is typically ablated by high-power femto- (Si) [4], pico- (Ta) [5] or nanosecond (CdTe) [6] laser pulses. Elemental materials are laser-exposed through a liquid layer. The resulting nanoparticle ensembles may have a bimodal size distribution [5] In this paper, we report for the first time the formation of a nanoparticle on semiconductor (PbTe) films exposed to cw-laser radiation in air.

PbSe(Te)/CaF$_2$/Si(111) heterostructures were grown by molecular-beam epitaxy at the ETH Zurich. The thickness of the PbSe(Te) film was varied from 0.3 to 4 mm. The CaF$_2$ buffer was 2 - 4 nm in thickness and served to compensate for the lattice mismatch between the silicon substrate and epitaxial film. The lead chalcogenides layer was single-crystal, with its (111) plane normal to the growth direction.

A Nd : YAG laser beam (LS-02-T laser, 5 to 15 W output power, λ = 1.06 mm) was focused to a spot diameter of 30 mm on the sample surface. The incident power density was thus 10^4 to 10^5 W/cm^{-2}. During the laser exposure, the sample was scanned with the laser beam on a positioning stage, which was translated at 80 mm s^{-1}. The laser-exposed zone on the sample surface was examined in real time using a laser monitor, which allowed us to directly control the exposure conditions.

We studied solid-state laser modification of the surface of PbX semiconductor films and identified surface self-organization at photon energies above the band gap of the semiconductor. Experimental data were used to construct a model for defect-deformation instability developing on the surface of an epitaxial film through strain-induced drift of laser-induced point defects. The model is capable of qualitatively describing the observed surface morphology and predicting the surface profile in laser modification experiments.

1. Mukherjee S., Li D., Kar A.G.J., Shi Z. Transworld Research Network (Kerala, India, 2010) p. 88.
2. Abtin L., Springholz G., Holy V. Phys. Rev. Lett., 97, 266103 (2006).
3. Zimin S.P., Gorlachev E.S., Amirov I.I., Zogg H. J. Phys. D:Appl. Phys., 42, 165205 (2009).
4. Shen M.Y., Crouch C.H., Carey J.E., Mazur E. Appl. Phys. Lett., 85, 5694 (2004).
5. Barmina E.V., Barberoglu M., Zorba V., Simakin A.V., Stratakis E., Fotakis C., Shafeev G.A. Kvantovaya Elektron., 39, 89 (2009) [Quantum Electron., 39, 89 (2009)].
6. Baidullaeva A., Vlasenko A.I., Kuzan L.F., Litvin O.S., Mozol' P.E. Fiz. Tekh. Poluprovodn., 39, 1064 (2005).

P2-21: Vapor phase epitaxy fabrication of self-organized Mn-doped InAs/GaAs quantum dot arrays

A.V. Zdoroveishev, M.V. Dorokhin, E.I. Malysheva, B.N. Zvonkov

Physico-Technical Research Institute of Nizhny Novgorod State University, 603950 Nizhny Novgorod, Gagarin Av., 23/3, Russia , e-mail: zdorovei@nifti.unn.ru

Magnetic semiconductor based structures find a number of applications in modern electronics and optoelectronics as elements of new nanoelectronic and spintronic devices. The application of self-organized quantum dot (QD) arrays as a ferromagnetic semiconductor reveals sufficient prospective [1]. The current work is dedicated to investigation of such arrays.

The structures were grown by means of original technique [2] combining atmospheric pressure metal-organic vapor phase epitaxy (MOVPE) and laser sputtering of solid targets. This technique is characterized by high productivity and efficiency as compared to the alternative techniques for quantum dot fabrication (low pressure MOVPE, molecular beam epitaxy - MBE). The buffer GaAs layer was grown on n+ GaAs (100) substrate at 650 °C. At the next stage the growth temperature was lowered down to (480-550) °C and selforganized InAs quantum dot array was deposited on sample surface. The quantum dots were fabricated with the application of basic technique described in [1].

During the process of QDs growth their doping with Mn or Cr atoms was carried out by means of sputtering of Mn (Cr) targets by pulse Nd:YAG laser. The dopants concentration was varied by laser beam attenuation. The concentration was estimated by a comparison with the control structures containing single delta-Mn layer in GaAs fabricated in the same growth mode. According to the estimation the concentration was varied within the range of $4 \cdot 10^{12} - 2 \cdot 10^{13}$ cm^{-2}. QDs were overgrown by the thin (12 nm) GaAs layer at the same growth temperature. In the paper the investigations of photoluminescence (PL) spectroscopy were carried out at 77 K. The PL was excited by 200 mW Ar laser. The morphology of InAs QD array uncovered bu the selective etching of a cap layer [2,3] was investigated with NT-MDT Solver Pro atomic force microscope (AFM).
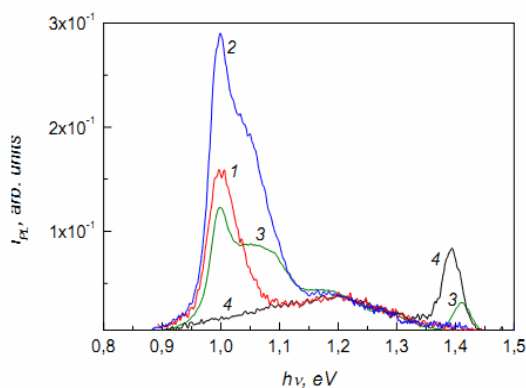
Fig.1. PL spectra (77 K) of samples with InAs/GaAs, QD arrays doped with Mn. Mn content, cm^{-2}:curve 1 – 0, curve 2 – $4 \cdot 10^{12}$, curve 3 – $8 \cdot 10^{12}$, curve 4 – $2 \cdot 10^{13}$.

At the photoluminescence spectra of undoped reference samples on can observe a doubled PL line (fig.1, curve 1) at the energies of ≈1 eV and (1,05 – 1,1) eV. According to the suppositions made in paper [2], the observed lines are due to the recombination in large and small size quantum dot arrays respectively. Both arrays may be present in a sample at the same time. Doping with Mn with threshold concentration of $2 \cdot 10^{13}$ cm^{-2} the sufficient changes in QD PL spectra occur (fig.1 curve 4): the lines corresponding to the radiative recombination in QDs is no longer observed. Instead the 1.4 eV peak is present. The origin of this peak cannot be interpreted unambiguously. Several centers may emit in 1.4 eV range, such as InGaAs quantum wells [5], isolated Mn levels in GaAs [4,5], or a wetting InAs layer which is formed at the first stage of QDs growth [2]. Supposedly in the case in point the radiation is due to InAs wetting layer. The layer mentioned is characterized by high non-uniformity due to Mn assisted In atoms diffusion. The non-uniformity is approved by a high PL line width (37 meV). Decreasing of Mnconcentration to $8 \cdot 10^{12}$ cm^{-2} leads to preservation of either low-energy (1 and 1.08 eV) or high-energy (1.4 eV) lines at the spectrum. Supposedly the latter Mn concentration allows to obtain an intermediate case. The decrease of concentration down to $4 \cdot 10^{12}$ cm^{-2} allows to obtain spectrum (fig.1 curve 2) which is analogous to a reference sample specrum. The introduction of Mn into QD region may be indirectly evidenced by a significant increase of photoluminescence intensity which is due to the increase of the hole concentration in the QDs.
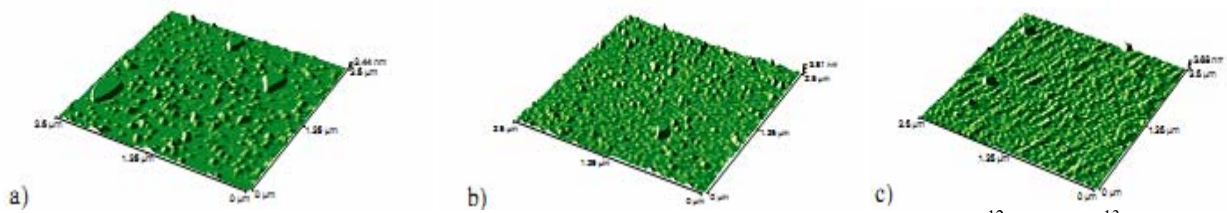
Fig. 2. AFM pictures of Mn-doped QD arrays. Mn content, cm-2:   a – 0, b – $8 \cdot 10^{12}$, c – $2 \cdot 10^{13}$.

The PL investigations may be corresponded by the measurements of the morphology of the surface of visualized QD array. The AFM investigation of the morphology of the reference undoped sample revealed (fig.2a) the QD array with the following parameters: lateral size – ≈60 nm, surface concentartion – ≈$5 \cdot 10^9$ cm^{-2}, height – ≈2.5 nm. In samples with InAs:Mn QD array with Mn concentration $8 \cdot 10^{12}$ cm^{-2} (fig.2 b), the average lateral size in the visualized array was increased to ≈ 90 nm, surface concentration decreased to ≈ $2 \cdot 10^9$ cm^{-2}, height decreased to ≈ 2 nm. In samples with $2 \cdot 10^{13}$ cm^{-2} Mn concentration (fig.2 c) the QD array was not revealed, instead relatively flat surface with ≈ 0.5 nm roughness was observed. Such picture is typical for InGaAs quantum well structure.

One may suppose that when high concentration of Mn is introduced large quantum dots are either not formed or formed with low surface concentration (lower than $5 \cdot 10^8$ cm-2), thus the QD identification by AFM picture becomes difficult. In this case only 1.4 eV peak is observed at the PL spectrum. Similar processes take place in structure with $8 \cdot 10^{12}$ cm^{-2} Mn content since the broad 1.4 eV line is also observed at the PL spectrum. This Mn concentration represents the threshold case: decreasing the Mn concentration leads to a "standard" QD arrays formation, increasing it prevents QD growth. In case of $8 \cdot 10^{12}$ cm^{-2} Mn content local regions with high Mn concentration are being formed on the surface (since the Mn distribution is non-unifrom). Within such regions QDs are not formed, instead InGaAs solid solution is formed. It leads to the decrease of QDs density.

This is the probable reason for the PL decrease in the sample as compared to the sample with lower Mn content. Within the regions with Mn content being lower than the threshold level the QD formation occurs. For that reason all 3 lines are observed at the spectrum.

Thus we have shown that the introduction of Mn into MOVPE reactor during the quantum dots growth allows doping the forming QD arrays. Mn doping increases structures PL intensity which is supposedly due to increase of hole concentration in the QDs because of doping. The QDs growth mechanism significantly depends on the Mn concentration. Within $(0,4-2) \cdot 10^{13}$ cm^{-2} range the transition from three-dimensional to layer-by-layer growth mode occurs which is accompanied by the decrease of QD density and of the intensity of the corresponding QD line.

1. A.V.Zdoroveishev, P.B, Demina, B.N. Zvonkov, "The influence of a periodic interruption of growth of InAs/GaAs quantum dots grown by vapor phase epitaxy at an atmospheric pressure on their morphology and optoelectronic spectra", Tech.Phys.Lett., 35, pp. 15–20, 2009 (in Russian).
2. I.A.Karpovich, et. al., "AFM investigation of the buried InAs/GaAs quantum dots with in situ monitoring of etching process by photoelectric and photoluminescence spectroscopy", Phys. Low-Dim. Struct., 3/4, pp. 191-196, 2003.
3. A.V.Zdoroveishev, "The effect of physic-chemical modification of cap layer on the morphology an photoelectric spectra of vapor phase epitaxy grown InAs/GaAs quantum dots" Author's abstract on PhD degree: 01.04.10, N.Novgorod, 22 p., 2006 (in Russian).
4. M.V. Dorokhin, et. al., "Formation of magnetic GaAs:Mn layers for InGaAs/GaAs light emitting quantum-size", Int. J. Nanoscience, 6, pp. 221-224, 2007.
5. S.V. Zaitsev, et. al., "Circularly polarized electroluminescence in LED heterostructures with InGaAs/GaAs quantum well and Mn d-layer", Physica E, 41, pp. 652-654, 2009.

P2-22: Multilayered photovoltaic structures based on tetrathiadiazoloporphyrazine/subphthalocyanine heterojunction

G. Pakhomov[1] , V. Travkin[1], A. Luk'yanov[1] , E. Gudkov[1] , P. Stuzhin[2] , M. Mikhailov[2]

1. Institute for Physics of Microstructures, Russian Academy of Sciences (IPM RAS), Nizhny Novgorod, Russia, E-mail: pakhomov@ipmras.ru. 2. Ivanovo State University of Chemical Technology (ISUCT), Ivanovo, Russia, E-mail address: stuzhin@isuct.ru

Surface physics and chemistry of thin layers of molecular semiconductors have received much attention in last decade, which is associated with rapid development of organic-based electronic devices, such as field-effect transistors (OFET), photovoltaic cells (OPVC) etc. There is continuous interest in new molecular architectures that would lead to unusual or improved functionalities of corresponding bulk phases. Tetrakis(thiadiazole)porphyrazines (TTDPz) are analogs of widely used in molecular electronics phthalocyanines; their synthesis was reported ~15 years ago [1].
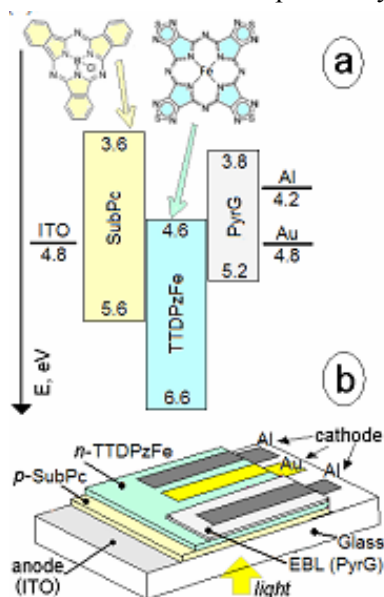
Fig. 1. Energy diagram with molecular structures (a) and schematic of OPVC (b).

Despite structural similarity with phthalo-cyanines, there are important distinctions that may stimulate a more intensive research on TTDPz complexes as materials for (opto-)electronic applications. First, introduction of π-electron-deficient thiadiazole rings instead of benzene rings leads to downward shift in energy positions of frontier molecular orbitals as compared with phthalocyanine compounds (Fig.1a), giving rise to negative sign of majority charge carriers [2]. Second, appearance of large peripheral sulfur atoms causes certain peculiarities in mutual arrangement of molecules in the bulk [2-5]. Third, there are no H-atoms in metallo-TTDPz complexes, so there is no hydrogen bonding, which is responsible for many features of molecular solid. Very recently, n-type conductivity of TTDPz was proved by measurements in OFET [2-4], in sandwich cells with different work function electrodes [4] and invertors [6]. Since phthalocyanine-like compounds are mostly p-type, opposite sign is often desired when manufacturing OPVC with p-n heterojunctions, as alternative to commonly used fullerene. In this work we report on first, to our knowledge, prototype of OPVC with a planar heterojunction based on TTDPz complex – Fig.1b. Iron tetrakis(thiadiazole)porphyrazine (FeTTDPz) was synthesized and purified at ISUCT according to Refs. [1,5]. Boron subpthalocyanine chloride (SubPc) was purchased from Aldrich and used as received. SubPc was chosen as a well-known p-type organic semiconductor [7] with appropriate energy band structure (Fig. 1a) and optical properties. The prototypes of OPVC were fabricated using standard vacuum evaporation technique by depositing thin layers of SubPc, FeTTDPz and top cathode, in that order, onto pre-cleaned glass/ITO substrate (anode) [7]. Thickness of layer was 35, 35 and 80 nm, respectively. Schematic of samples is shown in Fig. 1b. Three types of cathodematerials were tested: Au, Al and Al with pre-deposited 8 nm thick pyronine G (PyG) as exciton blocking layer (EBL) – see, Fig. 1b. Details of the sample preparation and testing are described elsewhere (see, [7] and references therein). At first, structural characterization of the single layer FeTTDPz thin films was carried out. Optical absorption measurements confirmed that FeTTDPz can successfully be sublimed under moderate vacuum ($<10^{-3}$ Pa) forming continuous layers without damaging molecular composition. As known [3,4], TTDPz films have a smoother surface compared to phthalocyanine films. Indeed, RMS surface roughness Sq is equal to 0.8 nm for a 90 nm thick FeTTDPz film deposited on ITO/glass substrate. In the UV/Vis spectra of FeTTDPz films all fundamental electronic transitions, such as Soret band (diffused through 330-380 nm), Q-band (peaked at ~660 nm) and less intensive CT band (~500 nm) are clearly seen [1-4]. FT-IR spectra (500-5000 cm^{-1}) show characteristic vibration bands that conform with those of initial FeTTDPz in powder.

X-Ray diffraction patterns do not reveal ordered packaging of FeTTDPz molecules in obtained film. This is similar to recently reported data [3] for a cone-shaped VOTTDPz derivative, which also forms

amorphous layers during vacuum sublimation. Note, however, that *Miyoshi et al.* obtained highly oriented films for other (planar) TTDPz compounds [3,4].Differences in crystallinity may be ascribed to different deposition rate (in out case – 0.1 nm/s), substrate material or temperature. Generally speaking, intermolecular interactions in the unit cell would be traced from Davydov splitting of electronic absorption bands. Unfortunately, all bands in UV-Vis spectrum of isolated FeTTDPz molecule are substantially broadened due to overlapping π-π^* and n-π^* transitions and presence of d-metal atom in the molecular core [1].
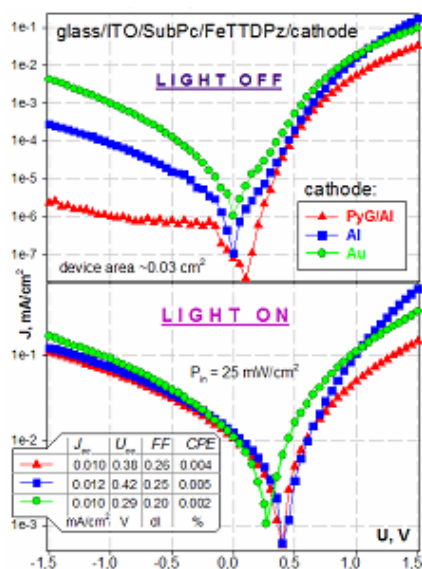
Fig. 2. J-V plots for OPVC with different cathodes in the dark (top) and under illumination (bottom).

Next, the completed OPVC prototypes were subjected to (photo) electrical testing. DC conductivity in the rang of +2…-2 V was measured in the dark and under white light illumination in laboratory conditions. Fig. 2 shows typical steady-state dependences of current density vs. applied voltage for OPVC with and without incident irradiation. Diode properties in the dark depend on the cathode material being the best for PyG/Al (rectification ratio $>5{\cdot}10^3$ @ 1V). When exposed to light, the cells generate output electrical power (positively biased ITO electrode), which manifests itself by displacement of curves in 4th quadrant of J-V plot.

Photovoltaic parameters are eakly affected by top cathode material – Fig. 2, inset. Better values are achieved with Al, mainly due to greater J^{sc}, and U^{oc}, with almost no effect of PyG interlayer. Lower values of U^{oc} and FF in case of Au may be explained by a barrier at Au/TTDPz contact [4]. A minor contribution of photogenerated carriers from FeTTDPz side is expected, since its own photoconductivity is much weaker than that of SubPc counterpart. Calculated power conversion efficiencies (CPE in Fig. 2) are very low, which is not surprising for OPVC without optimization of the layer thickness, heterojunction morphology, optical scheme etc. No especial care was taken on maintaining oxygen(water)-free conditions; yet, the cells degraded less notably than their full analogs, but with SubPc/C_{60} heterojunction. Therefore, we have demonstrated the working prototype of thin film OPVC employing a planar heterojunction, where n-type semiconductor was iron tetrakis(thiadiazole)porphyrazine, for the first time. The work was supported in part by RFBR project #12-02-01106-a and State Program "Leading Scientific School" (grant no. 3993.2012.3).

1. P.A. Stuzhin, E.M. Bauer and C. Ercolani, "Tetrakis(thiadiazole)porphyrazines. I.", Inorg. Chem., 37, pp.1533-1539, 1998 and ibid, 38, pp. 6114-6120, 1999.
2. X. Cai, Y.-X. Zhang, D.-D. Qi, J.-Z. Jiang, "Density functional theory study on organic semiconductor for field effect transistors: Symmetrical and unsymmetrical porphyrazine derivatives with annulated 1,2,5-thiadiazole & 1,4-diamyloxybenzene moieties", Science in China Series B: Chemistry, 52, pp.840-848, 2009
3. Y. Miyoshi et al. (10 authors), "Crystal Structure, Spin Polarization, Solid State Electrochemistry, and High n-type Carrier Mobility of a Paramagnetic Semiconductor: Vanadyl Tetrakis(thiadiazole) porphyrazine", Inorg. Chem., 51, pp. 456-462, 2012
4. Y. Miyoshi, T. Fujimoto, H. Yoshikawa, M. Matsushita, K. Agawa, T. Yamada, H. Ito "Photoconductivity and FET performance of an n-type semiconductor, tetrakis(thiadiazole)porphyrazine", Org. Electron., 12, pp. 239-243, 2011
5. Y. Suzuki, T. Fujimoto, H. Yoshikawa, K. Agawa, "Packing Motifs and Magneto-Structural Correlations in Crystal Structures of Metallo-Tetrakis(1,2,5-thiadiazole)porphyrazine Series, MTTDPz (M=H2, Fe, Co, Ni, Cu, Zn)", Chem. Eur. J. 10, pp. 5158-5164, 2004
6. T. Fujimoto, Y. Miyoshi, M. Matsushita, K. Agawa, "A complementary organic inverter of porphyrazine films: low-voltage operation using ionic liquid gate dielectrics", Chem. Comm., 47, pp. 5837-5839, 2011
7. G. Pakhomov, V. Travkin, A. Bogdanova, T.-F. Guo, "Photovoltaic properties of Schottky barrier cells utilizing subphthalocyanine layer" J. Porphyrins & Phthalocya., 12, pp. 1182-1186, 2008

P2-23: Kelvin Probe Microscopy Studies of the Surface Potential Variations on the Si(111)/Me Surface

S.V. Kazarinov[1], R.Z. Bakhtizin[1,2]

1. Department of Physical Electronics and Nanophysics Bashkir State University, Ufa, Russia, E-mail address: serjikk86@gmail.com; 2. Research and Education Center of Nanophysics and Nanotechnology Bashkir State University, Ufa, Russia, E-mail address: raouf@bsu.bashedu.ru

Kelvin probe force microscopy (KPFM) is a promising technique for studying conductive samples' surfaces in submicron scale [1]. Generally KPFM is a two-pass technique which is based on an atomic force microscopy (AFM). In the first pass, the probe is driven mechanically and the topography is imaged in tapping mode. In the second pass the probe retraces the previously captured topographic profile and the probe is driven electrically by applying to it excitation voltage V_{AC} with cantilever's resonance frequency ω. Capacitive force between probe tip and conductive sample:

$$F_z(\omega) = -\frac{\partial C}{\partial z}\left[(V_{DC} - \varphi(x,y)) \times V_{AC} \times \sin(\omega t)\right] \tag{1}$$

where C and z are the capacitance and distance between the tip and the sample, $\varphi(x,y)$ – local work function value in (x,y) point of the sample, V_{DC} и V_{AC} – voltages applied to the probe, while the sample is grounded. By adjusting of V_{DC} probe vibrations may be nullified then:

$$V_{DC}=\varphi(x,y) \tag{2}$$

i.e. then V_{DC} equals to surface potential in that point. Thus, KPFM allow us to obtain topography and surface potential distribution of the sample.

In this work we studied surface potential variations of metal (Au, In, Ti) films on the monocrystalline Si(111) surface. Au, In and Ti were evaporated onto silicon surface from an evaporator (W wire) under pressure $<10^{-3}$ Torr. The KPFM measurements performed with commercial SPM (NTEGRA Aura – NT-MDT) in ambient condition. A semicontact cantilever with TiN conductive coating was used as a probe.

The work function values of n-type Si(111), Au-, Ti-, In-films were 4.83, 5.1, 4.14 and 3.85 eV respectively. Obtained contact potential difference between Au and Si is approximately 0.3V. As silicon's work function is smaller than gold's, a surface potential will be greater in area, there is no Au film on Si surface. I.e. surface potential in this case distributes inversely to topographic profile. Figure 1 demonstrates respective topography and surface potential images.
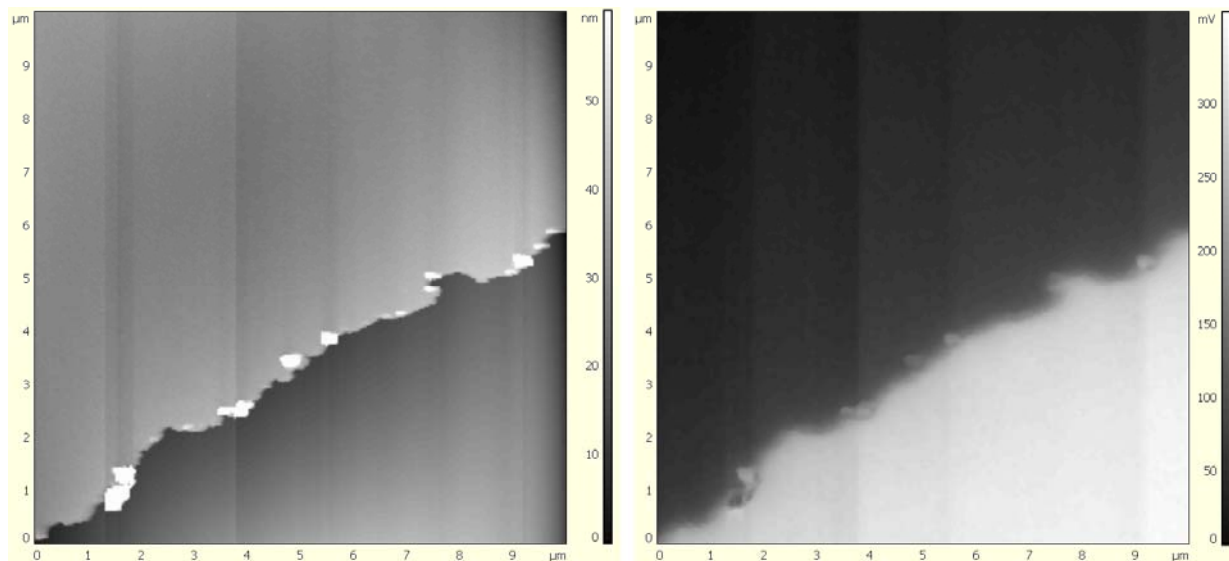
Fig. 1. Topography (left) and surface potential images of Au film on Si(111) surface.

1. P.K. Ingram, G.J. Wilson, R. Devonshire, "Measurements of the local work function of dispenser cathodes using an SPM technique", Appl. Surf. Science **146**, pp.363-370, 1999

P2-24: The carrier transport in the ferromagnetic quantum confined structures

A. Kudrin[1,2], O. Vikhrova[1], Yu. Danilov[1,2], I. Kalentieva[2], B. Zvonkov[1]

1. Physico-Technical Research Institute of University of Nizhny Novgorod, Nizhny Novgorod, Russia, kudrin@nifti.unn.ru. 2. Department of Physics of University of Nizhny Novgorod, Nizhny Novgorod, Russia

The Mn delta-doped GaAs layers are the subject of intensive studying by a number of research groups involved in the development of semiconductor spintronic devices [1-2]. One of the interesting areas of their application is a light-emitting diode, which produces circularly polarized light. As shown in [2], the presence of the Mn delta-doped layer resulted in a highly enhanced electroluminescence signal. In [3,4] it has been shown to us that Mn delta-doped GaAs layer itself possesses ferromagnetic properties. In GaAs structures only with single Mn delta-doped layer ferromagnetic properties were revealed by carrier transport investigations [3,4]. Galvanomagnetic measurements at low temperatures showed the presence of anomalous, planar Hall effect, anisotropic and negative magnetoresistance, and it is an evidence of ferromagnetism in the GaAs structures with Mn delta-doped layer. In particular at temperatures < 35 K the Hall resistance dependences on magnetic field ($R_H(H)$) were nonlinear without a hysteresis loop. The absence of the hysteresis loop on the $R_H(H)$ dependences can be related to the in-plane orientation of an easy magnetization axis. In this paper we present the investigation of the peculiarity of the carrier transport in GaAs structures containing InGaAs quantum well in addition to Mn delta-doped layer.

The structures were grown by the combined method of metal-organic chemical vapor deposition and pulse laser sputtering. Firstly a set of undoped layers was grown on *i*-GaAs (001) substrate by vapor-phase epitaxy at 600°C: 0.4 μm buffer GaAs layer, 10 nm thick $In_xGa_{1-x}As$ quantum well and 2 mn GaAs spacer layer. The vapor-phase epitaxy layers had *p*-type background doping with hole concentration about of $5 \cdot 10^{15}$ cm^{-3}. Then 0.2 monolayer thick Mn delta-doped layer and 20 nm thick GaAs cap layer were deposited at 400°C at reduced pressure in hydrogen flow using laser sputtering of metallic Mn and undoped GaAs targets, respectively. The In content was varied in range from $x = 0.1$ to 0.3 for different structures. Also the reference structure only with a single Mn delta-doped layer was fabricated.

The structure only with a single Mn delta-doped layer demonstrates at 10 K nonlinear Hall resistance dependence on magnetic field with hysteresis loop (coercive field ≈ 90 Oe) and saturation at magnetic field about 2000 Oe (Fig 1, dependence *1*). This indicate the presence of clear ferromagnetic properties and domination of anomalous effect in $R_H(H)$ dependences.
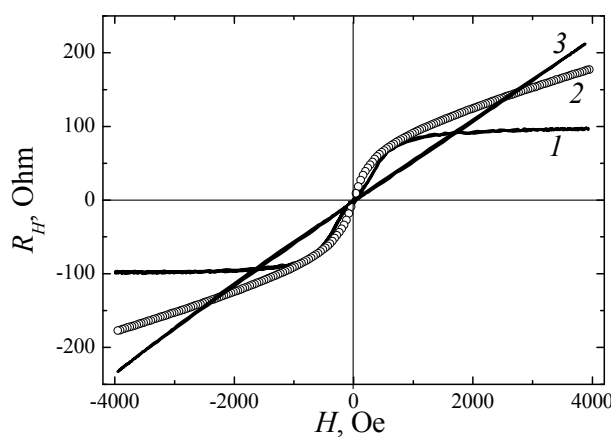
Fig. 1. Magnetic field dependences of Hall resistance at 10 K. *1* - The structure without InGaAs quantum well, *2* - The structure with InGaAs quantum well (In content is 0.15), *3* - The structure with InGaAs quantum well (In content is 0.3).

The structures with a quantum well beside Mn delta-layer demonstrate at 10 K differ character of the Hall resistance dependence. The shape of the RH(H) curves depends on indium content in InGaAs layer and consequently on the energy depth of a quantum well (Fig 1). With increasing In content the contribution from normal Hall effect increase. For the structure with the most deep quantum well the RH(H) dependence is linear, consequently, it determines by normal Hall effect (Fig 1, dependence 3). Is it indicates about the absence or weakening of ferromagnetic properties? In our opinion ferromagnetic properties of structures with Mn delta-doped layer have no direct relation to presence of InGaAs quantum well and its depth and related to intrinsic ferromagnetism of a Mn delta-layer. The insertion of a quantum well leads to appearance of an additional conducting channel for free charge carriers (holes). The distribution of charge carriers in a structure depends on quantum well depth. Fig. 2 shows

calculating band diagrams and carrier distribution at 77 K for the structure only with single Mn delta-layer (Fig 2a) and for the structures with Mn delta-layer and quantum well of different depth (Fig 2b and c).
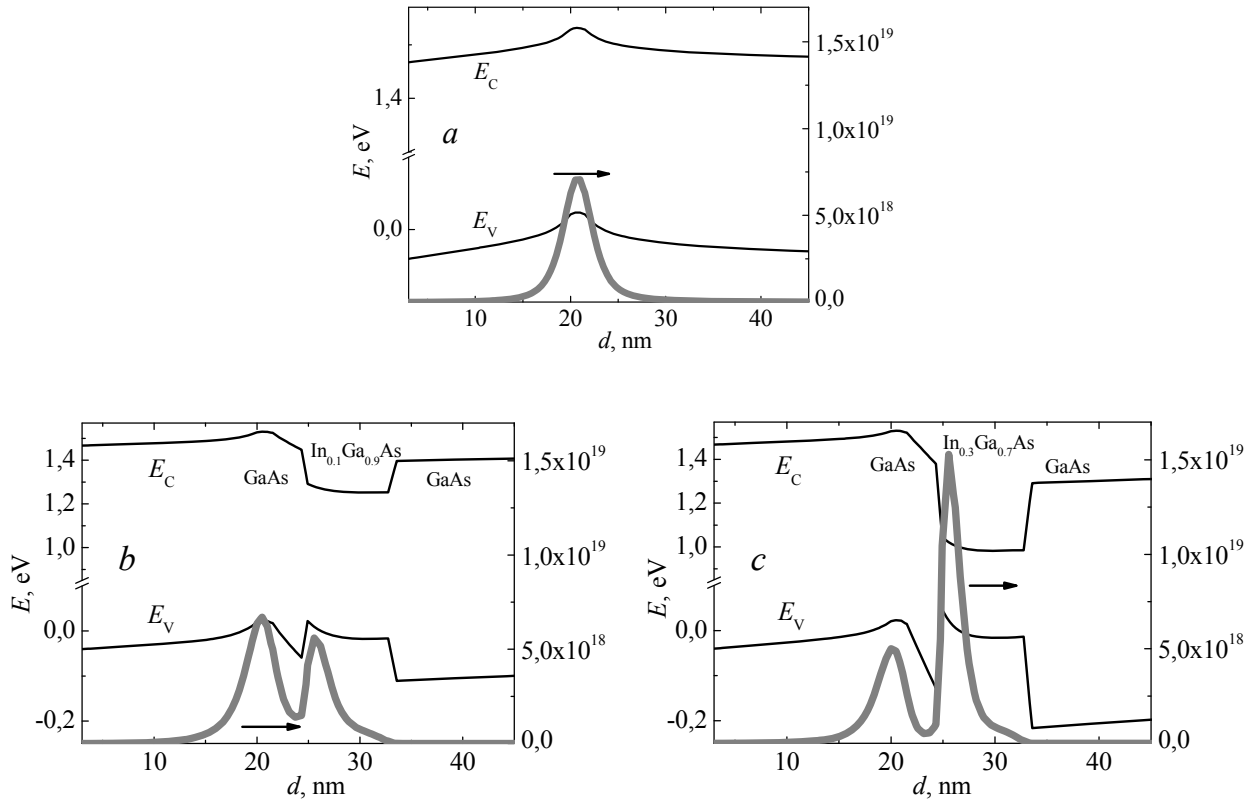
Fig. 2. Calculating band diagrams and carrier distribution at 77 K. *a* - The structure without InGaAs quantum well, *b* - The structure with InGaAs quantum well (In content is 0.15), *c* - The structure with InGaAs quantum well (In content is 0.3).

For the structure only with single Mn delta-layer all carriers is localized in the ferromagnetic region of delta-doped layer (Fig 2*a*) and only these carriers determine the transport properties of the structure. In contrast to this case, for the structure with deep quantum well (with In content is 0.3, Fig. 2*c*) the most part of free carriers is localized in the region of quantum well. Inasmuch as mobility of carriers localized in deep InGaAs quantum well at low temperatures is high, these carriers determine the transport properties of the structure. At the same time the carriers localized in region of Mn layer can determine the ferromagnetic properties of the structure. As the transport of carriers localized in InGaAs quantum well leads to predominance of the normal Hall effect, the question about the degree of spin polarization of these carriers still remains open.

1. A.M. Nazmul, T. Amemiya, Y. Shuto, S. Sugahara, M. Tanaka, "High Temperature Ferromagnetism in GaAs-Based Heterostructures with Mn δ Doping", Phys. Rev. B., **95**, pp. 017201-1-4, 2005
2. S.V. Zaitsev, V.D. Kulakovskii, M.V. Dorokhin, Yu.A. Danilov, P.B. Demina, M.V. Sapozhnikov, O.V. Vikhrova, B.N. Zvonkov, "Circularly polarized electroluminescence in LED heterostructures with InGaAs/GaAs quantum well and Mn δ -layer", Physica E., **41**, pp. 652-654, 2009
3. O.V. Vikhrova, Yu. A. Danilov, M.V. Dorokhin, B.N. Zvonkov, I.L. Kalent'eva, A.V. Kudrina, "Ferromagnetism in GaAs Structures with Mn-Delta-Doped Layers", Tech. Phys. Lett., **35**, pp.643-646, 2009
4. A.V. Kudrin, O.V. Vikhrova, Yu.A. Danilov, "Anisotropic Magnetoresistance and Planar Hall Effect in GaAs Structure with Mn-Delta-Doped Layer", Tech. Phys. Lett., **36**, pp.511-513, 2010

P2-25: Size effect in multilayer metallic nanocantilevers

I.V. Uvarov, V.V. Naumov, I.I. Amirov

Yaroslavl branch of the Institute of Physics and Technology, Institution of Russian Academy of Sciences,
Yaroslavl, Russia, ilnik88@mail.ru

The simplest and the most commonly used moveable element in NEMS is a cantilever - beam, one end of which is fixed. Reducing the size of beams can increase their sensitivity to external influences by increasing the resonant frequency and quality factor. At the same time, with decreasing size (for example, thickness) of the beam the ratio of surface area to volume increases, and the effect of the surface layer on the elastic properties of the beam becomes important. In [1, 2] the size effect associated with a decrease in Young's modulus of the material with decreasing thickness of the beam to 100 nm or less is observed. The size effect in multilayer metallic nanobeams is studied in this paper.

Nanocantilevers consisting of three metal layers (Cr, Al and Cr in the ratio of 1:10:1 in thickness) were fabricated. The beams had a length of 20 to 40 μm, a width of 2 to 6 μm and a thickness of 60 to 180 nm (fig. 1). Oscillations of cantilevers were obtained by electrostatic force. Registration of oscillations was carried out by the deflection of a laser beam reflected from the surface of the cantilever [3]. The resonant frequencies of the beams were measured.
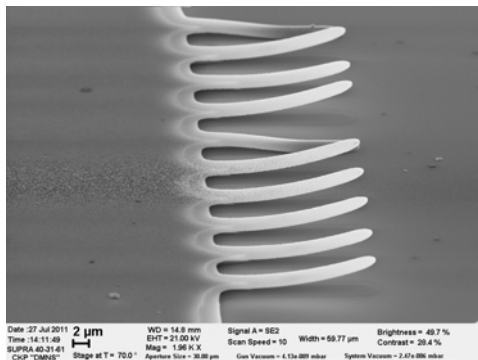
Fig. 1. SEM images of beams with dimensions 20×4×0,06 μm.
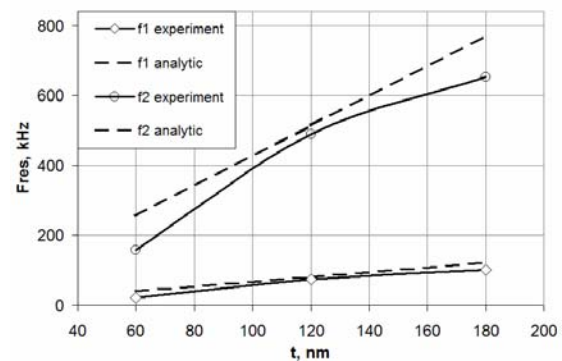
Fig. 2. Dependence of the 1st and 2nd resonant frequencies of beams with 40 μm length and 4 μm width on thickness.

Calculations of natural frequencies in accordance with the classical Euler-Bernoulli beam theory showed that the natural frequencies of flexural vibrations of a beam consisting of layers of Cr and Al in a ratio of 1:10:1 in thickness, at constant values of Young's moduli and densities of Cr and Al have to depended linearly on the total thickness of the beam [3]. The size effect, observed in [1, 2], leads to the fact that resonant frequencies of sufficiently thin beams are lower than that predicted by classical theory. In fig. 2 the theoretical and experimental dependences of 1st and 2nd resonance frequencies of beams on the thickness are presented. It is seen that the experimental values of resonance frequencies are lower than the theoretical values, but this is observed for all thicknesses and may be due to partial etching and modification of chromium layer on the surface of the beams in the fabrication process. In general, the experimental curves differ only slightly from linear curves, that is, the size effect in this experiment is not observed.

1. K. Babaei Gavan, H.J.R. Westra, E.W.J.M. van der Drift *et al.*, "Size-dependent effective Young's modulus of silicon nitride cantilevers", Appl. Phys. Lett., 94, pp. 3108-3110, 2009

2. H. Sadeghian, C.-K. Yang, J.F.L. Goosen *et al.*, "Effects of size and defects on the elasticity of silicon nanocantilevers", J. Micromech. Microeng. 20, 064012, 2010

3. I.V. Uvarov, V.V. Naumov, M.K. Aminov *et al.*, "The study of the resonance characteristics of the metallic micro- and nanobeams", Journal of Nano and Microsystem Technique, 12, pp. 45-48, 2011

P2-26: Influence of the conditions of ion-plasma sputtering on the surface roughness of platinum film

R.V. Selyukov, V.V. Naumov, I.I. Amirov

Yaroslavl branch of the Institute of Physics and Technology, Russian Academy of Sciences, Yaroslavl, Russia,
rvselyukov@mail.ru.

The processes of ion and ion-plasma sputtering of metal films are of interest due to the its possibility of surface modification including the creation of nanostructures [1]. The purpose of this work was to determine the influence of ion energy, substrate temperature and the structure of the original film on the surface roughness of platinum film.

Two kinds of platinum film with thickness of 100 nm were made. The first kind of film was prepared using RF-bias applied to substrate during deposition. The second kind of film was grown without bias on substrate. This variation of deposition conditions leads to structural differences between films. These differences include decrease of the number of grains with crystallographic orientation which different from the dominant orientation for the platinum film which is (111). Sputtering of the film was carried in argon plasma with ion energies 45, 60, 85 и 220 eV at the substrate temperature approximately of 200°C and of 25°C. The images of film surface were obtained using the scanning tunneling microscope (STM) Gpi-Cryo-SEM. STM-images were analyzed by WSxM software [2]. STM-images of the original film and of the two samples of treated films are shown in fig. 1 where the differences between objects on surface after sputtering under different conditions are shown.
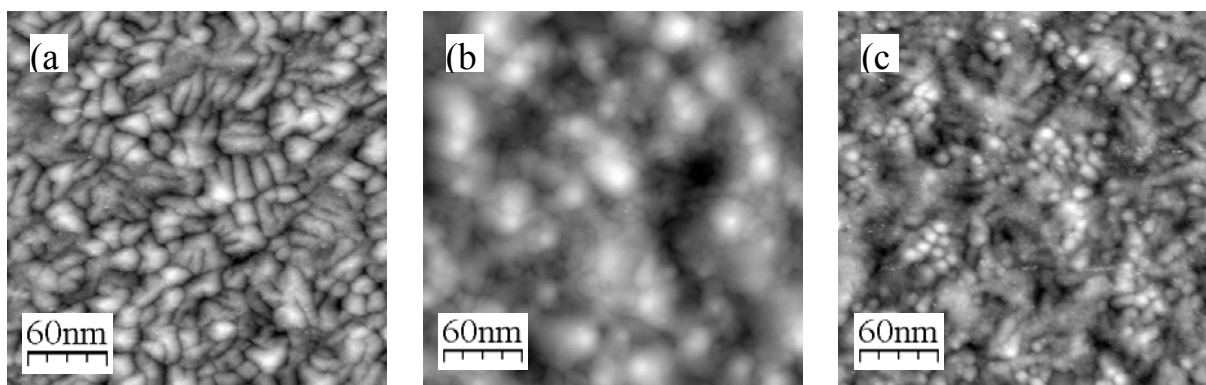
Fig. 1. STM-images of the platinum film surface with roughness of 1,1 nm before the ion-plasma sputtering (a), with roughness of 2,6 nm after sputtering with energy of 85 eV (b) and with roughness of 0.9 nm after sputtering with energy of 220 eV (c). Sputtering was carried at substrate temperature of 200°C.

The surface roughness dependencies on the ion energy have the form of hump with maximum at 60 eV. At low energies these curves differ for experiments which carried with various substrate temperatures. In the case of sputtering at 25°C the roughness is reduced from 2 - 2,5 nm to 0,9 - 1,2 nm while energy decreases from 60 eV to 45 eV whereas at the temperature of 200°C film roughness remains in the range of 2.2 - 2,7 nm. It's true for both kinds of platinum film. That difference may be explained by increasing of the grains sizes at elevated temperature of sputtering. This conclusion is confirmed by X-ray diffraction measurements. Difference between energy dependencies of roughness for both kinds of film is observed merely after sputtering at 25°C. Under this condition for all energies except 220 eV platinum film deposited with applying RF-bias has roughness about on 20 % less then film deposited without bias. In case of sputtering at 200°C energy dependencies of roughness for both film kinds are almost identical. This fact may be also explained by elevated temperature. At that temperature structural differences between films are eliminated.

1. D. Aurongzeb, E. Washington, M. Basavaraj, J. M. Berg, H. Temkin, and M. Holtz, "Nanoscale surface roughening in ultrathin aluminum films", J. Appl. Phys., 100, 114320, 2006
2. I. Horcas, R. Fernandez, J. M. Gomez-Rodriguez, J. Colchero, J. Gomez-Herrero, and A. M. Baro, "WSXM: A software for scanning probe microscopy and a tool for nanotechnology", Rev. Sci. Instrum., 78, 013705, 2007

P3-1: Laser synthesis of nanostructures

A. Antipov, A. Kucherik, S. Kutrovskaya, A. Osipov, D. Nogtev

Stoletov Vladimir State University, Vladimir, Russia, E-mail: aantipov@vlsu.ru

Development of integrated microcircuits, contact connections metal the semiconductor promotes working out and research of new methods of local spraying of metal, semi-conductor structures on dielectric surfaces. The greatest interest and prospect are represented by laser technologies as manufacture nanoparticles and their sedimentation on a surface. At the heart of laser methods there are various chemical reactions of decomposition or restoration which are initiated at the expense of influence of laser radiation lie. Such methods concern, the laser-induced transfer (laser-induced forward transfer, LIFT) [1], sedimentation from a firm phase at the expense of laser decomposition, laser sedimentation from a gas phase (laser chemical vacuum deposition, LCVD) [2,3].

The most actual method of sedimentation is the method of laser deposition of metals from solutions (LDMS), according to authors. A perspective method of reception nanoparticles is the method laser ablation in a liquid. In works [4,5] reception of colloidal solutions by a method laser ablation is considered. Laser radiation influences on targets (copper, brass, bronze) shipped in a liquid.

For deposition of nanoparticles from solutions it is necessary to receive colloidal solutions, therefore a target was located in a ditch with a liquid phase. The laser beam was focused on border a target – a liquid phase. As a result of influence of laser radiation occurred laser ablation targets in the liquids formed nanoparticles again came back in a laser bunch owing to convective movement that at big enough absorption on length of a wave of laser radiation led to change of function of distribution of particles in the sizes. Thus, nanoparticles were distributed in liquid volume, forming a colloidal solution [6]. Horiba LB-550 was used for definition of the size of particles in a solution the analyzer of the sizes of particles of dynamic dispersion of laser light. The sizes of particles were in a glycerin solution made 9.2nm, and in an ethanol solution 260nm.

Sedimentation was made on method LDMS. The substrate was located in a ditch with a colloidal solution. Focus of laser radiation was on border of the substrate and a colloidal solution. Deposition was carried out on a trajectory of movement of a beam. Research of area of sedimentation by AFM has shown that on a substrate placed in a colloidal solution of glycerin, the particles which average size made about 36 nanometers, and on a substrate, placed in an ethanol solution, particles in the size about 350 nanometers sat down.

Possibility of manufacturing of a colloidal solution in liquid environments of glycerin and ethanol is shown as a result. Research of the received solutions has shown that the size of the studied particles depends on property of environment. It is shown that the size of particles and concentration of a solution influence process of deposition and for particles with the sizes less than 20nm, it is necessary to use other methods of deposition.

1. Germain C, Tsui Y. Y. "Femtosecond laser induced forward transfer of materials", Proc. Int. Conf. MEMS, NANO and Smart Systems, Banff. p. 44.2003
2. Kordas K et al. "Laser-assisted metal deposition from liquid-phase precursors on polymers", Applied Surface Science, 172, pp. 178 – 179. 2001
3. Ryjenkov D.I. et al. Nanomaterialy.– M: BIN. Laboratory of knowledge, 363c. 2008
4. Kazakevich P. V, Ravens of Century B, Simakin A.V., Shafeev G. A "Formation nanoparticles copper and a brass at laser ablation in a liquid", Quantum electronics, 34, №10 pp.951 – 956.2004
5. Kazakevich P. V, Simakin A.V., Shafeev G. A "Formation of periodic structures at laser абляции metal targets in liquids", Quantum electronics, 35, №9, pp.831 – 834. 2005
6. Izgaliev A.T., Simakin A.V., Shafeev G. A "Alloy Formation of nanoparticles Au and Ag at a laser irradiation of a mix of their colloidal solutions", Quantum electronics, 34, №1 pp. 47-50, 2004

P3-2: Synthesis of transparent carbon films with operated morphology in constant electric field

A. Antipov, S. Arakelyan, S. Kutrovkaya, A. Kucherik, A. Osipov, V. Prokoshev

Stoletov Vladimir State University, Vladimir, Russia, E-mail patifon@mail.ru

Introduction
Synthesis of transparent carbon nanocoverings one of the perspective directions of receiving flexible contacts and monitors. Now methods of synthesis of grafenovy films are actively applied to the solution of this task from methane - a hydrogen mix on a nickel or copper foil [1-3]. A perspective method is possibility of synthesis of carbon nanotubes at ethanol deposition [4,5]. Advantage of this method is rather low temperatures to 750C and a high exit of a material, allegedly at the expense of availability of free oxygen [4,5] that allows to delete deposited amorphous and defective carbon from area.

Experimental conditions
For deposition of carbon on a surface of a glass substrate the scheme of direct laser sedimentation was used. The experimental scheme in a general view repeated the scheme offered in work, for management of process of deposition of the laser induced plasma.
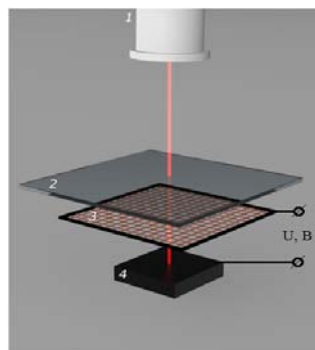
Fig. 1 Experimental scheme: 1–a source of continuous laser radiation (λ=1.06mkm), 2 – a transparent substrate (glass, quartz), 3 – a metal grid, 4 – a carbon target.

Intensity of laser radiation (λ=1.06мкм) on a target made $10^6 W/cm^2$. Laser influence was carried out in atmospheric air that allowed to avoid sedimentation of amorphous carbon at the expense of intensive oxidation.

Results and discussion
The structure of the deposited layer, also changed depending on distance between a substrate and a grid and potential differences between a grid and a target. At U = 600V both distance between a grid and a substrate 2mm in the course of sedimentation the layer consisting of separate carbon nanoparticles with the average size 250nm is formed. The layer densely fills a surface; the analysis shows that 312 particles of such size settle down in studied area in the size 20x20mkm.
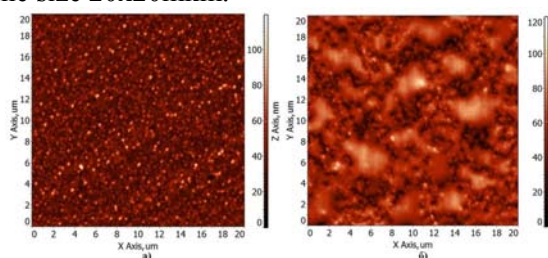
Fig. 2 AFM-images of the deposited nanostructured layer of carbon: a) distance between a grid and a substrate 2mm; б) U= 600V distance between a grid and a substrate 1mm.

With distance reduction between an accelerating grid and a surface of a transparent substrate, on a surface of

the last after sedimentation formation of structures similar to drop educations with the average lateral size 4mkm is observed. However, thus it was not observed characteristic for drop sedimentation of spreading of borders, at contact of a drop to a substrate that allows to assume about formation of similar structures in the course of condensation.

In a case when distance between a grid and a substrate 1.5mm, in the course of deposition the extended massifs of carbon nanostructures in extent to 5mkm, the average cross-section size 300nm and height to 100nm are formed. At increase in distance to 2nm it is fixed formations of carbon nanofibres, length more 20mkm and diameter of an order 300nm that allows to make the assumption of formation possibility on a surface of a glass substrate of the layer consisting of carbon nanotubes.

For confirmation of it tension between a grid and a target to U = 1000V (further the increase in tension led to air breakdown at formation of plasma) was increased. The distance between a substrate and a grid made 1.5mm, and between a target and a grid 0.5mm. The received structures are given on fig. 6. carbon nanofibres are formed.
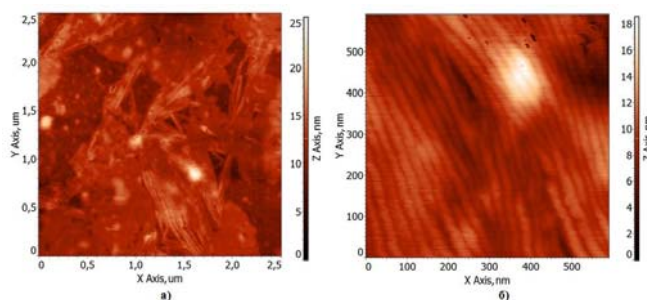
Fig. 3 AFM-images of the area of carbon deposition: a) formation of depositoin from the massif of carbon nanotubes; б) the increased image of the carbon nanotubes presented in drawing and.

The received type of a range with strongly dim maxima, answering amorphous (in the area 1380sm-1) and crystal (1560sm-1) to phases, is connected with substrate influence by sight a range since depth of penetration (to 500мкм) a laser bunch, a raman spectrometer (the Ar-laser, $\lambda = 0,488$ microns) considerably exceeded thickness of the besieged layer. The maximum in a range (600-800sm-1) is connected with formation in the field of sedimentation of multiwall carbon nanotubes.

Conclusion

Thus, in this work possibility of receiving the transparent nanostructured carbon coverings consisting of carbon nanotubes and/or nanostructured massifs of carbon nanoparticles at a laser dusting is shown. The received nanocoverings with operated topology can be used for manufacturing of carrying-out transparent layers of the necessary configuration on a surface of a glass surface, including for flexible displays.

Receiving possibility in laser experiment of nanostructures with the various morphology operated on micro and a nanolevel is shown. For the solution of a problem of synthesis of vertically focused nanotubes it is possible to use glasses with previously raised dust transparent layer, for example oxide of zinc and the etched matrix.

1. Geim A.K., Novoselov K.S. The rise of graphene. Nature Materials, 2007, v.6, No.3, p.183-191.
2. Kim K.S., Zhao Y., Jang H., Lee S. Y., Kim J.M., Kim, K.S., Ahn J.-H., Kim P., Choi J.-Y., Hong B.H. Large-scale pattern growth of graphene films for stretchable transparent electrodes. Nature, 2009, v.457, p.706-710.
3. Bae S., Kim H., Lee Y., Xu X., Park J.-S., Zheng Y. Balakrishnan J., Lei T., Kim H. R., Song Y. Il, Kim Y.-J., Kim K.S., Ozyilmaz B., Ahn J.-H., Hong B.H., Iijima S. Roll-to-roll production of 30-inch graphene films for transparent electrodes. Nature Nanotechnology, 2010, v.5, p.574-578.
4. Maruyama Sh., Kojima R., Miyauchi Y., Chiashi Sh., Kohno M. Low-temperature synthesis of high-purity singlewalled carbon nanotubes from alcohol. Chem.Phys.Lett., 2002, v.360, No.3, p.229-234.
5. Redkin A.N., Kipin V.A., Malyarevich L.V. Synthesis of carbon fibrous nanomaterials from ethanol on the nickel catalyst. Inorganic materials., 2006, т.42, No. 3, page 284-287.

P3-3: Oscillations profiles of thermoelectric parameters in nanostructures on the base of lead telluride

D. Freik, I. Yurchyshyn, A. Freik, L. Mezhylovlska

Physics and chemistry institute at PreCarpathian Vasyl Stefanyk National University,
Ivano-Frankivsk, Ukraine, E-mail: freik@pu.if.ua

The creation of highly effective thermoelectric materials led up to an intensification of research activity in low-dimensional structures [1]. The paper presents an analysis of new approaches to improve the figure of merit ZT for nanostructures on the base of compounds IV-VI. The optimal thermoelectric characteristics of quantum dots, wires and wells superlattices are determined.

A reduction the dimension of the material creates the conditions for observing the phenomenon of quantum-size effect, what leads to increase the density of states near the Fermi energy. This helps to preserve high conductivity at relatively low Fermi energy, where the high values of the Seebeck coefficient S have place. Significant influence of quantum effects on thermoelectric properties is probable only if the size of the structure in restricting direction is comparable with carriers de Broglie wavelength. This condition holds for structures in the form of quantum wells, quantum wires and quantum dots, where it have place a dimensional restriction in one, two and three directions, respectively. Thus, the electronic density of states shows marked deviation from the usual parabolic law in bulk materials.

The behavior of thermoelectric parameters (electrical and thermal conductivity, Seebeck coefficient) in bulk materials is usually described in terms of electronic and phonon properties, which vary greatly with decreasing sample size below the micrometer range, where the quantum effects become more significant. Spatial confinement of acoustic phonons and the corresponding modification of the group velocity leads to an increase of the phonon relaxation rate, resulting in reducing of lattice thermal conductivity In addition, nature of interaction between particles changes much. Taking into account the multiple energy bands in like-well structure can lead to nonmonotonous change in the various transport coefficients such as mobility, Seebeck and Hall coefficients.

Thickness dependences of kinetic parameters of quantum wells (QW) based on IV-VI compounds show non-monotonic oscillatory behavior that is associated with size quantization due to carrier movement restrictions in one direction .

On the basis of theoretical model of rectangular quantum well with infinitely high barriers the dependences of thermoelectric parameters on nanostructures thickness of IV-VI compounds (PbTe, PbSe, PbS, SnTe) are investigated. Theoretically shown that in such structures it has place nonmonotonous, oscillation change of power factor $S^2\sigma$ with well width. It was determined the d-dependence of Fermi energy and effective mass in the respective structures. Shown that experimental value of oscillations period are equal to QW thickness, when the bottom of lowest subband coincides with the Fermi energy. This thickness was explained as the minimum QW thickness, when quantum size effects are the main factor, that determines the nonmonotonous behaviour in thickness dependencies of thermoelectric parameters of the relevant structures.

It was identified and shown the determinative influence of geometric parameter on the band gap or overlap values of the quantum wire, quantum wells superlattice and the stack of quantum dots.

Fig. 1 shows that the experimental dependence of the thermoelectric power factor on the thickness of nanostructures PbTe: Bi on glassceramics at the room temperature is characterized by a nonmonotonic behavior. Natural to assume that such behavior is due to quantization of energy carriers by restricting their movement in the potential well. The increasing of the well width on the value of half the Fermi wavelength leads to a new subband below the Fermi energy. When a new subband is filled, in the density of states there is a jump, which leads to oscillating behavior.

The expressions for the Seebeck coefficient S and electrical conductivity σ can be written as [3]:

$$S = \frac{k_B}{e}\left[\frac{E_F}{k_B T} - \frac{A_1 + A_2}{A_3}\right] \tag{3}$$

$$\sigma = \frac{1}{2\pi d}\frac{2k_B T}{\hbar^2}\sqrt{\frac{m_X^*}{m_Y^*}}e^2\tau_0 A_3 \tag{4}$$
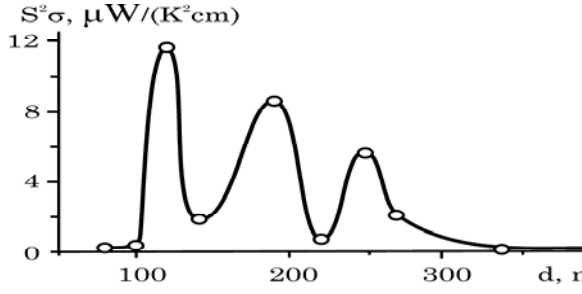
Fig. 1. Experimental dependence of the thermoelectric power $S^2\sigma$ on the thickness of the nanostructures PbTe:Bi on glassceramics at T = 300 K.

$$A_1 = \left(\sum_{n=1}^{En \le E_F} \int_0^\infty x^2 \left(-\frac{\partial f_n}{\partial x}\right) dx \right) \tag{5}$$

$$A_2 = \left(\sum_{n=1}^{En \le E_F} E' \int_0^\infty x \left(-\frac{\partial f_n}{\partial x}\right) dx \right) \tag{6}$$

$$A_3 = \left(\sum_{n=1}^{En \le E_F} \int_0^\infty x \left(-\frac{\partial f_n}{\partial x}\right) dx \right) \tag{7}$$

where $x = \dfrac{\varepsilon}{k_B T}$ - reduced carrier energy, and $\eta_n = \xi - E_n'$. Here $\xi = \dfrac{E_F}{k_B T}$ and $E_n' = \dfrac{E_n}{k_B T}$.

The value of the Fermi energy of condensate can be expressed by the well width (d) and concentration of carriers in the conduction band. Influence of doping level PbTe by bismuth on the Fermi energy can be evaluated by appropriate change of effective mass in the Fermi energy, based on empirical formulas derived in [4] as a result of approximating the experimental dependence of the effective mass on the electron concentration:

$$\frac{m^*}{m_0} = 0{,}111 \cdot 10^{-6} \cdot n_{ел}^{\frac{1}{3}} \tag{8}$$

where m0 - mass of the electron, nel - electron concentration in units of cm-3.

Using the above theoretical model there were obtained the dependences of TE coefficients on the width of QW PbTe:Bi, which are characterized by nonmonotonic oscillating behavior (Fig. 2). This calculation of values are in rather good agreement with the corresponding experimental dependences (Fig. 1).
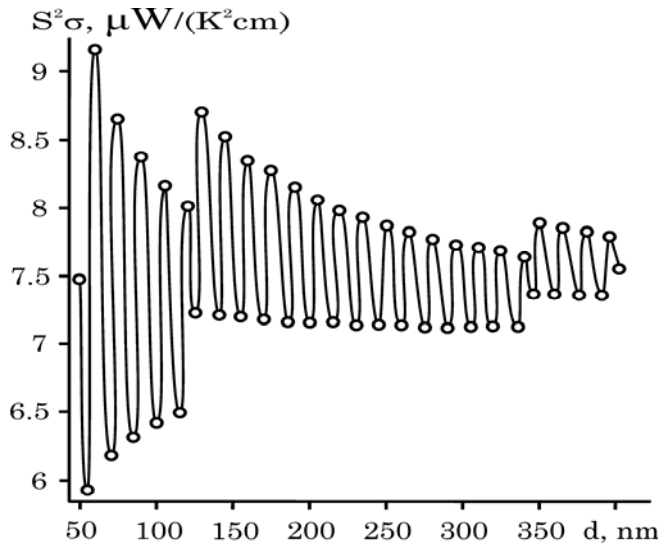
Fig. 2. Theoretical dependence of TE power $S^2\sigma$ on the width of the QW PbTe: Bi in the model of infinitely deep potential well at T = 300 K.

1. S.M. Sze. *Physics of Semiconductor Devices.* John Willey and Sons, New York, 1981.
2. J. Nishizawa and K. Suto, "Semiconductor Raman laser", J. Appl. Phys., 51, pp.2429-2431, 1980.
3. *CRC Handbook of Thermoelectrics* (Ed. D.M. Rowe) (CRC Press: 1995).
4. I.N. Dubrovkaya, Yu.I. Ravich, *SSP,* **8** No5, 1455 (1966).

P3-4: Technology features silicon nanostructured electrodes for lithium-ion batteries

Berdnikov A.E.[2], Churilov A.B.[1,2], Gusev V.N.[2], Kulova T.L.[3],
Mironenko A.A.[1,2], Naumov V.V.[1,2], Popov A.A.[2], Rudy A.S.[1,2], Skundin A.M.[3]

*1 - Facilities Sharing Centre "Micro- and Nanostructures Diagnosis", Demidov State University,
Yaroslavl, Russia, rudy@univ.uniyar.ac.ru.*
*2 - Yaroslavl Branch of Physics and Technology Institute of Russian Academy of Sciences,
Yaroslavl, Russia, rudy@univ.uniyar.ac.ru*
*3 - Frumkin Institute of Physical Chemistry and Electrochemistry, Russian Academy of Sciences,
Moscow, Russia, askundin@mail.ru*

Silicon, which has a theoretical capacity of an order of magnitude higher than of graphite (4200 mAh/g) is a promising anode material for lithium-ion batteries (LIB) [1]. However, the intercalation of lithium in crystalline silicon involves a strong increase in specific volume, until the destruction of the electrode. One of the most appropriate solutions to this problem is to manufacture the LIB negative electrode on the basis of silicon nanocomposites. Using this technology means slower destruction of the electrode as a result of charge-discharge cycles due to changes in the volume of damping material.

In this work we investigated the amorphous silicon film composite LIB anode, besides silicon containing oxygen and carbon. The processes of expansion and contraction during intercalation and deintercalation of lithium are damped by the large number of structural defects.

Experimental samples of the LIB anodes were prepared of titanium or copper foil by magnetron sputtering of silicon target. We studied the anode of pure amorphous silicon (α-Si), and with the addition of oxygen and carbon, which were introduced in the silicon film during magnetron sputtering. The results of elemental analysis of the composition series of silicon composite films derived from the data analysis of the Auger spectrometer PHI-660 are presented in the inset in Fig. 1. The study of surface morphology of anodic films of samples carried out on SEM SUPA-40 showed that the composite film, containing carbon, had more developed surface, in contrast to films of pure α-Si, had a smooth surface, roughness comparable to the surface of the silicon substrate. Transmission spectra of films of α-Si (O, C) were recorded using FTIR spectrometer IFS 113V at room temperature in the range 4000 - 400 cm^{-1} with a resolution of 4 cm^{-1}. This optical spectroscopy allows to draw conclusions about the chemical compounds formed of silicon with different stoichiometry with oxygen and carbon.

Fig. 1. Discharge capacity of the anodes vs charge-discharge cycles. Discharge voltage reduced: 1,2 samples to 0,05 V, sample 3 to 0,01 V, sample 4 to 0,07 V. The inset shows the data on the average content of Si, O, C in the studied films.

Sample	Si, at.%	O, at.%	C, at.%
1	100	0	0
2	94,5	5,5	0
3	86,6	8,6	4,8
4	70,6	24,5	4,9

Data obtained on the results of galvanostatic cycling at a current density 1.0 A/g displayed in Fig. 1, showed that film silicon anode material with oxygen in its composition (3) and carbon (4) have an initial capacity of 2730 mAh/g and 2010 mAh/g for samples 3 and 4, respectively, and the degradation of discharge capacity after 50 charge-discharge cycles is much less than in the samples containing carbon in the film.

In the present work it is established that the use of the battery to the negative electrode of pure amorphous silicon films and the content of 5 - 6 at.% oxygen satisfactorily maintain the discharge capacity for 50-60 charge-discharge cycles. The films based on amorphous silicon, having in its composition of oxygen and carbon, retain a high capacity of up to 300 charge-discharge cycles.

1. Wen C.J., Huggins R.A. // J. Solid State Chem. 1981, V. 37, P. 271
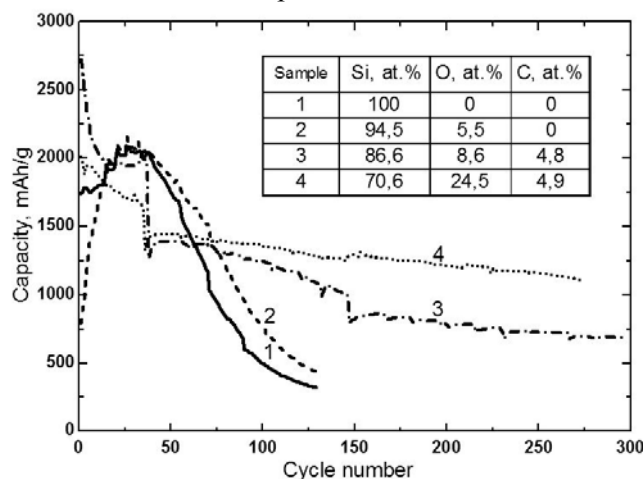
P3-5: Layer cold cathodes based on nanostructured diamond-like materials

A. Belyanin[1], A. Lamskij[1], P. Pashchenko[2]

[1]*Central Research Technological Institute "TECHNOMASH", Moscow, Russia, E-mail: belyanin@technomash.ru,*
[2]*Skobeltsyn Institute of Nuclear Physics, Moscow State University, Moscow, Russia*

The perspective for application of flat-panel displays with improved characteristics is associated with the elaboration of cold (field-emission) cathodes based on diamond-like materials (polycluster diamond (PCD), diamond-like carbon (DLC), AlN etc.). Emission properties were studied for layer structures: Ni(Ti)/DLC(PCD), Ni(Ti)/DLC(PCD)/dielectric, OM/Ni(Ti)/DLC, OM/Ni(Ti)/DLC/dielectric and OM/nanodiamond/Ni/DLC, where OM – opal matrix (perfect cubic packing of SiO_2 nanospheres with diameter d≈200±10 nm); dielectric – AlN, MgO_x, Al_2O_3 or ZnO; nanodiamond – diamond particles less than <5 nm. OM application [1] (up to 10 layers on Si substrates) resulted to increase of emission centres density to ~2,5·10^9 sm^{-2} (the distance between neighboring apexes (emission centres) were equal to d nanospheres of SiO_2). Diamond nanoparticles (deposited from alcoholic suspension by centrifugation) were placed as tetrahedral and octahedral cavity of SiO_2 nanospheres packing. PCD films were formed by arc discharge method and method of hot filament (diamond phase percentage C>99 vol.%), DLC films – by graphite sputtering by ionic beam (C≈1–10 vol.%), RF, SHF and glow discharges (X-ray amorphous) [2]. Ni, Ti, AlN, MgO_x, Al_2O_3 and ZnO films were obtained by magnetron sputtering, permitting to form films with controllable phase composition and phase structure. AlN; MgO_x; Al_2O_3 and ZnO films contained from 10 to 90 vol.% crystalline phase, and crystallites being axially textured on <0001> (AlN, ZnO and Al_2O_3) and <111> (MgO_x).
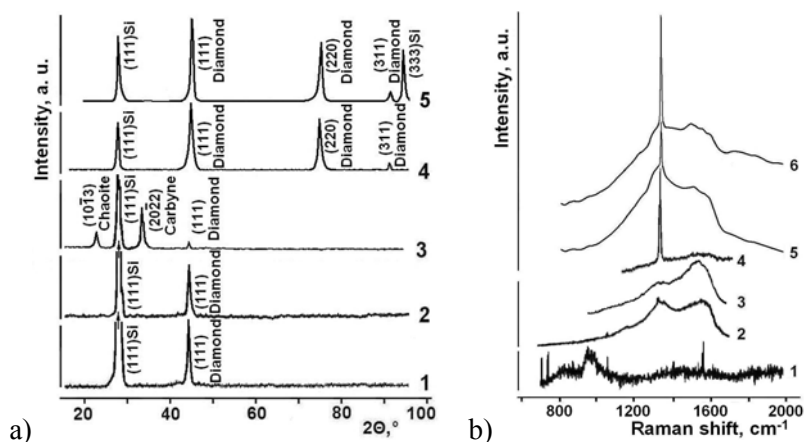
Fig. 1. Structure of films, formed on Si-substrates (deposition methods correspond to curves numbers: 1, 2 – graphite target sputtering by ionic beam; 3 – RF discharge; 4 – method of hot filament; 5, 6 – arc discharge: a) X-ray difractogram (Cu kα radiation); b) Raman scattering spectra

SiO_2 nanospheres on OM surface were sharpened by deposited layers of metals and insulators, and sharpening effect is associated with variation of film forming rates, placed under various angles relative to sputtering source. Depending on formation conditions structure and composition of emitting films is changed (fig. 1, 2). Emission properties of carbon films significantly improve after imperfection increase up to formation of Roentgen amorphous material with the main characteristic sp^3-hybridization of valence electron coupling in carbon atoms. For the emitters under consideration threshold value of electric field intensity with cold emission available varied at 2–20 V/μm.
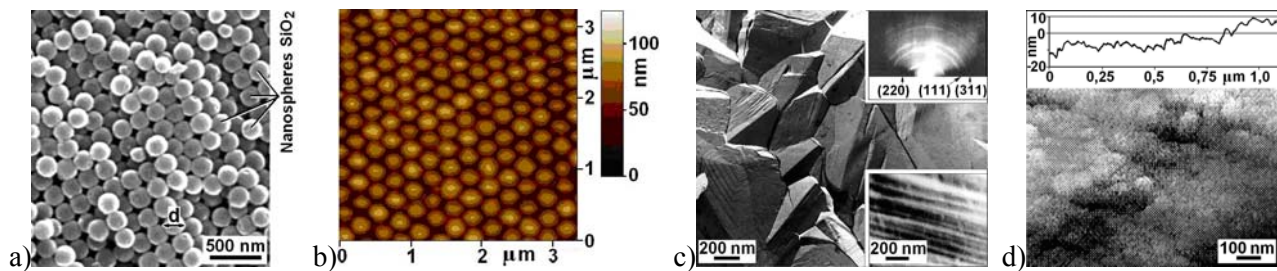
Fig. 2. Structure (a – SEM, b – APM, c, d – TEM) of surface: a, b) opal matrix; c) PCD film (inserted: top – reflected electron diffraction pattern; bottom – structure grain chip); d) DLC film (top – surface profilogram)

Emission characteristics measurements were provided under pressure $\sim 1{,}3 \cdot 10^{-3}$ Pa in pulse mode (frequency 50 Hz, duration 20–30 μs, cold cathode and anode gap (glass/InSnO$_x$/luminophor) 160–500 μm). Electron emission from PCD surface occured from plats edges only, forming crystallites, and emission with DLC – on edges of nanoglobules. Improvement of emission properties of DLC films was achieved due to deposition on emitting surface of AlN, MgO$_x$ and Al$_2$O$_3$ layers. For AlN films emission peaks current corresponded to microcrystallite (fibres) vertex of film, and the number of emission centers of AlN films without fibrous structure decreased on a few orders. MgO$_x$ or OM layers decreased emission threshold (fig. 3). Doping PCD (Si/PCD:B) and A1N (AlN:Mo, AlN:Sm, AlN:Eu и AlN:Zn) had no influence on emission threshold value.
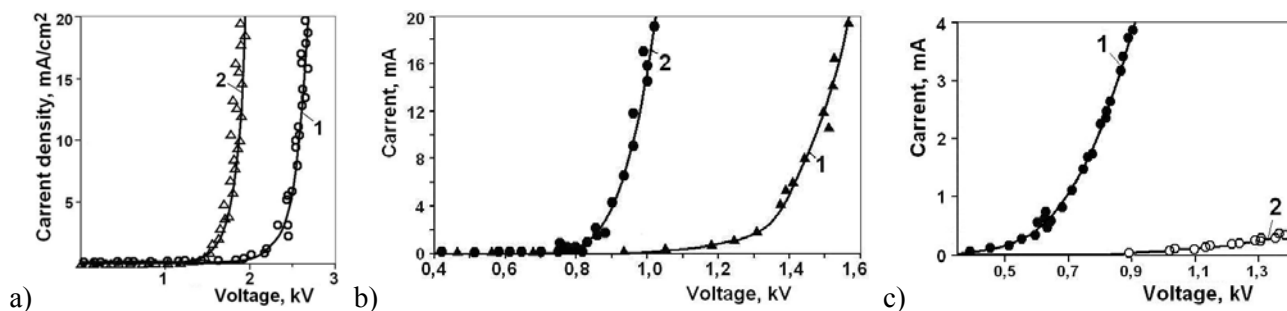
Fig. 3. Voltage-current characteristics of layer structures: a) Ti/DLC (1) and Ti/DLC/MgO$_x$ (2); b) Ni/DLC (1) and OM/Ni/DLC (2); c) Si/OM/nanodiamond/Ni/DLC (DLC film thickness: 1 – 0,7 μm, 2 – 1,4 μm)

1. *Nanomaterials. III. Photonic crystals and nanocomposites based on opal matrices*, Ed. M.I. Samoylovich. Moscow: Technomash. 2007. 303 pp.
2. A.F. Belyanin, M.I. Samoilovich. *Nanomaterials. IV. Thin films as nanostructured system*. Moscow: Technomash. 2008. 254 pp.

P3-6: Effect of annealing on formation of *high-k* insulators in the W/ultrathin HfO$_2$/Si (100) system

V.Rudakov, Yu.Denisenko, E.Bogoyavlenskaya, V.Naumov, S.Simakin

Yaroslavl Branch of the Institute of Physics and Technology, Russian Academy of Science, Yaroslavl, Russia,

E-mail address: den-yur55@mail.ru

The miniaturization of devices, in particular, the creation of CMOS-devices results in the need for ultrathin gate insulating layers, which would lead to reduction of leakage current and decrease of the equivalent oxide thickness (*EOT*, Equivalent Oxide Thickness). This, in turn, requires replacing of traditionally used gate dielectric SiO$_2$ on *high-k* materials, which possess high values of dielectric constant (*k*). HfO$_2$ is one of the perspective *high-k* dielectrics. This material is characterized by relatively high *k* values (~ 16-30) and large band gap (~ 8-5.7 eV). It is thermodynamically stable in contact with Si. Changing the SiO$_2$ gate dielectric on HfO$_2$ one is often accompanied by a selection of alternative materials for the gate other than polysilicon. Tungsten W is the most favorable material for this purpose. It is quite inert and does not tend to form an eutectic alloy. That generally improves the electrophysical characteristics of MOS-devices. During the process of creation these devices, especially on the stages of formation of silicide contacts and activation of impurities, the temperature effect on the W/HfO$_2$/Si (100) structure is of practical interest. The formation of HfO$_2$ films directly on Si-substrate and annealing of created structures are associated with the spontaneous formation of an interlayer (SiO$_2$, HfSi$_x$ or HfSi$_x$O$_y$) at the HfO$_2$/Si interface. Some of the main reasons of the appearance of this interlayer are the diffusion of oxygen atoms and probably the differences in the diffusion intensities of O, Si and Hf at different temperature conditions [1]. At that, in the case of W/HfO$_2$/Si (100) structure, the W film is the most likely oxygen source, rather than the HfO$_2$ film. In connection with the described phenomena, a great importance of the definition of the relationship between the changes in such electrical parameters as *k* and *EOT* in the W/ultrathin HfO$_2$/Si (100) structures with the physical processes that are activated during the annealing of these structures exists. In the present study we investigated the W(150 nm)/HfO$_2$(5 nm)/Si (100) structures, which were annealed at 500 °C in vacuum for 30 min and at 900 °C in N$_2$ atmosphere for 12 s in a rapid thermal annealing reactor. The HfO$_2$ and W films were deposited *in situ* on silicon wafers of *p*-type conductivity with a resistivity of 12 Ω·cm with (100) orientation by rf magnetron sputtering. By plasma etching through a photomask tungsten contact pads were formed. Determination of *k* and *EOT* belonged to the dielectric and of leakage current through the W/HfO$_2$/Si (100) structures before and after annealing was carried out on the basis of electrical measurements (*C-V* and *I-V*) investigated by a Keithley 4200-SCS electrometer. In addition, for the W/HfO$_2$/Si (100) structures in and out of region of the W contact pads, profiles of the intensity distribution of the negatively charged ions of Si, O, HfO$_3$, HfO$_2$, SiO$_2$, SiO, W$_2$ and WO, respectively, by using secondary ion mass-spectrometry (SIMS) performed on the time-of-light mass analyzer TOF.SIMS^5 were obtained. The calculations showed that for the as-deposited W/HfO$_2$/Si (100) structures $k \sim 27$ and $EOT \sim 0.7$ nm, and the leakage current was equal to 2.4×10^{-4} A/cm^2. The decrease of *k* up to 23 and the increase of *EOT* up to 1.1 nm, and also the slight reduction of the leakage current up to 2.1×10^{-4} A/cm^2 were the result of the annealing at maximum temperature (900 °C). The SIMS-investigations allowed to suppose the growth of oxide phases such as WO$_x$ at the W/HfO$_2$ interface and SiO$_x$ (and the formation of Hf-Si-O bonds) at the interface HfO$_2$/Si because of annealing in the absence of external sources of oxygen. The possible reasons of the presented behavior of *k* and *EOT* in accordance with the results of SIMS-profiles were discussed.

1. Tan Ting-Ting, Liu Zheng-Tang, Liu Wen-Ting, Zhang Wen-Hua "Chemical structure of HfO$_2$/Si interface with angle-resolved synchrotron radiation photoemission spectroscopy", Chin. Phys. Lett., **25** (10), pp. 3750-3752, 2008.

P3-7: Investigation of Cement Structure Formation by Small-Angle Neutron Scattering Experiments

A. Guryanov[1] , S. Korenkova[1] , V.M. Lebedev[2] , V.T. Lebedev[2] , U. Sidorenko[1]

1. Samara State University of Architecture and Civil Engineering, Samara, Russia, gurjanovam@mail.ru.
2. Petersburg Nuclear Physics Institute, Russian Academy of Sciences, Gatchina, Russia, lebedev@pnpi.spb.ru

Cement is one of the main functional construction materials. The hydration of cement is the chemical reaction of cement clinker components with water. During the hydration of anhydrous clinker minerals are converted into the corresponding crystallites (hydro silicates calcium, hydro aluminates calcium, hydro ferrites calcium), which fill the volume of a dense layering of gel particles, causing hardening. As a result of hydration, originally liquid or plastic cement glue turns into cement stone. The stages of this process are the setting and curing. The properties of a formed cement paste depend on the degree and rate of hydration.

The prevalence of Portland cement clinker compounds CaO and SiO_2 leads to the fact that in the process of determining the value of hydration is the formation of hydro silicates calcium (C-S-H). A complex framework of nanoparticles C-S-H formed as a result of hardening of the cement gel. Hydration process of cement depends on the size of grains (fineness), mineralogical composition of clinker, water-cement ratio, temperature hardening, and the introduction of various additives. It is important to understand what kind of structural changes occur in the cement paste or cement stone at the nanolevel.

In this work, the dynamics of changes in the structure of hydrated cement paste and cement stone samples as a function of time (up to 6 months) was investigated by method of small-angle neutron scattering (SANS) [1]. The measurements were performed on a diffractometer "Membrana-2", placed on the WWR-M reactor Petersburg Nuclear Physics Institute Russian Academy of Sciences. Neutron wavelength $\lambda = 0,3$ nm with a line width of $\Delta\lambda/\lambda = 0,3$. The range of momentum transfers $q = (4\pi/\lambda)\sin(\theta/2)$ was from 0.03 nm^{-1} to 0.8 nm^{-1}. The scattered neutrons were recorded of 41-channel ^{3}He-counter in the range of angles of $\pm2°$.

Scattering cross section $\sigma(q)$, per unit volume of the substance and unit solid angle as a function of the transferred neutron momentum q, obtained from the experimental spectra with the background and taking into account the contribution of the beam transmitted through the sample without the interaction of neutrons (transmission) with the normalization of data on the scattering intensity for the standard sample of known cross-section (1 mm H_2O).

For a system of identical scattering objects experimentally determined scattering intensity is averaged over all orientations (directions), the intensity of scattering by one particle in the Born approximation is the Fourier transform of the scattering structure. This allows us to define a number of structural characteristics of the scattering objects.

In situ dynamics of changes experimental ranges of sections of dispersion of neutrons on hardening samples of the cement paste is presented over time (up to 6 months).

From the experimental data for neutron-scattering cross-sections using the software GNOM 4.5 [2] the Fourier transform of the distribution of scattering objects recovered in the approximation of homogeneous spheres. When fitting the experimental data varied the maximum radius of the scattering objects in the range from 50 to 100 nm. The scattering data were described quite accurately, if the maximum size of the scattering region was chosen to be 80 nm. The average radius of the scattering structures distributed from 40 to 55 nm. Quantitative relationships that describe the growth dynamics of C-S-H nanoparticles is obtained.

The fractal dimension of the C-S-H nanoparticles is obtained from the experimental SANS data. It is shown that the process of evolution cement paste or cement stone occurs the growth of the fractal dimension structure of C-S-H nanoparticles.

Various additives effect on all the structural parameters of cement paste or cement stone. The mineral and organomineral technogenic and artificial origin additives were considered.

1. L.A. Feigin. D.I. Svergun. *Structure Analysis by Small-Angle X-ray and Neutron Scattering*. New York, 1987
2. D.I. Svergun, "Determination of the regularization parameter in indirect-transform methods using perceptual criteria", J. Appl. Crystallogr., **25**, pp.495-503, 1992

P3-8: Electrical properties of plasma-chemical silicon dioxide processed by boiling water in the metal - oxide - metal structure

V. Levin, V. Mordvintsev, S. Kudryavtsev

Yaroslavl Branch of the Institute of Physics and Technology, Institution of Russian Academy of Sciences, Yaroslavl, Russia, E-mail: el-bek@yandex.ru

This paper presents the investigation results of the influence of some technological factors on the surface of the dielectric properties of the insulating slit in a memory element based on self-forming nanostructures (MESN). In particular, a significant effect of moisture on the electrical properties of silicon dioxide was revealed, which is commonly used as an insulating layer in the MESN. The results of numerical calculations based on the model, which qualitatively explains the reasons for the influence of water on process of the electroforming are shown.

MESN [1], in a simplified design, is a plane-parallel capacitor system - "sandwich" structure consisting of two electrodes separated by a dielectric. The structure is not completely filled with dielectric, which is forming an insulating slit between electrodes. One of electrodes is a cathode and another is an anode. The butt end of the dielectric and the edge of cathode are usually aligned to facilitate the emission of electrons from it and to provide access a working medium to the dielectric surface. The dielectric layer is thin (tens of nanometers) to provide sufficient intensity for field emission in the insulating slit at low supplied voltages (5÷15 V).

In MESN the silicon dioxide (SiO_2) as the dielectric is used, which is a good insulator and has convenient functional properties as a storage medium, it is effortless to electroforming [1] In addition, the growing process of SiO_2 layers is widely used in conventional microelectronics, especially in the manufacture of MOS-devices and so well designed. There are various ways to create layers of SiO_2: thermal oxidation, anodic oxidation in plasma, plasma-chemical deposition, sputtering target of SiO_2 and Si in an oxygen atmosphere and CVD - processes.

In our experiments we used thermal oxidation and plasma-chemical deposition. We studied two options of design MESN, when n^+-type silicon layer and titanium nitride layer (TiN) as an anode are used. Schematically, the layers in these two options can be represented as n^+Si-SiO_2-W and n^+Si-TiN-SiO_2-W respectively. The top tungsten layer (W) is cathode, since has a good emission characteristics, it is a conventional material for field emission cathodes. Conductor layer of TiN protects active n^+Si surface against the influence of working medium and provides a functionally more stable electrical characteristics of the insulating gap. It is known that high-temperature oxidation of silicon in oxygen produces the highest quality of SiO_2 layers. They have low porosity and high breakdown voltage, which is especially important for very thin layers of nanometer thickness. Therefore it is important to understand how the insulating slit parameters are changing with the changing of the dielectric coating technology.

All experimental samples were fabricated on silicon wafers using the conventional methods of microelectronics technology, except for the important operation of forming an insulating slit - etching a thin dielectric [2]. SiO_2 layers were obtained by two ways. The first, the structure of n^+Si-SiO_2-W is the growing of a thin oxide layer on the n^+Si in the diffusion furnace at 850 °C in a dry oxygen flow, and the second, for the structure of n^+Si-TiN-SiO_2-W plasma-chemical deposition from a mixture of silane and nitrous oxide on the TiN layer at a silicon wafer temperature 380 °C. The thickness of the grown SiO_2 layer is typically near 20 nm, with small deviations in units of nanometers. The top W layer was deposited using magnetron sputtering. After the fabrication wafers are containing MESN and test structures, in particular, capacitors with a thin SiO_2. Then the photoresist mask was deposited on the wafer, only pads and scribing line were opened. Then the wafer is divided into chips, and they are arranged on glue in the glass-metal housings.

The technological process of manufacturing the memory matrix structure on the silicon wafers are subjected to various treatments, including operations of wet etching, after which the surface structure can contain contaminations which are difficult to delete. In forming the butt end of a thin dielectric insulating slit is particularly critical etching operation, as the butt end surface state significantly effects to the reliability of the MESN. Therefore, before the electroforming operation and after the removal of the protective layer of photoresist, it was decided to subject the open housings with chips to boiling in deionized water for further cleaning of the open butt ends of the dielectric from the possible ionic contamination.

Before the electroforming the quality of the obtained structures of the dielectric and electrical properties of

the insulating slit has been tested, to do this we measured current-voltage characteristics (I-U-characteristics) in a low current mode when the voltage (U_{10}) on the structure is limited when the current reaches the value of 10 nA.

The experimental I-U-characteristics of structures with a thickness of silicon dioxide about 20 nm before the electroforming are shown in figure. For the closed structure, i.e. capacitor with a continuous layer of SiO_2, the typical form of the I-U-characteristics are presented by curve 1 where there is a visible current only when the voltage applied to the structure more than 21 V, which is typical for high-quality layers of SiO_2. The curve 2 represents the I-U-characteristics of the opened structure, i.e. in which the butt end of SiO_2 is formed by method [2] in the layer of the same quality. After treatment in boiling water it was found that for the open Si-SiO_2-W structure with thermal silicon dioxide I-U-characteristics shifted toward lower values - curve 3, and for the open TiN-SiO_2-W structure with the plasma-chemical silicon dioxide I-U-characteristics shifted toward higher values - curve 4.
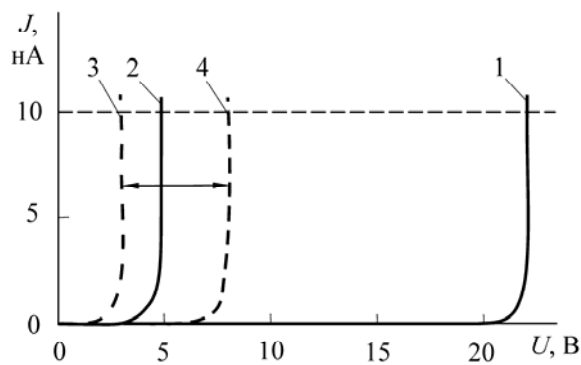
To explain this behavior of the I-U - characteristics the following assumptions can be made. In the dense thermal silicon oxide the defectiveness on the surface increases after treatment in boiling water, for this reason the density of surface states is increasing, which leads to an increase the initial conductivity of the butt end of the dielectric, while the water does not penetrate deeply into the oxide and is easily removed with conventional drying. On the contrary, plasma-chemical oxide has a higher porosity, that is indirectly confirmed by a comparatively higher rate of its etching (150 and 50 seconds respectively) due to rapid penetration of etchant into the pores. The increased porosity leads to the water penetration after boiling deep into the pores and can persist long in them. However, the mechanism of the effect of water on the initial conductivity of the open structure is not obvious, therefore, with such structure model numerical calculations were carried out for evaluation.

As the basis of the model the assumption is taken that the surface layer of the thin butt of the oxide can be represented as a matrix mix - nanoparticles of water with the relative permittivity $\varepsilon = 81$ (20 ^{o}C) in SiO_2-matrix with $\varepsilon = 3.8$. The effective dielectric constant ε^* of such media is very difficult to calculate, even if you know the geometry of the pores, but it is possible to estimate the limits within ε^*-value can lie, based on, for example, Hashin-Shtrikman formulas [3] derived from variational principles. In two dimensions, such an estimate gives the necessary limits for a possible porosity of SiO_2 up to cover the surface of a continuous thin film of water. The numerical simulation allowed us to find possible reasons for the growth of the test voltage U_{10} and probability increasing of breakdown structures with the plasma-chemical oxide. It is shown that with increasing concentration of water in the SiO_2 layer the field intensity near the open surface of the SiO_2 insulating slit is decreasing and in a narrow layer of insulating dielectric under the slit (in the residual oxide at the anode) – the intensity increases.

We can conclude that the silicon dioxide produced by plasma deposition on the TiN-surface is much more loose and porous in comparison with the high-temperature silicon dioxide. Due to the high porosity of the butt end the wetted dielectric surface with high dielectric constant can be formed. The accounting of this phenomenon at simulation explains our experiment results.

Calculations of the electrical fields in this paper were performed with the help of software package ELCUT [4].

1. V.M. Mordvintsev, S.E. Kudryavtsev, V.L. Levin, Rossiiskie nanotekhnologii, Vol. 4, N 1-2, pp.126-143, 2009.
2. V.M. Mordvintsev, T.K. Shumilova, Russian Mikroelektronika. Vol. 28, N 2, pp. 122-133, 1999.
3. T. D. Schermergor. *Teoriya uprugosti microneodnorodnyh sred*. Nauka, Moscow, 1977.
4. http://elcut.ru

P3-9: Photosensitive and luminescence porous silicon based structures

N. Latukhina, G. Pisarenko**,** A. Rogozhin, S. Saed, S. Sokolov, A. Surin, V. Timoshenko

Samara State University, Samara, Russia, natalat@mail.ru

Porous silicon is a perspective material for optoelectronic applications. In this work the layers of porous silicon were made on a textured surface of crystal silicon plates. The textured surface means a surface with a created microreliefe in the form of correct tetrahedral tripod signals with the basis square from 3 to 25

micrometers (Fig.1). During textured surface anode etching the origin of pores faces begins in dimples of microreliefe, i.e. on joints of tripod of pyramids where electric field intensity is maximum. Eventually the appeared pores that continue the growth deep into a silicon electrode. Peaks and edges of pyramids practically aren't exposed to etching [1]. The structures of similar type exhibit the good photosensitive and luminescence properties, and apart of usual porous silicon lays its have low electric resistance and high stability.

There the samples with p-n-junction (above 0.2 – 0.5 microns) on the working surface were used for obtaining of photodiode structures. The conducted researches have shown that such structure possesses good photo-electric
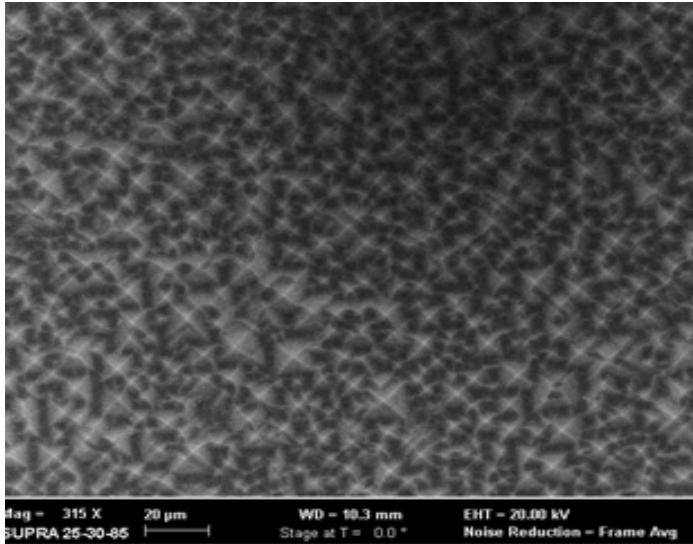
Fig. 1. SEM – image of textured surfaces with a porous layer

characteristics such as light absorption happening not only with edge, but also from a lateral surface of each photodiode column. Nanocrystalline structure of walls of pores leads to noticeable magnification of light absorption in a short wave part of a spectrum. Thus, structures with a porous layer, possess noticeably higher photo-electric characteristics, than structures with a textured surface without a porous layer (Fig.2). Therefore this technology is perspective for creation of photo-sensor elements of different functions.
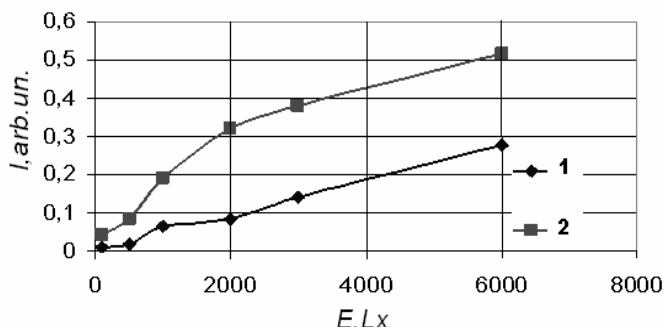
Fig. 2. Dependence of photocurrent *I* from light power *E for* samples without (1) and with (2) porous layer

The luminescence structures were prepared by soaking with a solution of rear earth (RE) in acid. Erbium (Er) and ytterbium (Ib) were used as RE elements Systems with Er doped silicon nanocrystals have luminescence at room temperature, which can be explained by transmission of excitation energy from nanocrystals to Er-ions with further transition $^4I_{13/2} \to {}^4I_{15/2}$. [2]. In order to optically activate Er- and Ib-related centers we used thermal annealing of the samples. The samples were annealed in air at different temperatures varied from 600 to 1100 ^{0}C for doping of porous silicon. Photoluminescence (PL) and electroluminescence (EL) measurements were performed using a PROSCAN HLS 190IR and HS 101H charge coupled detectors and a SOLAR TII monochromator. A Spectra Physics Beamlok 2065 laser with wavelength of 364 nm (laser power 50 mW) was used as an excitation source for the PL experiments. The measurements were performed at room temperature in air.

PL spectra of the Er-doped samples exhibit a complex structure (Fig. 3). The spectrum consists of a broad line with maximum at 750 nm, which corresponds to the radiative recombination of excitons confined in Si nanocrystals, and of a series of PL peaks in the infrared IR region. There are three Er-related lines: near

850 nm, 990 nm and 1530-1560 nm. The broad line at 1507 nm is probably related to the defect-related luminescence in Si nanocrystals. For some samples the PL line of defects was suppressed.
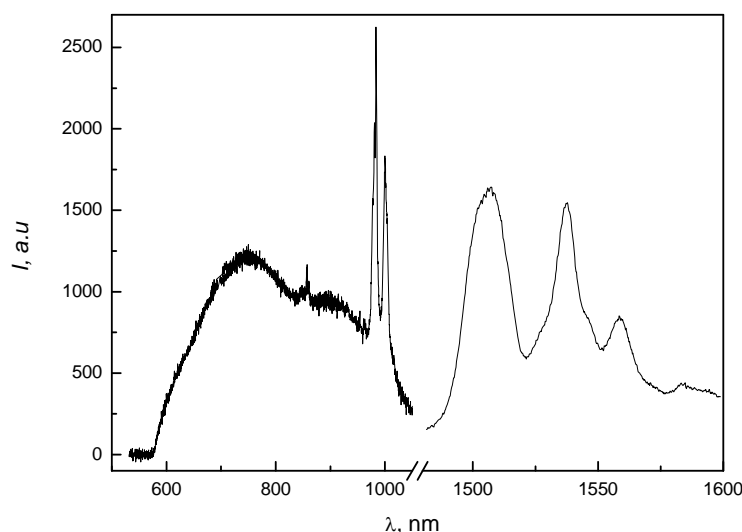
Fig. 3. Typical PL spectrum of a sample grown on the polished c-Si wafer (arbitrary units in the VIS and IR parts of the spectrum are different)

The EL was measured in the structures with nickel contact on the top of por-Si layer and Al-back contacts. The maximal dc-current under applied forward voltage of 10 V was about 1 mA. The EL spectrum was found to consist of mostly the defect-related line at 1500 nm. The intensive red light in the VIS part of spectrum was detected, caused by porous silicon EL.

Also in the samples doped with Yb by similar PL procedure we have observed a sharp line at 980 nm related to Yb-ions.

The electrical properties of some part of samples were researched. The high-frequency capacitance dependences and current-voltage characteristics were measured at room temperature. This researches show the conductivity inversion of silicon surface lays caused by diffusion RE in to silicon.

1. N.V. Latukhina., etc. "Photoelectric Properties of Sructures with Micro- and Nano-porous Silicon", News of the Samara centre of science of the Russian Academy of Sciences, 11, № 3 (29), pp. 66 – 71
2. V. Yu. Timoshenko etc., Comparative study of photoluminescence of undoped and erbium-doped size-controlled nanocrystalline Si/SiO2 multilayered structures, J. Appl. Phys., **96**, 2254 (2004).

P3-10: The features of interactions of disilane molecular beam with the epitaxial surface in conditions of silicon layer growth

N.L.Ivina[1], T.N. Smyslova[2], L.K. Orlov[3]

1. Nizhni Novgorod Management Institute, 2. Nizhni Novgorod State Technical Alexeev University,
3. Institute for Physics of Microstructures, Russian Academe of Science, orlov@ipm.sci-nnov.ru

Effects of interaction of molecular beams with a solid surface and the phenomena accompanying them proceeding on interphase boundary gas – solid state, underlie the various technological processes widely used in practice. Processes of a catalysis, membrane gases separation, gomo - and heteroepitaxy are the most important. It is obvious that achievement of necessary result at carrying out of any technological operations is impossible without detailed understanding of mechanisms and features of reactions on corresponding surfaces. This problem is especially actual in the connection with micro- and a nanoelectronics prospects, connected with the technology of growth of the heteroepitaxial layers and superficial nanostructures, using the method of molecular beam epitaxy with molecular beam sources of substance [1]. In this method, the growth of the layers occurs in the filling of surface states of a variety of gas pyrolysis products, which leads to the specifics of the growth process due to expression of a number of features in the decay kinetics of the epitaxial surface adsorbed molecules [2]. The silicon and germanium hydrides and dihydride are widely used for growing the layers for different applications of silicon electronics. So, it is obvious it is impossible to understand the features observed in the behavior of kinetic coefficients, without a detailed understanding of physical and chemical processes details occurring on the surface of the epitaxial [3].

In the literature, the discussion of the temperature dependence of the silicon layers growth rate is usually limited to the analysis of simple kinetic models that take into account in the kinetics equations only hydride molecule adsorption and hydrogen desorption terms. The corresponding model meets the conditions of full disintegration of the hydride molecules pyrolysis under the prechemosorbtion state, just in the vicinity of the growing surface. The terms that describe the hydrides molecules radicals' disintegration, trapped by surface, which play an important role in the range of typical growth temperatures, are excluded to simplify the calculation of the theoretical analysis. This procedure is generally consistent with results of known experiments to determine the composition of the pyrolysis products on the surface of the silicon layer in terms of growth and limits the ability to assess the degree of blur in the case of heterojunctions grown heterostructures for gas mixtures.

This paper discusses the features of kinetic models describing the basic physical and chemical processes occurring on the silicon crystal growth surface during the trapping and disintegration of the disilane molecules. Analytical expressions relating the hydrides molecules disintegration rate ν_{SiHj} on the Si surface with the other kinetic coefficients and the measured characteristics of the epitaxial process were fined. This expression has been obtained for the first time by us from kinetic equations for disilane disintegration models $Si_2H_6 \rightarrow 2SiH_j + (k+n)H$:

$$\nu_{SiHj} = \{j(1+1/j)^{n+1}/2(n+1)!\}\alpha /\{(\gamma - \alpha/r_{Si})\,[\gamma + (1+1/j)\beta^{1/(k+2)} - \alpha/r_{Si}]^n\}.$$

Heir r_{Si} – crystallization coefficient, $j = (3\div1)$ – type of radicals that is captured by the surface, $k = 0 \div (3\text{-}j)$ – hydride atoms number from hydride molecular are adsorbed by surface on the first forechemosorbtion stage, $n = 0 \div j$ - hydride atoms number from molecular radicals are adsorbed by surface on the second pyrolysis stage, α, β, γ – the functions of the growth rate (V_{gr}) and hydrogen covering (θ_H) which can be determined in temperature range 400-700°C from technological experiment. This parameters determine also on molecular capture coefficient, molecular flow and gas pressure in the chamber.

We defined region of the characteristic lifetimes of the radicals SiH_j molecules of silicon dihydride ($0.3c < \tau_{SiHj} < 5c$) on the surface of the plate for the various models and conditions of gas pyrolysis using the data of growth experiments. It was shown that the dependence of the molecules disintegration rate on temperature for all types of pyrolysis models cannot be described by simple dependencies of the activation form. The behavior of the curves (Figure) is determined not only by the condition where the hydride disintegration occurs: at the surface of silicon wafers ($j = 1$) or directly on it ($j = 3$), but also at what stage of the pyrolysis the hydrogen molecules is trapped in the silicon surface: if the hydride molecule is in prechermosorbtion

state k > n (b) , or have already invaded the surface k < n (a). A kinetic analysis of the temperature depending on the radicals molecules disintegration rate has shown that the nature of the collapse of the molecules of mono-and disilane trapped by the surface is quite different in different temperature regimes that meet the conditions of high and low coverage of the surface of silicon with hydrogen. In this case the temperature dependence of radicals molecules disintegration rate is described by the formula

$$\nu_{SiHj} = \nu_{01}(1-\theta_H)\times \exp(-E_{a1}/k_BT) + \nu_{02}(\theta_H)\times \exp(-E_{a2}/k_BT)$$

containing the sum of the activation dependence with the activation energies E_{a1} and E_{a2}. This energies are different for mono-and disilane $E_a (SiH_4) < E_a (Si_2H_6)$, and meeting the conditions of high temperature and low-temperature silicon layer growth on a clean and filled with hydrogen silicon surface with coefficients depending on the surface concentration of the hydrogen.
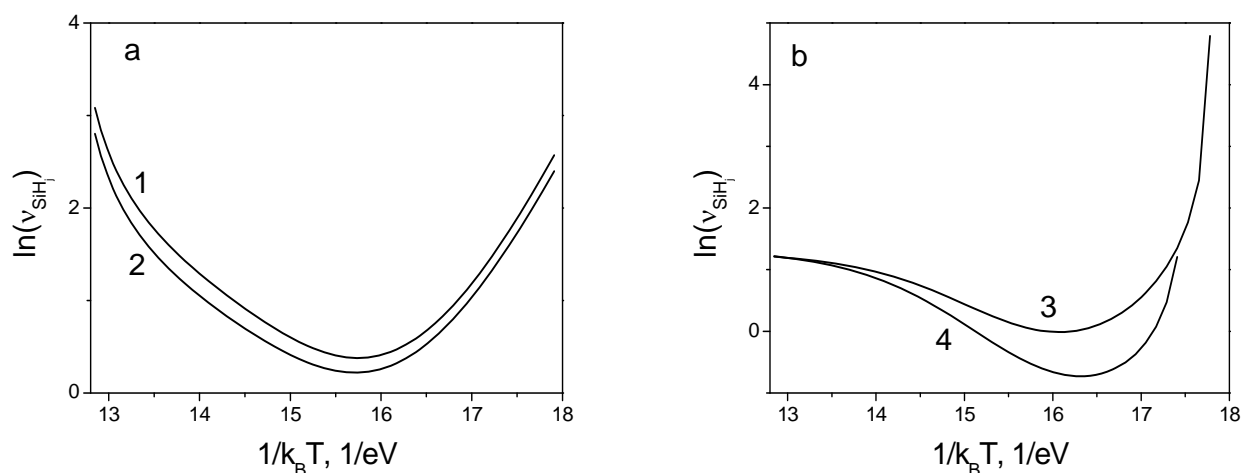
Figure. Temperature dependence of the disilane molecules pyrolysis frequency on the silicon layer surface in the kinetics model (jkn): a) 302 (1), 202 (2), b) 121 (3), 140 (4) and for the reactor gas pressure $P_{Si2H6} = 0.1$ mTor.

1. K.J. Kim, M. Suemitsu, M. Yamanaka, and N. Miyamoto, "Effects of mixing germane in silane GSMBE", Appl. Phys. Lett., 62, p.3461-3463, 1993.
2. B.A. Ferguson, C.T. Reeves, D.J. Safarik, and C.B. Mullins, "Trapping-mediated chemisorption of disilane on Si(100)-(2×1)", J. Phys. Chem., 113, p.2470-2478, 2000.
3. A.V. Potapov, L.K. Orlov, and S.V. Ivin, "The growth kinetics of SiGe layers from SiH4 and GeH4 ", Thin Solid Films, 336, p.191-195, 1999.
4. T. Murata, H. Nakazawa, Y. Tsukidate, and M. Suemitsu, "Role of adsorption kinetics in the low-temperature Si growth by gas-source molecular beam epitaxy: In situ observations and detailed modeling of the growth", Appl. Phys. Lett., 79, p.746-748, 2001.
5. L.K. Orlov, and S.V. Ivin, "Vacuum hydride epitaxy of silicon: kinetics of monosilane pyrolysis on the growth surface", Semiconductors, 45, p.557-566, 2011.
6. L.K. Orlov, S.V. Ivin, and T.N. Smyslova, "The spatial features of adsorption and the kinetics of decomposition of monosilane molecules on the epitaxial surface of silicon", Russian J. Phys. Chem. B, 5, p.168-175, 2011.

P3-11: Low-frequency noise spectroscopy as a diagnostic tool to study of surfaces

M. Makoviychuk

Yaroslavl Branch of the Institute of Physics and Technology, Russian Academy of Sciences, Yaroslavl, Russia,
E-mail:Makoviychuk@rambler.ru

The method of low frequency noise spectroscopy of structure-disordered semiconductors finds more and more broad application both in physical researches and in the analysis of different processes of micro- and nanotechnology. The practical realization of this method as a monitoring instrument of defect-impurity engineering for to solve the technological problems of silicon electronics are presented and discussed.

In presented activity the experimental results on analysis of flicker noise processes in disordered semiconductors on an example of designed production process of flicker noise gas sensor of a new generation are classified.

Studies concerned with the design of new approach for gas sensors based on ion-implanted silicon structures are analyzed. The influence of adsorbed molecules on the electronic state, electrical conductivity and flicker noise of the surface and inner interfaces in disordered silicon structures are discussed. The sensor properties of disordered silicon structures in the detection of various adsorbed molecules are described.

As they are grown and processed in microelectronics manufacturing, Si single crystals start to have different types of structural imperfection and impurity that may be detrimental to finished-device performance.

Defect/impurity flicker noise spectroscopy provides a rapid technique for investigating defect–impurity interaction and as such relates to defect/impurity engineering, which is concerned with reducing process-induced disturbances and impurity diffusion coefficients (in ion-implanted silicon) and with gettering metallic impurities. The above idea is implemented in a technology of new-generation flicker-noise gas sensors designed to be incorporated into microanalytical systems [1].

The highly effective diagnostic method is necessary for practical realization of defect-impurity engineering (DIE) in structure-disordered semiconductors. To such requirements there corresponds an offered method of a low-frequency noise spectroscopy (Fig.1).

Let's stay on nature and capabilities of each of components of a method at research of structure-disordered semiconductors.
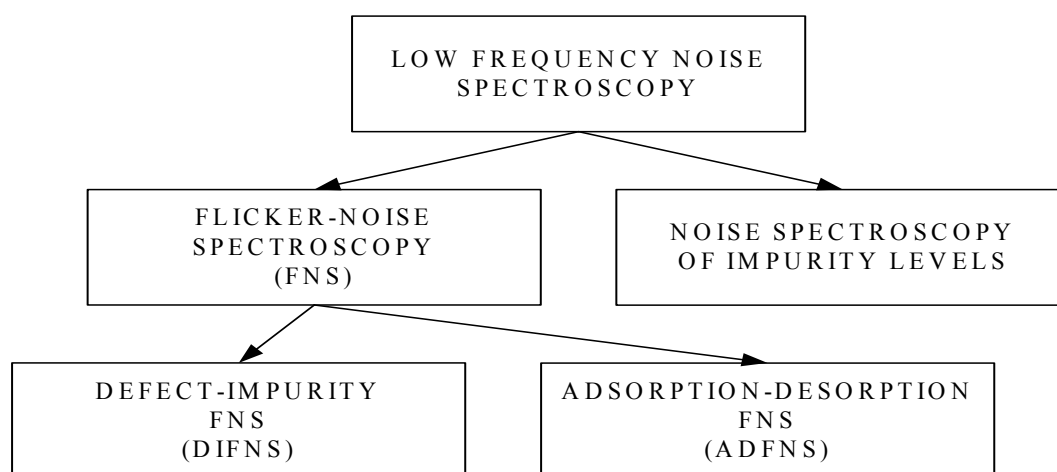
Fig. 1. Classification of methods of low frequency-noise spectroscopy of structure-disordered semiconductors.

Noise spectroscopy of impurity levels in silicon

The main advantage of the given technique is that a noise spectroscopy of impurity levels allows determining impurity the concentration on three orders is lower than equilibrium concentration of charge carriers in silicon [2]. The method of noise spectroscopy of impurity levels is irreplaceable for detection of small impurity concentrations in high-quality silicon: with his help it is possible to determine the impurity

concentrations about 10^{11}см$^{-3}$ and below (is depends on common concentration of free charge carriers in silicon) [3].

Flicker - noise in silicon systems with under dimension
In this case spectrum of low frequency noise has no a view such as 1/f, and represents a line (or sum of several lines) of Lorentzian form. The increase of temperature or geometrical sizes result to complicating of a spectrum and transition his to flicker type.
Kirton, Day and Uren have shown [4], that decreasing of the active area of n-Si MOS structure (from 350 μm^2 up to 0.4 μm^2) results in similar change of the form of a noise spectrum.
The decreasing of the sizes of investigated structure increase improve of a method of flicker-noise spectroscopy at the expense of a capability of research of parameters of local centers in silicon ground of analysis of behavior separate Lorentzian spectra at a temperature variation.
This was due to the fact that in the very small devices which they were studying (about 0.1 μm^2) it was not possible, even at elevated temperatures, to observe the fluctuations of more than a handful of traps at any particular gate voltage. Studies by Rogers and Buhrman [5] on small-area metal-insulator-metal (MIM) tunnel junctions, Restle *et al.* [6] on small-area silicon-on-sapphire resistors and Uren *et al.* [4] on a range of MOSFETs of different areas provided unambiguous evidence that 1/f noise in these systems is generated through the fluctuation in occupancy of individual defect states modulating the conductivity.
The experiments described in our report provide an elegant demonstration of the full decomposition of the 1/f spectrum into its constituent Lorentzian components and the sample-to-sample variation in the power spectra expected from very small systems.

Defect-impurity flicker-noise spectroscopy
The special role of defect-impurity flicker-noise spectroscopy (DIFNS) - in its application for information express-analysis of defect - impurity interaction at implementation of methods of defect - impurity engineering, namely methods of depressing of formation of residual disturbance, decrease of diffusion coefficients of impurity in ion-implanted silicon and gettering of metallic impurities.
The application DIFNS of silicon structures as the diagnostic tool of microtechnology is demonstrated at design of flicker - noise gas sensors of new generations tendered as the constituent of microanalytical systems [7].

Adsorption-desorption flicker noise spectroscopy
The tendered method adsorption–desorption flicker-noise spectroscopy (ADFNS) will use process of an adsorption and desorption of adsorbed particles from surface of the semiconductor for realization of the full electrophysical analysis of connection an adsorbate - adsorbent. Thus it is possible to receive also information about composition of a surface.
ADFNS - highly sensitive method of testing of surface phenomena in gas sensitivity semiconducting structures. The relation of flickers-noise performances to a structure of a gas phase can be utilized for essential sensitization both selectivity of detecting of gases and steams [1, 7].

1. M.I. Makoviychuk, A.L. Chapkevich, A.A. Chapkevich, V.A. Vinokurov, "Flicker-noise gas sensor", Biomedical Engineering, 43, No 3, pp.109-113, 2009
2. G. Bosman, R.J.J. Zijlstra, "Generation-recombination noise in p-type silicon", Solid-State Electronics, 25, No 1, pp.273 - 280, 1982
3. Z. Shoblitskas, V. Palenskis, "Noise spectroscopy of impurity levels and 1/f noise in high resistance silicon", Lietuvos fizikos rinkinys, XXV, No 3, pp.88 - 97, 1985
4. M.J. Uren, D.J. Day, M.J. Kirton, "1/f and random telegraph noise in silicon metal-oxide-semiconductor field-effect transistors", Appl. Phys. Lett., 47, No 11, pp.1195 - 1197, 1985
5. C.T. Rogers, R.A. Buhrman, Phys. Rev. Lett., 53, p.1272, 1984; Phys. Rev. Lett., 55, p.859, 1985
6. P.J. Restle, R.J. Hamilton, M.B. Weissman, M.S. Love, Phys. Rev. B, 31, p.2254, 1985
7. M.I. Makoviychuk, "Flicker-noise gas sensors as basis elements of microanalytical systems", Proceed. Int. Conf. " Micro- and nanoelectronics - 2007 ". (October 1rd -5th, 2007, Moscow-Zvenigorod, Russia), Moscow: IPT RAS, O1-22, 2007

P3-12: Neural network modeling for prediction of gas-sensitivity of Ag-containing polyacrylonitrile films

T.A.Bednaya[1] , T.V.Semenistaya[2]

1. Taganrog State Pedagogical Institute, Taganrog, Russia, bednayat@mail.ru.
2. Taganrog Institute of Technology – Southern Federal University, Taganrog, Russia, semenistaya@yandex.ru

Prompt development of a science and equipment demands receiving new structures and materials with qualitatively new properties. Recently it is given particular attention to gas-sensitive materials among which are most interesting to research films based on electroconducting polyconjuncted organic polymers. Application of such films as a sensitive layer of gas sensors is perspective due to its properties: functioning under normal conditions that gives the chance for creating not warmed up gas sensors.

Today the system of monitoring of environment widely applies electric chemical sensors of the resistive type which principle of action is based on change of electrophysical properties of a sensitive layer. They have a number of advantages before other known types of gas sensors thanks to high sensitivity, rather low cost and simplicity of a design.

In this work for receiving the electroconducting polyconjuncted organic polymer from a linear polymer polyacrylonitrile (PAN) pyrolysis under the influence of incoherent IR-radiation is used. Pyrolysis of organic polymers is the simplest way of receiving organic conductors and semiconductors from an insulator materials. Depending on intensity of IR-radiation structures of PAN with various length of π-conjuncted system are gained. So variation of technological parameters of fabrication the films based on such materials can essentially change their electrophysical properties. To increase the selectivity and adsorption activity of organic semiconductor PAN materials modification with transition metals are done. IR-annealing carried out in IR-chamber in two stages at a low vacuum (80 mTorr). Intensity of radiation at the first stage corresponded to $150 \div 450\,°C$, and the intensity of radiation at the second stage – $400 \div 500\,°C$. Time of exposure of IR-radiation were different ($5 \div 20$ minutes) at each temperature. About 100 samples of PAN/Ag films (argentum content by weight: : 0.0 wt.%, 0.02 wt.%, 0.05 wt.%, 0.07 wt.%, 0.09 wt.%, 0.1 wt.%, 0.2 wt.%, 0.5 wt.%, 1.0 wt.%, 1.5 wt.%, 2.0 wt.%, 3.0 wt.%) are fabricated.

To study the gas-sensing properties of a material of the received cobalt-containing PAN films measured their resistance on teraommetre E6-13A. Sensitivity of the films estimated by means of factor of gas-sensitivity S, which is calculated as:

$$S = (R_o - R_g) / R_o, \text{ when } R_o > R_g,$$

where R_o – value of resistance of a film on air, R_g – value of resistance of a film in the atmosphere of detected gas.

QSPR-methods (Quantitative Structure-Property Relationship) are used for prediction of dependence of technological parameters of PAN/Ag films formation on electrophysical properties of the gained metalorganic polymeric nanocomposites.

Of special interest are neural network approaches. Artificial neural networks, or neural networks, have become quite popular n recent years, as solutions to complicated, non-trivial problems where parametric or rule-based solutions have failed.

The true power and advantage of neural networks lies in their ability to represent both linear and non-linear relationships and in their ability to learn these relationships directly from the data being modeled. Traditional linear models are simply inadequate when it comes to modeling data that contains non-linear characteristics.

The objectively existing connection between the known input values and the unknown response is the important condition of applying any statistical methods. This connection can bear random nature, it is distorted by noise, but it must exist.

The neural networks design for prediction of gas-sensing properties of Ag-containing PAN films is done. An artificial neural network structure has been specified, implemented and optimized for the purpose of predicting the factor of gas-sensitivity of Ag-containing PAN films. The network was optimized to predict results obtained in experiments based on input data of technological parameters of fabrication the films. As input data are used temperatures and times of the first and the second phases of IR-annealing and mass portion of argentum; output data are factor of gas-sensitivity of the gained Ag-containing PAN films.

In order to develop the model of the neural network, the following steps are carried out:

1. Analysis and collection of data.

2. Separation of data into train, verify and test sets.
3. Transfer the appropriate data into the networks as input.
4. Set the conditions, train, verify and test the network.
5. Analyze the results.
Double-layer perceptron was the chosen network structure (fig.1). This network was trained by means of a standard backpropagation procedure and tested on selected data from experiment.
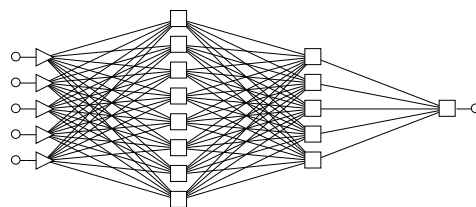

Fig.1. Double-layer perceptron of neural network.

With a test set consisting of technological parameters, the prediction error was only slightly larger than the statistical error in the training data itself. The weights in the trained neural networks were analyzed to qualitatively interpret the relation between the of technological parameters of fabrication the films and the factor of sensitivity of Ag-containing PAN films. Quality of work of an artificial neural network was determined by a root-mean-square error of predicting of values of property on a training sample (s_t), on factor of correlation between predicted and experimental values of property on a training sample of R and a root-mean-square error of a forecast on a control sample of s_v: $s_t = 0,07$; $s_v = 0,11$; $R = 0,927$.

Compiled equation correlation between the calculated and experimental values of factor of gas-sensitivity of PAN and Ag-containing PAN films looks like $S_{calc} = 0,991 S_{exp} + 0,001$. Visualization of the equation is presented in fig. 2.
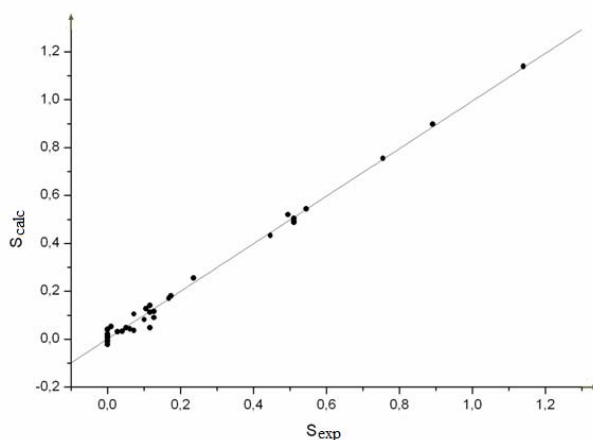
Fig.2. Experimental vs. estimated of factor of gas-sensitivity of PAN and Ag-containing PAN films

The optimum set of technological parameters for fabricating Ag-containing PAN films with the best values of gas-sensitivity to NO_2 is established: $\omega(Ag) = 0,05$ mass. %, $T_{drying} = 160\ ^{\circ}C$, $t_{drying} = 30$ minutes, $T_{IR-annealing\ 1\ phase} = 200\ ^{\circ}C$, $t_{IR-annealing\ 1\ phase} = 2$ minutes, $T_{IR-annealing\ 2\ phase} = 350\ ^{\circ}C$, $t_{IR-annealing\ 2\ phase} = 28$ minutes.

The objectively existing connection between the known input values and the unknown response is the important condition of applying any statistical methods. This connection can bear random nature, it is distorted by noise, but it must exist.

The elegant automated approach to the selection of the significant input variables can be realized with the use of the genetic algorithm, which it is possible to be called «intellectual» form of trial-and-error method.

P3-13: Three-dimensional model of adsorption-diffusion-reaction processes with a Tri-State

N. A. Rud[1], A. A. Astapkov[2], P. G. Morozov[3]

1. Yaroslavl Demidov State University, Yaroslavl, Russia, rud50@mail.ru;
2. Yaroslavl Demidov State University, Yaroslavl, Russia, ph4ntom@mail.ru;
3. Moscow Aviation Institute, Moscow, Russia, Pmorozov@bellintegrator.ru.

Micro- and nano- object related scientific researches and technical developments are nowadays actively held. There is also a growing interest in low-dimension structures research. It is known that low-dimension structures show several extraordinary properties. That is connected with specific energy redistribution in such structures. It is known that surface properties modifications has a significant influence on solid body volumetric properties especially in low size crystal regions when the surface area and the body volume are comparable. Molecules (atoms) that can change their charge state adsorption and desorption are able to show process in time dynamic periodicity. For example similar self-oscillating effects were found during potassium field desorption from the surface that has potassium-gold adsorbates mix.

Cellular automaton describing such dynamic processes is generally described in paper [1].

Input parameters of the algorithm are:

- model body size; in this case the body is a parallelepiped of size 100x100x50 elementary cells;
- a set of available cell colors(states);
- elementary cell life time that a cell can stay in one state;
- state change rules depending on neighbors states; in general rules are inequalities that look like $N(c)$ $\{>[=] | <[=]\}$ T_c, where $N(c)$ - state "c" neighbor cells quantity and T_c is a threshold by reaching which the state is changed;
- probabilistic transfer weight coefficients for each pair of states; influences probability of cell change state;
- anisotropic diffusion coefficient
- a portion of elementary cells that are in a specific state at the starting step if the algorithm: modeling surface adsorption (k);
- algorithm iteration number.

The algorithm represents an iterative whole modeled body bypass that includes every cell sate recalculation. Two operations are made every iteration in cycle by all the cells:

- reactionary interaction
- diffusion

If the life time of a cell has run out it can change its state. New cell sate depends on neighbor cells states that are in 26-tied neighborhood. If two or more conditions are accomplished then a new state is chosen randomly depending on given weights.

Diffusion occurs with given period (one time at step generally). Diffusion algorithm represents two cells states interchange. The first one is a diffusing cell and the last one is an empty place. The diffusion direction is chosen randomly depending on given diffusion coefficients. The output of the algorithm includes a 3d array [dx,dy,dz] that consists cell sates at one step for every step.

Modeling algorithm recalculates all the cell states over the whole body. To lower the algorithm complexity we applied paralleling using multi-agent system. The multi-agent system consists of three agent types: actor agent, parallel agent and rout agent. Actor agent performs cells state recalculation for cells that are in the given segment of the grid. Parallel agent divides the grid on segments depending on the number of actor agents and distributes the whole task between those agents. Route agent searches for new actor agents that are hosted into other applications and other computers. That way a new algorithm recalculates only those segments of the grid where the changes can actually take place. Also the recalculations in the independent segments are held simultaneously. These features allowed us to lower the number of operations and now it is generally independent of the modeling body size. It is worth mentioning that an innovative multi-agent platform was applied to achieve those results. That platform allows to use agents hosted on different computers (locally or globally connected) or even in the cloud. In its turn it allowed to make calculations on multiple computers that improved the performance even higher.

In the pic.1 near-surface layer evolution momentary images of 50 and 100 algorithm steps are shown.
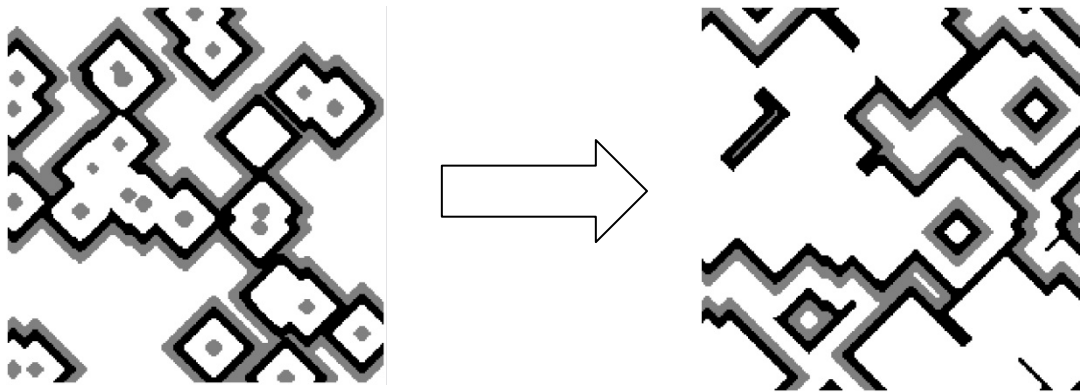
Fig.1 Near-surface layer evolution momentary images
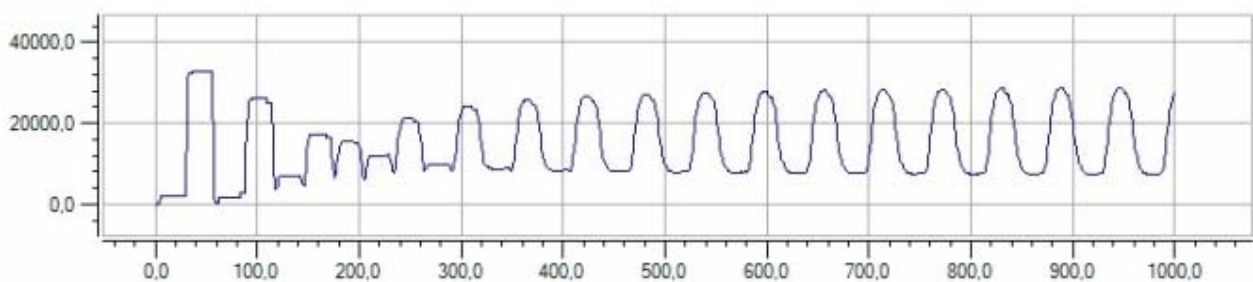
Fig. 2 Grey state cells concentration dependency on time

In the pic.2 grey state cells concentration dependency on time in the given body is shown. Constructed cellular automation can build similar dependencies for every investigated layer for every elementary cell state.

1. N. A. Rud, A. A. Astapkov, P. G. Morozov, Трехмерная модель адсорбционно-диффузионных процессов с тремя состояниями, труды международной заочной научно-практической конференции «Актуальные проблемы биологии, химии, физики», г.Новосибирск, 2011 г.

P3-14: Incorporation in grow film previously produced nanosize particles during low frequency PECVD

A.E.Berdnikov, S.V.Vasilev, A.A.Mironenko, A.A.Popov, A.V.Perminov, V.D.Chernomordick, V.N.Gusev

Yaroslavl Branch of the Institute of Physics and Technology, Institution of Russian Academy of Sciences; 150007
Universitetskaya 21, Yaroslavl, Russia, e-mail imiraslab4@yandex.ru

Plasma of low frequency discharge enhanced chemical vapor deposition (LF PECVD) has some features. As opposed to RF in LF discharge distance of ion drift in electric field is significant and can exceed distance between electrodes. As a result positively charged ions, which mass is not rather big, can achieve grow surface on electrode through half of cycle of applied power.

In other hand electrons in discharge are scattered and wall of plasma chemical reactor assumed negative charge. If nanosize particles are situated on the wall of reactor, they take negative discharge and levitate in gas phase. After that particles can moved in discharge region, drifted in applied electric field on grow surface and overgrow by deposited film. So, nanosize particle previously deposited on inner wall of plasma chemical reactor can incorporated in grow film.

Previously carries out process of LF PECVD in reactor provide nanosize particle producing. This particle can achieve inner wall of reactor. So, particle of material, which deposited in previous technology process, incorporated in film. For preventing this effect intermediate inert gas plasma treatment of reactor mast produced. In other hand this effect allowed fabricates, for example, dielectric film with incorporated clusters of material with low band gap for accumulation electric charge.

In figure 1 transparence electron microscope image of silicon oxide film with thickness 40 nm with incorporated particles of silicon nitride is show. It's obvious, that: 1) particles deposed on substrate in initial period of film deposition; 2) nanosize particles conglomerate in middle size (15-30 nm) clusters, and this clusters conglomerate in large size (50-100 nm) islands. This facts confirm the described mechanism of clusters incorporation in deposited in low frequency discharge films.
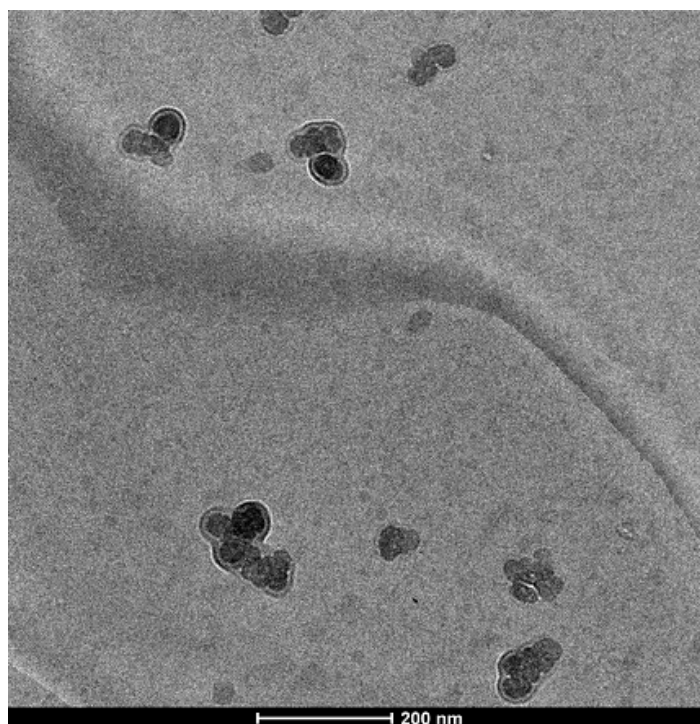

Fig.1. Transparence electron microscope image of silicon oxide film with thickness 40 nm with incorporated particles of silicon nitride

P3-15: Aluminum Nanoisland Films Formation under the Electron Irradiation of the Sapphire Surface

I.P. Ivanenko, A.A. Khaidarov, E.Yu. Zykova, I.K. Gainullin

Physics Department, Moscow State University; Russian Federation; Ivan.Gainullin@gmail.com

The controlled fabrication of nanostructures with arbitrary shapes and defined chemical composition is of great interest because of the special properties exhibited by these materials and their potential applications in electronics, optoelectronics, electrocatalysis, and thin film coatings.

In the present work we consider the possibility of use electron stimulated desorption (ESD) for the fabrication of structures on the nanometer scale on the surface of solids. It is known that low-energy electron bombarding of the binary compound surface may lead to emission of its components [1]. This phenomenon is observed for different types of materials such as oxides, alkali and alkali-earth metal halides. The more intensive ESD of anions can cause surface metallization and formation of nanoisland metallic film [2].

The aim of this study was experimental investigation of the ESD rate and formation of metallic islands on the surface of Al_2O_3 single crystal under low energy electron bombardment (E= 1—3keV) at the different sample temperature (20-320C). For estimation of ESD rate we used the method based on the dependence of the surface composition on the dosage of the electron irradiation. The surface composition was determined by Auger electron spectroscopy method. The metallic islands formed on the surface due to the electron irradiation were observed using atomic-force microscope (AFM). To reveal the optimal parameters for the nanoisland fabrication we investigated the dependence of the average size and density of metallic islands on the dosage and the energy of electron bombardment and sample temperature. It was found that Al islands of spherical form and diameter varied from 50 nm to 100 nm distributed irregularly on the Al_2O_3 surface.

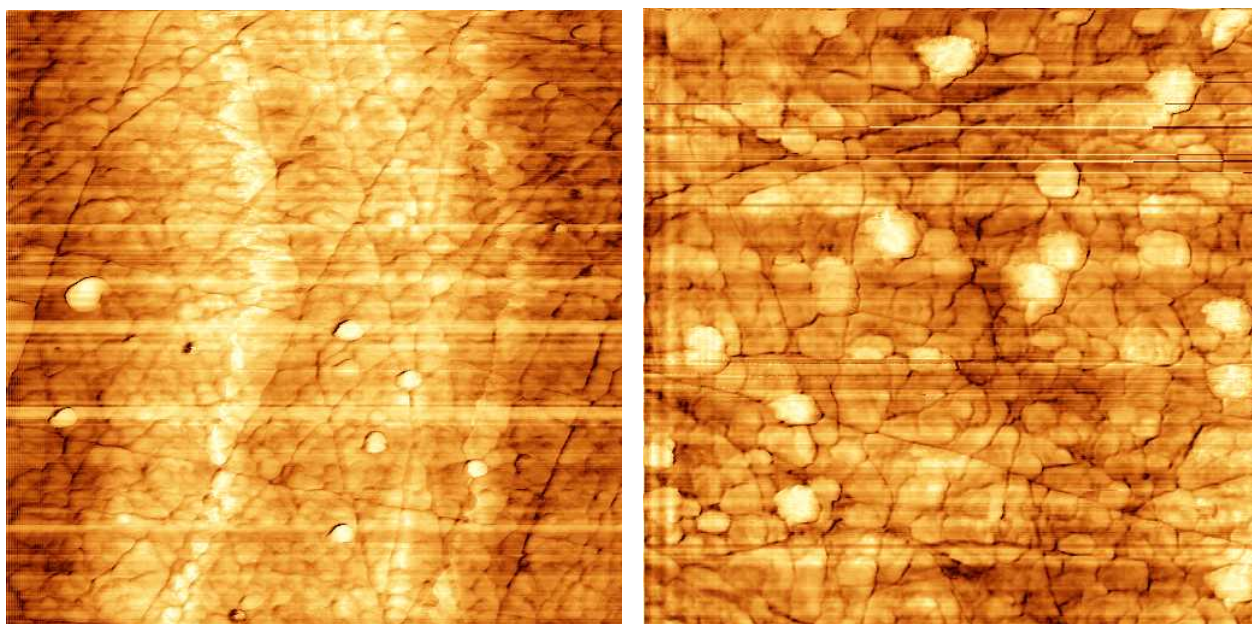Fig. 1 AFM image of Al_2O_3 surface (3x3 mkm) after electron irradiation with dose 10^{19} e/sm^2 (left) and 10^{21} e/sm (right).

1. Desorption Induced by Electronic Transitions DIET V (Springer Series in Surface Sciences 31, Springer-Verlag, Berlin, 1993.
2. M. Reichling, R. M. Wilson, R. Bennewitz, R. T. Williams, S. Gogoll, E. Stenzel, E. Matthias. Surface Science, 366 (1996) 531-544.

P3-16: Particle trapping in stainless steel in oxygen contaminated deuterium plasma

L. Begrambekov, A. Kaplevsky, Ya. Sadovskiy, P. Shigin and S. Vergasov

National Research Nuclear University (MEPhI), Moscow, Russia, alexk1989@mail.ru

The paper presents and discusses peculiarities and mechanisms of particle trapping and retention in stainless steel exposed in (D_2+O_2) plasma. The experiments were performed in the thermal desorption stand ("MIKMA") [1] intended for sample irradiation in gas discharge with heated cathode and thermal desorption analysis of irradiated samples.

The samples used in the experiments were made of 12X18H10T type stainless steel (SS) (0.12% C, 18% Cr, 10% Ni, ≤1% T) and of nickel (Ni). Residual gas (H_2O – 97%, H_2 – 3%) pressure in plasma chamber did not exceed $1.5×10^{-5}$ Pa, working gas (D_2+O_2) pressure was $(4-7)×10^{-1}$ Pa, and O_2 concentration in working gas was varied from 0 to 5%. Irradiation ion energy was changed from 20 to 700 eV/at. Samples were annealed before irradiation at 1450 K during 5 minutes. Irradiated samples were kept at 450-500 K, TDS temperature ramp up was 5 K/s.

It was found that irradiation of SS walls of plasma chamber with both deuterium atoms (which appeared in the working gas when tungsten cathode had been heated) or/and plasma particles initiates generation of "water" molecules (H_2O, HDO и D_2O) on the chamber wall surface from oxygen and deuterium of residual gas and hydrogen coming from the bulk of SS.
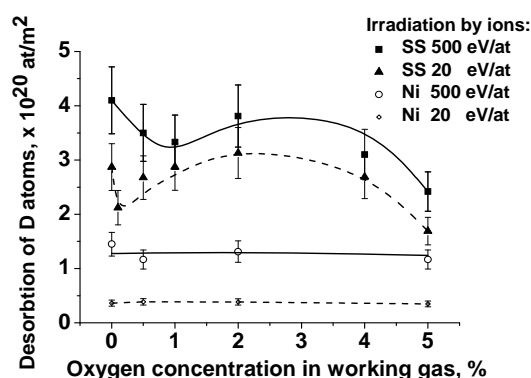
Fig. 1. The amount of deuterium atoms trapped in stainless steel and nickel in dependence on oxygen concentration in working gas.
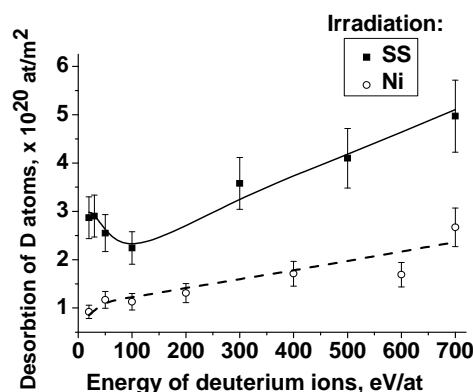
Fig. 2. The amount of deuterium atoms trapped in stainless steel and nickel in dependence on ion energy.

Deuterium trapping in SS and Ni in dependence on oxygen concentration in plasma and ion energy is showed on the figures 1 and 2. Thermal desorption analysis showed that basic features of trapping dependence on ion energy and oxygen concentration in plasma are defined primarily by oxygen concentration in oxidized SS surface layer (determined by the amount of oxygen in working gas) and correspondence between ions stopping range and thickness of SS surface layer. Under low energy irradiation trapped particles were bound predominantly with chromium atoms within oxidized layer. When ion energy exceeded 100 eV/at the particles were retained mainly behind oxidized layer in the traps related to iron atoms.

During deuterium atom irradiation of an annealed sample in working gas that consisted of $D_2+2\%O_2$ about 75% of hydrogen and deuterium trapping in SS and (40-50)% of trapping under plasma ion irradiation were provided by the "water" molecules sorbed on SS surface through the mechanism of "potential" trapping [2]. Trapping in Ni did not depend on oxygen concentration in plasma and proceeded by "kinetic" mechanism [2].

1. A.A. Airapetov, et al., "Glow discharge cleaning of carbon fiber composite and stainless steel", J. Nucl. Mater.. 415, pp. 1042-1045, 2011.
2. A.A. Airapetov, et al., "Deuterium trapping in carbon fiber composites exposed to D plasma", J. Nucl. Mater., 390–391, pp. 589-592, 2009

P3-17: Hydrogen trapping in zirconium and zirconium with chromium coating under hydrogen saturation in various conditions

L. Begrambekov, A. Gordeev, A. Grunin, A. Yevsin, A. Kaplevskiy

National Research Nuclear University "MEPhI", Moscow, Russia, evsin@plasma.mephi.ru

In spite of the long history of research into interaction between hydrogen and metals, some important aspects of hydrogen trapping and retention in metals with barrier layers of oxides on their surface and/or protective coatings have not been studied up to the present day. In this work the peculiarities of hydrogen trapping in zirconium and zirconium with chromium coating are investigated. Preference is given to zirconium as a material for research because it is used for producing of light-water reactors core elements so the investigation of peculiarities of hydrogen trapping in zirconium is of significant practical interest.

Zirconium samples (E110 alloy) and samples of zirconium with chromium coating have been exposed in overheated water steam (steam temperature T=400 °C), have been saturated by hydrogen ions in electrolyte (5% H_3PO_4, ion flux j_i=23 mA/cm^2), have been irradiated by deuterium atoms of thermal energy (atom flux j_i=0.16×10^{15} mA/cm^2, sample temperature T=330 °C), by ions and atoms of deuterium plasma (ion energy E_i=500÷750 eV/at, ion flux j_i=0.5 mA/cm^2, sample temperature T=380 °C). Hydrogen trapping during the deposition of chromium on zirconium in argon plasma of gas discharge with hot cathode has also been studied.

The amount of hydrogen atoms in zirconium has been measured by thermal desorption spectrometry (TDS). During the experiments the following regularities have been revealed:

1) In various conditions: under saturation of zirconium samples by hydrogen ions in electrolyte, under irradiation of them by deuterium atoms in vacuum, by ions of argon or deuterium plasma and during the deposition of chromium coating on zirconium in argon plasma – in thin subsurface slightly oxidized layer of zirconium trapping centers for hydrogen isotopes appears. Hydrogen releases from these trapping centers during thermal desorption at the temperatures of 1050 K and 1170 K, which are much lower than the temperature of hydrogen release from the bulk of metal (~1300 K). Under the irradiation of zirconium by atoms and ions of deuterium (hydrogen), hydrogen are mainly (more than 90%) trapped from the molecules of water (H_2O), sorbed on the surface of zirconium.

2) During the exposure of zirconium samples with chromium coating in water steam and in electrolyte, under irradiation of them by atomic particles and during the deposition of chromium coating on zirconium hydrogen is mainly trapped in zirconium.

3) The presence of carbon atoms in subsurface layer of zirconium stimulates hydrogen trapping in surface trapping centers during the deposition of chromium coating.

4) Under the irradiation of zirconium samples with chromium coating by the ions of deuterium plasma the deuterium uptake overdraws the uptake under the same irradiation of zirconium without coating by 3-4 times.

5) During the exposure of zirconium samples and samples of zirconium with chromium coating in overheated water steam periodical release of hydrogen occurs.

P3-18: Ion implantation of rolled copper-nickel foils and manifestations of long-range effect.

A. A. Novoselov, V. Ya. Bayankin, F. Z. Gilmutdinov

Physical-Technical Institute UrB RAS, Izhevsk, Russia, less@fti.udm.ru

40 mkm-thick rolled $Cu_{50}Ni_{50}$ foils with aluminum coating and rolled $Cu_{80}Ni_{20}$ foils had been irradiated with B^+ and Ar^+ ions of various energies with variuous ion current densities and irradiation doses. Chemical composition and mechanical properties of irradiated species had been studied with Auger-electron spectroscopy, X-ray photoelectron spectroscopy, Secondary ion mass spectroscopy and microhardness measurement methods.

According to Lindhard-Scharff-Schiott's model projected depth of implanted ions under set parameters of treatment should be less than 50 nm. As a consequence, compositional and structural changes of material due to ion implantation should be restricted to area of 1 mkm from the irradiated surface. The study has shown that some of the implanted B atoms make their way to the non-irradiated side of the foil. Simultaneously, redistiribution of sample's components takes place not only near the irradiated surface but also at the non-irradiated side of the foil. This redistribution was studied and confirmed both by methods of AES and XPS. SIMS study has shown that concentration of B atoms in the middle of the samples is negligible and much lower than near the non-irradiated side.

Microhardness of the non-irradiated side had also changed; as it is heavily dependant from stuctural parameters of the material, it could be assumed that irradiation led to changes of structure at extremely long distances from irradiated surface.

The dependency of implnted atoms' concentration, chemical redistribution and microhardness value non-monotonously depends from irradiation parameters.

It is suggested that this behavior is caused by initially non-equilibrium state of samples due to rolling. Ion implantation causes self-expanding structural changes: during irradiation of sample ions generate local thermal peaks. The excessive energy dissipates from these peaks in form of elastic waves and is enough for transformиation of initial defect structure, such as de-blocking of dislocations and annihilation of different types of defects, which leads to generation of more excessive energy. This allows elastic waves to support themselves. As a result, we observe redistribution of material's components on un-irradiated side due to connection of atoms of specific type with flows of defects.

In conclusion, ion beam treatment of metallic systems with corresponding set of parameters could be used for intended modification of thin-measured products for creation of ultra-thin surface layers of given composition, structure and topography.

P3-19: The features of interaction of disilane molecular beam with the epitaxial surface in conditions of silicon layer growth

L.K. Orlov[1,2], N.L.Ivina[3], T.N. Smyslova[1]

[1]NNSThU, [2]IPhM RAS, [3]VVASS

Effects of interaction of molecular beams with a solid surface and the phenomena accompanying them proceeding on interphase boundary gas – solid state, underlie the various technological processes widely used in practice. Processes of a catalysis, membrane gase separation, gomo - and heteroepitaxy are the most important. It is obvious that achievement of necessary result at carrying out of any technological operations is impossible without detailed understanding of mechanisms and features of reactions on corresponding surfaces. This problem is especially actual in the connection with micro- and a nanoelectronics prospects, connected with the technology of growth of the heteroepitaxial layers and superficial nanostructures, using the method of molecular beam epitaxy with molecular beam sources of substance [1]. In this method, the growth of the layers occurs in the filling of surface states of a variety of gas pyrolysis products, which leads to the specifics of the growth process due to expression of a number of features in the decay kinetics of the epitaxial surface adsorbed molecules [2]. The silicon and germanium hydrides and dihydride are widely used for growing the layers for different applications of silicon electronics. So, it is obvious it is impossible to understand the features observed in the behavior of kinetic coefficients, without a detailed understanding of physical and chemical processes details occurring on the surface of the epitaxial [3].

In the literature, the discussion of the temperature dependence of the silicon layers growth rate is usually limited to the analysis of simple kinetic models that take into account in the kinetics equations only hydride molecule adsorption and hydrogen desorption terms. The corresponding model meets the conditions of full disintegration of the hydride molecules pyrolysis under the prechemosorbtion state, just in the vicinity of the growing surface. The terms that describe the hydrides molecules radicals' disintegration, trapped by surface, which play an important role in the range of typical growth temperatures, are excluded to simplify the calculation of the theoretical analysis. This procedure is generally consistent with results of known experiments to determine the composition of the pyrolysis products on the surface of the silicon layer in terms of growth and limits the ability to assess the degree of blur in the case of heterojunctions grown heterostructures for gas mixtures.

This paper discusses the features of kinetic models describing the basic physical and chemical processes occurring on the silicon crystal growth surface during the trapping and disintegration of the disilane molecules. Analytical expressions relating the hydrides molecules disintegration rate on the Si surface with the other kinetic coefficients and the measured characteristics of the epitaxial process were obtained. We defined region of the characteristic lifetimes of the radicals SiH_j molecules of silicon dihydride ($0.3c < \tau_{SiHj} < 5c$) on the surface of the plate for the various models and conditions of gas pyrolysis using the data of growth experiments. It was shown that the dependence of the molecules disintegration rate on temperature for all types of pyrolysis models cannot be described by simple dependencies of the activation form. The behavior of the curves (Fig. 1) is determined not only by the condition where the hydride disintegration occurs: at the surface of silicon wafers ($j = 1$) or directly on it ($j = 3$), but also at what stage of the pyrolysis the hydrogen molecules is trapped in the silicon surface: if the hydride molecule is in prechermosorbtion state ($k > n$), or have already invaded the surface ($k < n$). A kinetic analysis of the temperature depending on the radicals molecules disintegration rate has shown that the nature of the collapse of the molecules of mono-and disilane trapped by the surface is quite different in different temperature regimes that meet the conditions of high and low coverage of the surface of silicon with hydrogen. In this case the temperature dependence of radicals molecules disintegration rate is described by the formula containing the sum of the activation dependence with the activation energies E_{a1} E_{a2}. This energies are different for mono-and disilane $Ea (SiH_4) < Ea (Si_2H_6)$, and meeting the conditions of high temperature and low-temperature silicon layer growth on a clean and filled with hydrogen silicon surface with coefficients depending on the concentration of the hydrogen.
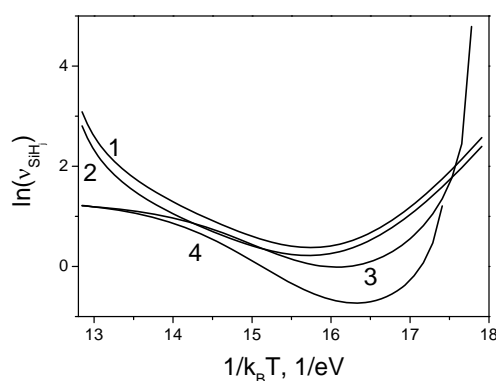
In Fig. 1. Depending of the disilane molecules pyrolysis frequency of the temperature on the silicon layer surface, obtained for the pyrolysis model (jkn): 302 (1), 202 (2), 121 (3), 140 (4) when the gas pressure in the reactor $P_{Si2H6} = 0.1mTor$.

1. Kim K.J., Suemitsu M., Yamanaka M., et.al. // Appl. Phys. Lett. 1993. V.62. P.3461.
2. Ferguson B.A., Reeves C.T., Safarik D.J., et.al. // J. Phys. Chem. 2000. V.113. P.2470.
3. Potapov A.V., Orlov L.K., Ivin S.V. // Thin Solid Films. 1999, V.336. P.191.
4. Murata T., Nakazawa H., Tsukidate Y., et.al. // Appl. Phys. Lett. 2001. V.79, P.746.
5. Орлов Л.К., Ивин С.В. // ФТП. 2011. Т.45. № 4. С.566.
6. Орлов Л.К., Ивин С.В., Смыслова Т.Н. // Химическая физика. 2011. Т.30. № 2. С.88.

P3-20: Investigation of the surface structure of solids and liquids by ellipsometry in a severe mathematical incorrectness of the inverse problem

A.I. Semenenko[1], I.A. Semenenko[2]

1. State University*, Sumy, Ukraine, sem199@mail.ru*
2. Medical Academy. I.M. Sechenov*, Moscow,* Russia*, semenenko1979@mail.ru*

Investigation of the surface structure of solids and liquids is one of the complex and practically important scientific problems. This structure is manifested in various forms. It is ultra thin natural oxide film on semiconductors and metals. It is broken layers at the surface of solids, resulting from a particular treatment. In addition, it is also a natural structure of the surface of liquids associated with their general properties and changing with the addition of various substances. In all these cases the inverse problem of ellipsometry is mathematically incorrect. The mathematical incorrectness is shown that even relatively weak experimental errors significantly distort the true values of the parameters characterizing the surface structure. Very often, these distortions become absurd. However, it must be understand that such a manifestation of the mathematical incorrectness is directly related to the classical approach to solving the inverse problem. In this case the solutions chosen by the parameters determining the point of absolute minimum of the functional inverse problem. In the presence of experimental error causes that lead to mathematical incorrectness, may be very different. For natural oxides expressed incorrectness of the inverse problem is due to their extremely short (a few nanometers) thick. For the disturbed layer thickness does not play a special role, and the leading cause significant manifestation of incorrectness is little difference between the optical parameters of such layers from their by volume values. Broken layers always occur, and this fact should be considered in the study of ultra thin films with a different nature. But also the disturbed layer usually has a more pronounced at the top of the optical parameters with a relatively small, including the ultra, thick. Such a structure seemingly have and the surface of liquids. Thus, the task to study the surface structure of solids and liquids is quite complex. It is not limited to the determination of the parameters of a surface film at the given parameters of the substrate.

In [1] proposed a new approach to the solution of mathematically incorrect inverse problem of ellipsometry for ultra thin superficial films. This approach is based on the using of measurements of the polarization angles corresponding to a set of angles of incidence of the light beam. In [1] provides a general description of the rules of selection of optimal solutions. Using these rules allow with high accuracy to find a solution to the inverse problem with respect to thickness and refractive index of the film at known values of the optical constants of the substrate. This is convincingly demonstrated a numerical experiment based on the simulation of the experimental errors. However for real objects under study the optical constants of the substrate can not be defined precisely. First, this is due to the complex structure of the surface of any material, and hence the substrate. Second, between the film and the substrate is always a certain transition layer. These factors are the reason that the substrate is characterized by some effective values of optical parameters. These effective values can differ markedly from the optical parameters that determine the by volume properties of the substrate. In [1] it is shown that the mathematical incorrectness of the inverse problem is greatly enhanced due to the inaccurate setting of the optical parameters of the substrate. This occurs even when the inaccuracy in setting the refractive index of the substrate is shown in the fourth or fifth decimal place. Therefore, we can talk only about the simultaneous determination of all parameters of a single-layer system, as the surface film and the substrate.

In subsequent studies for solving mathematically incorrect inverse problem of ellipsometry in its general formulation the method of successive approximations is proposed. The basis of this method make rules of selection of optimal solutions for the parameters of the ultra thin film or broken layer at fixed, at each stage of the solution, the optical parameters of the substrate. In this case consider the process of rapprochement between the two points. One of these points is determined by the parameters of the film at an absolute minimum of the functional

$$(d_{min}, n_{min}) \tag{1}$$

The second point is represented by the optimal values of these parameters

$$(d_{opt}, n_{opt}) \tag{2}$$

Obviously, both points correspond to the same fixed for each step of the method parameter values $n_0^{(0)}$, $\kappa_0^{(0)}$ of the substrate. The choice of values $n_0^{(0)}$, $\kappa_0^{(0)}$ is relative. It is important only to the first step in any type of experimental error must satisfy the condition

$$n_{min} < n_{opt}, \qquad d_{min} > d_{opt} \tag{3}$$

Condition (3) is achieved easily. This is due to the fact that point (1) is very mobile even at a weak change in the refractive index of the substrate. At the same time, the point of optimal values (2) has limited mobility. This ensures that the transition of the minimum point through the point of optimal values, followed by divergence of data points

$$n_{min} > n_{opt}, \qquad d_{min} < d_{opt} \tag{4}$$

The main role in the movement of the minimum point (1) is the refractive index n_0 of the substrate, i.e. its variation along an increasing sequence of values. Consequently, the shift of the minimum point (1) through the point of optimal values (2) is observed for any value of the absorption coefficient κ_0 of the substrate. The problem is that of the set transitions of the minimum point through the point of optimal values choose that transition, which corresponds to an optimal solution that best approximate the exact solution of the inverse problem. And since each such transition corresponds to a specific value κ_0, then the right choice of transition means and the choice the value κ_0 as one of the parameter of optimal solutions of inverse problem. This procedure is described in detail in [2]. Particular attention is given to the establishment of character that determines the optimal value of the absorption coefficient of the substrate.

The method of successive approximations worked out in the numerical experiment. This experiment involves modeling of the experimental errors in the assignment of the polarization angles Ψ and Δ for a set of angles of incidence of the light beam. Using a set of angles of incidence of the light beam on the sample is a prerequisite for the successful application of the method. At the same time, the method demonstrated good reliability and features in the study also real reflect systems such as the semiconductor substrate - the ultra thin film. It was successfully tested in the study of silicon and gallium arsenide with the natural super thin oxide films. This involves the determination of all 4 parameters of such systems. Also successfully carried out and processing the experimental results obtained with distilled water with the addition of surfactants. It should be noted that the successful use of this method requires a high accuracy of the computational process. In this regard, substantially modified by a well-known complex method of Box [3], which is the basis of the inverse problem.

1. A.I. Semenenko, I.A. Semenenko, "Optimal solution choice of inverse problem in studying of ultra thin superficial films", Nauchnoe priborostroenie, v. 20, № 4, pp. 132 – 142, 2010.
2. A.I. Semenenko, I.A. Semenenko, "About real possibilities of successive approximations in the solution of the inverse problem", Nauchnoe priborostroenie, v. 22, № 1, pp. 44 – 51, 2012.
3. Box M.J., "A new method of constrained optimization and a comparison with other methods", Comp. Journ., v. 8, pp. 42 – 51, 1965.

P3-21: Simulation of bone tissue/carbon nanotubes interaction during biomineralization

N. Zakharov, M. Sentsov, T. Zakharova

Kurnakov Institute of General and Inorganic Chemistry of the Russian Academy of Science, Moscow, Russian Federation, zakharov@igic.ras.ru

The work is directed in the solution of the fundamental problem connected with development of bioengineering principles for design of materials for bone implants and estimation of perspectives of carbon nanotubes (CNT) application for modification and improvement of nanocomposite characteristics for implants materials.

The key aim of the work was the vital basic task about interaction of CNT with bone tissue of mammals, in particular, with inorganic component of bone tissue – calcium phosphates (CP) with apatite structure. CNT are the form of carbon with unique properties and morphology, which is similar to collagen fibers of native bone. Perspectives of CNT application in the bone engineering shall connect formerly with opportunity of improvement of mechanical properties of biocomposites based on CP, with perspectives of composite materials properties control (primarily – with biochemical, medical and biological) with electrical methods (owing to electrical conductivity CNT) and opportunities of nanoctructured coatings development for improvement of biocompatibility of implants surface.

The solution of problems for utilization of CNT unique advantages in bone tissue bioengineering, estimation of biological potential CNT perspectives, clarification of CNT toxicological characteristics, nature and degree of their participation in metabolism processes suppose following approaches:

– simulation of biomineralization processes of bone tissue main inorganic component – calcium hydroxyapatite $Ca_{10}(PO_4)_6(OH)_2$ (HA) with present of CNT in the course of synthesis of HA/CNT composites;

– development of direct synthesis methods for HA/CNT composites controlled in the course of synthesis and following processing of physical, chemical, medical and biological characteristics;

– analysis of fundamental interrelations "composition – synthesis conditions – structure – dispersiveness – properties" (inclusive of biocompatibility property) of HA/CNT nanocomposites.

Preparation methods are based on the biomimetic synthesis of CP/CNT nanocomposites in the course of calcium and phosphorus salts precipitation and CNT from water solution that simulate of native liquids.

Identification methods of investigation objectives and definitions of their physical and chemical characteristics include chemical analysis, X-ray analysis, infrared spectral analysis, thermal analysis (DTG, DTA), ESCA, electron microscopy (SEM, TEM), electron diffraction, determination of thermally activated characteristics (thermally activated currents, dielectric spectroscopy).

For estimation of biocompatibility characteristics *in vitro* solubility methods (degree and character of solubility in liquids) shall be used.

Composites HA/CNT were produced by biomimetic synthesis in the system $Ca(OH)_2$-H_3PO_4-CNT-H_2O. Multiwall CNT "Taunit" (Tambov) with outer diameter 20-70 nm, inner diameter 5-10 nm and length 5-10 μm were used for the investigation. In Table 1 the residual concentrations and compositions of synthesized products are presented. Synthesized compositions were included in own composition nanocrystalline (NC) HA (Table 2). The increase of CNT content in composites caused growth of solubility of composites HA/CNT NC HA (Fig. 1).

These results allow to assume opportunity of CNT effect on metabolism processes during interaction of CNT with bone tissue.

Table 1. Residual concentrations, pH and compositions of solid phases in the system

Speci-men number	CNT concent-ration, wt.%	Residual concentrations, mmol/l		pH	Ca/P, calculated	Solid phases composi-tions (data of chemical analysis, TGA)
		Ca^{2+}	PO_4^{3-}			
1	0	0,047	0,023	7,23	1,667	$Ca_{10}(PO_4)_6(OH)_2 \cdot 4H_2O$
2	0,1	0,060	0,007	7,14	1,667	$Ca_{10}(PO_4)_6(OH)_2 \cdot$ $0,08C \cdot 8H_2O$
3	1	0,073	0,010	7,21	1,666	$Ca_{10}(PO_4)_6(OH)_2 \cdot$ $0,8C \cdot 6H_2O$
4	5	0,070	0,005	7,32	1,666	$Ca_{10}(PO_4)_6(OH)_2 \cdot$ $4C \cdot 6H_2O$

Table 2. Crystallographic and morphological properties of NC stoichiometric NC HA: NC HA (0 wt. % CNT) and nanocomposites HA/CNT (0.1; 1; 5 wt. % CNT).

Speci-men number	CNT content in initial pro-ducts of synthesis, wt.%	Unit cell parameters, Å		Geometric parameters of HA crystals, *nm* *		Product synthesis gross-formula
		a	*c*	$\| C$	$\perp C$	
1	0	9,421	6,888	39	22	$Ca_{10}(PO_4)_6(OH)_2 \cdot$ $4H_2O$
2	0,1	9,414	6,876	37	19	$Ca_{10}(PO_4)_6(OH)_2 \cdot$ $0,08C \cdot 8H_2O$
3	1	9,414	6,886	35	17	$Ca_{10}(PO_4)_6(OH)_2 \cdot$ $0,8C \cdot 6H_2O$
4	5	9,419	6,885	27	15	$Ca_{10}(PO_4)_6(OH)_2 \cdot$ $4C \cdot 6H_2O$

*HA crystals dimensions in stoihiometric NC HA (1) and in composites HA/CNT (2-5) parallel ($\| C$) and perpendicular ($\perp C$) to crystallographic axis "*C*" of HA.
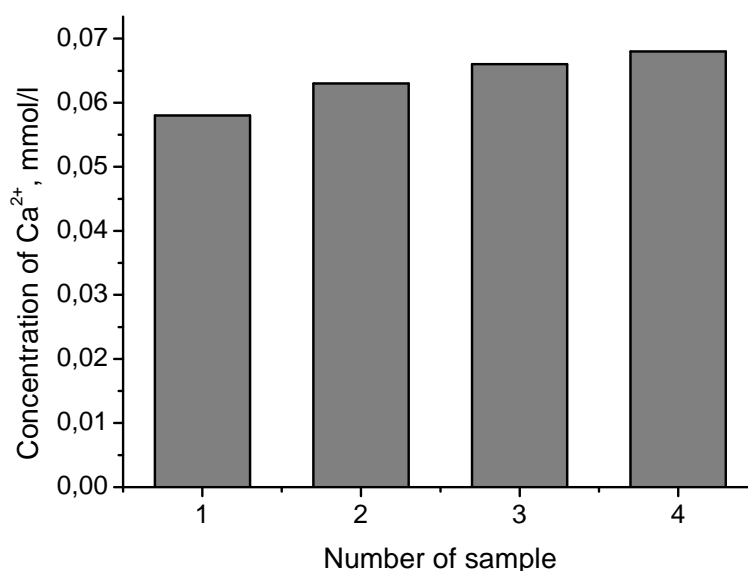
Figure 1. Solubility (based on Ca^{2+} ions) stoihiometric NC HA (1) and composites HA/CNT with CNT contents 0.1 wt. % (2), 1 wt. % (3), 5 wt. % (4).

P3-22: Effect of multi – walled carbon nanotube on tribological properties of field and lubricant

N. Savinski 1, M. Gitlin 1, A. Shornikov, V. Naumov 1,
A. Zharov 2, A. Kiselev 2, D.Boikov 3, S. Vasilev 4

1. Yaroslavl branch of of Physics & Technology Institute of Russian Academy of Sciences
2. Yaroslavl State Technical University
3. Avtodiesel Yaroslavl Motor Works (YaMZ)
4. Facilities sharing centre "Micro and Nanostructures Diagnosis"
E-mail Savinski1@yandex.ru

Nowadays, the automobile industry is progressively imposing the use of gasoline direct injection system to enhance the fuel efficiency and to reduce, at the same time, the harmful emissions to the atmosphere. The new demanding operating conditions linked to the high injection pressure (above 50 MPa) accompanied by the insufficient lubrication response of gasoline, promote the extensive friction and wear of the metallic sliding components, with improved tribological performances [1].

Since the discovery of carbon nanotubes (CNTs) in 1991[1], the CNTs attracted a great deal of have attracted a great deal of attention because of their unique structural electronical, mechanical properties. Many potential application of CNTs, such as nanodevices, sensors, ultrahigh –strength engineering fibers have been found. It is well known, that the CNT are chemically inert, and reinforcing elements will suffer from poor dispersion capability and weak interfacial interaction. Currently, chemical modification of CNTs is an efficient means for modifying the chemical properties and wettability of CNTs. In this paper, a simple approach to modify MWNTs with cobalt salt of Stearic Acid (SA), which is one of the most important lubricant and dispersant, was proposed as good candidate for practical application. The modified carbon nanotube as lubricant additive were utilized to prepare lubricant, and effects of carbon nanotubes on the tribological properties were investigated by using four ball wear tester ((DIN 51 350, ASTM D 2266, ГОСТ 9490-75, РД 50-531-85).

The MWCNTs were produced by the catalytic decomposition of propanol - 2 vapor using IR tube furnace which can be operated up to a temperature of 7500 C at atmospheric pressure. The experimental set-up is somewhat like that reported elsewhere [2]. The quartz tube used to carry out the deposition has a length of 100 cm with a 25 mm inner diameter. The MWCNTs were grown using argon as carrier gas. As prepared MWCNT were purified by immersing in concentrated HNO3 and HCl acids. The purified MWCNT were mechanically milled with planetary ball mill for 24h. The presence MWCNTs of can improve the friction reduction and anti-wear ability of pure lubricant of mineral oil SN-400 about 40%. The concentrated MWCNTs additive in lubricant

is 1% mass. The result imply, that modified MWCNTs with SA can improve the friction reduction and anti-wear ability of pure lubricant of mineral oil SN-400 60%. The MWCNTs as field additive offer many advantages. Because their ability to trap free radical, carbon tube can function as anti-khock additive. Adding MWCNTs in diesel field increasing the cetane number.

The collected MWCNTs were examined by a SEM (Supra), X-ray spectrometry ARL X`tra (Thermo Fisher Scientific) FTIR Bruker -113 to measure the length, diameter and uniformity.

1 J.P. Hantsche and U.Spicher, "Ceramic component for high pressure gasoline fuel injection pump, Mat.-wiss.u.Werkstofftech., 2005,36,108

2 H.Oshima, Y.Suzuki, T. Shimazu, and S.Maruyama "Novel and Simple Synthesis Method for Submillimeter Long Vertically Aligned Single-Walled Carbon Nanotubes by No-Flow Alcohol Catalytic Chemical Vapor Deposition" Japanese Journal of Applied Physics,V. **47**, No. 4, , pp. 1982–1984, 2008

P3-23: The study of the dynamics of calcifying nanoparticles

Vasilev S.V.[1], Churilov A.B.[2], Prikhodko O.Y.[1], Rudy A.S.[2],
Shekhovtsova N.V.[3], Yagushkina A.Y.[3]

*1. Facilities Sharing Centre "Micro- and Nanostructures Diagnosis", Demidov State University, Yaroslavl, Russia,
E-mail address: ginger89@yandex.ru*
*2. Yaroslavl Branch of Physics and Technology Institute of Russian Academy of Sciences, Yaroslavl, Russia, E-mail
address: rudy@univ.uniyar.ac.ru*
*3. Department of Biology, Demidov State University, 14, Sovetskaya street, Yaroslavl, Russia, E-mail address:
ninval@mail.ru*

This paper presents the results of studies of nanoparticles from the Vorotilovskaya deep scientific well (VDSW). The morphology and phase composition of nanoparticles were studied by means of scanning and transmission electron microscopy.

Pure culture of bacteria *Planomicrobium sp.* extracted from gneiss VDSW where investigated and the objects with size from 50 to 400 nm have been detected (Fig.1, 2a). These objects, reminiscent of a colony of unusually small spherical or coin-shaped bacteria, were significantly smaller than any bacteria known today, fungal spores or cells of tissues of multicellular organisms[1].
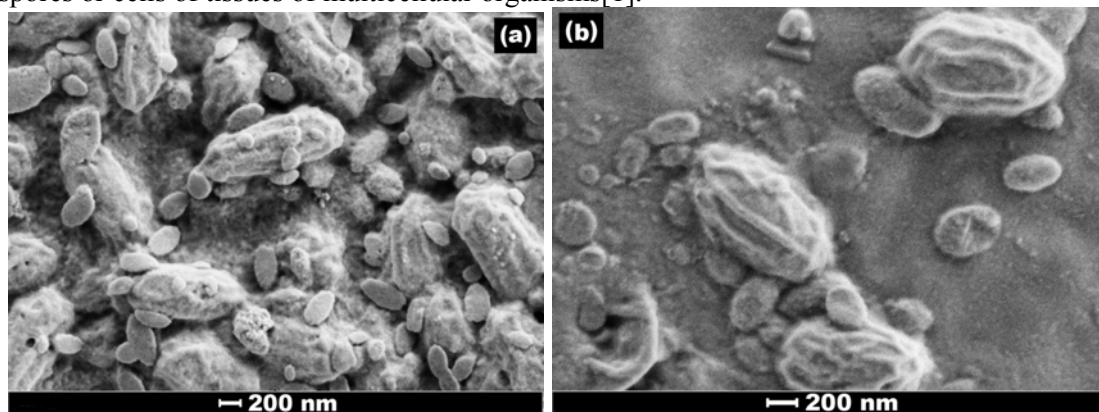

Fig. 1. Images of bacteria *Planomicrobium sp.* and calcifying nanoparticles obtained on SEM Supra 40.

Similar «colonies» have been previously detected in many different samples by biochemists, microbiologists, geologists [2]. The main compound of these particles is hydroxyapatite $Ca_5(PO_4)_3OH$. This statement is based on the data from the X-ray microanalysis, which has been carried out by hydroxyapatite as internal standard. However, calcium, phosphorus and oxygen create a big number of different compounds. This makes the interpretation of X-ray microanalysis results varied.
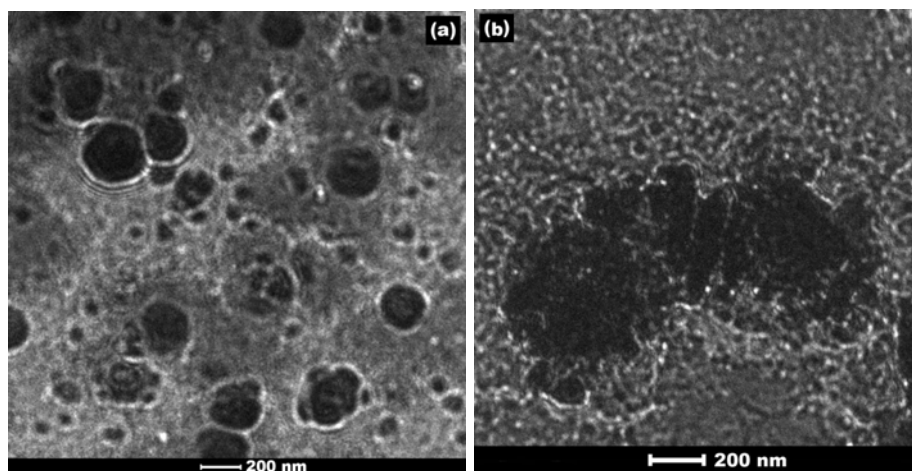

Fig.2. Images of calcifying nanoparticles obtained in the transmission electron microscope Tecnai G2 F20 U-TWIN.
a) primary research, b) research after 2 months.

We have tried to solve this problem by means of electron diffraction using a transmission electron microscope Tecnai G2F20 U-TWIN and find two compounds: $Ca_2Fe(PO_4)_2(OH)H_2O$ and $Mg(NH_4)_8(P_3O_{10})_2 \cdot 8H_2O$. These studies were repeated by the same research methods after 2 months (Fig.2b) of storage initial suspension of nanoparticles at room temperature under normal atmospheric pressure in a glass flask. The procedure for sample preparation was similar to the primary research.

Based on the comparisons with the diffraction results database it was concluded that the shell of re-examined nanoparticles is composed of aragonite with the chemical formula $CaCO_3$. Results of Fourier transform infrared (FTIR) measurements suggest that a chemical reaction, which took place in solution in the six-week period between successive registrations of electron diffraction, has transferred phosphate ions into solution.

The feature of the detected objects is their capability to phase composition and morphology transformation with time. In contrast with stable objects earlier observed E.O. Kajander [3] and other scientists [2, 4] these nanoparticles in two months has changed their morphology and phase composition from $Ca_2Fe(PO_4)_2(OH) \cdot H_2O$ and $Mg(NH_4)_8(P_3O_{10})_2 \cdot 8H_2O$ [14] to $CaCO_3$.

1. B. Alberts, D. Bray, J. Lewis, M. Raff, K. Roberts. *Molecular Biology of the Cell*, fifth ed. Garland Science, 2007.
2. V.A. Kordyum et.all, "Biopolymers and cells dimension in architecture microcenosis", Biopolym. Cell, 25, pp. 403-423, 2009.
3. E.O. Kajander, "Nanobacteria - propagating calcifying nanoparticles", Letters in Applied Microbiology, 42 (6), pp. 549-552, 2006.
4. J.C. Lieske, "Human-derived nanoparticles and vascular response to injury in rabbit carotid arteries Proof of principle ", Int. J. Nanomedicine , 3(2), pp. 243-248, 2008.

P3-24: Fraktalnaja processing of surfaces of cancer diseases of a skin

L. Nefed'ev, I. Rusanova, R. Nabiev

Physics institute, the Kazan (Privolzhsky) federal university, Kazan, Russia, e-mail: irusanova@yandex.ru

Fraktalnye structures are found out in many areas of physics, chemistry, biology and medicine and allows to find out the general principles and laws of the difficult dynamics which has been not enough opened of physical essence of observable processes in such casual systems as polymers, rough and porous surfaces, colloidal units, structures of arteries etc. Presence of self-similar properties specifies that dynamics of the processes which result they are, has also the self-similar nature and is characterized by the certain algorithm operating according to the general principles and laws of development of disease, and functioning on each hierarchical level.

Concept of scale invariancy (скейлинга) and self-similarity have arisen independently in different areas. One of them – the physics of phase transitions studying the critical phenomena, another – fraktalnaja the geometry including concept nonintegral dimension. Definition fraktal dimensions of objects allows not only to study their structure, but also communication between structure and processes of its formation. Now a perspective direction of development of noninvasive methods of diagnostics is increase of their quality, reduction of time of inspection, and also working out of the new visual methods which are not demanding any external influences on the patient.

In work sensitivity of application of [1-4] researches of images of non-uniform structures of surfaces developed before a technique for increase in the diagnostic information is investigated at cancer diseases of a skin and nail plates, at an early stage of occurrence of irreversible changes of living tissues, with allocation fraktal and self-similar properties of surfaces.

As objects of research were electronic pictures of surfaces of a skin and nail plates for different groups of diseases, in comparison with pictures of surfaces of healthy fabrics are taken. The description of experimental data by means of fractals allows to represent them rationally. The set of experimental data can be described corresponding fraktal dimension and in self-similarity factor. We will consider partially ordered final set $A(N^2)$, where N^2 - number of elements $a_{i,j}$ in set $a_{i,j} \in A(N^2)$, where $i,j = 1...N$. Let's consider, that the partial order on final set is set by diagramme Hosoe and set elements possess some properties $H_\xi(a)$ (the size, colour, volume, the form etc), inherent only elements of the given set $\forall a_{i,j} \left(a_{i,j} \in \left\{ a \middle| H_\xi(a) \middle| \right\} \right)$. If it is some general properties $(\xi > 1)$, that description of set should be made by means of several fraktal dimensions. Let's define fraktal dimension D_ξ множества $A(N^2)$ on property $H_\xi(a)$ in angular factor of dependence $\log \Gamma_\xi(n^2)$ from $\log s_\xi n^2$, where $\Gamma_\xi(n^2)$- number of not adjoining surfaces of the cubes covering subsets, $s_\xi n^2 = S_\xi(n^2)$ - the area occupied with elements of a subset

$$D_\xi = \sum_\gamma \frac{\log \Gamma_\xi\left(n^2_{\gamma+1}\right) - \log \Gamma_\xi\left(n^2_\lambda\right)}{abs\left(\log S_\xi\left(n^2_{\gamma+1}\right)\right) - abs\left(\log S_\xi\left(n^2_\gamma\right)\right)} \left(\frac{\alpha_{\gamma+1} - \alpha_\gamma}{N-1} \right).$$

Self-similarity factor we will define as $K_\xi = \dfrac{D_\xi^0}{D_\xi}$, где D_ξ^0 - fraktal dimension of self-similar set

$$D_\xi^0 = \frac{\log \Gamma_\xi\left(N^2\right) - \log \Gamma_\xi(1)}{abs\left(\log S_\xi\left(N^2\right) - abs\left(\log S_\xi(1)\right)\right)}$$ [3]. For example, at research fraktal properties of the image as properties $H_\xi(a)$ it is possible to choose three colours: the red (ξ =K), green ($\xi = C$) and dark blue ($\xi = $ B). Thus, the description of structure of the image in this case is carried out by three fraktal dimensions DR, DG and DB with which help it is possible to construct some size SRGB (the triangle area in co-ordinate system of properties), possessing high sensitivity to change of structure of the image: $SRGB = \frac{1}{2} M[-2(D_R + D_B) + (D_B + D_G) + (D_G + D_B)]$.
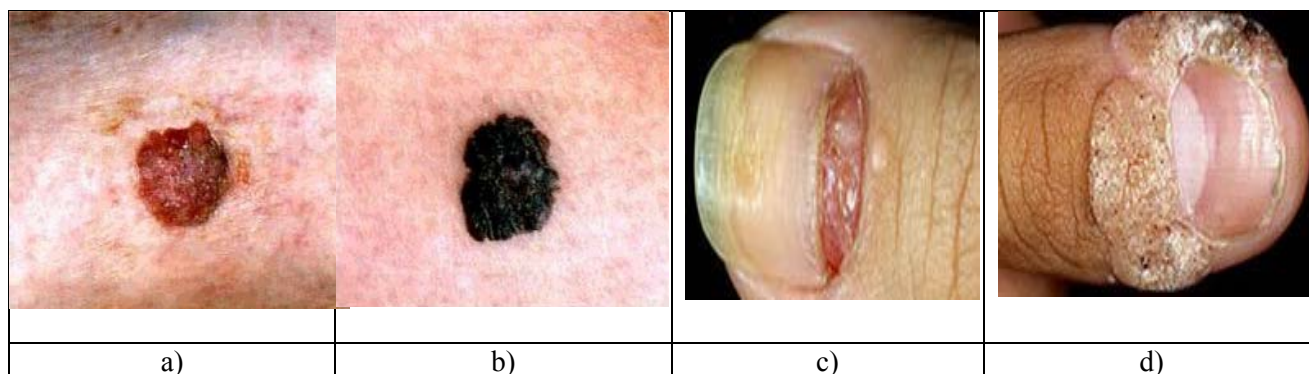
Fig. 1. Pictures of surfaces of a skin of the basic types of cancer diseases:
a) bazalno-cellular carcinoma skin; b) scaly cellular carcinoma;c) acral lentigo melanoma; d) warts about a nail.

It is shown, that, despite distinction in character of changes of a surface of a skin near to the centre (fig. 1. a, b) in the form of consolidations and colour colouring очаговой zones, the general behaviour of the characteristic changes which visually are not observed, is shown in size fraktal dimensions of various sites of

an investigated surface of a skin $D_1 \approx D_2$, $D \begin{cases} \neq D_1 \\ \neq D_2 \end{cases}$, где D - fraktal dimension of all amazed area, D_1

- the centre and D_2 - close centre sites. It is revealed, that fraktal dimension of a healthy skin surface is less фрактальной than dimension of the amazed sites of a skin surface. At research of surfaces of 8 groups of diseases (a Fig. 1. c, d) nail plates (48 pictures) it is revealed, that average value of sizes SRGB for investigated sites of different diseases in most cases are various and negative, in times smaller on size, in comparison with healthy nails. For healthy nail fabrics average value SRGB of investigated sites are close on size. Method SRGB is more sensitive in comparison with definition фрактальной dimension and self-similarity factor. It is shown, that the applied method is sensitive to research of changes of superficial structure of a skin and nail plates, and allows to spend diagnosing at an initial stage of disease, considering, that фрактальность not always proves distinctly, she hides in the casual statistics of colour scale and structure changes.

1. E. Feder, *Fractals.* M: the World, 1991.
2. L.A. Nefed'ev and I.A. Rusanova, Fraktalnaja processing of images//Article of the Tenth International youth school of thought «Coherent optics and optical spectroscopy». Kazan, on October, 24-26th, 2006. C.147-151
3. I.A. Rusanova, Research of irreversible processes of non-uniform surfaces of an eye bottom and cancer diseases of a skin.// Article of V All-Russia conference «Irreversible processes in the nature and the technician». Moscow, on January,   pp. 247-250, 2009.
4. I.A. Rusanova, , Fraktalnaja images of nuclear magnetic resonances-tomograms of a brain.//Theses of 6th Winter youth school-conference «the Magnetic resonance and its appendices». St.-Petersburg, pp. 202-203, 2009.

P3-25: Self-organization of oligopeptides thin films due to organic vapors

I.G. Efimova[1], M.A. Ziganshin[1], V.V. Gorbatchuk[1], S.A. Ziganshina[2], A.P. Chuklanov[2], A.A. Bukharaev[2]

1 - Kazan (Volga region) federal university, Kazan, Russia
2 - Zavoisky Physical–Technical Institute of KSC of RAS, Kazan, Russia, iefimova@ksu.ru

Ability of molecules peptides to self-organizing with formation tubular or layered nanostructures with various functional features has caused considerable interest to them in the last some years.

Research objective is studying of processes of the directed self-organizing nano-structured films of and change of morphology of a film surface as a result of their interaction with organic vapors (guest).

In present study receptor properties the thin layer of oligopeptides L-alanyl-L-valine (AV), L-valyl-L-alanine (VA) and L-leucyl-L-leucyl-L-leucine (LLL) were estimated using the quartz crystal microbalance technique (QCM). The morphology of thin films of oligopeptides on surfaces of the HOPG (Highly Oriented Pyrolytic Graphite) was studied using the atomic force microscopy (AFM).

It was observed that sorption ability of oligopeptides AV, VA and LLL decrease with increase molecular size of organic guests.

The binding of vapors of big or hydrophobic guest by thin flat dipeptides layer lead to the formation of the stable nanosized islands on the dipeptide surface (Fig. 1).
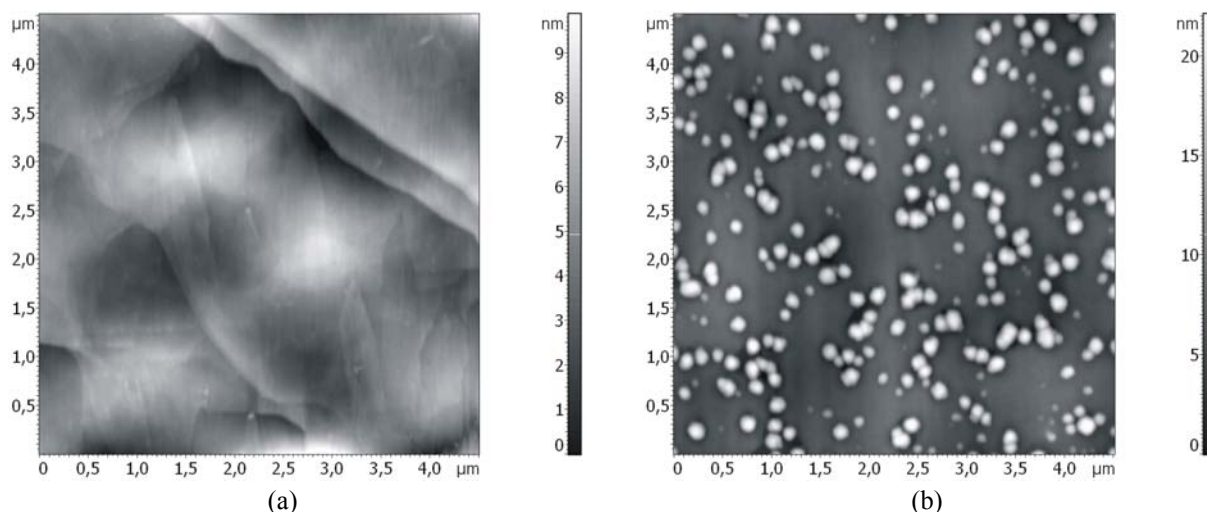

Fig. 1. AFM images of the L-alanyl-L-valine film befor (a) and after (b) the binding of toluene vapor and futher purge with hot air.

It was found that sorption of a relatively large and/or hydrophobic molecules are caused an irreversible change in the initially flat dipeptides surface morphology, with the formation of nanoislands with varying topology.

It was shown that micro- and nanocrystals formed on the surface of the thin film tripeptide LLL prepared from solution in methanol.

It was found that the sorption of organic compounds which able to effective binding with the tripeptide, leads to significant deformation of microcrystals LLL on the surface of thin film.

The data obtained in the present study will allow to create a fundamental reserve for the solve of a problem of controllable self-organizing of oligopeptide that is necessary for making new biocompatible nanomaterials with the useful properties for bionanomedicine, new biocatalytic systems and intelligence systems for recognition of smell and taste.

P3-26: Application of ion beam cutting for multi-layered metal/oxide system

E. Fedorova, N. Suhodoeva

Polytechnic institute of Siberian Federal University, Krasnoyarsk, Russia, fedorova.elena.85@gmail.com
me-zon@list.ru

Ion beam preparation of cross-section for optical and SEM observations has essential advantages compared with conventional techniques as mechanical grinding/polishing and focused ion beam (FIB) [1]. Ion beam processing allows the deformation-free preparation and also the layers damaged during mechanical treatment can be removed followed by special ion beam polishing procedures to get smooth areas for material contrast imaging and elemental analysis [2].

In the present work, Gatan Precision Etching Coating System (PECS Model 682) equipped with Slope Cutter Tool was used to prepare the cross-section of the thermally grown oxide (TGO) formed during the high temperature isothermal oxidation Ni-based superalloy. Single crystal superalloys AM1[3] were provided by Snecma-Safran Group. Oxidation resistance of Ni-based superalloys and bond coating materials in high-temperature environments is largely dictated by their ability to preferentially form an adherent oxide scale on the metal surface [4]. In the previous work published recently it was shown that the oxide scale formed on AM1 after short term isothermal oxidation at 1100 °C has a multi-layered structure. This structure of TGO must be accurately known for a correct analysis of the interfacial adherence of studied metal/oxide system [5]. A detailed description of oxidation test conditions was presented in [5].

The three-step procedure cutting-selective etching-coating was carried out (Fig 1, a). Multiple tests were performed to determine the optimal operating parameters in order to obtain the cross-section of the multi-layered TGO on the alloy surface. The cutting step was performed with argon ions using a special holder with 90 ° sample stub (Fig. 1, b). Selective etching provides eliminating the effect of transfer of material and improves the contrast structure of the surface. Ion beam sputter coating of Pt conductive layer using Film Thickness Monitor aimed to accurate control of film thickness for high resolution SEM imaging was carried out. Parameters using for sample cross-section are presented in Table 1.
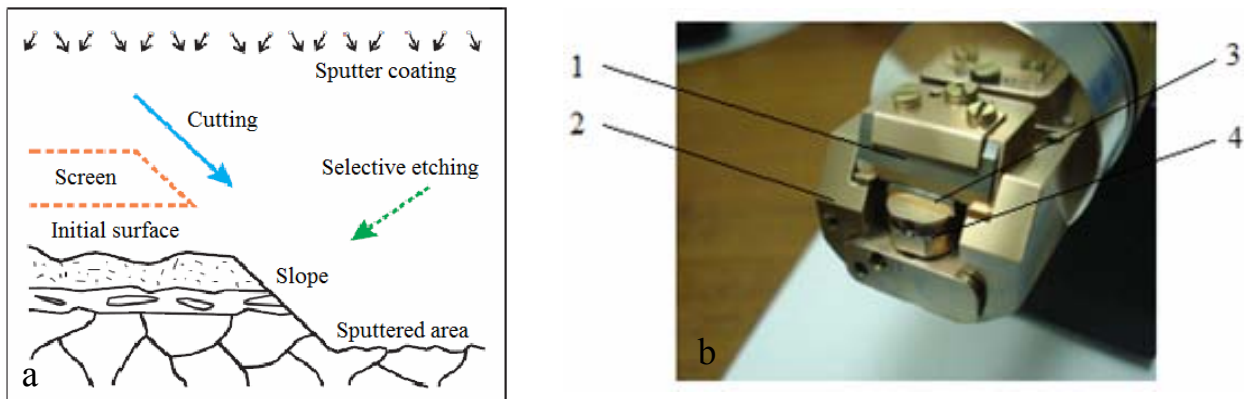

Fig. 1: a - Schematic representation of the ion beam processing steps [2]; b – Slope Cutter Tool with the sample (1-screen, 2- holder, 3 – sample, 4- stub)

Table 1 – Operating conditions of procedure

Parameters	Ion beam cutting	Selective etching	Ion beam sputter coating
Ion beam energy, keV	7	5	5
Rocking angle,	30	45	30
Sample rocking/sec	12	0	12
Time, min	120	5	1

The ability of the of ion beam cutting technique for cross-section of multi-layered metal/oxide system was evaluated. In order to understand the sources of possible imperfections and problems which arise

during the process different operating parameters were used. It was found that to minimize the damage of thin layers during the cutting lower ion beam energies and increased time could be used.

Acknowledgments:

References:

1. Gatan product information 2007 http://www.gatan.com
2. W. Hauffe, "Production of Microstructures by Ion Beam Sputtering", Chapter 6 in Sputtering by
Particle Bombardment III (Eds. R.Behrisch and K.Wittmaack), Springer Ser. Topics in Appl. Phys., Vol. 64 Springer-Verlag Heidelberg, New York, 1991.
3. P. Caron, T. Khan, "Evolution of Ni-based superalloys for single crystal gas turbine blade applications" Aerospace Science and Technology, 3, pp. 513–523, 1999.
4. M.A. Smith, W.E. Frazier, B.A. Pregger, "Effect of Sulfur on the Cyclic Oxidation Behavior of a Single Crystalline Nickel-Based Super-alloy", Mater. Sci. Eng., A 203, pp. 388–398, 1995.
5. E. Fedorova, D. Monceau, D. Oquab, "Quantification of growth kinetics and adherence of oxide scales formed on Ni-based superalloys at high temperature", Corrosion Science 52, pp. 3932–3942, 2010.